ornl

ORNL/Sub/83-43374/1/V2

OAK RIDGE NATIONAL LABORATORY

MARTIN MARIETTA

Study to Assess the Effects of High-Altitude Electromagnetic Pulse on Electric Power Systems Phase I Final Report

J. R. Legro
N. C. Abi-Samra
J. C. Crouse
A. R. Hileman
V. J. Kruse
E. R. Taylor, Jr.
F. M. Tesche

OPERATED BY
MARTIN MARIETTA ENERGY SYSTEMS, INC.
FOR THE UNITED STATES
DEPARTMENT OF ENERGY

Changed on *[illegible handwriting]*

OAK RIDGE NATIONAL LABORATORY

OPERATED BY MARTIN MARIETTA ENERGY SYSTEMS, INC.

March 14, 1986

To: Recipients of Subject Report

Report No.: <u>ORNL/Sub/83-44374/1/V2</u>   Classification: <u>Unclassified</u>

Authors: <u>J. R. Legro, N. C. Abi-Samra, J. C. Crouse, A. R. Hileman,</u>

          <u>V. J. Kruse, E. R. Taylor, Jr. F. M. Tesche</u>

Title: <u>Study to Assess the Effects of High-Altitude Electromagnetic Pulse</u>

       <u>on Electric Power Systems. Phase 1: Final Report</u>

The report number ORNL/Sub/83-44374/1/V2 that appears on the cover and title page of this report is in error. Please correct by placing the enclosed self-adhesive pages on you copy(ies) of this report.

We regret any inconvenience this error may have caused and appreciate your cooperation in correcting the error.

W. N. Drewery, Supervisor
Laboratory Records Department
Information Resources Organization

WND/db

Enclosure(s)

cc: Master File - ORNL/Sub/83-43374/1/V2

Energy Division

STUDY TO ASSESS THE EFFECTS OF HIGH-ALTITUDE ELECTROMAGNETIC PULSE ON ELECTRIC POWER SYSTEMS
PHASE I
FINAL REPORT

J. R. Legro
N. C. Abi-Samra
J. C. Crouse
A. R. Hileman
V. J. Kruse
E. R. Taylor, Jr.
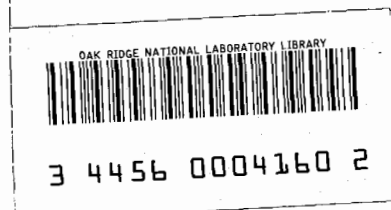F. M. Tesche

Date Published - February 1986

ACKNOWLEDGMENTS

CONTENTS

CONTENTS (Cont'd)

LIST OF FIGURES

LIST OF TABLES

STUDY TO ASSESS THE EFFECTS OF
HIGH-ALTITUDE ELECTROMAGNETIC PULSE
ON ELECTRIC POWER SYSTEMS

J. R. Legro
N. C. Abi-Samra
J. C. Crouse
A. R. Hileman
V. J. Kruse
E. R. Taylor, Jr.
F. M. Tesche*

ABSTRACT

The high-altitude burst of a nuclear device over the continental United States can expose civilian electric utility systems to transient electromagnetic pulses (EMP). The electromagnetic fields experienced within one second after the burst have been collectively defined by the term high-altitude EMP (HEMP). The phenomena has been subdivided, for this report, into an early-time HEMP field followed by an intermediate-time HEMP field.

This volume documents a preliminary research effort to: (1) investigate the nature and coupling of the HEMP environments to electric power systems, (2) define the construction of approximate system response models and, (3) document the development of a methodology to assess equipment and system vulnerability.

The research, to date, does not include an attempt to quantify power system performance in HEMP environments. This effort has been to define the analytical methods and techniques necessary to perform such assessments at a later time. It is anticipated that the HEMP methodology will be incorporated into a comprehensive EMP assessment process to investigate total system risk.

---
*LuTech Incorporated, Lafayette, CA

1. INTRODUCTION

In the event of single or multiple high-altitude nuclear bursts over the continental United States, it is predicted that large geographic areas of the country can be illuminated by transient electromagnetic fields known as high-altitude EMP (HEMP). The initial electromagnetic environment experienced at or near the earth's surface is a fast transient having characteristic rise times strongly related to the prompt gamma radiation output rate of the nuclear device. This HEMP environment, known as early-time HEMP, may have the potential to cause direct and consequential damage to unhardened, civilian electric utility systems, as well as system operational upset. Immediately following the initial, HEMP transient, scattered gamma photons and inelastic gammas from weapon neutrons create additional ionization resulting in the second (intermediate-time) HEMP environment. The HEMP environments are followed at much later times (seconds to hundreds of seconds after the burst) by very low frequency excitation due to magnetic bubble formation followed by hydrodynamic motion of the heated atmosphere. This type of electromagnetic transient has been defined by the term magnetohydrodynamic EMP (MHD-EMP).

Since the United States electric power network of generation, transmission and distribution may be exposed to EMP environments, it is of critical importance to national security that a quantitative and comprehensive methodology be developed to assess the vulnerability of electric power systems to this, externally imposed, transient environment. The creation of such an assessment technique would enable all interested parties to quantify the potential risk to existing systems, and to explore alternate system hardware applications and operational strategies. EMP assessments have been performed for other types of electrical systems, such as military aircraft, missiles and communications facilities. The unique properties of the electric power system, such as its complex electrical interconnection over a wide geographic area strongly indicates that an EMP assessment methodology should be developed with specific focus on the electric power system.

Section 2 of this report presents a brief overview of the physics related to HEMP formation as a prelude to characterization of HEMP transient environments. Previous approaches to HEMP environmental description, predicated upon concepts of "worst case" threat definitions suitable in the assessment of spatially local, hardened military facilities, are compared to alternate techniques to incorporate the spatial dependence of the phenomena necessary to more realistically assess the system interaction of a geography dispersed civilian electric utility system.

In Section 3, the HEMP interaction with the civilian electric utility system is discussed. Such interaction includes direct "coupling" of the transient electromagnetic fields to electrical conductors, such as power lines and cables, and the subsequent propagation of EMP energy throughout the system. In addition, interaction of the HEMP environment directly on system components by direct field penetration into enclosures via apertures and by direct diffusion is developed. Models are developed in order to define applicable electrical "stress" at points of interest.

Section 4 considers the necessary elements of a civilian electric utility assessment methodology for HEMP environments. The methodology encompasses assessment techniques specifically orientated towards the generation, transmission, distribution and operations function of the utility system as well as total system response.

Section 5 presents the development of power system equipment models and vulnerability criteria to support the assessment methodology. The applicability of existing power system assessment digital codes is discussed and the development of additional codes is considered. This section also considers the scope of an experimental program to determine equipment vulnerability, and system responses.

The report concludes with a summary of recommended areas of additional research to refine the environmental definition, modeling techniques and assessment methodology.

The research to date does not include any attempt to quantify power system performance in HEMP environments. The Phase I effort has been to define the methods and techniques necessary to perform such assessments in subsequent phases of the research program.

2. HEMP ENVIRONMENTAL DESCRIPTION

2.1 Introduction

Any methodology developed to investigate the interaction of HEMP with civilian electric utility systems must incorporate an electromagnetic environmental description as part of the specification of initial conditions. The environmental description should incorporate an appreciation of the physics associated with the generation of the EMP transient phenomena and the suitability of the environmental specification with respect to the physical and functional properties of the system under investigation.

Much of what is empirically known about the HEMP signal cannot be discussed in an unclassified sense. However, the unclassified literature does present at least one measured HEMP waveform [1] ascribed to the 1962 high-altitude, nuclear device test series. This measurement, designated as curve C, is reproduced in Figure 1 of this report. Figure 1 also depicts the results of an EMP computer code (curve A) developed to simulate the phenomena and investigate the accuracy of various approximations made in analytical investigations employing high-frequency models. Curve B represents the convolution of the computer simulated waveform and the measurement instrument response.

This section presents an overview of the physical mechanisms associated with the creation and propagation of the radiated HEMP signal(s) from a high-altitude nuclear detonation and develops the parameters of interest which could be expected at or near the earth's surface. The approach of HEMP "worst case" threat environmental definition is discussed and contrasted to specifications incorporating the spatial and time variance of the HEMP environment within the area of direct illumination. The section concludes with a recommendation of a HEMP environmental format designed to specifically investigate the interaction of EMP and the civilian electric utility system.
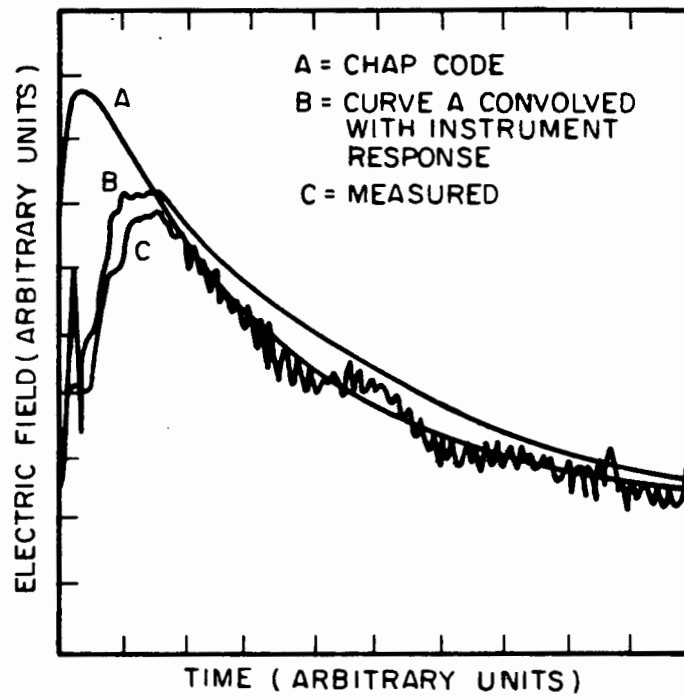
Fig. 1.   Experimental and theoretical HEMP waveforms [1].

2.2 The Physics of EMP Generation

The HEMP phenomena is initiated by a nuclear detonation at an altitude greater than approximately 40 km above the earth's surface. This event results in a radiated, transient electromagnetic field(s) that can illuminate large areas of the earth's surface. These signals are distinctly different from other natural or man-made sources of electromagnetic phenomena with respect to their large amplitudes and short rise times. In addition, within the limitations of the speed of light, large areas of the earth are simultaneously illuminated.

The HEMP pulse is generated in the electromagnetic source (deposition) region where gamma rays emanating from the nuclear device collide with air molecules and lose part of their energy by producing Compton electrons [2]. This interaction is shown in Figure 2. The result is an ionized region in which an approximately radially directed Compton current is able to flow. The physical extent of the deposition region is a strong function of the height of the burst and the weapon yield. For a nominal one megaton burst, the respective deposition regions for heights of 50, 100, 200 and 300 km are shown in Figure 3 [3].

It is the Compton electron interaction with the earth's magnetic field and resulting motion within the source region which ultimately produces the HEMP electromagnetic radiation. The electron motion is also affected to some degree by the EMP fields themselves, and a self-consistent solution for the fields, Compton currents and air conductivity can be obtained using Maxwell's equations with the appropriate source and boundary conditions and air chemistry relations [1,4,5].

As is shown in Figure 3, the asymmetry of the source (deposition) region evokes the existence of HEMP radiated fields outside of the region. The physical mechanisms responsible for source region and HEMP radiated field asymmetry arise from: (1) gradients in the earth's atmospheric density, (2) the presence of the earth's magnetic field
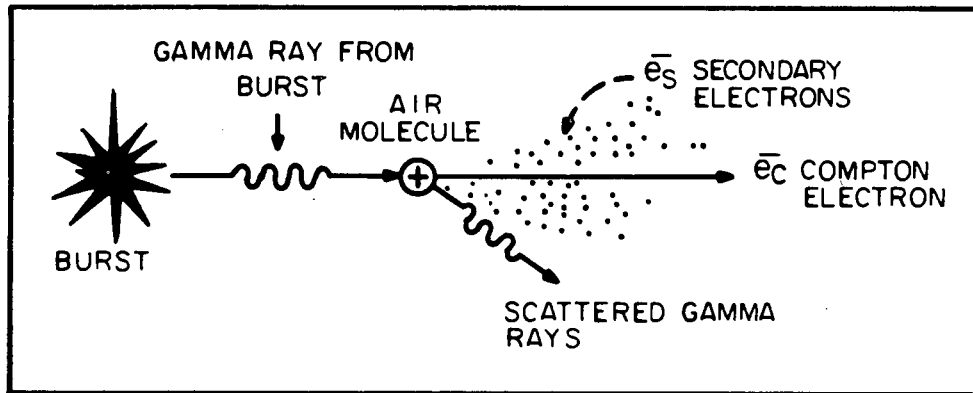
Fig. 2. The Compton scattering process.
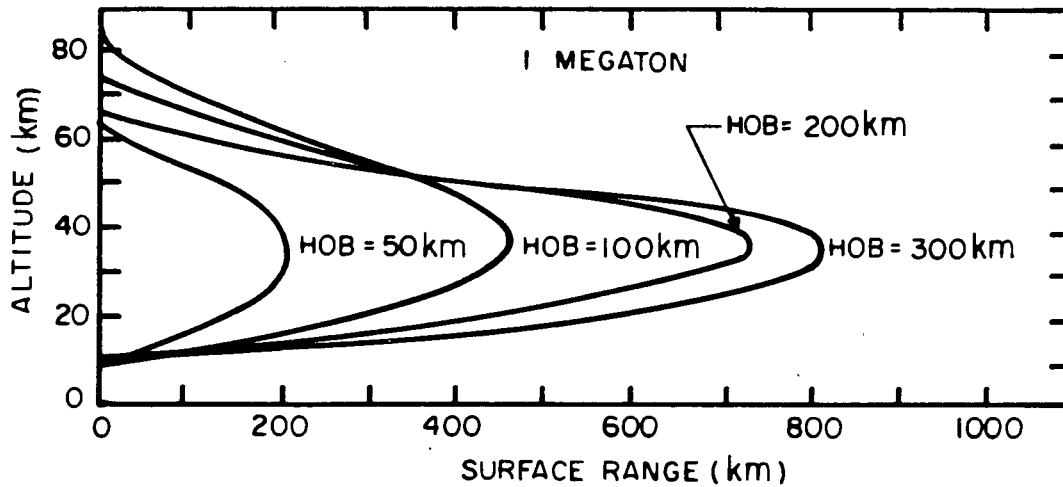
Fig. 3. Physical extent of the deposition (source)
region for a 1 MT burst at several heights of
burst (HOB) [6].

which affects electron motion, and (3) asymmetries in the initial gamma ray flux due to weapon design. The net effect of such asymmetry is shown in Figure 4. Downward gammas from the burst travel practically unaffected until they reach an altitude of about 40 km, where the earth's atmosphere has sufficient density to produce Compton electrons. The presence of the earth's magnetic field at this point causes the electrons to spiral around the magnetic field lines, resulting in a transverse component of the Compton current. This current component creates a magnetic dipole moment. The highly peaked, early-time characteristic of the HEMP radiated field, exhibited in the measured signal shown in Figure 1, has been attributed to this turning of electrons in the earth's magnetic field [3].

Beyond the source (deposition) region, the radiated HEMP electro-magnetic transient is considered to propagate according to the free-space propagation velocity of $3x10^8$ m/s and with a free-space characteristic impedance of 377 ohms. At an observation point on the earth's surface, the incident HEMP electromagnetic field appears as a local plane wave having transverse electric and magnetic field components, a specific polarization, angle of incidence and temporal waveform. The exact behavior of these quantities depend on the burst location and weapon design, the geomagnetic field in the source region and the observation point.

The preceding physical development of the HEMP radiated field is predicated on the concepts of a high-frequency EMP model and focuses on the prompt gamma flux produced by the weapon. Thus, the theory accounts for the early-time of the total HEMP signal, i.e., signal times less than one microsecond. Scattered gamma ray photons and inelastic gammas from weapon neutrons create additional ionization later in time. It is the HEMP signal produced under this additional ionization that has been defined as intermediate-time HEMP. The attributes of both types of HEMP are discussed in the next subsection.
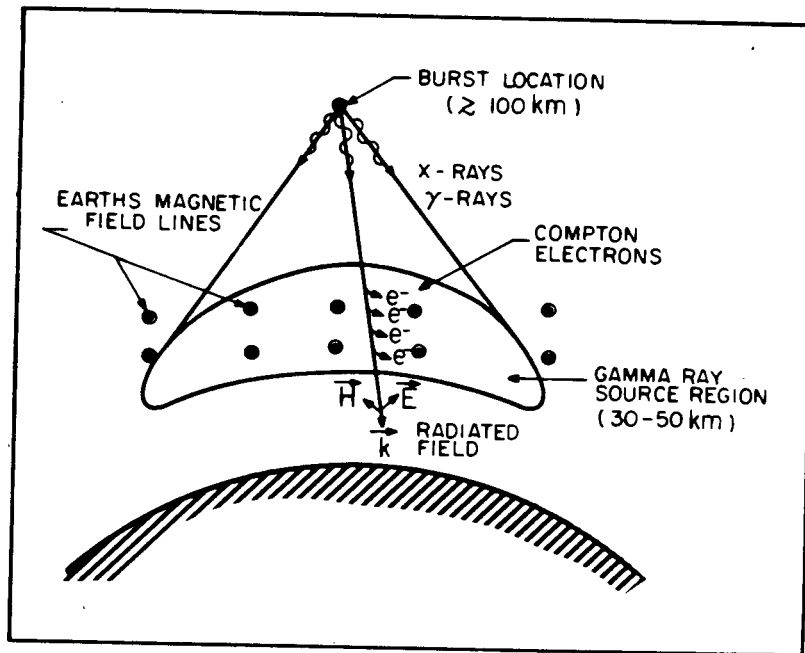
Fig. 4. Schematic representation of high-altitude EMP generation [1].

2.3 Description of Early-Time HEMP Fields

The early-time HEMP field description of interest, for civilian electric utility system assessment, is the specification of the incident electric field on the earth's surface. For any nuclear event, a complete field description requires the following quantities be specified:

- Spatial extent of the fields
- Angle of incident and polarization
- Spatial variation of the fields
- Temporal behavior

Each of the required quantities will be discussed in detail. It is noted that a definition of the incident electric field alone is adequate for representing the HEMP environment, since the corresponding incident magnetic field is directly related to the electric field through the free-space impedance.

2.3.1 Spatial Extent of The Fields

As illustrated in Figure 4, the HEMP source region is not in a localized volume of space, but extends in a pancake-like geometry under the burst point. The radiated fields observed on the ground include contributions from all parts of the source region, a fact that has some importance in determining the late-time response of the field.

For early-time in the HEMP signal, it is possible to approximately determine the extent of HEMP coverage by using a simple geometric optics argument. As shown in Figure 5a, it is possible to draw a tangent line from the burst point to the earth, thereby defining the extent of coverage of the HEMP. The lower frequency (late-time) components of the fields are able to diffract around the earth and enter the "shadow" region thereby contributing to the later response. Generally, these fields are much smaller in magnitude than those in the directly illuminated region.

Figure 5b shows the spatial extent of the HEMP fields in relation to the continental United States for several different heights of burst (HOB).

2.3.2 Angle of Incidence and Polarization

As with the determination of the spatial extent of the HEMP, geometrical considerations can be used to infer the approximate angle of incidence and the polarization of the incident field. Figure 6 shows a burst point at a height h above the earth's surface and described by the polar angles θ_b and ϕ_b. Similarly, an observation point on the earth's surface is given by θ_o and ϕ_o. The line of sight from the observation point to the burst point defines the direction of incidence of the EMP. Given the coordinate system of Figure 6, the x,y,z coordinates of the observation point can be expressed as:

$$x_o = a \sin \theta_o \cos \phi_o \tag{1}$$

$$y_o = a \sin \theta_o \sin \phi_o \tag{2}$$

$$z_o = a \cos \theta_o \tag{3}$$

where a is the earth's radius. The corresponding coordinates for the burst point are:

$$x_b = (a+h) \sin \theta_b \cos \phi_b \tag{4}$$

$$y_b = (a+h) \sin \theta_b \sin \phi_b \tag{5}$$

$$z_b = (a+h) \cos \theta_b \tag{6}$$
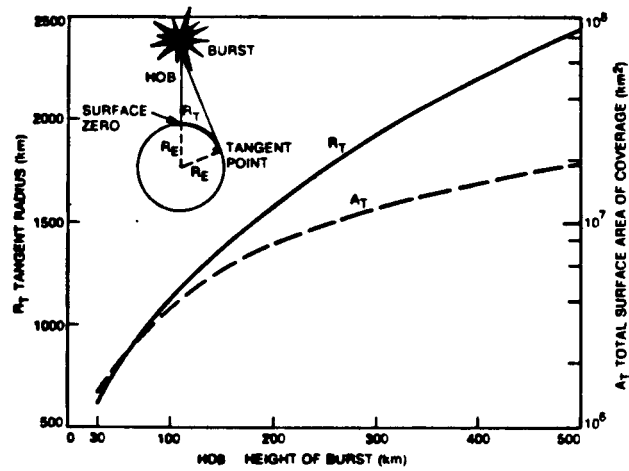
a) Tangential coverage distance (R$_T$) and coverage area (A$_T$) for burst height.
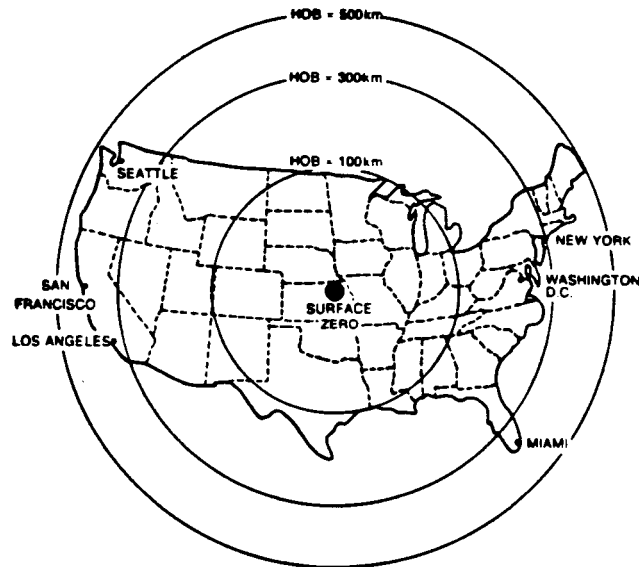
b) Overlay of HEMP coverage for 3 burst heights.

Fig. 5. Geometrical coverage of HEMP fields [5].
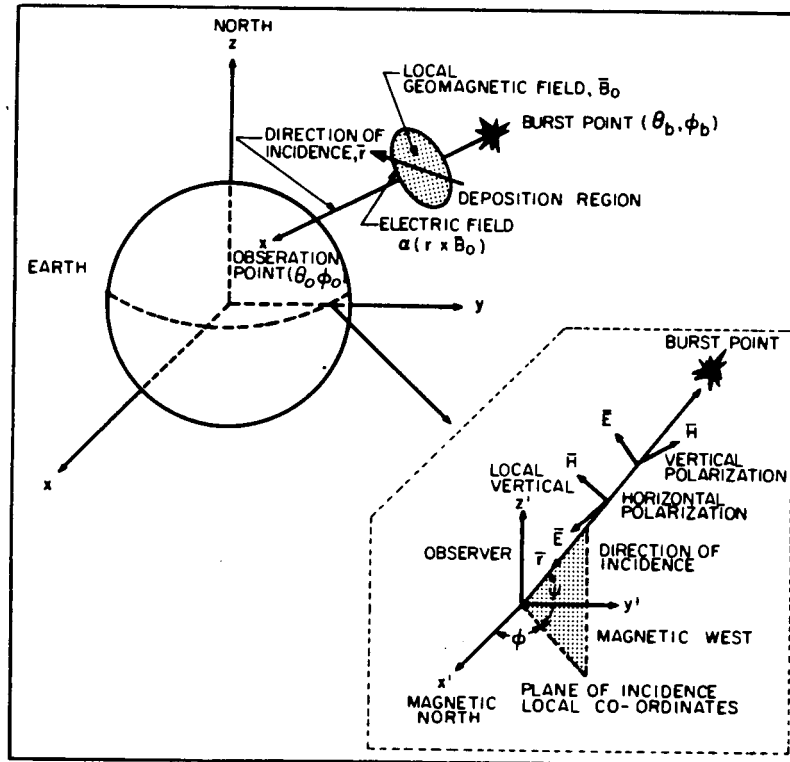
Fig. 6. Geometry of burst and EMP observation point.

This permits the vector $\bar{r}$, which defines the direction of incidence, to be defined as:

$$\bar{r} = (x_o - x_b)\hat{x} + (y_o - y_b)\hat{y} + (z_o - z_b)\hat{z} \qquad (7)$$

Locally, on the surface of the earth, it is convenient to define another coordinate system related to the local vertical direction and the magnetic north direction. In this coordinate system, the two angles Ψ and ϕ are used to define the angles of incidence of the incoming HEMP, as indicated in Figure 6.

As discussed in the Bell Laboratories publication [5], the polarization of the radiated electric field is such that it is perpendicular to both the direction of propagation of the HEMP and the local magnetic field, of the earth in the deposition region. Mathematically, this is expressed as:

$$\hat{E} = \bar{r} \times \bar{B}_o / |\bar{r} \times \bar{B}_o| \qquad (8)$$

where the ^ symbol represents the unit vector direction.

For the continental United States the earth's magnetic field has a typical dip angle (i.e., the angle between the field and the horizon) of approximately 67 degrees [5]. Geometrical considerations indicate that for observation points due north or south of the burst point, the HEMP field is horizontally polarized. Thus, the electric field vector is parallel to the earth as it arrives at the observation point.

For observation points east or west of the burst point, the electric field can have a vertical component, and the orientation of this field can be as much as 23 degrees in the vertical direction.

For the purpose of performing coupling calculations of the HEMP fields, it is convenient to divide the incoming field into two
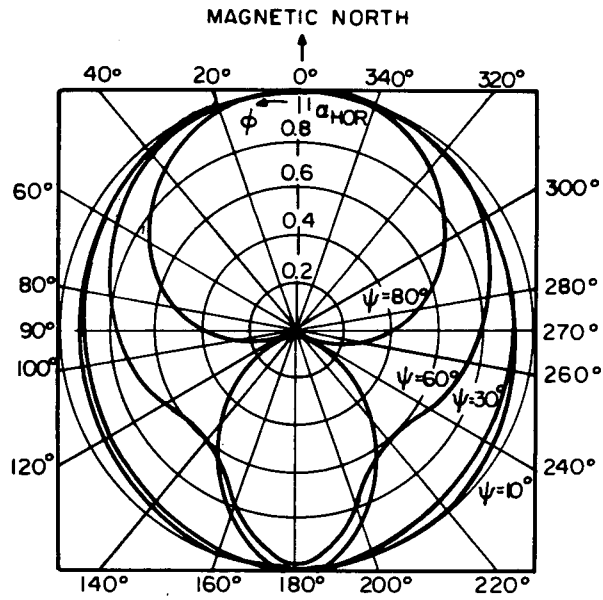
a) Horizontally polarized fraction (α_{hor})
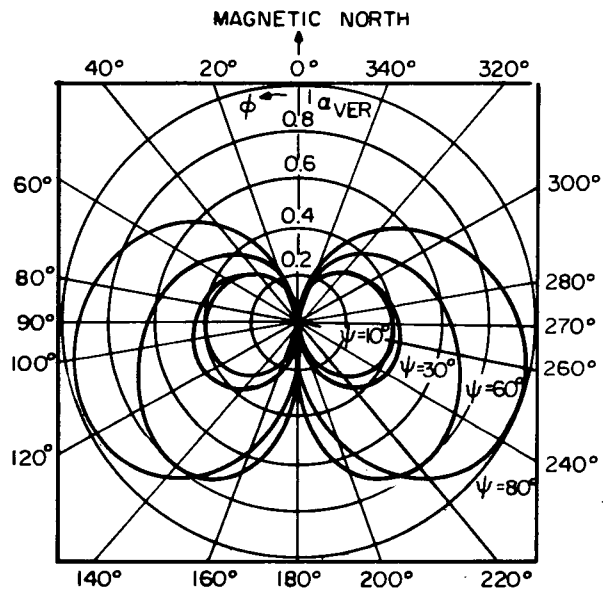
b) Vertically polarized fraction (α_{ver})

Fig. 7. Polarized fractions of incident HEMP field as a function of angles of incidence [5].

components, referred to as the horizontally polarized and the vertically polarized components. As illustrated in Figure 6, the horizontally polarized field always has its electric field parallel to the x'-y' plane, (i.e., the surface of the earth), whereas the vertically polarized field has its electric field vector in the plane of incidence. Note that a vertically polarized electric field generally has both vertical and horizontal components with respect to the earth's surface.

The fraction of the total incident field occurring as vertically or horizontally polarized components can be expressed as:

and:

$$E_V^{inc} = \alpha_{ver} \ E^{inc} \tag{9}$$

$$E_H^{inc} = \alpha_{hor} \ E^{inc} \tag{10}$$

where the coefficients α_{hor} and α_{ver} obey the relationship:

$$\alpha_{hor}^2 + \alpha_{ver}^2 = 1 \tag{11}$$

The Bell Laboratories report [5] presents plots of these polarization coefficients as a function of the angle of incidence, based on the assumed constant magnetic dip angle. These plots are reproduced in Figure 7. As may be noted, the polarization of the incident HEMP is primarily horizontal in nature, a fact that is important in determining the HEMP-induced currents in power lines as will be discussed in Section 3.

2.3.3 Spatial Distribution of The HEMP Fields

In addition to the determination of the area illuminated by HEMP, it is necessary to determine the variations of the incident field strength in this region. By referring to Figure 8a [4] it can be shown that the field on the earth is a function of position. At observation points on the ground, where the direction of incidence of the HEMP is parallel to the earth's geomagnetic field, the observed HEMP field is

seen to be small. At earth observation points where the field and the direction of incidence are perpendicular, the field is the largest. The reason for this effect is shown in Figure 8b. Neglecting the longitudinal motion of the electrons, at any point in the source region, the electrons tend to precess around the geomagnetic field lines, creating a magnetic dipole moment. This dipole produces both electric and magnetic fields which radiate away with particular spatial features. Specifically, the electric field is in the ϕ_1 direction in the figure, and the magnetic field is in the θ_1 direction. Furthermore, this type of radiation has a null in the $\theta_1 = 0^\circ$ direction and a maximum in the $\theta_1 = 90^\circ$ direction. Applying this model to the various observation regions on the earth shown in Figure 8a shows the reason for the maximum and minimum field regions.

Figure 9 presents a contour map of electric field magnitude on the earth's surface. A commonly used value for the peak magnitude, E_{max} of the radiated early-time HEMP field is about 50 kV/m, which occurs in the region of maximum field slightly south of the burst point. At other points on the earth's surface, the peak amplitude of the radiated field will be less, according to the data in Figure 9. Clearly, the details of this field variation will depend on the magnetic field and weapon characteristics in any particular case. However, in the absence of source-specific data, Figure 9 could form the basis for a detailed specification of the early-time HEMP environment for power system assessment.

2.3.4 Temporal Behavior of The Fields

The final important feature of the radiated HEMP field is the shape of the waveform. The waveform varies as a function of position on the earth [5]. Directly under the burst (point 1), the HEMP has a 10 to 90 percent rise time on the order of 5 ns, a time that is commensurate with the rise time of the prompt gamma pulse. The fall time corresponding to a half the peak value is on the order of 20 ns. Away from this region, the rise and fall times tend to be greater. For example, in the region
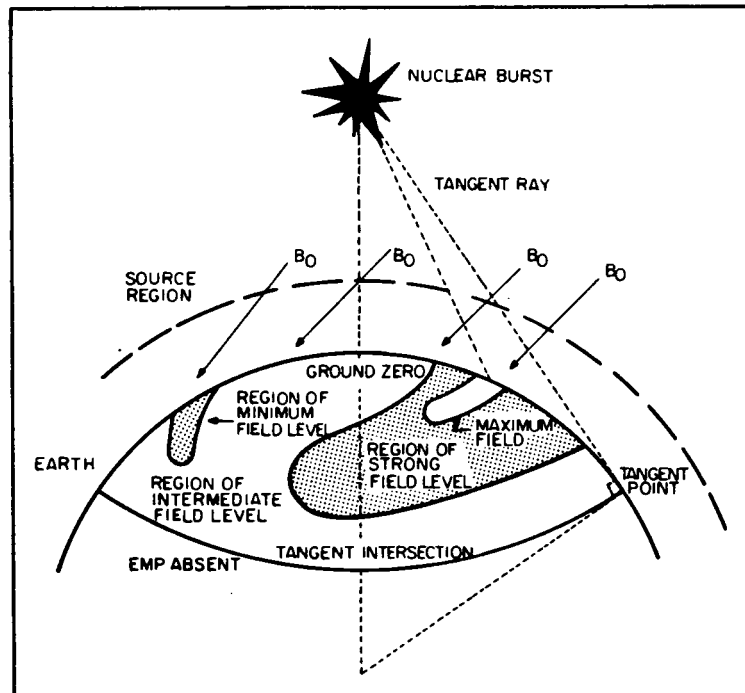
a) Variations of HEMP signal strength
   on earth's surface [4].
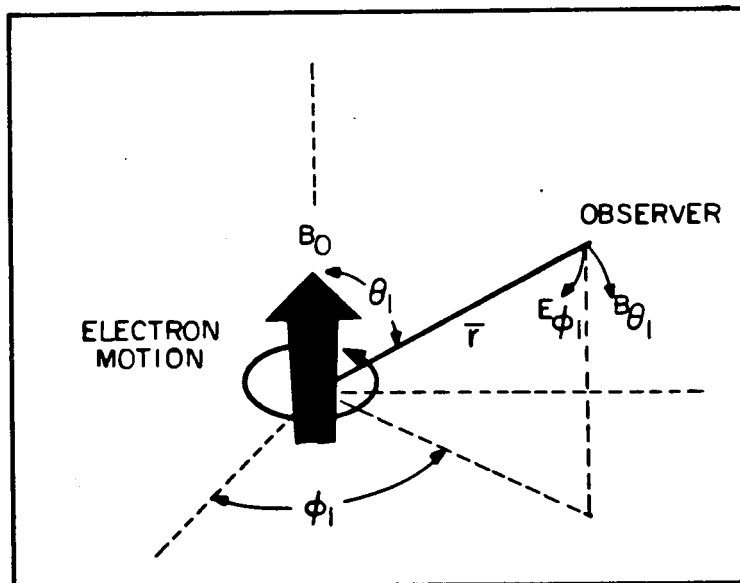
b) Geometry for orbiting electron.

Fig. 8. Spatial variations of HEMP fields.
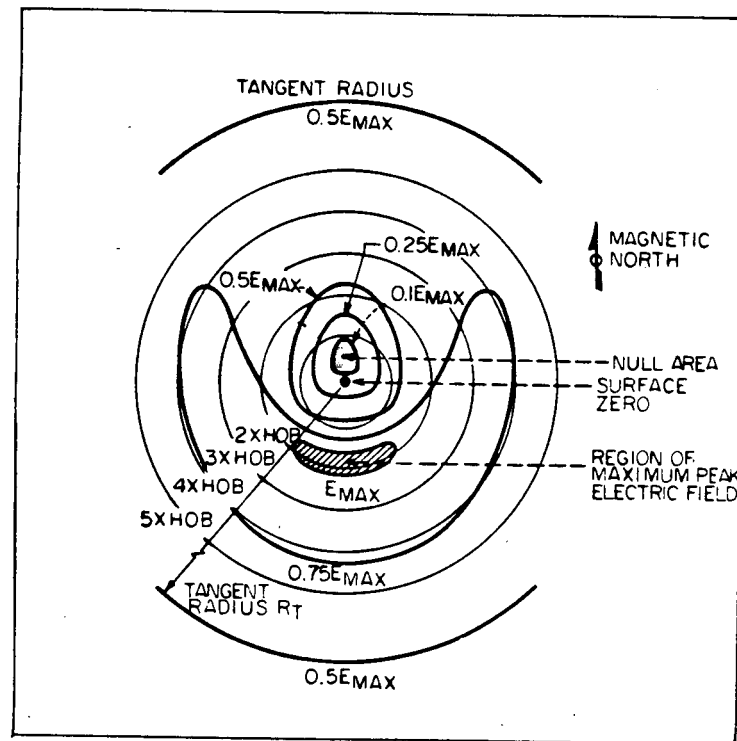
Fig. 9. Variations in high-altitude EMP peak electric field on surface of continental United States [5].

of the maximum field strength (point 2), due south of the burst, the field has a rise time of slightly under 10 ns and a fall time of about 50 ns [5]. On the horizon (point 3), near the tangential distance, the pulse has broadened considerably, having a rise time somewhat longer than 10 ns and a fall time on the order of 200 ns [5]. The waveforms can be represented by a double exponential expression as:

$$f(t) = \Gamma(e^{-\alpha t} - e^{-\beta t}) \hspace{3cm} (12)$$

In Equation (12), the α^{-1} and β^{-1} terms are the applicable time constants and the Γ is a normalizing factor calculated so that the peak value of f(t) is unity. The appropriate values for the above waveforms are presented in Table 1.

Table 1

WAVEFORM PARAMETERS FOR EARLY-TIME HEMP TEMPORAL BEHAVIOR

Point	Location	Γ	$\alpha(s^{-1})$	$\beta(s^{-1})$
1	Under burst	1.348	3.46×10^7	4.40×10^8
2	E_{max}	1.259	1.38×10^7	2.44×10^8
3	Horizon	1.031	3.46×10^6	2.00×10^8

Figure 10 presents the f(t) time domain waveform of the electric field at each point and the corresponding frequency spectra.

2.4 Description of Intermediate-Time HEMP Fields

In contrast to the unclassified body of knowledge developed to characterize the early-time HEMP fields, little unclassified data is available to describe the intermediate-time HEMP signal. All of the unclassified data supplied to the authors by ORNL consists of the following:
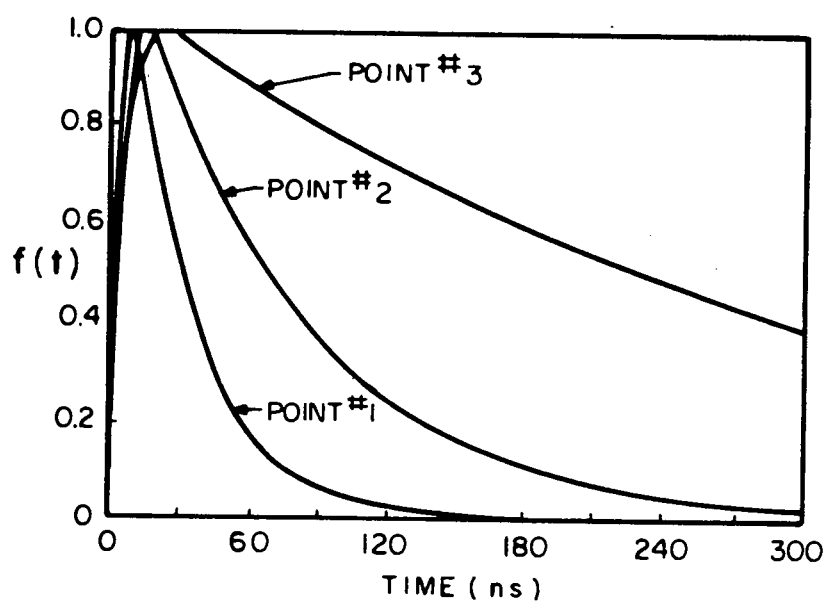
a) Time-dependent functions
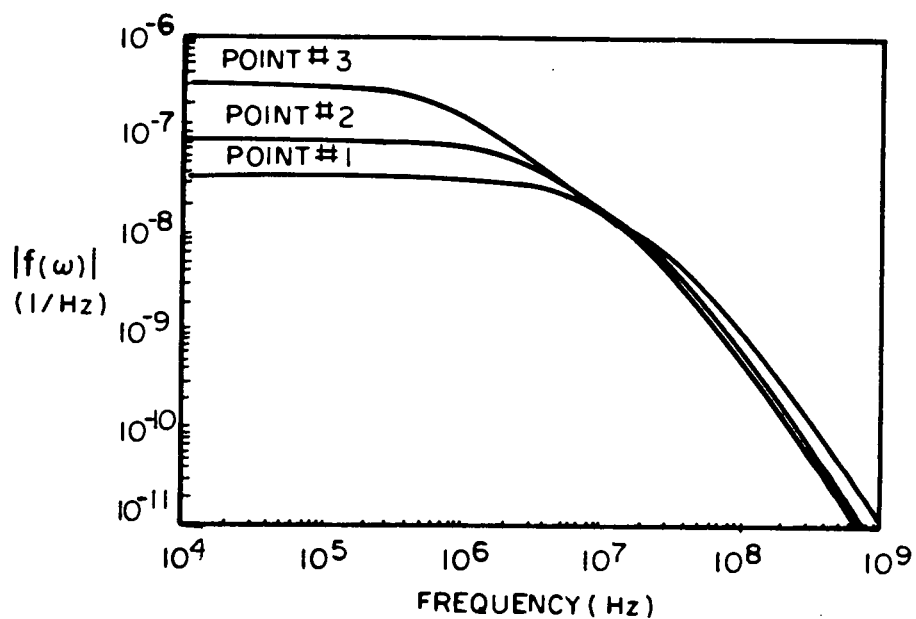
b) Frequency spectra

Fig. 10. Time-dependent functions (a) and resulting frequency domain spectra (b) for HEMP waveforms at various points.

- An average peak magnitude of 100 volts/meter
- Frequency spectra from 10^1 Hz to 10^5 Hz
- Signal duration from 10^{-6} seconds to 1.0 seconds

In the absence of any other technical guidance, a single exponential waveform has been chosen to represent the incident electric field associated with intermediate-time HEMP. The temporal behavior of this waveform is expressed as:

$$E_{inc}(t) = E_1 e^{-\gamma t} \tag{13}$$

where E_1 = 100 volts/meter and $\gamma = 10^3 \ s^{-1}$.

Figure 11 presents this transient waveform. It must be kept in mind that this waveform occurs in conjunction with the early-time HEMP signal. If the early-time HEMP component were plotted on Figure 11, it would appear almost like a delta function occurring at t=0.

Details concerning the spatial extent of the fields, angles of incidence and polarization are unknown. For the purpose of this document, these details are assumed to be the same as early-time HEMP fields.

2.5 HEMP Environmental Specification

The HEMP radiated field has been shown to contain spatially dependent properties within an extensive coverage pattern of the earth's surface. Such a distributed EMP environment and its interaction with spatially local military systems, such as a hardened communication facility or missile silo, have been previously considered by a number of investigating organizations. Various reports [4,6,7] illustrate many of the techniques which have been developed for estimating HEMP response and system survivability. In performing an assessment on a spatially local system to HEMP, a commonly used approach is to define a "bounding case" HEMP threat environment, apply it to the system of interest and assess system response. The rationale for the development of this
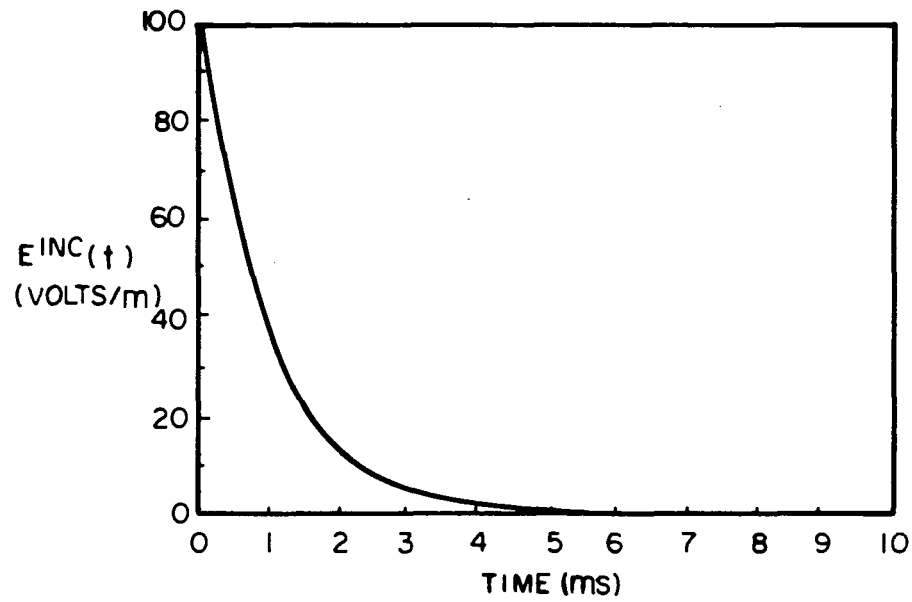
Fig. 11.   Intermediate-time HEMP waveform.

threat environment incorporates the fact that such systems may be located in a region of maximum excitation. Therefore, it is necessary to consider the worst possible excitation in order to insure system survivability.

An unclassified example of a threat HEMP incident field is presented in the Bell publication [5]. For the purpose of this document it is denoted as the "Bell" waveform. The incident electric field is assumed to have a peak magnitude of 50 kV/m. The waveform, defined as a double exponential as expressed in Equation (12), incorporates a fast rise time and a long fall time. An alternate threat waveform, denoted in this document as the "DoD" waveform, has been suggested to the authors by ORNL [8] as more applicable to early-time HEMP illumination. The waveform parameters appropriate for the "Bell" and "DoD" waveforms are shown in Table 2. The time domain waveforms and corresponding frequency spectra are plotted as Figure 12.

Table 2

WAVEFORM PARAMETERS FOR THREAT
HEMP ELECTRIC FIELDS

Waveform	Γ	$\alpha(s^{-1})$	$\beta(s^{-1})$
Bell	1.050	4.0×10^6	4.76×10^8
DoD	1.285	3.0×10^7	4.76×10^8

The complete threat HEMP environmental specifications is obtained by the determination of the polarization, angle of incidence and system orientation such that there is maximum interaction between the HEMP environment and the system under assessment. This approach develops a "bounding case" scenario. Often, such excitation is not physically realizable, but it does serve to place an upper bound on possible system responses and reflects a conservative approach to the assessment of an intentionally hardened system.
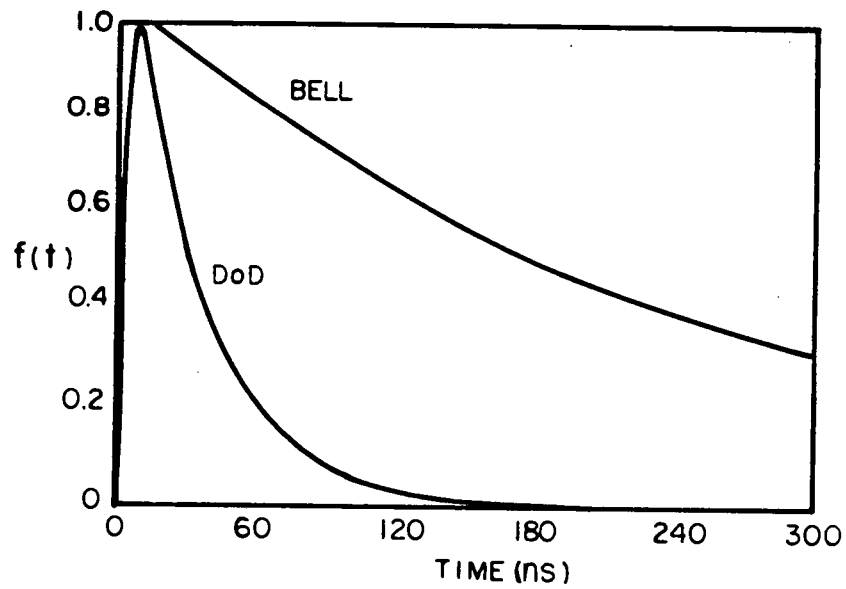
a) Time-dependent functions
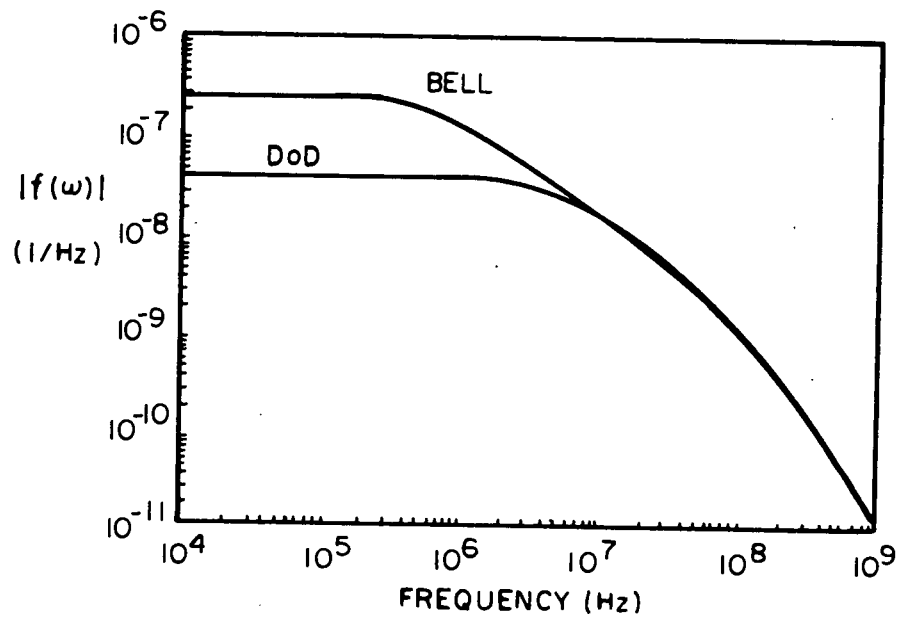
b) Frequency spectra

Fig. 12. Time-dependent functions (a) and resulting frequency spectra (b) for "Bell" and "DoD" waveforms.

The above approach to HEMP environmental specification, developed to provide a uniform "bounding case" interaction with a spatially small, hardened system could be invoked in the assessment of the civilian electric utility network. However, the significant geographic size of the power system and the nature of system network properties evaluated under such an environmental specification may provide unrealistic estimates of system excitation and response.

In lieu of the use of the above threat environmental specification, the authors recommend that the spatial variation inherent in HEMP illumination be maintained in the early-time HEMP environmental specification for power system assessment. The discussion of early-time HEMP field behavior in the previous subsections suggests techniques to attain such a specification. For a specified, high-altitude burst location, a more realistic estimate can be developed for any spatially local observation point on the earth's surface. At any such point of interest, the details of the incident, early-time HEMP signal, such as the waveform (amplitude and waveshape) polarization and angle(s) of incidence are retained. For the purpose of this document, the incorporation of intermediate-time HEMP effects can be linked to the early-time HEMP characterization by the assumptions discussed in Subsection 2.4.

From the initial specification of the geographic location and altitude of the nuclear detonation, the surface spatial extent of direct illumination can be determined by the geometrical techniques shown in Figure 5. For any observation point on the earth's surface, a knowledge of the local polarization of the incident field (Equation 8) and the angle of incidence (Figure 6) can be determined. The details of the local temporal waveform can be obtained by first expressing the HEMP incident field in the form:

$$E_{inc} = E_0 \Gamma(e^{-\alpha t} - e^{-\beta t}) + E_1 e^{-\gamma t} \tag{14}$$

where E_o is determined from a contour plot similar to Figure 9 plus the specification of a maximum value of E_o expressed in volts per meter. For the purpose of this document, E_1 is defined as 100 volts per meter and γ equals 10^3 s^{-1}. The appropriate values for Γ, α and β are determined for the local observation point of interest.

2.6 Summary

This section has discussed an overview of the physical generation, propagation and spatially varying behavior of incident early-time HEMP electric fields produced by high-altitude nuclear detonation. A technique to incorporate the signal known as intermediate-time HEMP has been developed from a minimum set of available, unclassified data.

The recommended environmental specification for early-time HEMP assessment retains the spatial variance of incident waveform, polarization and angle of incidence as a function of position on the earth's surface for a specified burst location. These details are retained in order to simulate a spatially changing environment over a spatially large and unhardened system.

The approach to specification of the intermediate-time HEMP incident field is a preliminary attempt to account for such stimulus based on unclassified data. It is strongly recommended that the EMP community review such an approach and that the sensitivity of the civilian electric utility system to intermediate-time environments be investigated in subsequent phases of the ORNL research program.

3. HEMP INTERACTION WITH ELECTRICAL POWER SYSTEMS

3.1 Introduction

A practical power system is a very complex collection of massive, electrically robust components such as towers, transmission lines, lightning arresters and the like, as well as electrically fragile components such as the integrated circuitry found in modern communications and control subsystems which form part of the overall power system. In order to perform an assessment of the effects of EMP on the power system, it is first necessary to obtain a functional description of the system. After that is done, an electrical description (often referred to as a topological description) may be developed, and this may be used along with the EMP environments described in Section 2 to estimate the responses at points of interest within the system.

Part of this calculational process involves determining how the incident EMP fields "couple" to important parts of the power system. This involves determining the response (voltage or current, for example) of electrical conductors, such as antennas or power lines, which are directly excited by the incident EMP. This response depends strongly on the local geometry of the conductor, as well as on the characteristics of the incident field.

Such a response is generally able to "propagate" from one point to another in the system, so that the effects of an EMP striking one point of the power system can be observed at an entirely different point. Usually, this propagation of EMP energy occurs on guided wave structures, such as transmission lines, coaxial lines, etc., but at times, direct field propagation of energy is possible.

Finally, the EMP energy is able to "penetrate" into shielded portions of the system. For example, in a communications facility, there is usually a shielded enclosure protecting equipment from unwanted radio frequency interference (RFI) which serves as a barrier to the unwanted EMP energy that might cause internal damage to the equipment.

Such barriers are not perfect, and energy can penetrate into the barrier at holes in the shield. Similarly, the process of an EMP-induced voltage surge coupling to a transmission line and then propagating to the input terminals of a transformer can be thought of as then penetrating into the interior regions of the transformer and possibly causing damage.

This overall process involving coupling, propagation and penetration, is referred to as EMP "interaction" with the system. A number of standard calculational models have been developed by investigators in the EMP community and these may be directly applied to the power system assessment process, and details of these will be presented later in this section.

In choosing the various calculational models for performing an assessment, it is necessary to define the "observable" quantities which are to be determined. For example, the voltage induced across a transformer winding is one important quantity to know, since it can be directly related to damage within the insulation. However, the electromagnetic field penetrating into a window in an otherwise shielded enclosure might induce a voltage in a critical control circuit, causing upset or failure. Thus, this quantity might play an important role in the system assessment process.

As discussed in this section, it is important to carefully define the observable quantity. Generally, these are voltages, currents, electric fields or magnetic fields, and details of their time histories (rise and fall times and peak amplitudes) which are useful in performing an assessment of the system. In addition, the derived quantity of the total energy delivered to a load is commonly used.

In examining a typical power system, the most striking feature is the transmission and distribution line network linking the generation and load facilities. Obviously, the EMP interaction with this network of conductors forms an important excitation mechanism for the system. Detailed models describing the EMP coupling to such lines and the EMP propagation along lines are needed for an assessment.

Various types of antenna structures are also found in power systems. Although not used for the direct transmission of electrical energy, these components are typically found in the command and control subsystems and perform a critical function in maintaining the integrity of the power system. Such antennas occur in several forms, such as wire structures for the HF region, blade antennas in the UHF regime, and dish and waveguide antennas for microwave frequencies. In addition, such antennas have supporting towers and equipment which themselves might interact with an incident EMP. Because antennas are designed to radiate electromagnetic energy efficiently in a particular band of frequencies, reciprocity dictates that they will be equally good receptors of energy. Thus, antennas designed to operate at frequencies in which the EMP spectrum is large will generally be highly excited. Detailed electrical models have been developed for predicting the EMP interaction with antennas, and these also will be discussed in this section.

Models are also needed for predicting the EMP penetration through apertures in shielded enclosures. Apertures occur in the form of doors and windows in shielded facilities, cracks and seams in metallic covers, and in any other opening in a shield. This form of EMP penetration is important to consider for highly shielded systems. For a normal building, however, where no real attempt has been made to exclude EM interference from the interior, it is difficult to define a "shield" and the associated apertures. Such may be the case for many power system facilities.

A final phenomenon affecting the EMP penetration into a facility is that of field diffusion through imperfect conductors. As in the case of apertures, this effect is only important for highly shielded facilities.

In the following subsections, details of the EMP coupling models for lines, antennas, apertures, and diffusion are discussed, with special emphasis placed on those models that are adaptable for incorporation into a computer assessment code.

3.2 Introduction to Transmission Line Modeling

In electrical power systems, long runs of conductors above a ground plane are frequently encountered. These occur in the transmission and distribution lines connecting load, generation and distribution stations, as well as in the switchyard where there are sections of electrical buses interconnecting equipment. In addition, there are lengths of electrical cables found in communications and control subsystems which take the form of a conducting line over a ground plane. Buried conductors are also encountered.

An incident EMP impinging on such conductors can induce substantial voltage and current traveling waves on the line, and these can propagate to other points within the system. By virtue of its relatively simple geometry, it is possible to easily compute the interaction of an incident EMP with these lines, thereby allowing the possibility of estimating the EMP-induced response of excited power system components.

In this subsection, several different analysis approaches for treating the case of EMP-excited above-ground conductors are outlined. One particular approach involves the use of quasi-TEM transmission line theory to predict the behavior of induced currents and voltages, and the fundamentals of this approach are discussed in detail in Section 3.2.1. Furthermore, the extension of this theory to the case of EMP excitation of buried conductors is also discussed. Section 3.2.2 then presents several examples of the use of TEM models for power system applications.

The basic geometry of the problem to be treated in this section is illustrated in Fig. 13, which shows a conductor of radius a located at a height h over a conducting earth. The earth is assumed to have a conductivity of σ_g mhos/meter, and a relative dielectric constant of ε_r. For illustrative purposes, only a single conductor line has been depicted here. More generally, we might be interested in the response of a multiconductor line having a similar configuration above the ground, and this will be discussed later in Section 3.2.1.
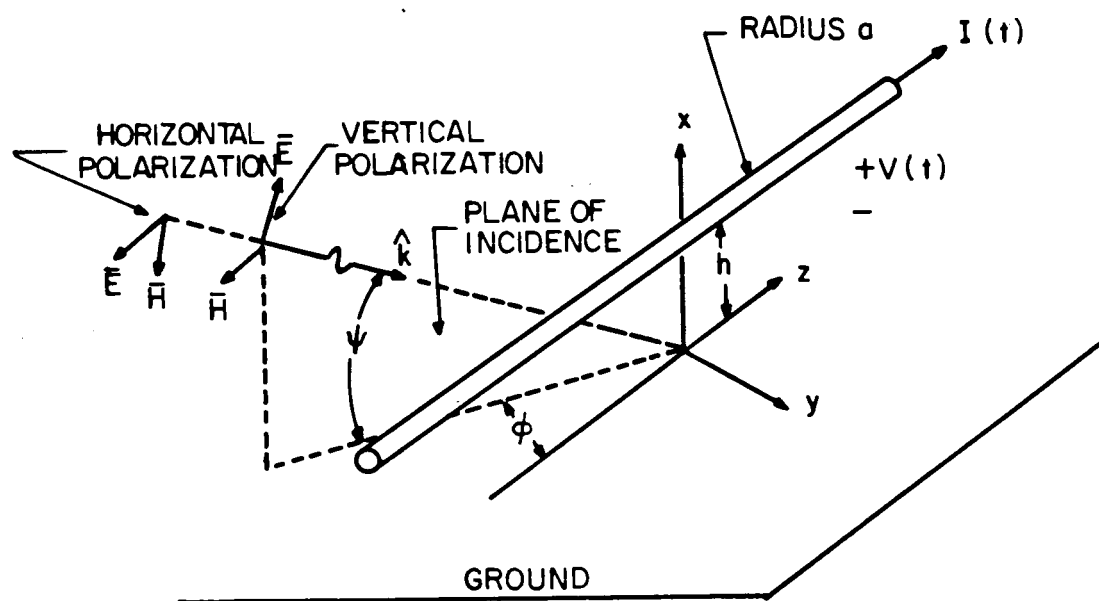
Fig. 13. Above-ground conducting line excited
by HEMP.

The line is assumed to be illuminated by an incident transient plane wave arriving with an elevation angle ψ and with an azimuthal angle ϕ with respect to the line's direction. For convenience, it is desirable to decompose the actual polarization of the incident electric field vector into two independent polarizations, one vertical and the other horizontal as discussed in Section 2. The vertically polarized component is an incident field having its electric field vector contained in the plane of incidence (i.e., the plane which contains the propagation (k) vector of the incident field and is perpendicular to the ground). The horizontally polarized incident field is that having its electric field vector always parallel to the earth, regardless of the incidence angles. Figure 13 shows these two polarization types.

Of prime concern in the analysis of the EMP interaction with this class of electrical structures is the determination of the time history of the induced voltage (or charge) and current on the conductor. Perhaps the most fundamental and rigorous analysis is through the use of frequency domain electromagnetic scattering theory [9], which has the potential of providing accurate line responses. Such an approach, however, is rather complex and can be time consuming. An alternate approach using time dependent scattering theory is also possible [10], but its solution is efficient only for relatively early times. Moreover, the inclusion of lossy ground effects is difficult in such direct time domain analyses.

A third calculational approach for such problems is also available in the form of quasi-TEM transmission line theory. This approach has been used by a number of investigators [11,12,13] and permits a rapid solution for the induced line responses. Although there are errors found in the responses due to various simplifications introduced in the analysis, studies [1,13,14] indicate that for EMP responses, this approach is adequate. Later, in Section 3.2.2 this point will be illustrated with a comparison of some calculated TEM response data with similar data obtained from a scattering calculation.

The basic idea behind the analysis of lines using the TEM approach is to assume that the electromagnetic energy induced by the EMP striking the line propagates along the line in the form of a transverse electromagnetic field which is closely bound to the conductor. These fields can be alternately described in terms of the voltage and current on the line, and these are usually viewed as being the fundamental quantities of interest.

The determination of the behavior of the voltage and current can be accomplished by considering the line to consist of a large number of ladder-type L-C circuits, and then perform a circuit analysis. Such an approach, known as lumped parameter modeling (LPM) is possible when the length of line is sufficiently small that only a limited number of L and C elements are needed. For an electrically long line, however, such an analysis approach is difficult.

An alternate approach, and one which is discussed in more detail in the next subsection, involves the analytical solution of the voltage and current behavior on the line, regardless of its length. This approach, then, permits the consideration of much longer lines, and is one of the chosen approaches for many of the power system assessment calculations.

However, one difficulty with this calculational approach is including the effects of corona, flash-over on lines, and other nonlinear behavior of components, since it is based on a frequency domain analysis. Because the concept of superposition of responses is not possible in systems containing nonlinearities, it is necessary to conduct such analysis directly in the time domain. Details of this alternate analysis using the TEM concepts will also be outlined in the next subsection.

Due to the complexity and diversity of the EMP interaction problems with long runs of conductors, it is not possible to use just one type of analysis procedure. In performing an analysis, therefore, it is necessary to have several different calculational models available for use, and know the attributes and limitation of each. In the following subsection, several different calculational models are summarized, and their use in performing an EMP assessment on a power system indicated.

3.2.1 Fundamentals of Quasi-TEM Analysis

As mentioned in the previous subsection, it is desired to develop models useful for predicting the response of electrical equipment connected to long lengths of electrical conductors excited by EMP. Ultimately, what is desired is a knowledge of the voltage across the terminals of a piece of equipment and the current flowing into the equipment, as illustrated in Fig. 14a. These responses are a function not only of the EMP-excited line, but also on the electrical characteristics of the load equipment.

The description of the EMP response of the isolated line without the load present is facilitated through the use of a Thevenin equivalent circuit, as illustrated in Fig. 14b. There, the line and the incident EMP is replaced by an equivalent open circuit voltage source and an input impedance. These load-independent parameters may then be combined with a knowledge of the equipment load impedance to compute the actual response.

Thus, in most of the development of the calculational models for EMP interaction with long lines, it is desired to reduce the problem to that of specifying the equivalent circuit. Note also that the dual Norton equivalent circuit involving a short circuit current source and an input admittance could be specified, as shown in Fig. 14c.

It is important that the representation of the behavior of the EMP-excited line through the use of an equivalent circuit is possible in both the time and frequency domain. The frequency domain representation is a bit simpler, with the input impedance and open circuit voltage being complex-valued functions of frequency. In the time domain, both of these quantities are real-valued functions of time with the time domain input "impedance" really being the time dependent voltage across the line when it is driven by an impulsive voltage source (a delta function) across its terminals.

In developing EMP coupling models for transmission line-like conductors, the use of a frequency domain analysis is usually the most
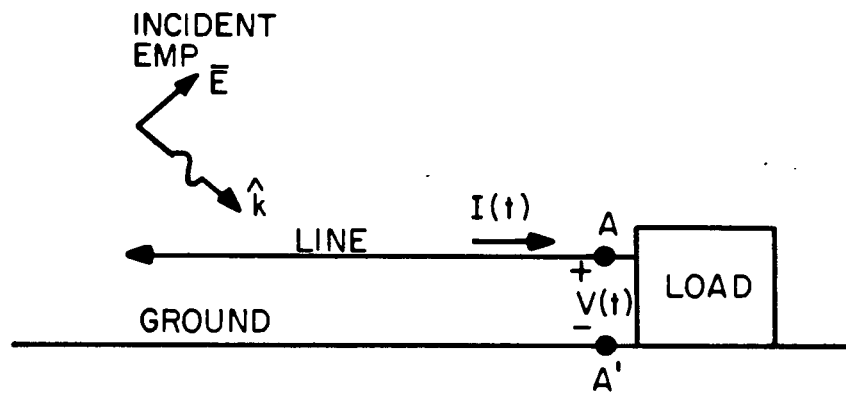
a) Simplified electrical configuration
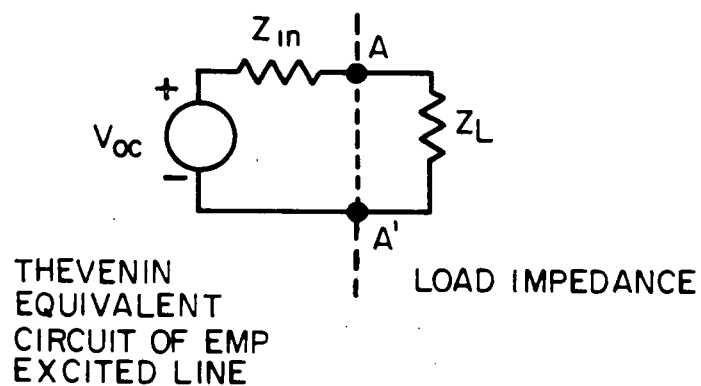
b) Thevenin equivalent circuit
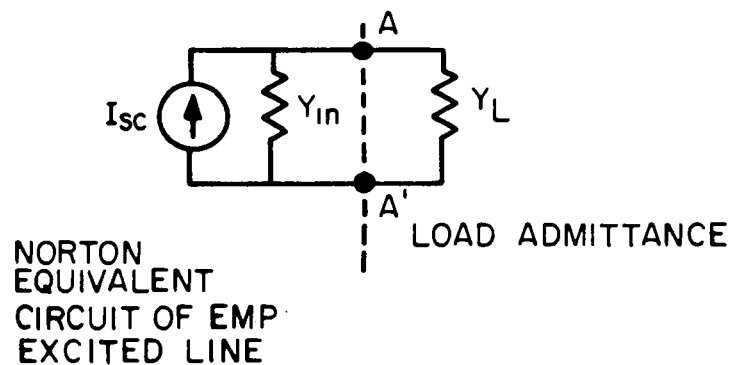
c) Norton equivalent circuit

Fig. 14. Analysis of EMP-excited lines using equivalent circuit.

straight forward. As an example, consider the case of a semi-infinite, single wire line located above a conducting ground.

3.2.1.1 Transmission-Line Frequency Domain Analysis - Single Line Above Ground

The transmission-line (TEM propagation mode only) calculation method used for this analysis assumes that the surge (characteristic) impedance of conductors above earth remains constant at the value defined by the series impedance and shunt reactance. This implies the surge impedance of the conductor does not change from early time (time before which the presence of ground through reflection is fully established), typically between time zero and $(2h \sin \psi)/c$ and late time, where the effects of ground are fully accounted for. The response in early time becomes questionable if the height of the conductor is greater than the longest wave length of the field (or said in other words, the round trip time from the conductor to ground exceeds the rise time of the field by two or more times). However, comparisons of early time response results obtained by transmission-line method to those calculations obtained from more rigorous "exact" methods were very favorable, as discussed in Section 3.2.2.1. The late time response obtained by the transmission line response is accurate, by virtue of the assumptions made.

The EMP induced response on an above-ground conductor depends on how the incident electromagnetic field couples to the conductor and on how the conductor propagates this surge. To illustrate this, consider, as in Figure 13, a single conductor of radius a and electrical conductivity σ_ω located over a conducting earth at a height h. The earth is assumed to be homogeneous with a conductivity σ_g and dielectric constant $\varepsilon_g = \varepsilon_r \varepsilon_o$.

When an incident electromagnetic field strikes this conductor, it induces both voltage and current waves which tend to propagate down the conductor. In reality, the behavior of these currents may be described accurately through the use of antenna (scattering) theory. Through the

use of approximate transmission-line (or TEM propagation) analysis, we can define a set of forward and reverse propagating voltage and current waves on a conductor of the form:

$$V(z) = V_1 e^{-\gamma z} + V_2 e^{+\gamma z} \qquad (15)$$

$$I(z) = I_1 e^{-\gamma z} + I_2 e^{+\gamma z} \qquad (16)$$

where the (+) sign refers to the forward propagating set of waves, and the (-) refers to those in the negative direction. The term γ is the propagation constant, which generally consists of an imaginary component describing the wave-like propagation on the line, and a real part which is positive and describes the attenuation along the conductor. The amplitudes of the voltage and current waves are related through the characteristic impedance of the conductor, Z_0 as:

$$I_1 = V_1/Z_0 \qquad (17)$$

$$I_2 = -V_2/Z_0 . \qquad (18)$$

Under the assumptions of TEM mode propagation, the equivalent circuit shown in Fig. 15 may be used to determine the propagation constant and the characteristic impedance on the conductor. Once these quantities are known, the conductor response may be determined.

As discussed in Ref. 13 the inductance in the equivalent per-unit-length model of the conductor in Fig. 15 is given by the relation:

$$L' = \frac{\mu_0}{2\pi} \cosh^{-1} \frac{h}{a} \simeq \frac{\mu_0}{2\pi} \ln \frac{2h}{a} = 0.2 \ln \frac{2h}{a} \ \mu H/_m \qquad (19)$$

and is that which would be expected if both the ground and the conductor were perfectly conducting. The per-unit-length capacitance of the conductor is given by:

$$C' = \frac{2\pi\varepsilon_0}{\cosh^{-1}(h/a)} \simeq \frac{2\pi\varepsilon_0}{\ln(2h/a)} = \frac{10^{-3}}{18\ln(2h/a)} \frac{\mu F}{m} \qquad (20)$$

and likewise it is that for the conductor over a perfectly conducting earth.

The term Z_g represents the effective complex impedance of the earth in the propagation and is given by:

$$Z_g \simeq - \frac{j\gamma_g}{4\pi h\sigma_g} \frac{H_0^{(1)}(j\gamma_g 2h)}{H_1^{(1)}(j\gamma_g 2h)} \qquad (21)$$

where the parameter γ_g is the plane wave propagation constant in the earth and is expressed as:

$$\gamma_g = \sqrt{j\omega\mu_0(\sigma_g + j\omega\varepsilon_g)} \qquad (22)$$

$H_0^{(1)}$ and $H_1^{(1)}$ are the Hankel functions of the first kind and orders 0 and 1 respectively.

The additional per-unit-length impedance term Z_i represents the effect of the internal impedance of the lossy conductor, and is:

$$Z_i = \frac{j\gamma_\omega}{2\pi a \sigma_\omega} \frac{J_0(j\gamma_\omega a)}{J_1(j\gamma_\omega a)} \qquad (23)$$

where the term γ_ω is the wave propagation constant in the wire material and has the same form as Eq. 22, but with the wire conductivity σ_ω used instead of the earth conductivity. J_0 and J_1 are the Bessel functions.

The final additional term is Y_g, which is a per-unit-length suscep-
tance accounting for the admittance effects of the soil currents. This
is estimated in [13] as:

$$Y_g \simeq \frac{\gamma_g^2}{Z_g} \qquad (24)$$

Once these quantities are defined, it is possible to define total
per-unit-length impedance and admittance values of the conductor as:

$$Z' = j\omega L' + Z_g + Z_i \qquad (25)$$

and

$$Y' = \left[Y_g^{-1} + \frac{1}{j\omega C'} \right]^{-1} \qquad (26)$$

The propagation constant for the TEM voltages and currents on the
conductor is then defined as:

$$\gamma = \sqrt{Z'Y'} \qquad (27)$$

and the conductor characteristic impedance is given by:

$$Z_o = \sqrt{\frac{Z'}{Y'}} \qquad (28)$$

Determination of Conductor Response

Once the propagation characteristics of the conductor are
determined, it is possible to develop expressions for the field-induced
surges on the conductor.

As a starting point for the analysis, consider the conductor shown
in Fig. 16a. A section of conductor of length L is terminated at z=0
with an impedance Z_L. At z=ξ a lumped voltage source V_s is used to
excite the conductor. Using the transmission-line expressions it is
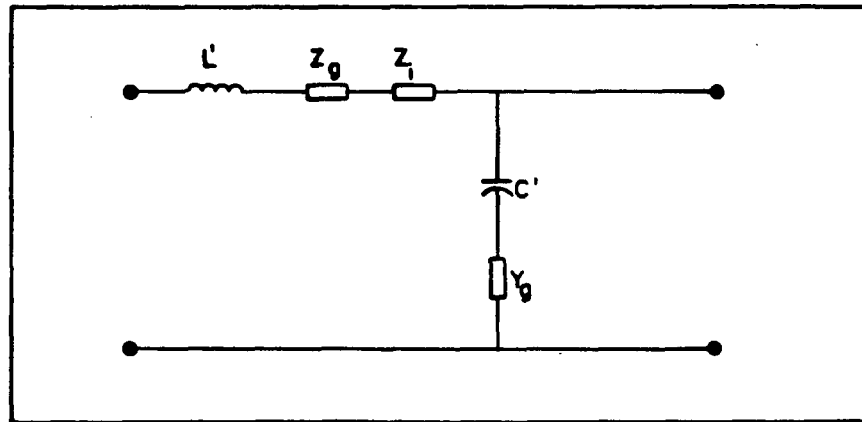
Fig. 15. Differential section of line over lossy ground
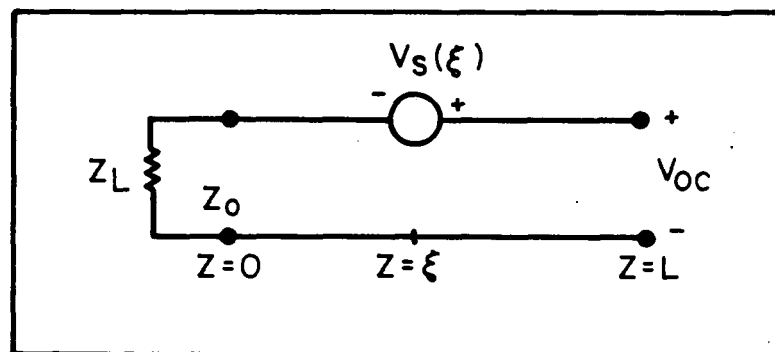
Fig. 16a. Lumped source excitation.
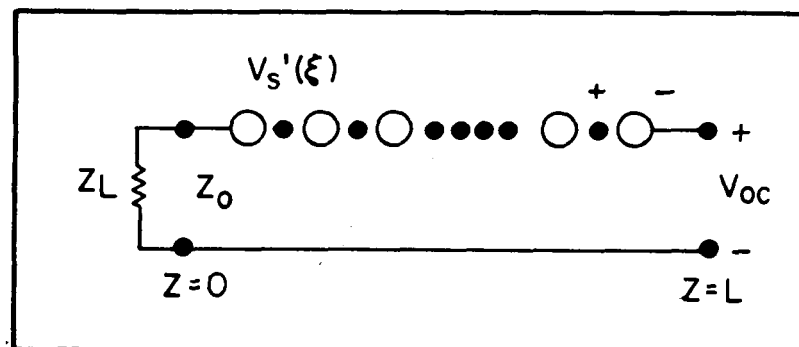
Fig. 16b. Distributed source excitation.

possible to write an expression for the open-circuit voltage at the z=L end of the conductor as:

$$V_{oc} = \frac{e^{-\gamma L}}{1 - \rho e^{-2\gamma L}} \; V_s(\xi) \left[e^{\gamma \xi} - \rho e^{-\gamma \xi} \right] \qquad (29)$$

where the term ρ is a reflection coefficient defined as:

$$\rho = \frac{Z_L - Z_o}{Z_L + Z_o} \qquad (30)$$

Similarly, the input impedance of the loaded conductor at z=L is given by:

$$Z_{in} = Z_o \left[\frac{1 + \rho e^{-2\gamma L}}{1 - \rho e^{-2\gamma L}} \right] \qquad (31)$$

For the case of an incident electromagnetic field exciting the conductor, the excitation sources are not isolated, but are distributed along the conductor as illustrated in Fig. 16b. In this case, the solution of Eq. (29) for the open-circuit voltage may be regarded as a Green's function, and used in an integral to determine the total response, as:

$$V_{oc} = \frac{e^{-\gamma L}}{1 - \rho e^{-2\gamma L}} \int_o^L V_s'(\xi) \left[e^{\gamma \xi} - \rho e^{-\gamma \xi} \right] d\xi \qquad (32)$$

The distributed sources in this case are given by the tangential electric field along the conductor, and these are comprised of both the incident and earth-reflected fields as:

$$V_s'(\xi) = E_z^{tot}(\xi) = E_z^{inc}(\xi) + E_z^{ref}(\xi) \qquad (33)$$

Equation 32 is the most general form of the open circuit voltage induced at the end of a horizontal conductor due to an arbitrary HEMP plane wave. The determination of the closed form response to a

vertically or a horizontally polarized HEMP wave necessitates the knowledge of the values of the incident and ground reflected electric fields in order to evaluate the intergal in Equation (32).

In Ref. 13 explicit expressions for the vertical and horizontal fields at a height h above the earth are given for both the vertically and horizontally polarized incident fields. For the case of a vertically polarized field incident on the conductor with angles Ψ and ϕ, as defined in Fig. 13 electric field components normal and tangential to the earth at the height h are given by:

$$E_x(h,z) = E_0^{inc}(\omega) \; e^{-\gamma_0 z \cos\Psi \; \cos\phi} \left(1 + R_v \; e^{-\gamma_0 2h\sin\Psi} \right) \cos\Psi \quad (34)$$

$$E_z(h,z) = E_0^{inc}(\omega) \; e^{-\gamma_0 z \cos\Psi \; \cos\phi} \left(1 - R_v e^{-\gamma \; 2h\sin\Psi} \right) \sin\Psi \; \cos\phi \quad (35)$$

where $E_0^{inc}(\omega)$ is the frequency domain spectrum of the transient incident field , $\gamma_0 = jk = j\omega/c$ is the free space propagation constant, and R_v is the plane-wave reflection coefficient for vertical polarization which is given by:

$$R_v = \frac{\varepsilon_r \left(1 + \dfrac{\sigma_g}{j\omega\varepsilon_g} \right) \sin\Psi - \left[\varepsilon_r \left(1 + \dfrac{\sigma_g}{j\omega\varepsilon_g} \right) - \cos^2\Psi \right]^{1/2}}{\varepsilon_r \left(1 + \dfrac{\sigma_g}{j\omega\varepsilon_g} \right) \sin\Psi + \left[\varepsilon_r \left(1 + \dfrac{\sigma_g}{j\omega\varepsilon_g} \right) - \cos^2\Psi \right]^{1/2}} \quad (36)$$

where ε_r is the relative dielectric constant of the ground and $\varepsilon_g = \varepsilon_r \varepsilon_0$.

In Equations (34) and (35) the point z=0 is taken to be the zero phase point, implying that the incident field strikes this point at t=0 in the time domain. For a good conductor this reflection coefficient approaches the value of 1 so that the vertical component of the field near the surface of the earth becomes twice that of the incident field, and the horizontal component tends to zero.

In a similar manner, the electric fields due to a horizontally polarized field may be expressed as:

$$E_x(h,z) = 0 \qquad (37)$$

and

$$E_z(h,z) = E_0^{inc}(\omega)\, e^{-\gamma_0 z \cos\Psi \cos\phi} \left(1 + R_H\, e^{-\gamma_0 2h\sin\Psi} \right) \sin\phi \quad (38)$$

where the horizontal reflection coefficient is:

$$R_H = \frac{\sin\Psi - \left[\varepsilon_r \left(1 + \frac{\sigma}{j\omega\varepsilon} \right) - \cos^2\Psi \right]^{1/2}}{\sin\Psi + \left[\varepsilon_r \left(1 + \frac{\sigma}{j\omega\varepsilon} \right) - \cos^2\Psi \right]^{1/2}} \qquad (39)$$

The resulting expressions for the electric field components tangential to the conductor for the vertically and horizontally polarized fields may be used in Eq. (32) and the integration performed analytically to yield expressions for the open circuit voltage at z=L. Equations (40) and (41) show the result of such integrations for vertical and horizontal polarizations respectively.

$$V_{oc}^{(V)}(\omega) = \frac{E_0^{inc}(\omega)\, \sin\Psi\, \cos\phi \left[1 - R_V\, e^{-\gamma_0 2h\sin\Psi} \right] e^{-\gamma L}}{1 - \rho e^{-2\gamma L}} \times$$

$$\left(\frac{e^{-(\gamma-\gamma_0\cos\Psi\cos\phi)L} - 1}{(\gamma-\gamma_0\cos\Psi\cos\phi)} + \rho \left(\frac{e^{-(\gamma+\gamma_0\cos\Psi\cos\phi)L} - 1}{(\gamma+\gamma_0\cos\Psi\cos\phi)} \right) \right) \quad (40)$$

$$V_{oc}^{(H)}(\omega) = \frac{E_0^{inc}(\omega)\, \sin\phi \left[1 + R_H\, e^{-\gamma_0 2h\sin\Psi} \right] e^{-\gamma L}}{1 - \rho e^{-2\gamma L}} \times$$

$$\left(\frac{e^{-(\gamma-\gamma_0\cos\Psi\cos\phi)L} - 1}{(\gamma-\gamma_0\cos\Psi\cos\phi)} + \rho \left(\frac{e^{-(\gamma+\gamma_0\cos\Psi\cos\phi)L} - 1}{(\gamma+\gamma_0\cos\Psi\cos\phi)} \right) \right) \quad (41)$$

The effect of conducting vertical elements, such as steel transmission/distribution line towers, line drops to substation entrance, cables connecting pad mounted transformers to distribution feeder, etc., on the horizontal conductor response, is to add additional length to the current path for either polarization, and modify the response (induced voltage or current) in the case of vertical polarization. No response will be induced on vertical elements due to horizontal polarization since the electric field will be orthogonal to the elements.

The effect of the vertical elements at z=0 and z=L for vertical polarization, can be represented, to a first approximation, by two lumped sources at these two points. The values of these end sources are given by the product of the local vertical electric field times the height of the elements. These vertical elements are then treated as passive loads at z=0 and z=L for determing the propagation characteristics of the system. Hence to include the effect of the vertical elements on horizontal conductors, Equation (40) becomes:

$$
V_{oc}^{(V)}(\omega) = \frac{E_0^{inc}(\omega)\ \sin\Psi\ \cos\phi \left[1 - R_v\ e^{-\gamma_0 2h\sin\Psi}\right] e^{-\gamma L}}{1 - \rho e^{-2\gamma L}} \quad \times
$$

$$
\left[\frac{e^{-(\gamma-\gamma_0\cos\Psi\cos\phi)L}-1}{(\gamma-\gamma_0\cos\Psi\cos\phi)} + \rho\ \frac{e^{-(\gamma+\gamma_0\cos\Psi\cos\phi)L}-1}{(\gamma+\gamma_0\cos\Psi\cos\phi)}\right]
$$

$$
+ \frac{E_0^{inc}(\omega)\cos\psi\ e^{-\gamma L}}{1 - \rho e^{-2\ L\gamma L}}\ (1 + R_v)h
$$

$$
- E_0^{inc}(\omega)\ \cos\psi\ e^{-\gamma_0 L\cos\psi\cos\phi}\ (1 + R_v)\ h \qquad (42)
$$

In this expression, the first bracketed terms account for the distributed field excitation of the horizontal conductor and the last two terms represent the vertical field excitation at the loads (vertical

elements). Equation (41) for horizontal polarization is, of course, not effected.

The above method is an approximate one since the variation in the strength of the incident electric field with height is not accounted for. Vance in [13] develops a more elaborate representation for this excitation which is more accurate when the height of the line becomes an appreciable fraction of a wavelength.

Case of Long Conductors (Semi-Infinite)

The above equations are the general forms, as developed from TEM transmission line theory, for the open circuit voltage of a conductor excited by HEMP. Under certain circumstances, it is desirable to simplify these equations. For example, in the case of a matched load at z=0, the reflection coefficient ρ may be set to zero.

Often, it is desirable to study the effects of field excitation on an infinite or semi-infinite line. By setting ρ to zero, letting the conductor length L go to infinity, and changing the zero phase reference to the observation point end of the line, the following expressions result for the open circuit voltage on the long (semi-infinite) line:

$$V_{oc}^{(V)}(\omega) = E_0^{inc}(\omega) \, \sin\Psi\cos\phi \, \frac{1 - R_V \, e^{-\gamma_0 2hs in\Psi}}{(\gamma - \gamma_0 \cos\Psi\cos\phi)} \quad (43)$$

and

$$V_{oc}^{(H)}(\omega) = E_0^{inc} \, \sin\phi \, \frac{1 + R_H \, e^{-\gamma_0 2hs in\Psi}}{(\gamma - \gamma_0 \cos\Psi\cos\phi)} \quad (44)$$

The short circuit current at this point may be evaluated as:

$$I_{sc}(\omega) = V_{oc}(\omega)/Z_0(\omega) \quad (45)$$

where $Z_0(\omega)$ is the characteristic impedance of the conductor.

The above equations may be solved by use of computer programs implemented on an IBM PC. The programs use a Fourier transform to obtain the HEMP excitation field in the frequency domain. The solution, either short circuit current or open circuit voltage, is obtained in the frequency domain and then changed back to the time domain through an inverse Fourier transform.

Through the use of approximations that are valid for many cases, a closed form solution may be obtained for the time domain open circuit voltage (or short circuit current) if the incident field is of the form $E(t)=E_0 e^{-at}$ [13]. For cases in which the approximations are valid, solutions can be obtained through the use of tabulated functions and a calculator.

3.2.1.2 Responses of Above Ground Multiconductor Transmission and Distribution Lines

The preceding sections discussed the attributes of the HEMP-induced responses on isolated conductors in free space. The responses of the multi-conductor, multi-phase power lines used in transmission and distribution system, however, are more complicated than those isolated conductors in free space. Table 3 illustrates the major factors influencing the responses of such lines and, hence, indicates their complexity.

Table 3

Factor Affecting the Response of Power Lines

1 - The span length
2 - The length of the line insulators
3 - The presence and number of shield (ground) wires
    and their grounding scheme
4 - The type of towers supporting the line
5 - The tower-footing resistance (TFR)
6 - The (non-corona) attenuation on the line
7 - The geometrical layout of the phase and shield
    (ground) wires
8 - The ground resistivity
9 - The polarization of the EMP
10 - The angles of incidence and orientation of the line
11 - The corona attenuation on the line
12 - The line sag

Consider the problem illustrated in Fig. 17. A multiconductor transmission line having n individual conductors and a total length L is located above the earth. At each end of the line, a generalized load impedance matrix $Z_{L_{n,m}}$ is defined to relate the individual line voltages to the line currents.

It is assumed that the line is illuminated by an incident electromagnetic field as indicated in the figure. Generally, this field could be a plane wave arising from a high altitude detonation, or it could be a radiated field from a surface burst, in which case the field would have a 1/r amplitude fall-off from the burst point and not be perfectly planar.

It is further assumed that for performing an assessment of the connected power equipment, it is necessary to estimate the line currents and voltages at the load of interest, say at the load at z=L. As in the single line case, it is common to replace the transmission line, its load impedance at z=0, and the incident EMP field by an equivalent Thevenin open circuit which is then connected to the load impedance at z=L. This is illustrated in Fig. 18. Characterizing the line in this load-independent manner thus permits the determination of many different responses, depending on the nature of the load on the line.

The details of the analysis of a general multiconductor line are reviewed in Appendix A and this results in a matrix equation (Eq. A9) for the individual wire currents at both ends of the multiconductor line, given in terms of the line, load and excitation parameters. This equation may be used to determine the Thevenin equivalent circuit at the z=L end on the line.

First, a useful approximation in the analysis of many practical multiconductor line configurations is to assume that all of the TEM modes on the line propagate at the same velocity. For a set of closely-bundled conductors having dielectric coatings, this approximation is not accurate, but for widely separated conductors, the resulting errors are not significant. Moreover, it has been shown in
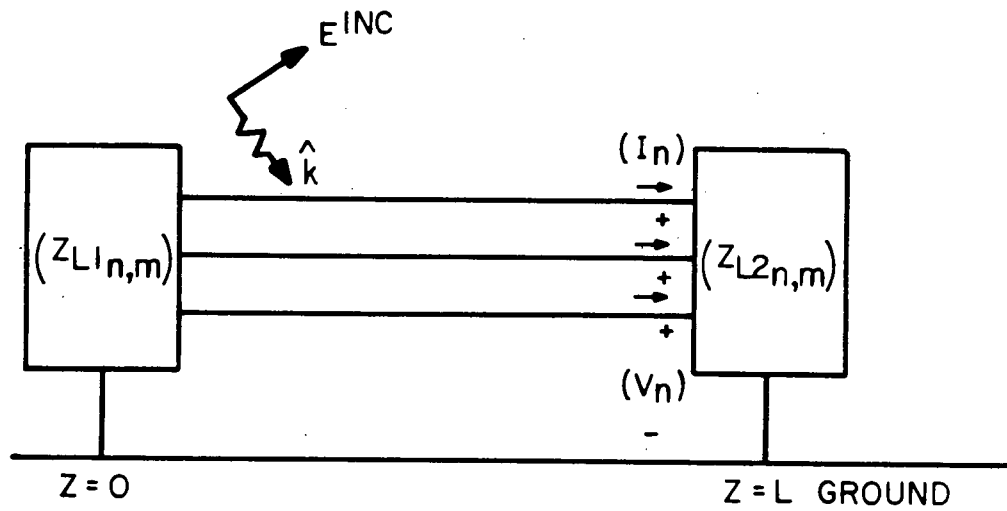
Fig. 17. Field-excited multiconductor line over ground.
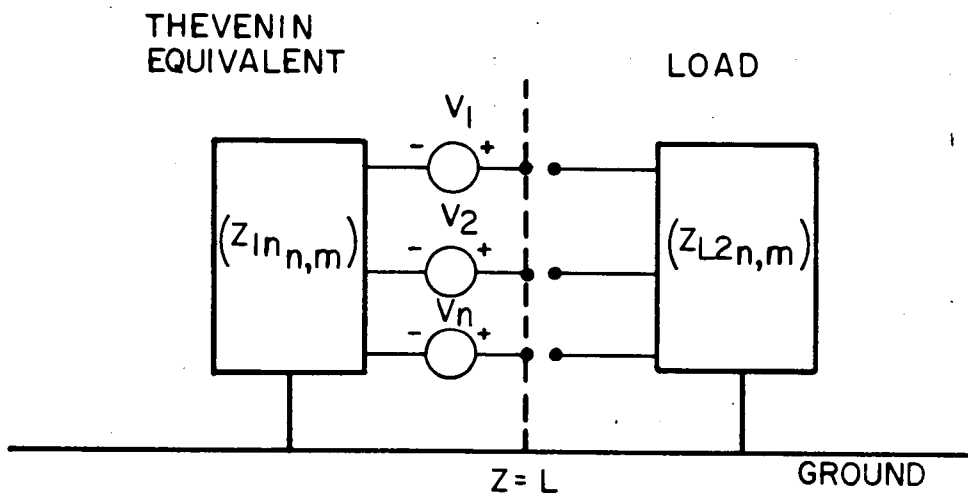
Fig. 18. Generalized Thevenin circuit of multiconductor line at z=L.

Ref. [15] that the use of single velocity modes does not lead to large errors in the terminal response of practical lines. Thus, it is a practical approximation for increasing the ease of calculations.

As a result of this single velocity approximation, the propagation matrix term $e^{(\gamma_{n,m})\ell}$ in Eq. (A9) in the appendix becomes equal to the unit matrix multiplied by a simple scalar propagation term as:

$$e^{(\gamma_{n,m})\ell} = e^{\gamma_c} (\delta_{n,m}) \tag{46}$$

where γ_c is a scalar propagation constant given by:

$$\gamma_\psi = \omega/v \tag{47}$$

Here ω is the angular frequency and v is the velocity of propagation on the line.

As a result of this assumption of single velocity propagation on the line, it is possible to choose any linearly independent set of modal distributions for the current modes on the line. One possible choice of the modal current distribution is for a unit current to exist on one wire with zero current on the remainder of the conductors. Of course, the ground (reference conductor) has a negative unit return current. This choice of modal currents results in the matrix $(T_{n,m})$ in Appendix A being simply a diagonal matrix, thereby simplifying the resulting expressions considerably.

In order to determine the Thevenin equivalent circuit for the line in Fig. 17, it is necessary to open-circuit the line at z=L and compute the voltage at the various terminals. From Eq. (A10), it is noted that in the open-circuit case, the reflection coefficient at z=L is the unit matrix. This may be used in Eq. (A9) along with the characteristic impedance matrix of the line to determine the open circuit voltage at z=L. In this case, the effective source terms are those determined by the distributed field sources given in Eqs. (A13) and (A14).

Similarly, Eq. (A9) along with the lumped source excitation terms of Eqs. (A11), and (A12) can be used to obtain an expression for the Thevenin impedance at the point z=L.

Under the above assumptions and after much algebraic manipulation, the Thevenin voltage source for the multiconductor line may be shown to be expressed as:

$$\left(V_{oc_n} \right) = \left(e^{\gamma_c L}(\delta_{nm}) + e^{-\gamma_c L}(\Gamma_{nm}) \right)^{-1} \left((V_n) + (Z_{c_{nm}})(I_n) \right) \quad (48)$$

where the excitation terms $(\overline{V_n})$ and (I_n) may be expressed using the distributed voltage and current sources as:

$$(V_n) = \int_0^L \left(e^{\gamma_c z}(\delta_{nm}) + e^{-\gamma_c z}(\Gamma_{nm}) \right) \left(V_n^{'(s)}(z) \quad dz \right) \quad (49)$$

and

$$(I_n) = \int_0^L \left(e^{\gamma_c z}(\delta_{nm}) - e^{-\gamma_c z}(\Gamma_{nm}) \right) \left(I_n^{'(s)}(z) \quad dz \right) \quad (50)$$

The individual terms $(V'^{(s)}(z))$ and $(I'^{(s)}(z))$ are the n-vector distributed source terms defined in Eqs. (A15) and (A16).

In Eq. (48), the matrix $(Z_{c_{n,m}})$ is the nxn characteristic impedance matrix of the line which is given by Eq. (A7) in the most general case. For the single velocity case being discussed here, this reduces to:

$$\left(Z_{c_{n,m}} \right) = v \left(L_{n,m} \right) \quad (51)$$

where $(L_{n,m})$ is the per-unit-length inductance matrix of the line, and v is the propagation velocity.

Similarly, the expression for the Thevenin impedance is given by:

$$\left(Z_{in_{n,m}}\right) = \left(Z_{c_{nm}}\right)\left(e^{\gamma_c \ell}(\delta_{nm}) + e^{-\gamma_c \ell}(\Gamma_{nm})\right)^{-1}\left(e^{\gamma_c \ell}(\delta_{nm}) - e^{-\gamma_c \ell}(\Gamma_{nm})\right) \quad (52)$$

In each of these expressions, the reflection coefficient term is that due to the load at z=0 and is given by:

$$(\Gamma_{n,m}) = \left((Z_{L1_{n,m}}) + (Z_{c_{n,m}})\right)^{-1}\left((Z_{L1_{n,m}}) - (Z_{c_{n,m}})\right) \quad (53)$$

The expressions in Eqs. (48) and (52) above may be reduced in complexity in the case of an open, short, and matched load at z=L. In these cases, the reflection coefficient matrix becomes the negative unit matrix, the unit matrix and the null matrix respectively, thereby simplifying the expression for the Thevenin response.

In order to understand the excitation of the multiconductor line by an incident field, it is convenient to assume that the wave reflections at the z=0 end of the line are zero. This, in effect, permits the understanding of the induced line response due to the initial interaction of the exciting field without having subsequent reflections from the end of the line adding to the complexity of the waveform.

With $(\Gamma_{n,m})=0$ in Eq. (48) the following expressions result for the Thevenin equivalent circuit:

$$(V_{oc_n}) = e^{-\gamma_c L}\int_0^L e^{\gamma_c z}\left((V_n^{'(s)}(z)) + (Z_{c_{n,m}})(I_n^{'(s)}(z))\right)dz \quad (54)$$

and

$$(Z_{in_{n,m}}) = (Z_{c_{n,m}}) \quad (55)$$

The open circuit voltages on each conductor in the line in the above expressions differ in form somewhat from that for a single wire conductor developed in Section 3.2.1.1. In the present formulation, a contribution to the transmission line source terms contains both the electric and magnetic fields. Furthermore, in the present formulation the electric field of interest is that component perpendicular to the conductors and the magnetic field is that component which links the conductor and the reference ground plane. In the case in Section 3.2.1.1, the only excitation was that due to the tangential component of the electric field on the conductors, as well as on the terminating conductors.

That these two alternate representations for the line response are identical can be shown by using the curl(E) Maxwell equation to express the magnetic field in the distributed voltage term in terms on the electric field. Then, upon combining the voltage and current source contributions into a single term, it may be noted that only the tangential components of the electric field are present in the sources.

In this manner, the expression for the Thevenin voltage at the end of the matched multiconductor line can be written in an alternate form as:

$$(V_{oc_n}) = e^{-\gamma_c L} \int_0^L e^{\gamma_c z} \left[E_{tan_n}(z)\right] dz + e^{-\gamma_c L}(E_{1_{\perp n}}(0) \cdot h_n)$$
$$- (E_{1_{\perp n}}(L) \cdot h_n) \qquad (56)$$

where the first term represents the effect of the electric field along the length of the conductor, and the second two terms account for the excitation of the loading terminations by the incident field. Note that in this notation (E_{tan_n}) represents the total incident plus ground-reflected tangential electric field on each of the n conductors and $(E_{1_{\perp n}})$ represents the total incident electric field normal to the n conductors and terminating on the ground plane.

As discussed in Reference [13], the electric field exciting the line in Eq. (56) consists of contributions from the direct (incident) wave, as well as from the electric field reflected from the ground, as illustrated in Fig. 19. Reference [13] shows that these may be written as:

$$E_{tan} = E_0 e^{-jkz \cos\Psi} (1 - R_v e^{-jk2h \sin\Psi}) \sin\Psi \qquad (57)$$

and

$$E_{\underline{1}} = E_0 e^{-jkz \cos\Psi} (1 + R_v e^{-jk2h \sin\Psi}) \cos\Psi \qquad (58)$$

where E_0 is the incident field strength, and Ψ is the angle of incidence. In these relations, the incident field is assumed to be vertically polarized.

The term R_v is the plane wave reflection coefficient for vertically polarized fields and is given by Eq. (36).

In looking at these relations, it may be noted that for conductor heights which are small compared with a wavelength, the excitation of each conductor varies linearly with the height above ground. Thus, if the excitation term is known on one conductor, the corresponding excitation can be estimated for another in the same line.

For example, consider the typical transmission line cross sections for a 69 kV line as shown in Fig. 20. For the single circuit line shown in Fig. 20a, each phase conductor is at the same height over the earth, so that each receive the same amount of excitation from the incident field. (This neglects any phase differences in the excitation field across the cross section of the line.) Based on an estimation of the various heights of the phase conductors in Fig. 20b where a double circuit line is shown, it may be estimated that there will be a variation of approximately 30% of the voltage source on the top conductor over that for the bottom conductor. This difference may or may not be important in the final outcome of the analysis, and depends on how the calculated results are to be used. If there are similar uncertainties in the modeling of components and their susceptibilities,

INCIDENT FIELD

E^{INC}

E_{TAN}

CONDUCTOR

GROUND-REFLECTED
FIELD

E^{REF}

E_I
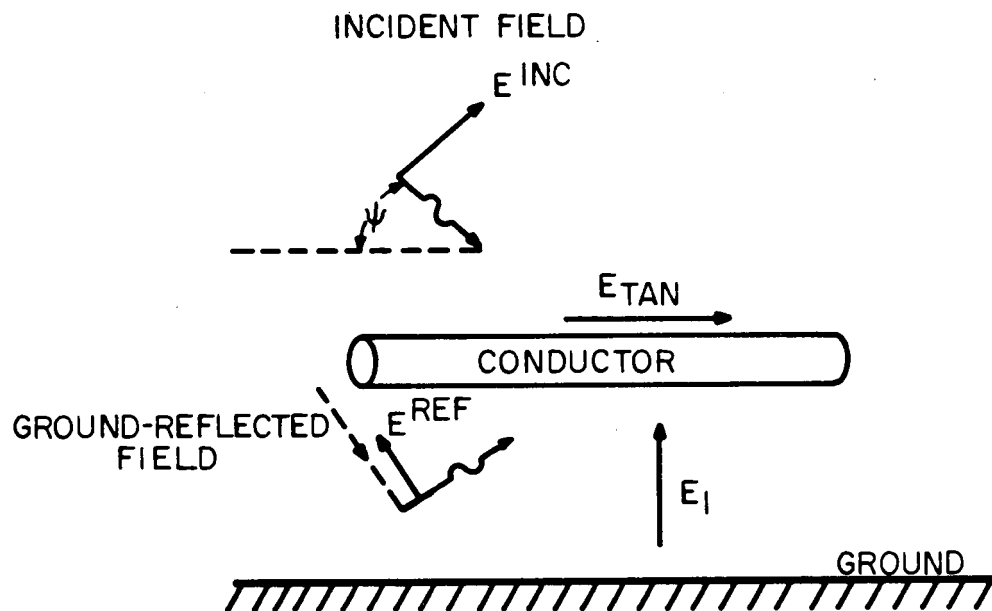
GROUND

Fig. 19. Reflection of incident field at ground plane.

AVERAGE SPAN=1000 FT.   AVERAGE SPAN=900 FT.

SINGLE CIRCUIT   DOUBLE CIRCUIT
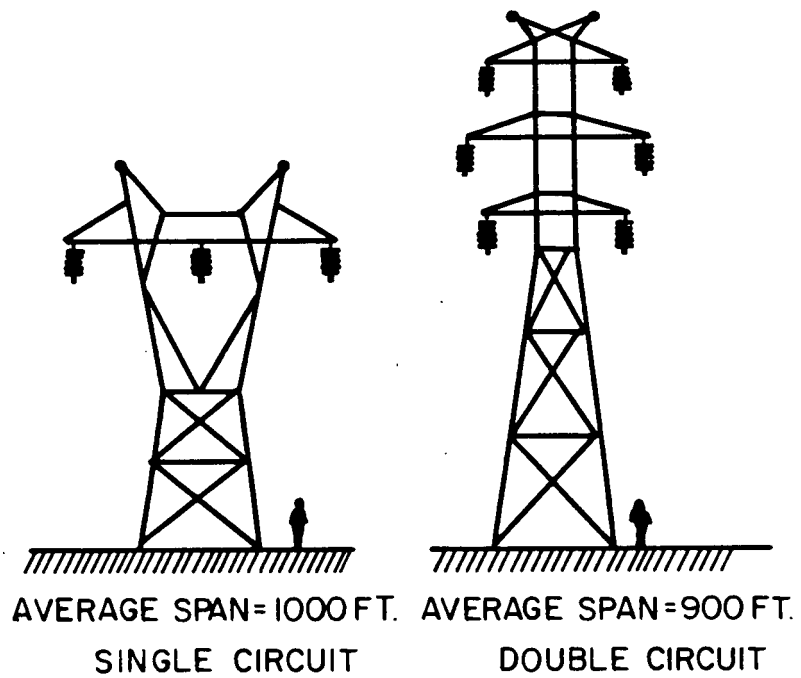
Fig. 20. Steel tower construction for transmission lines at voltages of 69 kV and above.

or if there are larger uncertainties in the EMP environments exciting the line, it may not be necessary to take the multiconductor line behavior into account. In this case, an approximate single line may suffice.

3.2.1.2.1 Equivalent Single-Conductor Response

In the cases where the inaccuracies in using a single line model for a multiconductor line response are low enough to permit the use of a single line model to estimate individual phase conductor currents or voltages, it is necessary to determine the appropriate single line parameters for modeling the line. These parameters include the characteristic impedance and wave velocity on the single line equivalent, the field coupling parameters, and the effective load impedances. A knowledge of these parameters then permits the representation of the excited line as a single Thevenin equivalent circuit as shown in Fig. 21.

This problem has been addressed by several investigators [16,17] and their results will be summarized here. The determination of the propagation velocity for the equivalent single conductor line is obtained by looking at all of the multi-mode propagation velocities on the multiconductor and choosing the fastest velocity. The fastest mode is always the bulk (or common) mode on the line, and thus corresponds most closely to the quantity being calculated in the single line model.

In addition to this, the single line characteristic impedance can be defined as:

$$
Z_C = \left(\sum_{i,j=1}^{N} (Z_{c_{ij}})^{-1} \right)^{-1}
\tag{59}
$$

where $(Z_c)_{ij}^{-1}$ represents the ij^{th} element of the inverse of the impedance matrix (i.e., the characteristic admittance matrix of the line).
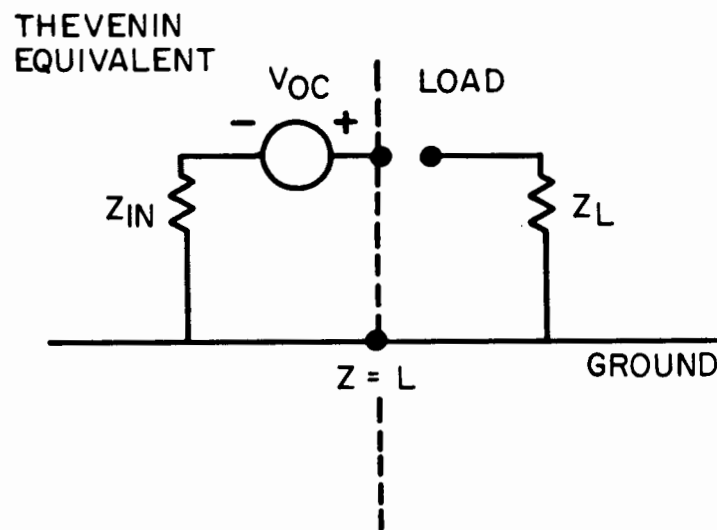
Fig. 21. Single line Thevenin equivalent circuit.

For determining the appropriate load impedance at the end of a single conductor line, Eq. (59) may also be used, but with the load impedance (Z_L) used in place of the characteristic impedance matrix.

For the field coupling parameters, it is necessary to determine an average height of the conductors above the ground and use this to find the excitation terms in the single line equivalent of Eq. (56). This is the same as defining an average of all excitation voltage sources on the multiconductor line and using this for the single line excitation.

Doing this leads to the definition of the single-line voltage and currents as:

and

$$V_s = \frac{1}{n} \sum_{i=1}^{h} V_i \qquad (60)$$

$$I_s = \sum_{i=1}^{h} I_i \qquad (61)$$

where n is the number of conductors in the line, and V_i and I_i are the wire voltages and currents on the multiconductor line.

Once a single line analysis has been conducted, and the load voltages and currents have been determined, it still remains to estimate the individual phase conductor responses from the bulk response. This may be accomplished by assuming that the loads are balanced on the line and that the phase voltages are identical. This then permits the estimation of the phase conductor response as:

and

$$V_i = V_s \qquad (62)$$

$$I_i = I_s/n \qquad (63)$$

Obviously, there are many different errors introduced in using a single line analysis for a multiconductor line. Unfortunately, it is very difficult to quantify the degree of error in a general sense. As a result, there have been several numerical studies performed to assess the accuracy of this modeling, but they are unable to permit any general statements regarding the accuracy.

In a general power system, a preliminary screening of the load and line configurations must be carried out and an assessment of the desired calculational accuracy made prior to deciding whether a single or multiconductor analysis is required.

3.2.1.3 Network Modeling in Frequency Domain

The EMP coupling models discussed to this point have all been related to a single length of line, containing one or more individual conductors. In actual practice in a power system, the topology of the electrical conductors connected to a particular piece of equipment may not be this simple. There may be branching of electrical conductors, as well as significant changes of line impedance, such that a transmission line network model is more suitable for the analysis of the Thevenin equivalent circuit at the observation end of the line. While such analysis is possible [1], the resulting complications can be severe and this type of analysis is best avoided if possible.

Consider the electrical transmission network shown in Fig. 22 which is comprised of a number of individual transmission line sections (either single wire or multi-wire) which are interconnected at each of the nodes or junctions in the system. It is desired to determine the open circuit response at the observation point, denoted as 0.

From the experience gained from the analysis of single wire lines, it is clear that the very early time response of the line at 0 is dictated by the coupling of the EMP with the line conductor in the vicinity of the observation point. As time progresses, the effects of the coupling to the line at points further away from the observation point have time to propagate and influence the response.
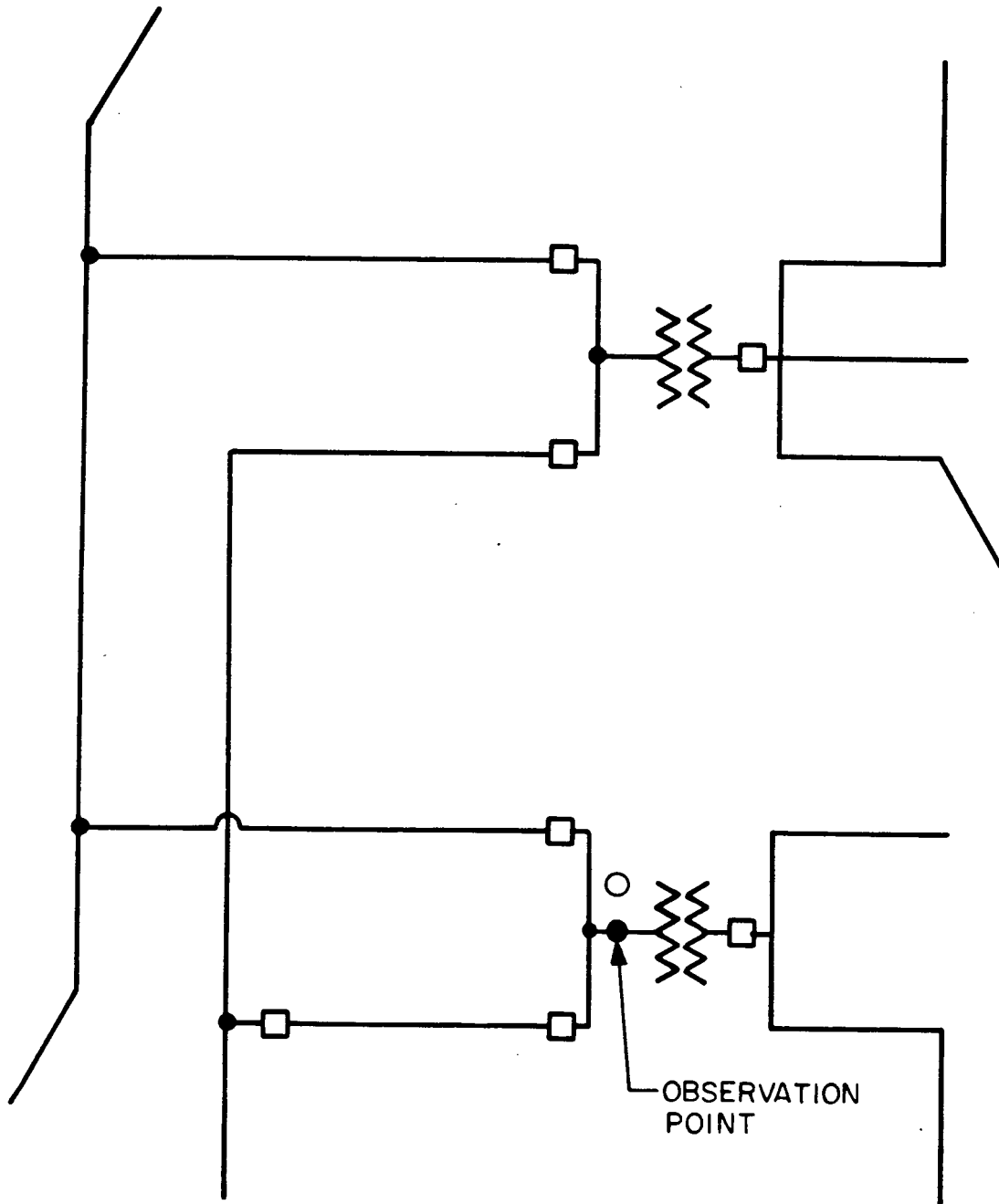
Fig. 22. Transmission line network with observation point indicated.

Using the concept of the critical line length permits us to extract a portion of the network and analyze its EMP response as if it were isolated from the remainder of the network. Clearly, if the calculated response is desired for later times, the resulting size of the sub-network to be analyzed is correspondingly larger. In most cases, however, the peak EMP-induced response occurs well within the first microsecond after the incident field strikes the observation point, and the required sub-network size is small, perhaps consisting of only a single line less than a kilometer in length.

The critical line length of a single conductor is expressed as:

$$Lc = \frac{c \ tmax}{(1 - \cos(\Psi) \cos(\phi))} \tag{64}$$

where tmax is the maximum time for which the response of the single length line is to be identical to that of the line imbedded in the network. Note that the above equation is developed for a line located over a highly conducting earth, where the wave velocity on the line is the same as that in free space.

Assuming that a maximum time of 1 microsecond is acceptable for estimating the effects of EMP on a component in the power system, the above equation becomes:

$$Lc = \frac{300}{(1 - \cos(\Psi) \cos(\phi))} \tag{65}$$

Table 4 presents this critical line length for several values of the angles of incidence Ψ and ϕ. Thus, depending on the angles, a complete EMP network coupling analysis may not be necessary in assessing a particular piece of equipment.

There may be, however, times when a network analysis is needed. For example, in studying the effects of intermediate time HEMP, it will be necessary to consider times on the order of milliseconds, and the

Table 4

Critical Line Lengths (in Km) for a 1 μs Clear Time

Ψ (Degrees)

ϕ (Degrees)	90	80	70	60	50	40	30	20	10	0
90	0.30									
80	0.30	0.31								
70	0.30	0.32	0.34							
60	0.30	0.33	0.36	0.40						
50	0.30	0.34	0.38	0.44	0.51					
40	0.30	0.35	0.41	0.49	0.59	0.73				
30	0.30	0.35	0.43	0.53	0.68	0.89	1.20			
20	0.30	0.36	0.44	0.57	0.76	1.07	1.61	2.56		
10	0.30	0.36	0.45	0.59	0.82	1.22	2.04	4.02	9.95	
0	0.30	0.36	0.46	0.60	0.84	1.28	2.24	4.97	19.75	∞

SYMMETRIC

corresponding critical line lengths become large. Similarly, in estimating the response of distribution systems, a network model may be required, since the network size may be comparable to the critical line length.

In cases like these, there are several different approaches which may be used. The first is a simple network reduction technique which permits the reduction of a simply connected (i.e., no closed loops) network into its Thevenin equivalent through a series of transformations.

Consider the simple network shown in Fig. 23 which consists of five lines located above the ground. At the ends of three of the lines there are terminating impedances, and the Thevenin equivalent circuit is desired at the terminal 0. Through the use of the transmission line transformation indicated in Fig. 24, it is possible to sequentially collapse each line at the extremities of the network into lumped impedance and voltage sources in parallel, and then combine their contributions. This process is continued until the network is completely reduced to a single Thevenin equivalent circuit, as is illustrated in Fig. 25.

Note that in collapsing a line as indicated in Fig. 24, the incident field on the line, as well as the presence of a previously excited line, contribute to the line's response. The contribution to the open circuit voltage by the incident field is directly given by Equations (40) and (41) for the two different polarizations, and the part of the open circuit voltage due to lumped source at the far end of the line in Fig. 25 is given by:

$$V_{oc} = \frac{V_1 e^{-\delta L}(1-\rho)}{1 - \rho e^{-2\delta L}} \qquad (66)$$

where ρ is the reflection coefficient for the line previously defined in Eq. (30). Similarly, the expression for the input impedance for the line segment is given by Eq. (31).
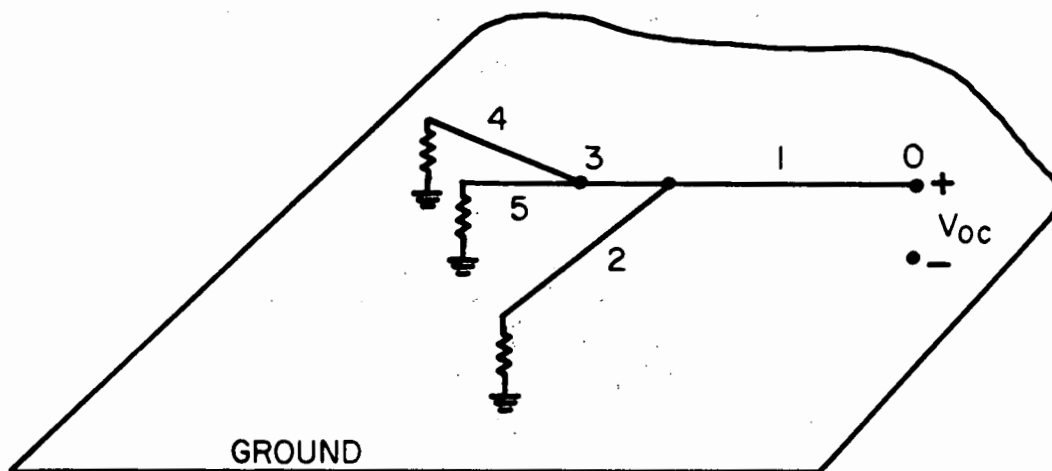
Fig. 23. Tree-like transmission line network.
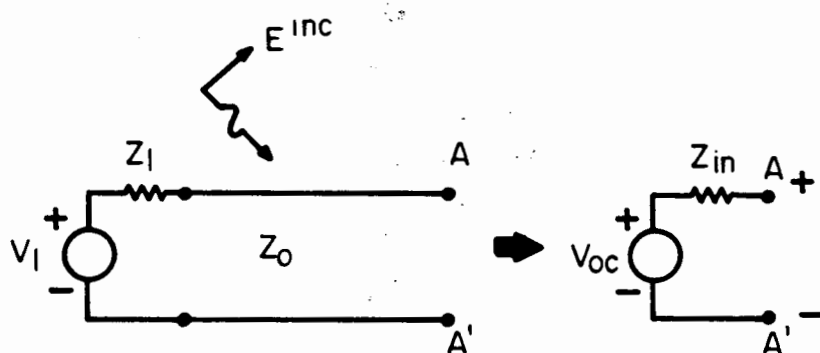
Fig. 24. Fundamental circuit for network reduction.
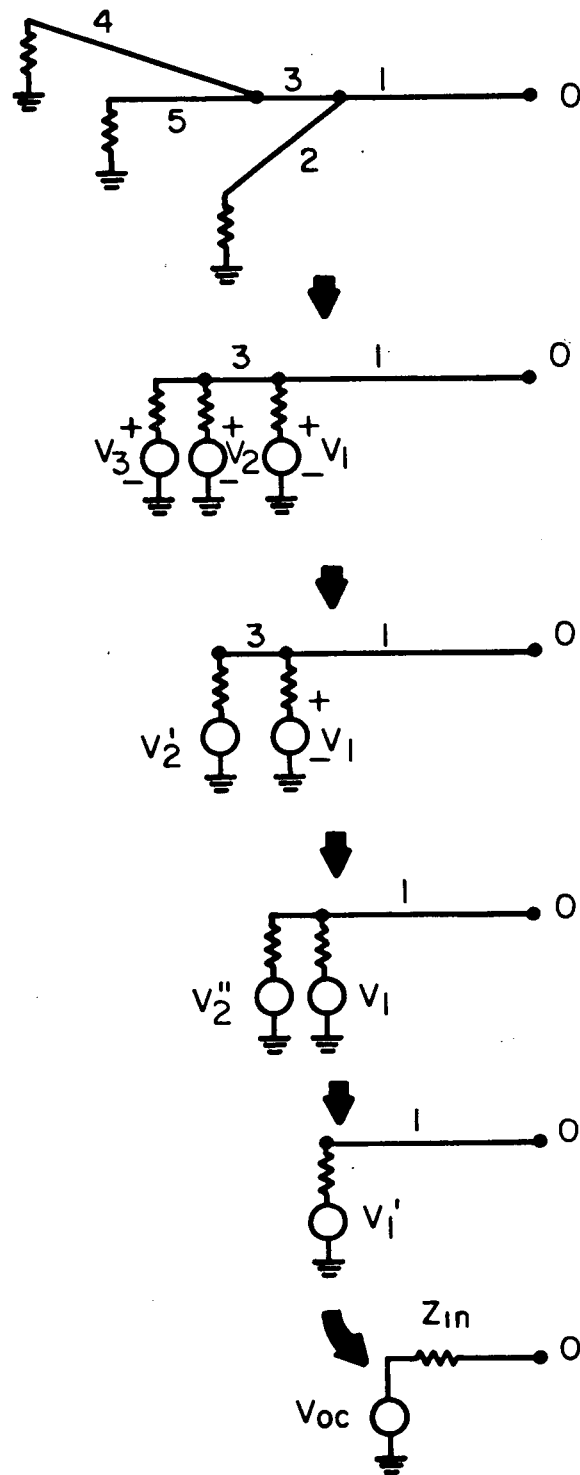
Fig. 25. Series of transformations of network to a Thevenin equivalent.

There are some cases where the transmission line network contains loops, as illustrated in Fig. 26. In this instance, the simple node reduction method previously described is not applicable for the determination of the equivalent circuit at the observation point. A more general analysis approach is required.

The analysis of general transmission line networks has been discussed recently in several different References [18,19] and involves an analysis procedure that is similar to that used in the solution of large circuit problems, also involving loops: instead of simplifying the circuit, a set of node (or possibly loop) equations are written, and the entire circuit is analyzed at once. This formalism will not be re-derived here, but the salient aspects of the analytical approach will be summarized.

For the transmission line network, however, the individual elements linking the nodes in the network are long compared with a wavelength, thereby complicating the analysis. From the physical description of the transmission line network, it is possible to develop a topological representation of the same, as shown in Fig. 26b. Each branch of the network represents a particular length of transmission line, either single or multiwire, and each are assumed to be excited by an incident EMP.

The previous discussions of EMP coupling to single and multiwire lines permit the determination of the amplitudes of positive and negative traveling waves on each of the lines in the network. How each of these traveling waves interact with each other at the junctions in the network is a function of the connections of the conductors at the junctions, as well as the details of the load impedances at these points. This knowledge is incorporated in one large matrix equation, known as the BLT equation [18], which may be solved for the line traveling waves. These may then be combined to yield the line voltages and currents at all of the junctions in the network.
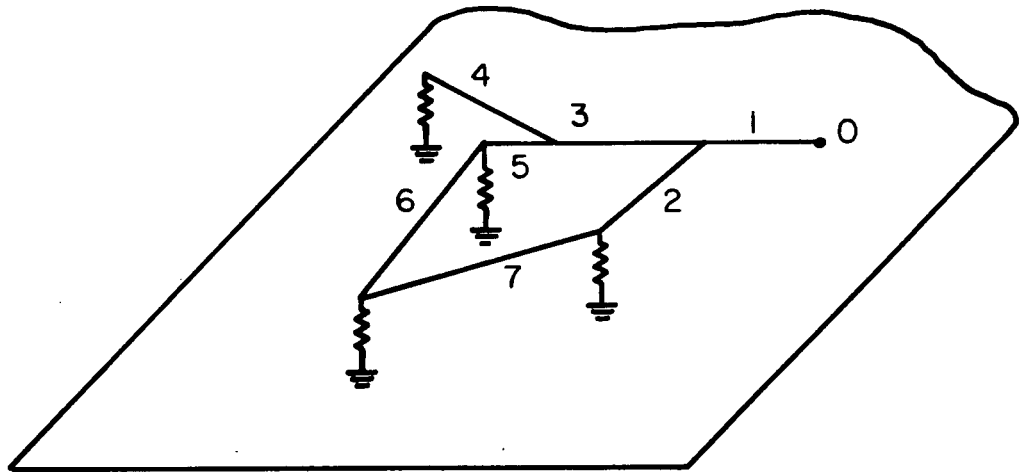
a) Transmission line network involving loops

① = NODE

I = BRANCH
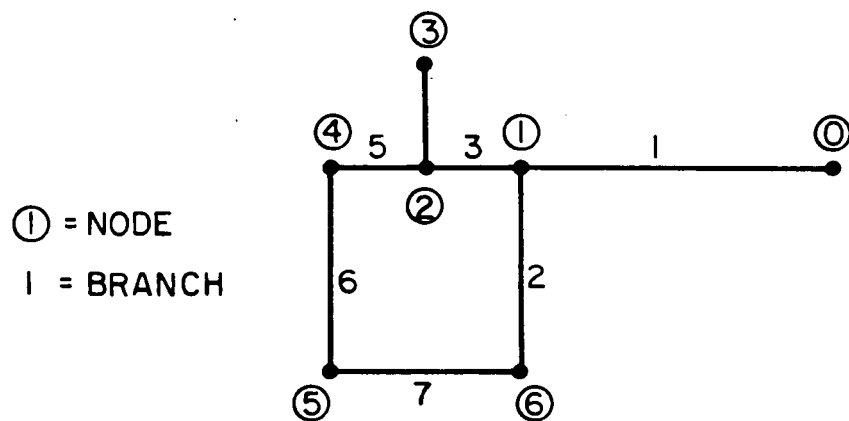
b) Linear graph showing network topology

Fig. 26. Pictorial representation (a) and topological representation (b) of a transmission line network with loops.

As this analysis is performed in the frequency domain, any transient results are obtained by performing such an analysis at many different frequencies, and then using a Fourier transform.

This calculational approach has been incorporated in a general computer code for treating multiconductor transmission line networks [20], and is available for use in power system assessments, if necessary. However, it is presently thought that the need for such an analytical tool will be infrequent, due to the fact that the largest EMP response at a specific component occurs within the first microsecond and the critical line length concept allows a reduction of the size of the network to be analyzed.

3.2.1.4 Underground Conductors

This section covers the analysis of the response of buried conductors to HEMP. This analysis can be applied directly applied to pipe type cables, insulated cables, bare cables, conduits, and metalic water pipes. This section discusses the case of both electrically long and short buried conductors.

The analysis described here is based basically on the analysis by Vance in References [13 and 21].

Long Buried Conductors

Consider the problem shown in Figure 27. An infinitely long, highly conducting conductor of radius a and covered with an insulating jacket of radius b is located a distance d below the surface of the earth. The earth is assumed to be a homogenious half-space having a conductivity σ_g and a dielectric constant ε_g. An incident HEMP impinges on the earth with angles of incidence ψ and ϕ, and has either vertical or horizontal polarization as defined in Section 3.2.1.1. It is desired to determine the time-dependent current induced on the line conductor.

As discussed in Section 3.2.1.1, the analysis of this problem can be carried out through the development of a transmission line model having the differential section shown in Figure 28. Once the various
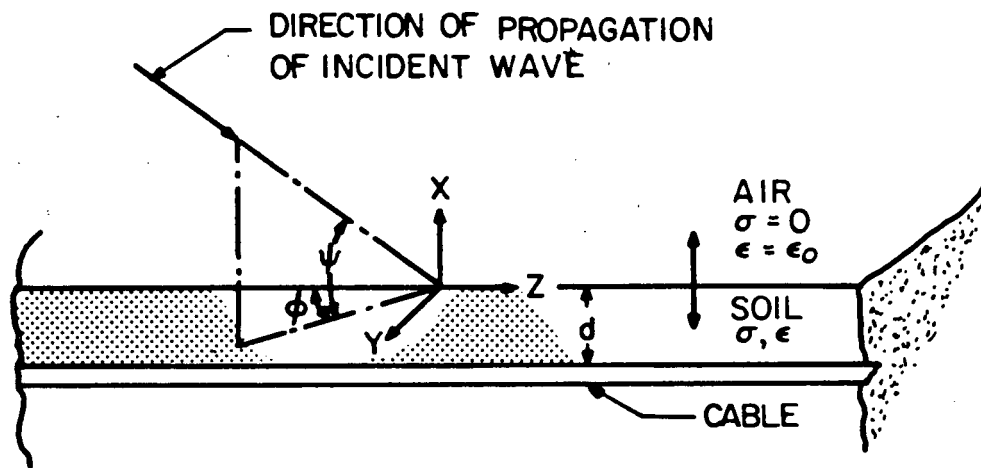
a) Perspective view
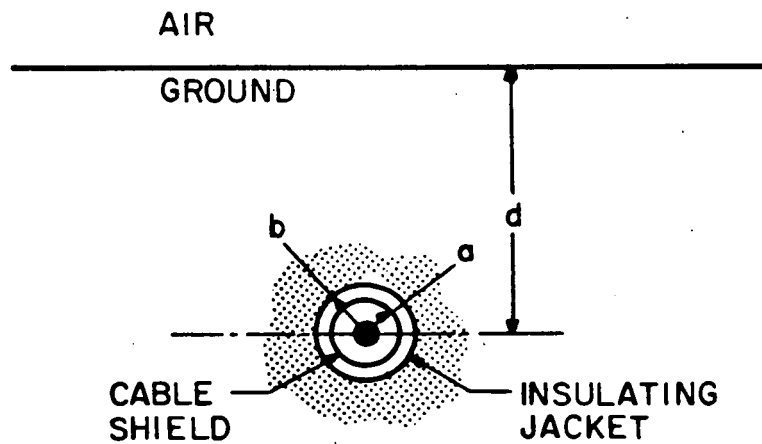
b) Cross sectional view

Fig. 27. Geometry of HEMP excited buried cable [21].
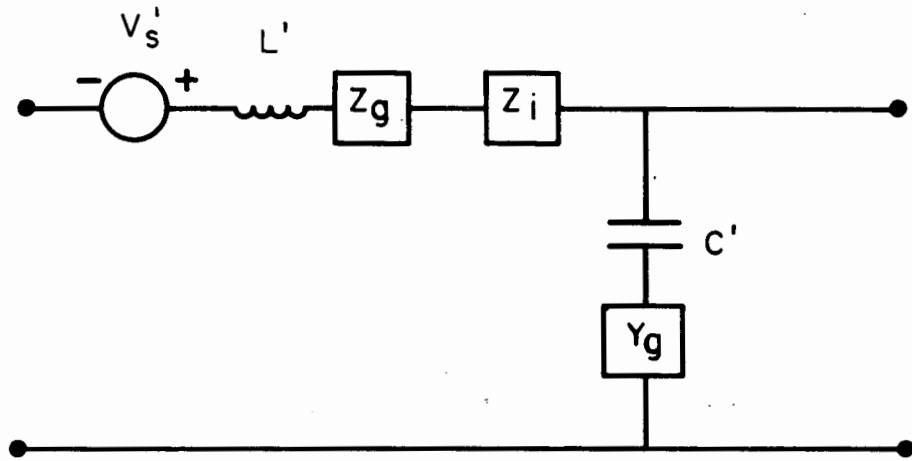
Fig. 28. Differential section of buried conductor
excited by HEMP.

impedance and admittance elements are defined, and the excitation voltage source related to the incident EMP electric field, the conventional transmission line relations developed in Section 3.2.1.1 may be used to determine the conductor current. In this particular case, the conductor is taken to be infinite, so the effects of current reflections at the ends of the line are not taken into account.

In Fig. 28, the total per-unit-length impedance for the transmission line model is given by:

$$Z'(\omega) = Z_g(\omega) + Z_i(\omega) + j\omega L'$$ (67)

where the first term Z_g represents the effective impedance of the ground-return path of the current. Ideally, the transmission line current flowing on the buried conductor at one end must flow out of the end, into the near-by soil, and propagate back to the opposite end of the conductor to complete the circuit. This term accounts for the impedance of this current path and is given in Ref. 13 as:

$$Z_g(\omega) = \frac{-j\gamma_g}{2\pi b \sigma_g} \frac{H_0^{(1)}(j\gamma_g b)}{H_1^{(1)}(j\gamma_g b)}$$ (68)

where $H_0^{(1)}$ and $H_1^{(1)}$ represent the cylindrical Hankel functions and γ_g is the propagation constant in the lossy earth given by:

$$\gamma_g = \sqrt{j\omega\mu_0(\sigma_g + j\omega\varepsilon_g)}$$ (69)

which for low frequencies may be approximated as:

$$\gamma_g \simeq (1 + j)\sqrt{\pi f \mu_0 \sigma_g} = \frac{(1 + j)}{\delta}$$ (70)

where δ is the skin depth defined as:

$$\delta = 1/\sqrt{\pi f \mu_0 \sigma_g}$$ (71)

Figure 29 from Ref. 21 shows plots of skin depth vs. frequency for several different ground conductivities. In these relations, f is the frequency given by $f = \omega/2\pi$.

For the cases when the depth of burial of the conductor is significantly less than the skin depth, the earth impedance contribution to the transmission line model can be approximated as:

$$Z_g(\omega) \simeq \frac{\omega\mu_0}{8} + \frac{j\omega\mu_0}{2\pi} \ln \left[\frac{\sqrt{2}}{\Gamma_0} \frac{\delta}{b} \right] = R_g + j\omega L_g \qquad (72)$$

where Γ_0 is Euler's constant given by 1.781...

The second term in the per-unit-length impedance in Eq. 67 pertains to the internal impedance of the conductor itself which is given approximately as:

$$Z_i(\omega) = (1 + j)/2\pi a \sigma \delta \qquad (a >> \delta) \qquad (73)$$

In developing this last relation, it is assumed that the conductor is a highly conducting cylinder.

The last term in the line impedance is due to the impedance of the dielectric jacket of the cable having a thickness b-a. This is given as:

$$j\omega L' = \frac{j\omega\mu_0}{2\pi} \ln(b/a) \qquad (74)$$

The overall per-unit-length admittance of the conductor is seen to be a series combination of two individual admittance elements, $j\omega C'$ and Y_g. The first is due to the capacitive effect of the dielectric sheath which is expressed as:

$$j\omega C' = j\omega \, 2\pi\epsilon_i/\ln(b/a) \qquad (75)$$
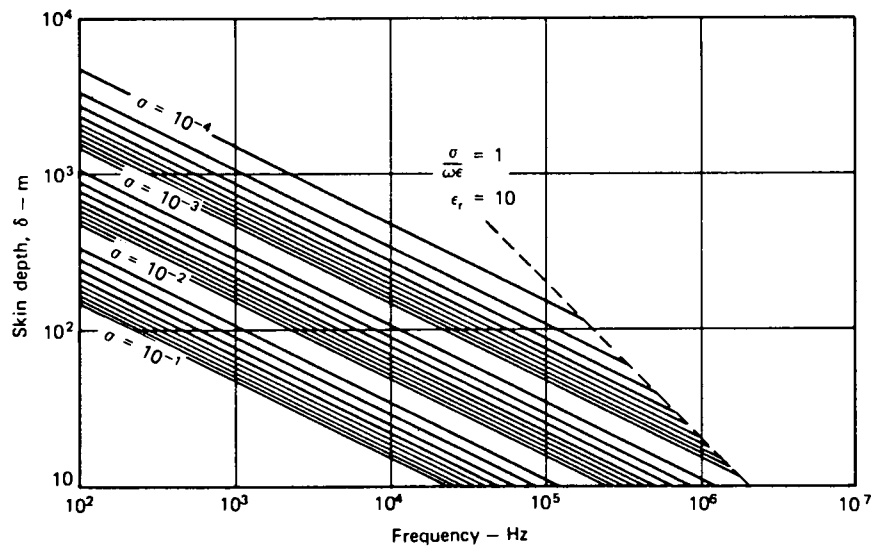
Fig. 29. Skin depth in imperfectly conducting soil [21].

where ε_i is the dielectric constant of the cable jacket. The second term pertains to the shunt susceptance of the soil, and according to Vance [13], is given approximately as:

$$Y_g(\omega) \simeq \gamma_g^2/Z_g(\omega) \qquad (76)$$

The resulting total per-unit-length admittance of the line is thus the series combination of these two admittances and is given as:

$$Y'(\omega) = \frac{j\omega C' \; Y_g(\omega)}{j\omega C' + Y_g(\omega)} \qquad (77)$$

Note that for a bare conductor or for a conductor with a very thin jacket, the jacket capacitance approaches a large value and the per-unit-length admittance of the line reduces to just that of the surrounding earth. With the line impedance in Eq. (67), and the admittance in Eq. (77), the propagation constant for induced currents on the buried bare conductor may be calculated as:

$$\gamma(\omega) = \sqrt{Z'(\omega) \; Y'(\omega)} \simeq \gamma_g \simeq \frac{(1 + j)}{\delta} \qquad (78)$$

and the characteristic impedance is given as:

$$Z_c(\omega) = \sqrt{Z'(\omega)/Y'(\omega)} \quad \frac{j\omega\mu_0}{2\pi\gamma_g} \; \ln \frac{\sqrt{2}\,\delta}{r_0\,b} \qquad (79)$$

These latter quantities permit the description of the behavior of the EMP-induced conductor current using the simple transmission line expressions.

The final quantity needed to complete the description of the per-unit-length model of the buried conductor is the distributed exciting voltage sources. As for the above ground conductors, these

distributed sources are equal to the tangential electric field on the conductor. Because the conductor is buried in the earth, it is expected that this excitation field will be considerably reduced in magnitude, due to the reflection of much of the incident field from the ground surface.

Vance, in Ref. 13 has developed two approximate expressions for the frequency-domain tangential electric field at a depth d for both vertical and horizontal polarization. These are given as:

$$E_z \simeq 2 \, E_0 \, (\omega) \, \cos\phi \sqrt{\frac{j\omega\varepsilon_0}{\sigma_g}} \, e^{-(1+j)d/\delta} \quad \text{(vertical)} \quad (80)$$

and

$$E_z \simeq 2 \, E_0(\omega) \, \sin\psi \, \cos\phi \, \sqrt{\frac{j\omega\varepsilon_0}{\sigma_g}} \, e^{-(1+j)d/\delta} \quad \text{(horizontal)} \quad (81)$$

where $E_0(\omega)$ is the spectrum of the incident HEMP wave.

The description of the buried conductor response through the quantities in Eq. (79), (80), and (81), are sufficient to permit the application of the transmission line formalism of Section 3.2.1.1 to develop a solution for the frequency domain line current.

Instead of doing this, however, Vance [21] has illustrated how it is possible to obtain a relatively simple expression for the time-domain cable current without resorting to a numerical evaluation of the current spectrum and performing a Fourier transform. First, it is necessary to simplify the form of the incident waveform somewhat. Instead of using a double exponential, a single exponential waveform in the form of:

$$E_0(t) = A_0 \, e^{-t/\tau} \quad (82)$$

is suitable with A_0 = 50 kV/m, and τ = 0.25 x 10^{-6}, in order to represent the HEMP field. Note that this does not represent the early time part of the field accurately, but the effects of the lossy earth

serve to markedly broaden the transmitted fields into the earth, so that the actual field is not at all strongly dependent on the details of the very early time part of the incident waveform. For a double exponential input waveform, one can obtain the response by supposition of the results of the two single exponential responses.

Using concepts similar to those developed for the transmission line analysis for above ground conductors, the frequency-dependent current on the infinite line at a depth d can be expressed as:

$$I(d,\omega) = \frac{E_z(d,\omega)}{Z_c(\omega)\,\gamma(\omega)} \simeq \frac{2D(\psi,\phi)\,\sqrt{j\omega\tau_e}\;e^{-(1+j)/\delta}}{j\omega\,\frac{\mu_0}{2\pi}\,\log\frac{\sqrt{2}}{\Gamma_0}\frac{\delta}{b}}\,E_0(\omega) \qquad (83)$$

where the term τ_e represents a time constant for the earth and is given by:

$$\tau_e = \varepsilon_0/\sigma_g \qquad (84)$$

The term $D(\psi,\phi)$ in Eq. (83) is the directivity function which accounts for the polarization of the incident field and is given by:

$$D(\psi,\phi) = \cos\phi \qquad \text{(vertical polarization)} \qquad (85)$$

$$D(\psi,\phi) = \sin\psi\,\sin\phi \qquad \text{(horizontal polarization)} \qquad (86)$$

In attempting to develop an analytic solution for the time-domain response for the current, it is necessary to make an additional simplification in Eq. (83) in order to perform the transform from the frequency-domain into the time-domain. As illustrated in Fig. 30, the log term in the denominator of Eq. (83) is a weak function of frequency. As discussed by Vance, the choice of a constant value of about 10 appears to be a reasonable one, and in doing this, the inverse Fourier
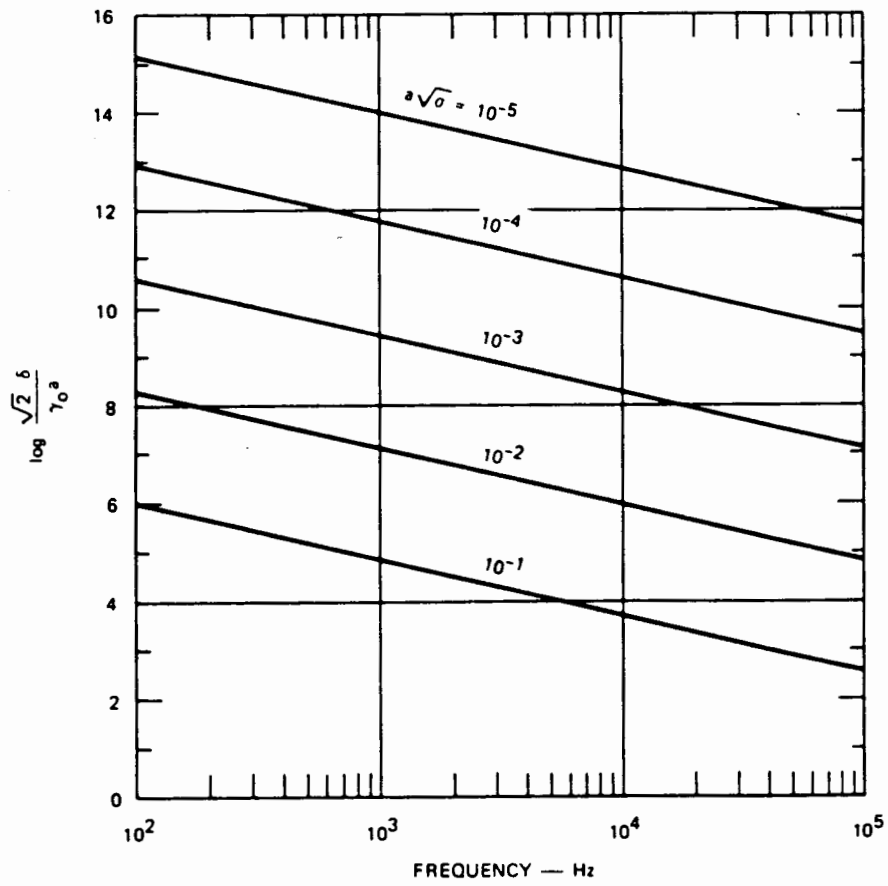
Fig. 30. Plot of log ($\sqrt{2}\,\delta/\gamma_0$ a) vs. frequency [13].

transform may then be taken analytically. This permits the final expression for the transient current in the buried cable to be written as:

$$i(d,t) = 2 \times 10^6 \sqrt{\frac{\tau_e \tau}{\pi}} \; A_o \; D(\psi,\phi) \; e^{-t/\tau} \int_0^{\sqrt{t/\tau}} e^{-p/\xi^2} \, e^{\xi^2} \, d\xi \quad (87)$$

where the parameter p is a constant and is given by

$$p = \left[\frac{d}{c}\right]^2 /4\tau\tau_e \quad (88)$$

The evaluation of Eq. (87) is rather straightforward. The only potential problem is that the evaluation of the integral must be done carefully so as to not cause unwanted errors in the response. Additionally, for large times, the positive exponential term must be treated carefully, since there is a possibility of this resulting in numerical overflows. As a quick reference, Fig. 31 from Ref. [21], shows the variation of the normalized current as a function of time and the incident field.

Figure 32 from Ref. [21] shows the variation of the peak induced current with respect to incidence angles for both vertical and horizontal polarization. For an arbitrary polarization, the techniques of superposition can be applied to determine the response of cable.

Special Case: Buried Conductors In Non-Metalic Conduits

A special case of the under-ground conductor are those enclosed in non-metalic conduits or mechanical shields. The shield in this case does not offer any shielding to the inner conductor, but serves only to alter the capacitance between the soil and the conductor. In addition to this, the insulation in the shield (either air or any other form of insulator) tends to make the response of such a conductor different than the bare conductor in direct contact with the soil. These effects lead
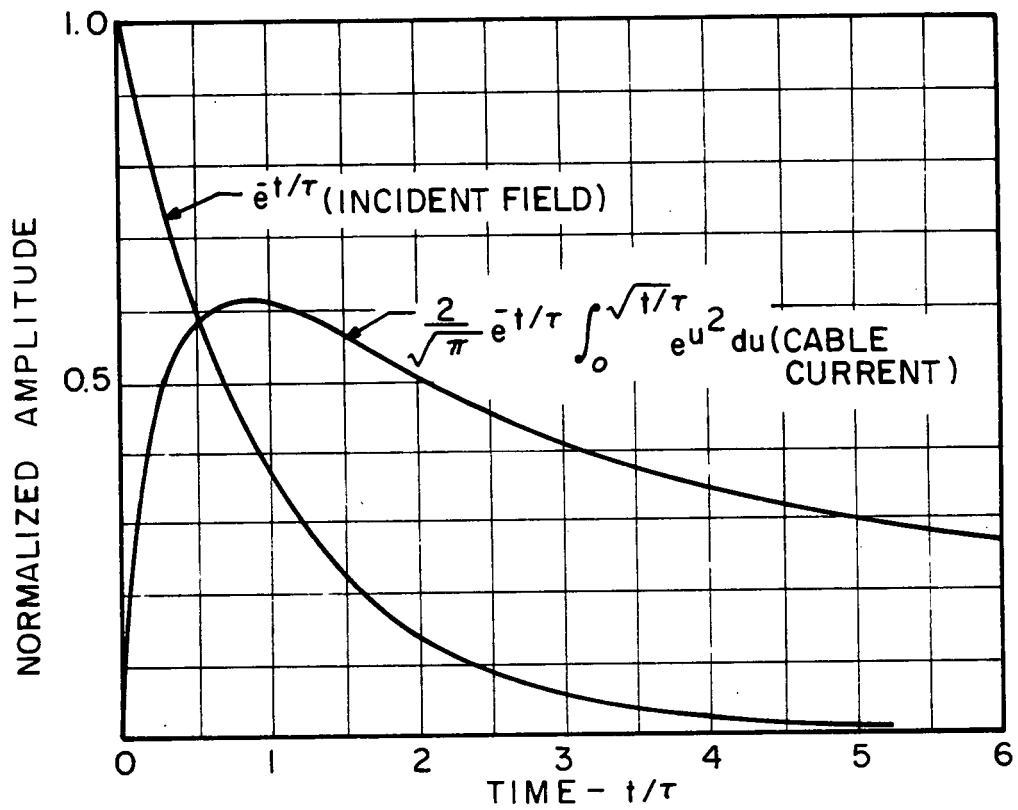
Fig. 31. Normalized waveforms of the incident field and cable current as functions of time [21].
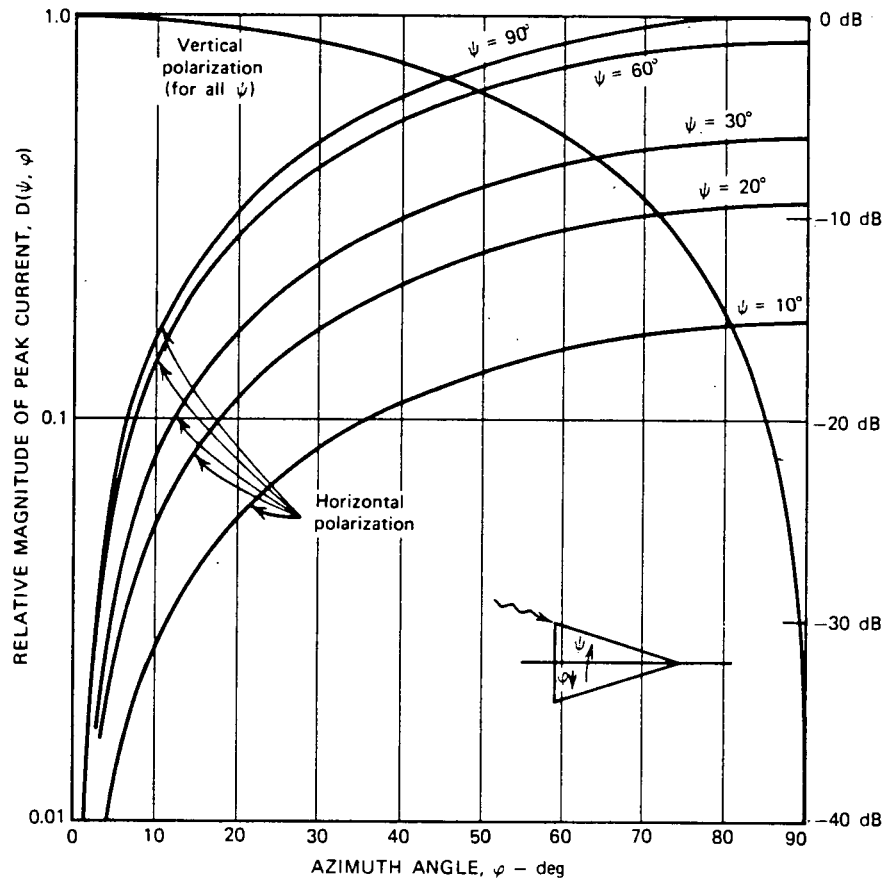
Fig. 32. Variation of peak conductor current as azimuth (φ) and elevation (ψ) angles of incidence change [21].

to less attenuation of the induced current at low frequencies (since the coupling to the inner conductor is through the capacitance between it and the soil). At high frequencies, the admittance per-unit-length is dominated by the admittance of the soil. The two types of conductors will have approximately the same response.

Short Buried Conductors [21]

If the conductor is short electrically (few tens of meters in poor to average soils) with respect to a skin depth in soil for the frequencies of interest, it can be analyzed as an electrically short dipole in a finitely conducting medium. The current at the center of such a conductor of length ℓ is then given as:

$$I \simeq \frac{E_z \ell Y}{2} \tag{89}$$

where E_z is the field strength in the soil.

Y is the admittance of a center-fed dipole of length π and radius a

For $\sigma \gg \omega\epsilon$ we can write:

$$Y \simeq G \simeq \frac{\pi \sigma \ell}{2 \log \ell/a} \tag{90}$$

where σ is the conductivity of the earth

Then:

$$I \simeq \frac{\pi \sigma E_z \ell^2}{4 \log \ell/a} \tag{91}$$

Using Eq. (80) and (81), Vance gives the following relationships for the current in terms of a single exponential incident field of the form of Eq. (82):

$$I \simeq \frac{\pi \sigma A_0 \ell^2}{2 \log \ell/a} \tau_e \frac{\sqrt{j\omega}}{j\omega + \frac{1}{\tau}} \sin \psi \sin \phi \tag{92}$$

$$I \simeq \frac{\pi \sigma A_o \ell^2}{2 \log \ell/a} \quad \tau_e \frac{\sqrt{j\omega}}{j\omega + \frac{1}{\tau}} \cos \phi \qquad (93)$$

Equations 92 and 93 are for horizontal and vertical polarization respectively.

The waveform of the current at the center of the conductor is hence given by:

$$i(t) \simeq l_o \left[\frac{1}{\sqrt{\pi \tau t}} - e^{-t/\tau} \frac{2}{\sqrt{\pi}} \int_0^{\sqrt{t/\tau}} e^{u^2} du \right] (t > \tau_e) \qquad (94)$$

where

$$l_o = \frac{\pi \sigma A_o \ell^2}{2 \log \ell/a} \sqrt{\tau_e \tau} \; D(\psi, \phi) \qquad (95)$$

$$\tau_e = \varepsilon_o / \sigma \qquad (96)$$

$D(\psi, \phi) = \sin \phi \sin \psi$ (horizontal polarization)

$\qquad\qquad = \cos \phi$ (vertical polarization)

τ = Time constant of incident exponential field pulse.

Equation (94) is only valid for $t > \tau_e$ and gives the maximum current along the conductor [21].

3.2.1.5 Coupling to the Inner Conductors of Shielded Cables

Shielded cables are used for many applications in today's power systems. Some of these applications are found in energy delivery, communications, and control sub-systems. This subsection of the report describes the coupling of HEMP to the inner conductor of such cables, and, hence, this completes the coupling aspects to all kinds of conductors.

This subsection starts with the description of a transmission line model for the shielded cable, followed by a discussion on the transfer impedance and admittance of shield, followed by the responses of short

and arbitrary-length cables. A discussion on multi-shields and ferrormagnetic saturation concludes this subsection.

Transmission-Line Model

There are basically two types of shielded cables. The first kind is the type with a braided-wire shield, and the second is the type with continuous solid (with no cavities and no apertures) sheath. In both cases, however, the transmission-line model can be used to analyze the effects of an incident HEMP plane wave. In the case of the first type (shield with apertures), the transmission-line model will contain both distributed series voltage and shunt current sources, as in Fig. 33. In the case of the second type of shielded cables (with continuous shields) only the series voltage sources are present in the model.

Formulation of the Response

The differential element, dz, of the cable of Fig. 33 contains a distributed voltage source of the form:

$$V_z'(z) = Z_T \, I_0 \, (z) \tag{97}$$

where, $I_0(z)$ is the current in the shield, per Fig. 33a. Z_T is the transfer impedance of the shield.

The distributed current source is of the form:

$$J_z'(z) = -Y_T \, V_0(z) \tag{98}$$

where, $V_0(z)$ is the external voltage of the shield, per Fig. 33a. Y_T is the transfer admittance of the shield.

The inner conductor voltage V and current I are defined by the following two differential equations:

$$\frac{dV}{dz} + ZI = V_z'(z) \tag{99}$$
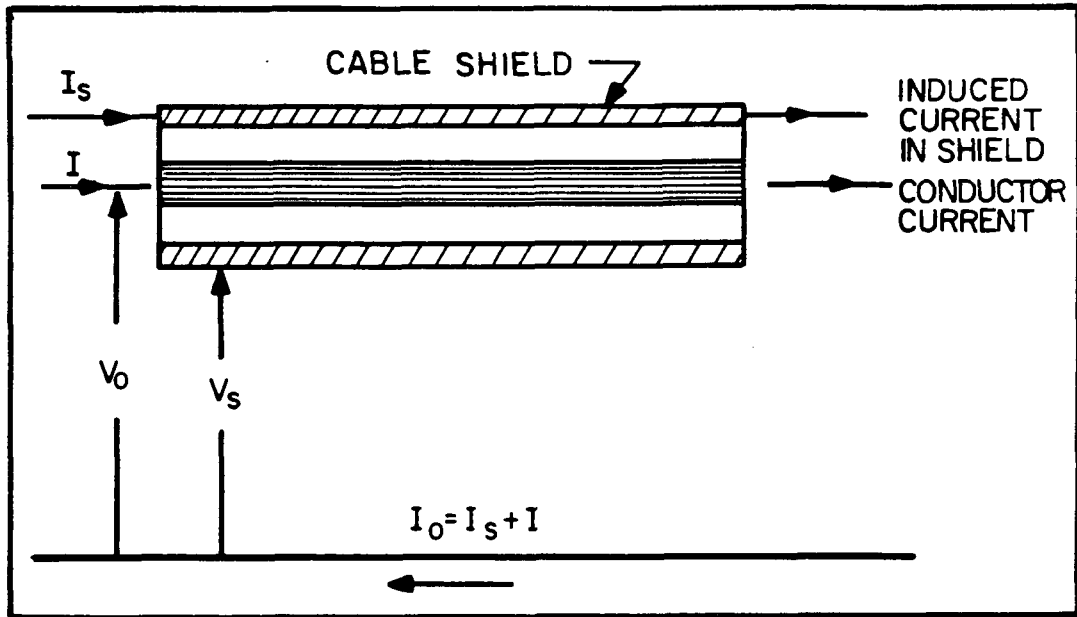
a) Cross section of a shielded cable
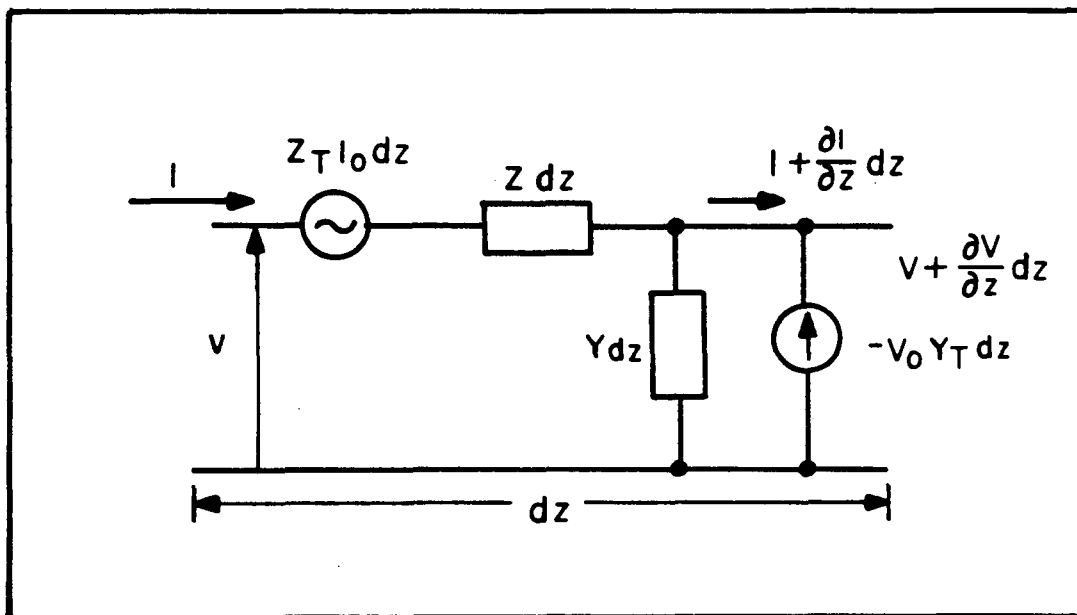
b) Equivalent circuit for the internal circuit when both the transfer impedance and the transfer admittance are included [13].

Fig. 33. Model for a shielded cable.

$$\frac{dI}{dz} + YV = J_z^{\prime}(z) \tag{100}$$

where, Z and Y are the series and shunt admittance per unit length, respectively. $V_z^{\prime}(z)$ and $J_z^{\prime}(z)$ are as defined in Equations (97) and (98) respectively.

In the case of a solid shield, $J_z(z)$ is negligible compared to $V_z^{\prime}(z)$.

The Transfer Impedance, Z_T

The transfer impedance of the shield depends on the characteristics of the shield and is the given by:

$$Z_T = \frac{1}{I_o} \left. \frac{dV}{dz} \right|_{I=0} \tag{101}$$

Where, I_o is the current in the shield.

$\frac{dV}{dz}$ is the voltage per unit length along the cable.

Z_T gives the open circuit voltage developed between the internal conductor and the shield for one ampere of shield current in a cable one meter long. In other words, Z_T, is the ratio of the voltage induced across the ends of a one meter cable divided by the current induced on the outside shield by the incident HEMP.

Properties of Z_T

For both types of shields, Z_T always contains a diffusion component which defines the longitudinal electric field inside the shield to the current on the finitely-conducting shield. For shields with apertures, there is also a mutual inductance term to account for the coupling to the inner conductor.

For solid shields, Schelkunoff [22] defines Z_T as follows:

$$Z_T = \frac{1}{2\pi a \sigma T} \frac{(1+j)T/\delta}{\sinh(1+j)T/\delta} \qquad (102)$$

whereby a is the outer radius of the shield.

T is the thickness of the shield.

δ is skin depth in the shield given by:

$$\delta = \frac{1}{\sqrt{\pi f \mu \sigma}} \qquad (103)$$

(μ and σ are the permeability and conductivity of the shield.)

Equation (102) assumes the following:

- a is small compared to the smallest wavelength of the incident field.
- σ is high (conduction current >> displacement current)

For low frequencies, $T/\delta << 1$ and Z_T is real and is given by:

$$Z_T \simeq \frac{1}{2\pi a \sigma T} = R_0 \qquad (104)$$

where R_0 is the dc resistance of the shield per unit length.

For high frequencies, $T/\delta >> 1$ and Z_T is given by:

$$|Z_T| = \frac{2\sqrt{2}\, e^{-T/\delta}}{2\pi a \delta \sigma} \qquad (105)$$

with a phase angle, $\theta_z = -\frac{T}{\delta} + \frac{\pi}{4}$

Figure 34 shows the variation of normalized Z_T as a function of T/δ. This figure indicates that as T/δ increases, $|Z_T|$ decreases implying that the higher the frequency the less coupling to the inner conductor of shielded cables.

An alternative expression for Z_T is given by Vance [13] as:

$$Z_T = \frac{R_0 \sqrt{j\omega\tau_s}}{\sinh \sqrt{j\omega\tau_s}} \tag{106}$$

where τ_s is the shield diffusion time constant given by:

$$\tau_s = \mu_0 \sigma T^2 \tag{107}$$

The Transfer Admittance, Y_T

The transfer admittance of the shield is dependent on both the characteristics of the shield and the surroundings of the cable. It is given by:

$$Y_T = -\frac{1}{V_0} \frac{dI}{dz} \Big|_{V=0} \tag{108}$$

where V_0 is as defined in Figure 33.
and:

$\frac{dI}{dz}$ is the current into the internal conductor from the surrounding of the cable.

Y_T gives the short-circuit current induced in the inner conductor of a one meter long cable when it is shorted to the shield at one end, and one volt is applied at the other end between the inner conductor and and the shield.
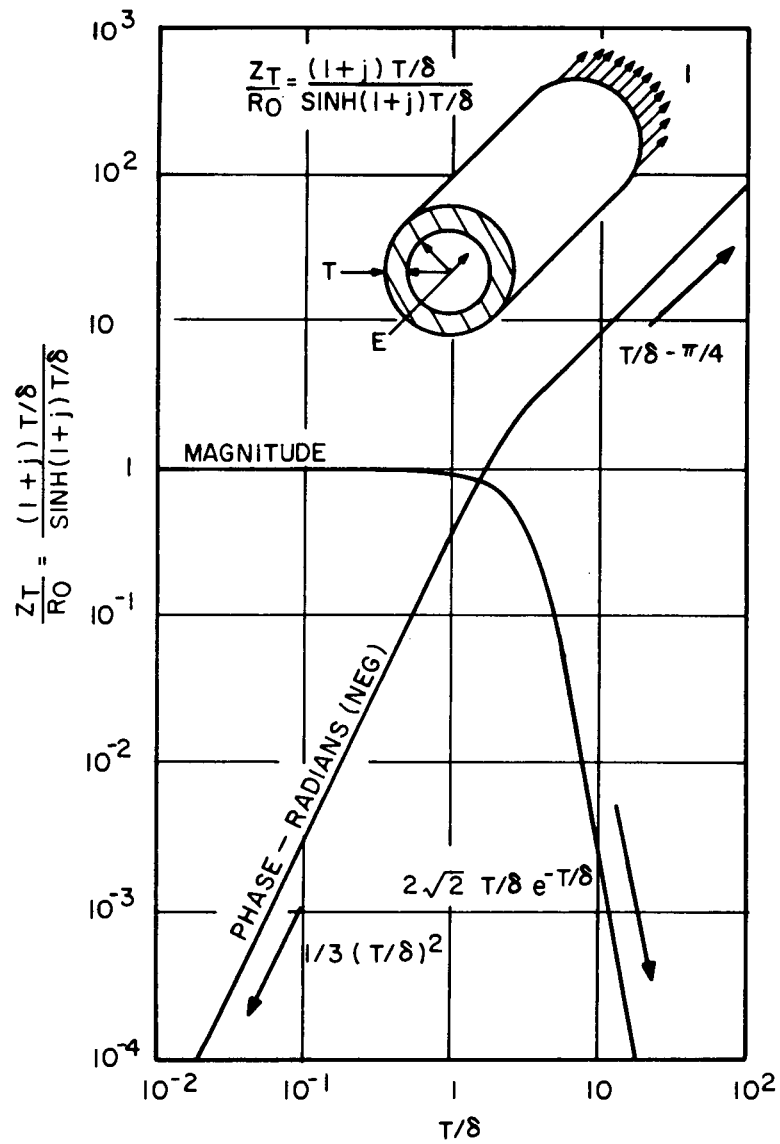
Fig. 34. Normalized transfer impedance for thin-walled solid cylindrical shields [13].

Properties of Y_T

For solid shields, Y_T is negligible. For braided wire shields, or those with apertures, Y_T contains a mutual capacitance term that accounts for the capacitance coupling between the inner conductor and the surroundings of the cable which serves as a return path for the shield current.

Response of Shielded Cables of Arbitrary Length

The response of cables that are not much shorter than the shortest wavelength of interest in the incident field is obtained by the transmission line method. Hence, Fig. 33 can be used here as a building block. The response of this transmission line problem can be most easily obtained by the method of superposition. Thus the total response of the cable is the sum of the response due to the distributed voltage and current sources along the cable, each considered separately. This is described below.

Response Due to Distributed Voltage Sources [13]

The solution of the transmission line equations for the inner conductor voltage and current can be written in the following form:

$$I_v(z) = [K_1 + P(z)]e^{-\gamma z} + [K_2 + Q(z)]e^{\gamma z} \qquad (109)$$

$$V_v(z) = Z_0 \ [K_1 + P(z)]e^{-\gamma z} - [K_2 + Q(z)]e^{\gamma z} \qquad (110)$$

whereby

$\gamma = \sqrt{ZY}$ is the propagation factor for the transmission line (formed of the inner conductor and the shield)

$Z_0 = \sqrt{Z/Y}$ is the characteristic (surge) impedance line:

$$P(z) = \frac{1}{2Z_0} \int_{z_1}^{z} e^{\gamma v} E_z(v) \ dv \qquad (111)$$

$$Q(z) = \frac{1}{2Z_0} \int_{z}^{z_2} e^{-\gamma v} E_z(v) \ dv \qquad (112)$$

$E_z(z) = I_0(z) \, Z_T$, where $I_0(z)$ is the current flowing on the shield induced by HEMP and Z_T is the transfer impedance of the shield.

The constants K_1 and K_2 are determined from the terminating impedances Z_1 at $z = z_1$, and Z_2 at $z = z_2$ (where $z_1 < z < z_2$) and are:

$$K_1 = \rho_1 e^{\gamma z_1} \frac{\rho_2 P(z_2) e^{-\gamma z_2} - Q(z_1) e^{\gamma z_2}}{e^{\gamma(z_2 - z_1)} - \rho_1 \rho_2 e^{-\gamma(z_2 - z_1)}} \qquad (113)$$

$$K_2 = \rho_2 e^{-\gamma z_2} \frac{\rho_1 Q(z_1) e^{\gamma z_1} - P(z_2) e^{-\gamma z_1}}{e^{\gamma(z_2 - z_1)} - \rho_1 \rho_2 e^{-\gamma(z_2 - z_1)}} \qquad (114)$$

where ρ_1 and ρ_2 are the reflection coefficients given by:

$$\rho_1 = \frac{Z_1 - Z_0}{Z_1 + Z_0} \, , \quad \rho_2 = \frac{Z_2 - Z_0}{Z_2 + Z_0} \qquad (115)$$

Response Due to Distributed Current Sources [13]

Similarly, the internal current and voltage, when the distributed current source $J(z,\omega) = -Y_T V_0(z,\omega)$ is acting alone, and $E_z(z,\omega) = 0$, are:

$$I_i(z) = \frac{1}{Z_0} \left[[K_{1e} + P_e(z)] e^{-\gamma z} - [K_{2e} + Q_e(z)] e^{\gamma z} \right] \qquad (116)$$

$$V_i(z) = [K_{1e} + P_e(z)] e^{-\gamma z} + [K_{2e} + Q_e(z)] e^{\gamma z} \qquad (117)$$

where

$$P_e(z) = \frac{Z_0}{2} \int_{z_1}^{z} J(v) e^{\gamma v} \, dv \qquad (118)$$

$$Q_e(z) = \frac{Z_0}{2} \int_z^{z_2} J(v)e^{-\gamma v} \, dv \qquad (119)$$

$$K_{1e} = \rho_1 e^{\gamma z_1} \frac{Q_e(z_1)e^{\gamma z_2} + \rho_2 P_3(z_2)e^{-\gamma z_2}}{e^{\gamma(z_2-z_1)} - \rho_1\rho_2 e^{-\gamma(z_2-z_1)}} \qquad (120)$$

$$K_{2e} = \rho_2 e^{-\gamma z_2} \frac{P_e(z_2)e^{-\gamma z_1} + \rho_1 Q_e(z_1)e^{\gamma z_1}}{e^{\gamma(z_2-z_1)} - \rho_1\rho_2 e^{-\gamma(z_2-z_1)}} \qquad (121)$$

Total Response of The Cable

The currents and voltages of Equations (109), (110), (116), and (117) are added together to get the total response of the cable:

$$I_{Total} = I_v + I_i \qquad (118)$$

and

$$V_{Total} = V_v + V_i \qquad (119)$$

Responses for Short Cables

For a cable with a length ℓ, where ℓ is much shorter than the shortest wavelength of interest, in the incident field that is terminated in impedances Z_1 and Z_2, the induced response at the two ends is given by [13]:

$$I_1 \simeq I_0 Z_T \ell \frac{1}{Z_1+Z_2} + V_0 Y_T \ell \frac{Z_2}{Z_1+Z_2} \qquad (120)$$

$$V_1 \simeq - I_1 Z_1 \qquad (121)$$

$$I_2 \simeq I_0 Z_T \ell \frac{1}{Z_1+Z_2} - V_0 Y_T \ell \frac{Z_1}{Z_2+Z_1} \qquad (122)$$

$$V_2 \simeq I_2 Z_2 \qquad (123)$$

Internal Responses of Short Cables with Solid Shields

For a short cable, the induced voltage, $V(\omega)$, across the inner conductor for an exponentially decaying shield current ($I_0 = I_m e^{-t/\tau}$) can be found given the transfer impedance, Z_T. From the previous section one can write $V(\omega)$ as follows:

$$V(\omega) = Z_T \, I_m \, \ell = \frac{R_0 \, \sqrt{j\omega\tau_s}}{\sinh \sqrt{j\omega\tau_s}} \, \frac{I_m}{j\omega + \frac{1}{\tau}} \, \ell \qquad (124)$$

In deriving Equation (124), it is assumed that the inner conductor and the shield are shorted together at one end, and open-circuited at the other. If the inner conductor and the shield are open circuited at both ends, half of the voltage given by Equation (124) will appear at either end between the two. In this case, however, these two voltages will be of opposite polarity.

The time domain inner conductor voltage waveform is given by Vance [21] as:

$$V(t) = \frac{I_m R_0}{2} \, \ell \left[\frac{\tau}{\tau_s}\right] \frac{1}{\sqrt{\pi}} \left[\frac{\tau_s}{t}\right]^{3/2} \sum_{n=1}^{\infty} \left[\frac{(2n-1)^2}{2t} \, \tau_s - 1\right] e^{\left[-(2n-1)^2 \frac{\tau_s}{4t}\right]}$$

$$\text{for } \tau \ll \tau_s \qquad (125)$$

$$V(t) = \frac{I_m R_0}{2} \, \ell \left[\frac{\tau}{\tau_s}\right] \frac{2}{\sqrt{\pi}} \left[\frac{\tau_s}{t}\right]^{1/2} \sum_{n=1}^{\infty} e^{\left[-(2n-1)^2 \frac{\tau_s}{4t}\right]}$$

$$\text{for } \tau \gg \tau_s \qquad (126)$$

The normalized waveforms of V(t), for different ratios of $\frac{\tau}{\tau_s}$, are illustrated in Figure 35. Table 5 presents the peak magnitude and rise time (t_{10-90}) of v(t) when the inner conductor is open circuited at both ends [21]. Typical values of τ_s and R_o for common shielding material are shown in Figures 5.7 and 5.8 of Reference [13].

Table 5

SHIELDING MATERIAL RESPONSE

Condition	Peak Open Circuit Voltage	Rise Time
$\tau \gg \tau_s$	$\dfrac{I_m R_o \ell}{2}$	$.236 \tau_s$
$\tau \ll \tau_s$	$5.9 \dfrac{\tau}{\tau s} \dfrac{I_m R_o \ell}{2}$	$.038 \tau_s$
$\tau = \tau_s$	$.77 \dfrac{I_m R_o \ell}{2}$	$.15 \tau_s$

Response of The Inner Conductor of A Buried Cable

The results of Section 3.2.1.4 of this report can be used in conjunction with the results presented in this section to calculate voltage between the inner conductor and shield of buried cables. The exciting HEMP waveform is considered to be a single exponential. The results apply to cable lengths which are short compared to the shortest wavelength penetrating the shield, but long compared to the skin depth, δ, in the soil. It is also assumed the inner conductor is open circuited at both ends (with respect to the shield) and the shield current is uniform. For the case of solid shields, Vance [21] gives the following expression for the voltage:

$$V(\omega) = \frac{I_o R_o \ell}{2} \sqrt{\frac{\tau_s}{\tau}} \frac{1}{(j\omega+1/\tau) \sinh \sqrt{j\omega\tau_s}} \qquad (127)$$
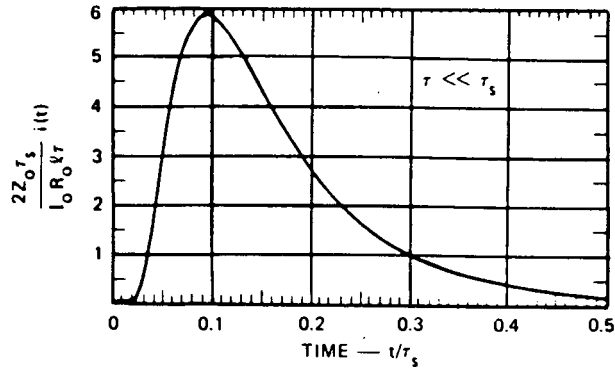
a) Impulse response
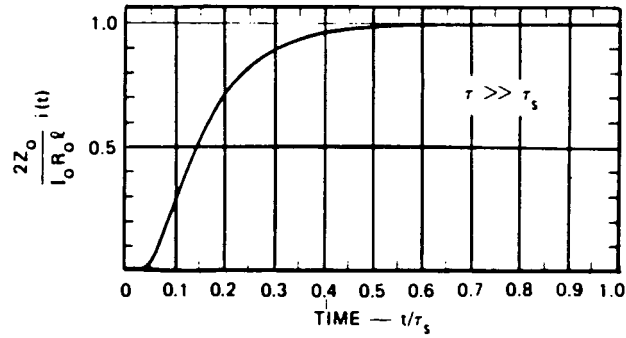
b) Step function response
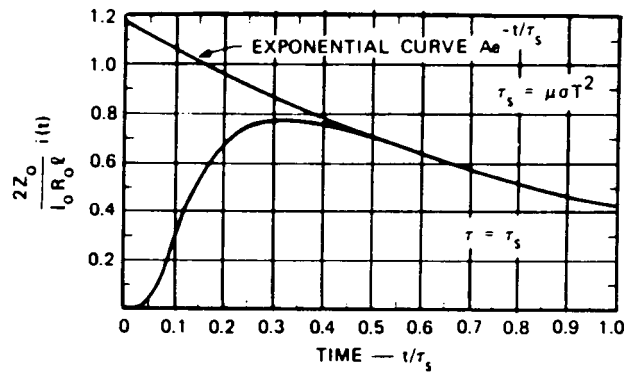
c) Exponential response

Fig. 35. Normalized voltage waveforms produced by an exponential pulse $I_m e^{-t/\tau}$ of current in the shield (normalized to $V_o/Z_o = I_m R_o \ell$) [21].

where:

$$I_0 = 10^6 \sqrt{\tau \tau_e} \quad E_0 \; D(\psi,\phi)$$

and

$$\tau_s = \mu \sigma T^2 \tag{128}$$

The time domain waveform is hence: (129)

$$v(t) = K \, e^{-t/\tau} \int_0^{t/\tau_s} \left[e^{(\tau_s/\tau)y} \sum_{n=1}^{\infty} \frac{n}{y^{3/2}} \; e^{-\frac{(2n-1)^2}{4/y}} \right] dy$$

$$\text{where } K = \frac{I_0 R_0 \ell}{2} \sqrt{\frac{\tau_s}{\pi \tau}} \tag{130}$$

The variation of $v(t)$ with respect to different $\frac{\tau_s}{\tau}$ is shown in Figure 36.

3.2.1.3 Time Domain Analysis

The analysis described in the previous sections does not take into account the presence of non-linear effects such as corona and flashovers. This section presents a time domain method of accounting for non-linearities.

Single Wire Above Ground

Consider the idealized problem geometry shown in Fig. 37a.. An above-ground transmission line of length L is located at a height h over a lossy ground. At the z=0 end of the line, there is a load impedance from the line to the ground, and, at this point, there is a supporting tower. The other towers supporting the line are assumed to occur at distances d_t, and are normally not connected electrically to the tower. However, when the line to tower voltage exceeds a critical flashover value, it is assumed that there is a conducting arc formed to the tower, and part of the EMP-induced energy is shunted to ground.
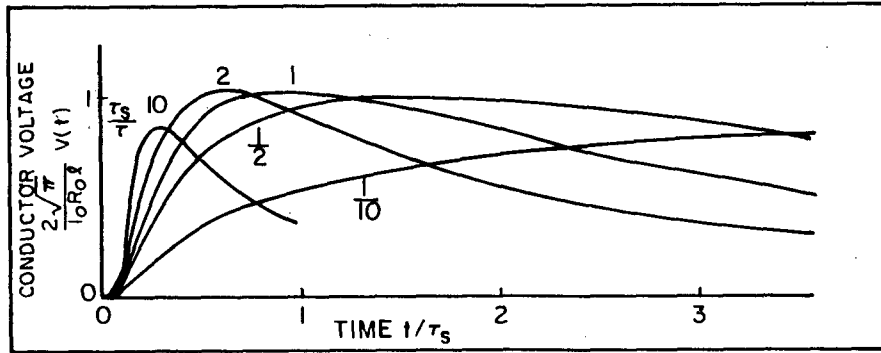
Fig. 36. Normalized induced voltage on the inner conductor
of buried cables for different decay time constants of a single
exponential incident field [21].
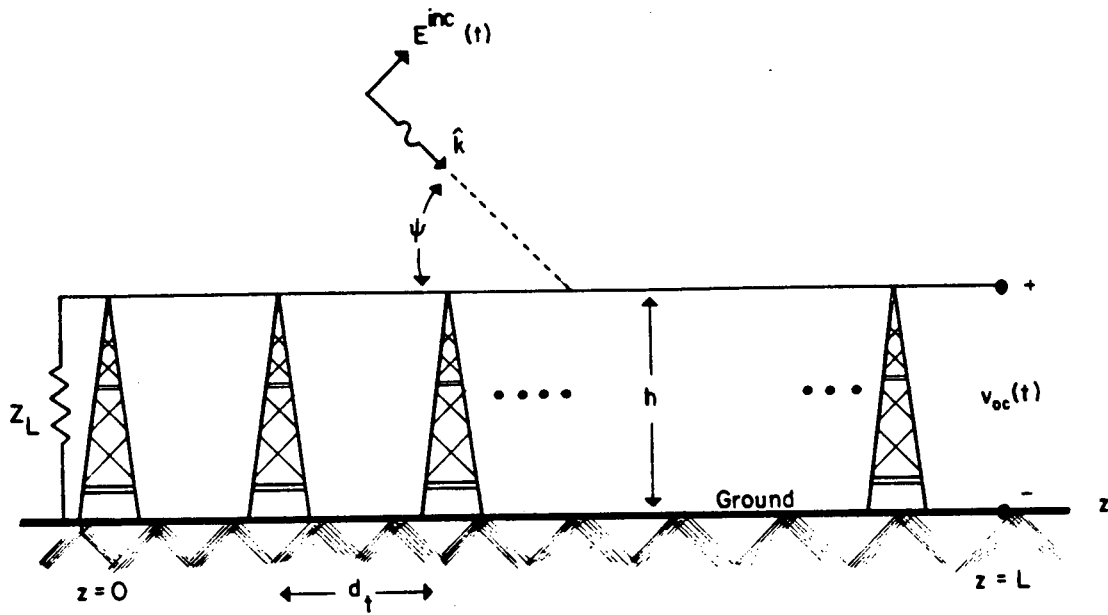
a) Simplified physical model
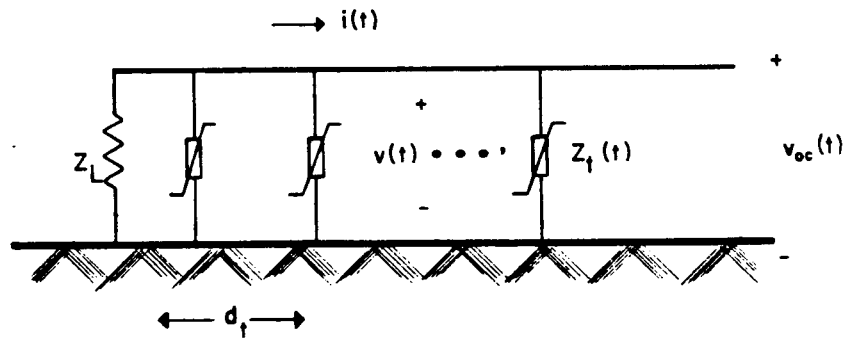
b) Electrical model

Fig. 37. Transmission or distribution line
with towers.

As in the previous sections, the open circuit voltage at the z=L end of the line is taken as a measure of the electrical behavior of the line. However, unlike the previous cases, this quantity (along with the corresponding input impedance), does not serve to uniquely determine the excitation for an arbitrary load on the line at this point, due to the fact that the line involves non-linearities. Hence, in the case of tower flashover, both the line and the actual load must be analyzed together. However, in this section, the same open circuit voltage response as determined in the previous section is computed so as to permit a comparison of results, and, hopefully, allow us to make some general statements regarding the importance of non-linearities on the system behavior.

For the line in Fig. 36a, a simple electrical model can be developed as shown in Fig. 36b. The line is assumed to be described by per-unit length inductance, resistance, capacitance, and conductance denoted by L', R', C', and G'. The effects of the towers are in the form of a time dependent impedance which is a virtual open circuit for line to tower voltages less than the tower flashover value, and a low impedance value, say on the order of the tower footing resistance, when the line voltage exceeds the critical voltage. Other, more detailed models for the tower flashover can be postulated, but it is sufficient in the present example to consider only the simple model.

The time dependent voltage and current along the line are solutions to:

$$\frac{\partial}{\partial z} v(z,t) + R'(z,t)\, i(z,t) + \frac{\partial}{\partial t} [L'(z,t)\, i(z,t)] = v_s'(z,t) \quad (131)$$

and

$$\frac{\partial}{\partial z} i(z,t) + G'(z,t)\, v(z,t) + \frac{\partial}{\partial t} [C'(z,t)] = i_s'(z,t) \quad (132)$$

Note that generally the line per-unit-length parameters, L', R', C', and G' may be functions of both position along the line, the time variable, as well as some other parameter, such as the local voltage or current on the line. Thus, developing a solution technique for

Equations (131) and (132) will permit the analysis of a large class of non-linear and time-dependent transmission line problems.

The direct time domain solution of Equations (131) and (132) have been treated by a number of investigators. For the special case when the per-unit-length coefficients of the line are constants, the method of characteristics [23] may be used to rapidly determine the voltage and current. However, when the line parameters vary in a non-linear fashion, such an approach is difficult to use. An alternate method is to simply develop a finite-difference representation for the two equations and "step" the solution along in time.

Using a first order differencing scheme, Equations (131) and (132) can be approximated as:

$$
i(z_i, t_i) = \left(\frac{R'(z_i,t_i)}{2} + \frac{L'(z_i,t_i)}{\Delta t}\right)^{-1}\left[\left(\frac{L'(z_i,t_{i-1})}{\Delta} - \frac{R'(z_i,t_{i-1})}{2}\right)i(z_i,t_{i-1})\right.
$$

$$
\left. + \frac{v(z_{j+1},t_j) - v(z_j,t_j)}{\Delta x} + \frac{v'_s(z_j,t_j) + v'_s(z_{j+1},t_j)}{2}\right] \qquad (133)
$$

and

$$
v(z_j,t_j) = \left(\frac{G'(z_j,t_j)}{2} + \frac{C'(z_j,t_j)}{\Delta t}\right)^{-1}\left[\left(\frac{C'(z_j,t_{j-1})}{\Delta} - \frac{G'(z_j,t_{j-1})}{2}\right)v(z_j,t_{j-1})\right.
$$

$$
\left. + \frac{i(z_{i+1},t_i) - i(z_i,t_i)}{\Delta x} + \frac{i'_s(z_i,t_i) + i'_s(z_{i+1},t_i)}{2}\right] \qquad (134)
$$

where Δz represents the spacing between the individual observation points along the line, and Δt is the spacing between time points. The space-time diagram shown in Fig. 38 illustrates the relation between the current and voltage on the line. The equation for the currents (Eq. 133) at points z_i and t_i are staggered both in time and space with respect to that for the voltage (Eq. (134)) which is written at points z_j and t_j.
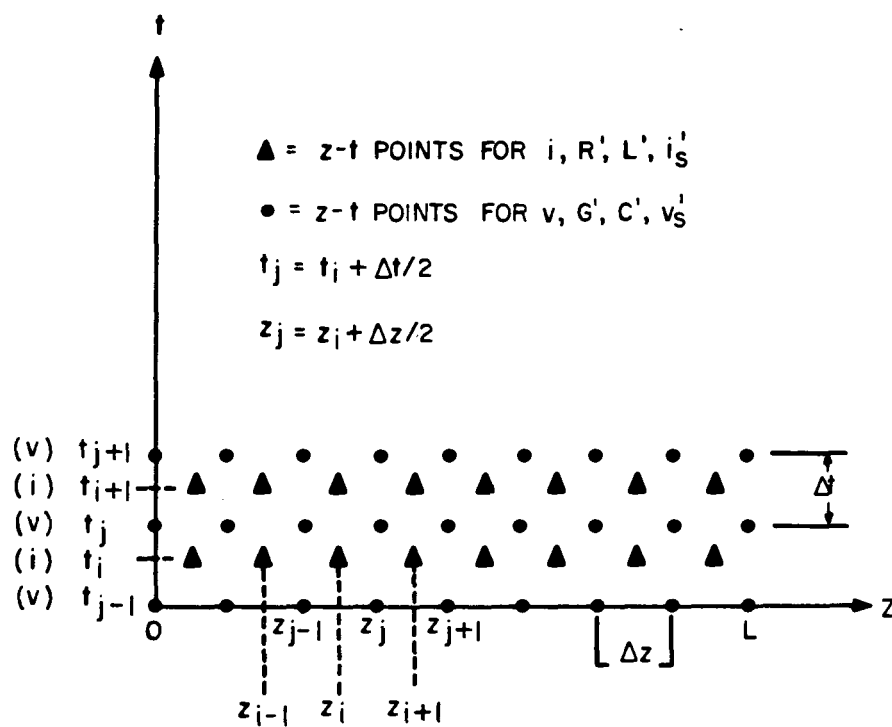
Fig. 38. Space-time diagram for finite-difference
solution of Equations (132) and (133).

Note that each equation has a source or excitation term. The current Eq. (133) has a distributed voltage source term and Eq. (134) has distributed current terms. In treating the excitation of a line by an incident EMP, one possible way to account for the coupling is to have a distributed voltage source on the line whose value is equal to the total incident tangential electric field (incident plus ground-reflected) on the line, as well as the lumped voltage sources at the conducting vertical elements of the line. Thus, in Eq. (134), the current source term is zero for the present problem.

The overall solution for the line voltage and current is obtained by stepping along in time, first solving Eq. (133) at a time t_i for all z_i by representing the equation as a sparse matrix equation and inverting it directly. Then, this solution is advanced by a time $\Delta t/2$ to t_j where the voltage equation is solved in a similar manner. For each equation, the values of the function (voltage or current) are related to the other quantity (current or voltage) through the boundary impedance conditions at both ends of the line.

This time marching process is repeated iteratively until the solution is completed. It is tempting to make the time steps Δt large, so that the overall solution is not time consuming and the late time behavior of the line response can be evaluated rapidly. It is well known, however, that for a convergent, stable solution of these equations, the time steps are constrained to be such that $\Delta t < \Delta z/v$, where v is the propagation velocity. This Courant condition effectively dictates the rate at which the transmission line solution develops in time; and, if a late time solution is desired, a considerable amount of computation time might be required.

Time Domain Multiwire Analysis

As in the case of a single wire line, it is possible to carry out an EMP coupling analysis of a multiconductor line directly in the time domain. Using a lumped parameter approach, a multiconductor line as illustrated in Fig. 39a can be represented through a complex interconnection of interwire capacitances, conductor inductances and
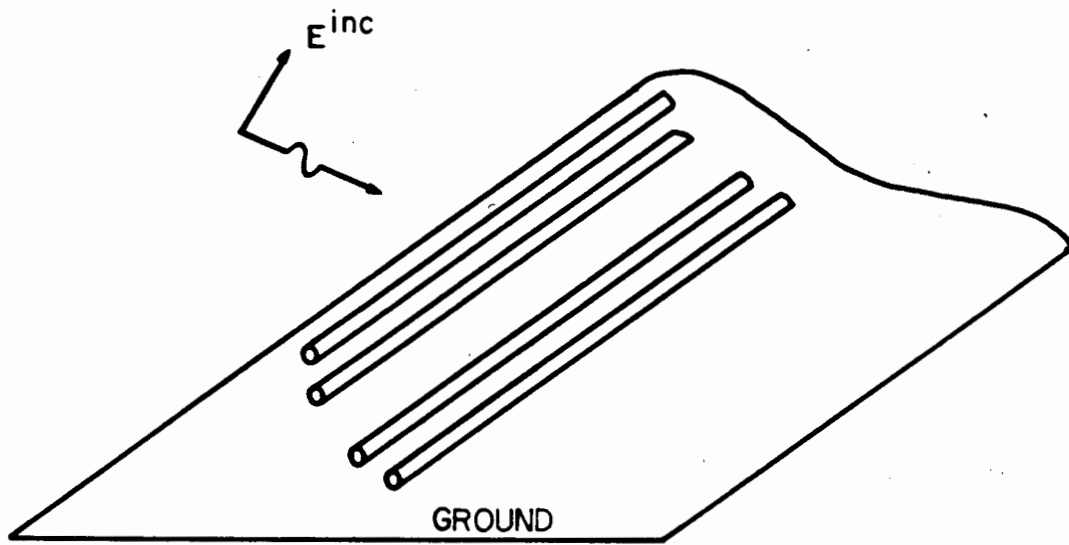
a) Multiconductor line over ground
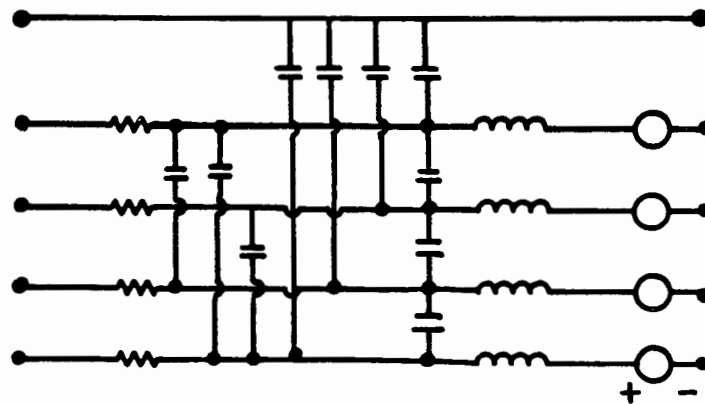
b) Per-unit-length lumped circuit model of
   four-wire multiconductor line. (Shunt
   conductances neglected)

Fig. 39. Multiconductor line (a) and LPN equivalent
circuit (b).

resistances, and distributed voltage sources representing the excitation of the line by the incident field. This is shown in Fig. 39b.

The transient behavior of this line can be evaluated by using a time marching approach similar to that used for the single wire line. Such calculations have been performed in the past, and the results agree well with those obtained by the frequency domain analysis methods. However, some difficulties arise in attempting to obtain a solution for late times, since the iterative "time marching" procedure can be very time consuming in terms of computer resources, and can become unstable.

It should be pointed out that this calculational method is similar to that used in the EMTP code which enjoys widespread use in the power community for computing the behavior of transients on power systems. This code, however, does not presently have the capability of treating distributed excitation sources along the lengths of transmission lines, a prerequisite for carrying out an EMP coupling analysis.

Thus, the use of EMTP in its present state is not recommended for EMP coupling studies. Either existing frequency domain coupling codes must be used or a time domain analysis procedure involving distributed sources similar to that previously described must be developed. However, the EMTP code may be useful in permitting an understanding of the propagation of EMP-induced transients on realistic line configurations as illustrated in Section 3.2.2.3.

Time Domain Network Analysis

As it is possible to envision carrying out a transient analysis of a single transmission line, it is also possible to think of analyzing an entire network in the time domain. Unfortunately, such an analysis on a network of reasonable size and complexity is difficult, due to the large number of unknowns required for the solution.

Consider a complex transmission line network consisting of a number of interconnected branches, each being modeled by a lumped parameter network as shown in Fig. 39. For a very large network, computer

resources could be severely taxed. Instead of performing a lumped parameter analysis on the lines, a time-dependent travelling wave analysis could be envisioned as described by Agrawal [24] in order to reduce the number of unknowns in representing the response of a single line segment in the network. However, as discussed in that reference, multiple reflections at all nodes in the network must be tracked in time, and the number of such reflected waves in the network grows exponentially as time progresses, rapidly exceeding the capability of existing computers.

In summary, it is clear that many problems exist with the analysis of transmission line networks, both in the time and the frequency domain. The frequency domain analysis models which have been discussed have the potential for treating the largest size of a distributed network, but cannot handle nonlinear behavior of components in the network. Time domain methods are costly to run, but can treat the nonlinearities.

In assessing an actual power system, it is desirable to avoid the complications introduced by considering EMP coupling to networks. This is achieved by using the critical line length concept to reduce to the size of the network required for analysis to (hopefully) a single line or to at least a simple, smaller network.

3.2.2 Examples of Transmission Line Solutions for Power System Applications

In this subsection several examples of numerical solutions to the equations developed in the previous subsections are presented for selected transmission line geometries and HEMP electromagnetic fields.

The results of the numerical solutions for many other single line above ground geometries and HEMP excitations are contained in Appendices B, C, and D and are summarized in this subsection.

The first example presented shows a comparison of solutions obtained with the transmission line approach and with antenna (scattering) theory.

3.2.2.1 Validation of Transmission Line Approach

References 13 and 21 present a comparison between the responses of a long conductor due to a step function of incident field as calculated by 1) Vance and Scharfman using the transmission-line method [25] and, 2) more exact method used by Flammer and Singhaus [26]. Figure 40a compares the results of the two methods for vertical polarization, azimuthal angle of incidence, $\phi = 0$ and elevation angle of incidence, ψ. Figure 40b compares the results of the two methods for horizontal polarization.

Figure 41 shows a comparison of the early time results obtained with the transmission line method and the more exact antenna theory used by Lee [10]. The two figures show that, for early time, the transmission line approach is remarkably accurate for nongrazing incident elevation angles. For small incident elevation angles and highly lossy ground the two results do not compare as well.

The transmission-line approach seems to give good results at early time where the concept of the transmission line surge or characteristic impedance does not strictly apply for the following reasons according to Scharfman and Vance [25]:

1. The field strength of the wave scattered from the wire and reflected back to the wire by the ground is small so that the current it induces in the wire is small compared to that induced by the incident field.

2. In the frequency spectrum of a pulsed incident electric field with a rise time of about 5ns, the scattering impedance (i.e., the ratio of the tangential component of the incident electric field to the current induced in the wire) is nearly equal to twice the characteristic impedance, Z, of the wire above ground. Hence, the induced current is almost the same whether viewed in early times as a transmission line (low frequency model) or as a scattering cylinder in space. For faster rise times of the incident field, the transmission line approach would lead to lower responses due to the fact that the scattering impedance is less than 2Z.
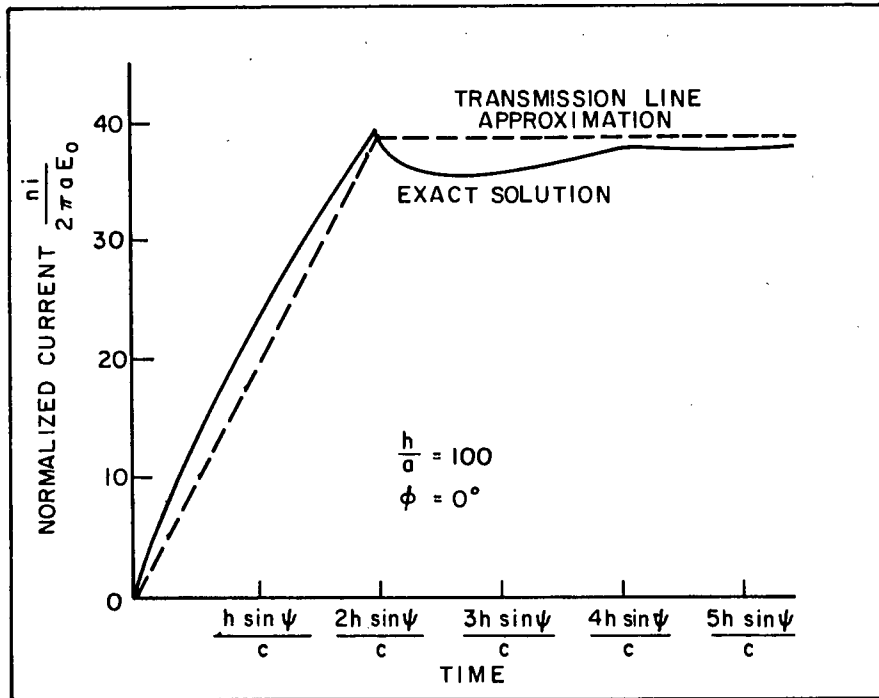
Figure. 40a. Comparison of the transmission-line approximation and the exact solution for the current in a wire over a perfectly conducting ground plane -- step-function incident field, vertically polarized [13].
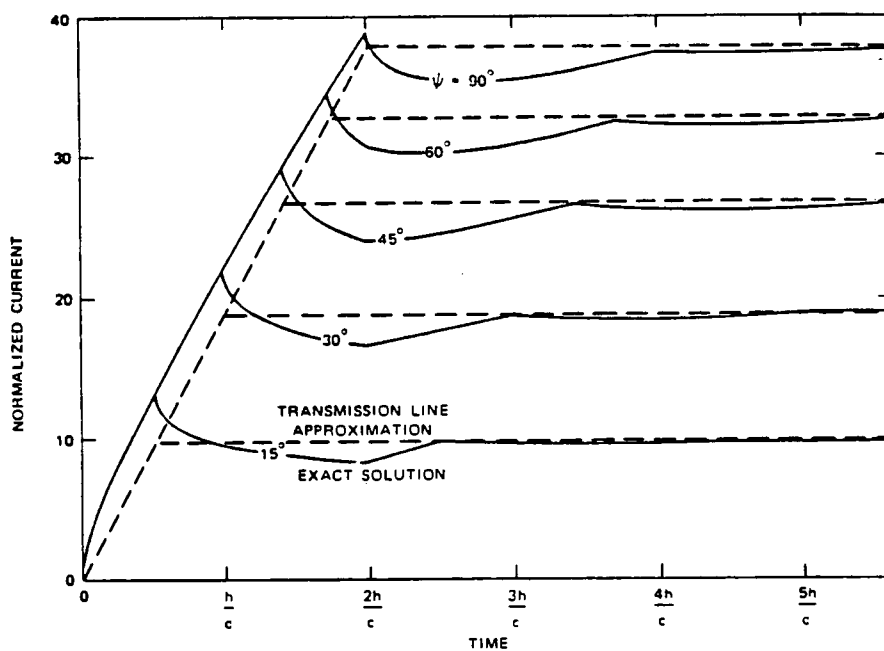
Fig. 40b. Comparison of the transmission-line approximation and the exact solution for the current in a conductor over a perfectly conducting ground plane -- step-function incident field, horizontally polarized [21].
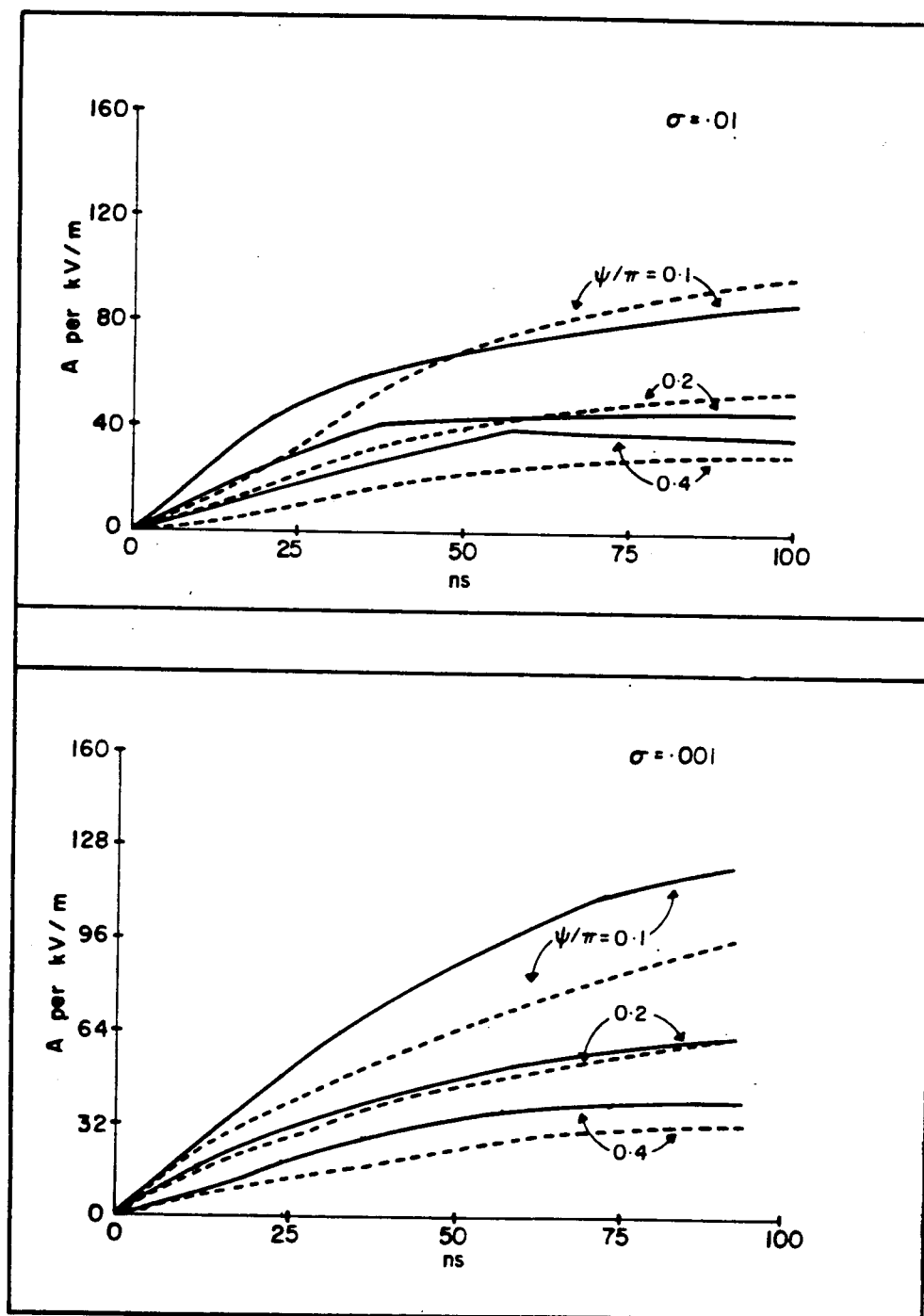
Fig. 41. Comparison of early time HEMP-induced current on a long conductor 2mm in radius and 9m over a lossy ground with different conductivities (E_r=10) polarization as calculated by antenna theory (solid line) and the TEM approach (dashed line); vertical polarization of EMP assumed.

It can be concluded from the above that the transmission line approach is sufficiently accurate for engineering purposes to calculate the response of conductors to HEMP. The accuracy of the response for late time is much better than that for early time HEMP.

3.2.2.2 Response of A Single Line Above Ground to Vertically Polarized Fields

The effects of variations in parameters such as line orientation, angle of incidence, soil resistivity, waveshape of the applied HEMP electromagnetic field, and line length for a single horizontal line above ground are shown in Section B.2 of Appendix B. A vertically polarized wave was used in these examples since this polarization generally produces a larger response (voltage or current) [5].

Section B.3 shows how HEMP fields can be separated into their horizontal and vertically polarized components, the response calculated for the two components separately, and the total response determined by combining the responses for the two components. This approach works if the system is linear.

Section B.4 gives the response of transmission lines at eight different geographic points for a HEMP burst at a specific location. The actual HEMP fields that would be produced at these points per currently available information is used in calculating the responses at these points. The response at one of the points is calculated for an assumed intermediate time HEMP waveform.

In Section B.5 a time domain solution is shown that takes into account the effects of transmission tower flashovers.

3.2.2.3 Response of Multiple Lines Above Ground to Vertically Polarized Fields

Numerical solutions for selected multiconductor geometries and HEMP excitations are presented in Appendix C.

Frequency domain solutions are presented in Section C.2. These solutions show the effect of shield wires and line terminations on the response of multiconductor lines.

Scattering theory solutions for multiconductor transmission lines are presented in Section C.3. These solutions are shown only for the early time period (t<100ns) because of the difficulty in obtaining solutions for longer time periods.

In Section C.4 a method for using a time domain multiconductor solution, which does not include distributed voltage sources to estimate the effect of shield wires and multiconductor propagation on the HEMP response of multiconductor transmission lines, is given.

In Section C.5 an approximate method for determining the effect of shield wires and multiconductor propagation on the HEMP response is presented.

3.2.2.4 Response of Buried Conductors

Numerical examples for responses of buried conductors are presented in Appendix D. Responses for various combinations of HEMP waveforms, burial depths, and soil conductivities are shown.

3.2.2.5 Conclusions and Summary on The Coupling of
HEMP to Conductors

The following can be concluded from the preceding Section 3.2.

Above Ground Non-Shielded Conductor

1) The transmission-line method can be used to predict accurately the behavior of above ground conductors. There seems to be some discrepancies between this method and the more rigorous methods for highly lossy grounds (.001 mhos/m conductivities and lower) and for small angles of incidence ($\Psi<36°$).

2) Effect of waveshape of the incident electric field:

Lossy Earth

● Neglecting corona, the response of conductors are directly proportional to the magnitude of the incident electric field.

● The tail of the incident electric field is critical in the determination of the peak and the waveshape of the response of the conductors. Both the peak magnitude and tail of the response increase with an increase in the tail of the incident field.

● The front of the incident electric field is only critical in determining the initial rate of rise of the response of conductors. The peak magnitude of the response is a weak function of the front of the incident electric field. Hence, a zero front (single exponential) waveshape is a good approximation of the incident electric field.

Perfect Earth

● The effect of a longer tail in the incident field is only manifested as a longer tail of the response leaving the peak magnitude of the response unchanged.

● The effect of the front of the incident field is minimal.

3) Effect of the height above ground for power transmission lines

● The response of above ground conductors increases with increasing height.

● The incremental increase of the response of conductors with height is more pronounced in the case of more conductive grounds (.1 mhos/m or better).

● The use of perfect ground ($\sigma = \infty$) is a good approximation for calculating the response of conductor 7 m or more above lossy grounds of .1 mhos/m or better conductivities.

4) Effect of ground conductivity

- The peak and the time-to-peak of the response of above ground conductors increases with decreasing ground conductivity.

- The ground effect becomes more important than the height effect as the ground becomes less conducting (typically for ground conductivities of .01 mhos/m or less).

- The effect of ground is more pronounced for vertical polarization compared to horizontal polarization.

5) Effect of angles of incidence

- The response of above ground conductors increases with decreasing elevation and azimuth angles of incidence.

6) Effect of polarization of the incident HEMP

- Vertical polarization of the incident HEMP wave yields the largest response.

- Assuming linearity, the response to arbitrary polarization can be obtained by superimposing the responses of the vertically and horizontally polarized components.

7) Effect of length

The time peak and time-to-peak of the response of conductors remains unchanged from those of the long (semi-infinite) conductor cases if the length, L, satisfies the following relationship:

$$L > \frac{ct_p}{1 - \cos \Psi \cos \phi}$$

where c is the speed of light, tp is the time-to-peak for the long conductor case, and Ψ and ϕ are the angles of incidence.

8) Flashovers between conductors and ground (or grounded structures, as in the case of transmission and distribution line flashovers to towers) act to isolate the conductor into segments. The results of each of these

segments is then estimated independently by assuming a short circuit at the flashover points. The rigorous determination of the response of the conductor requires detailed modeling of the arc characteristics and the impedance to ground (e.g., the tower surge impedance).

Underground Non-Shielded Conductors

1) The transmission line analysis method can be applied to determine the response of such conductors to HEMP.

2) Effect of waveshape:

   The loss in the ground tends to broaden the transmitted fields into it, hence, the actual fields at the buried conductor are very weakly dependent on the details of the very early time of the incident field. As in the case of above ground, the response of underground conductor is a strong function of the late time characteristics of the incident field.

3) Effect of ground conductivity:

   The induced response is nearly proportional to the inverse square root of the conductivity of the earth.

4) Effect of the burial depths:

   The response of underground conductor decreases, as expected, with increasing burial depths. The effect of ground conductivity for highly conducting grounds is however more pronounced than the depth effect (responses of conductor with buried depths of up to 5 m are nearly identical for σ = .001 mhos/m). As the ground becomes less conducting, the effect of buried depth dominates.

5) Effect of angles of incidence:

   The response of underground conductors increases with increasing elevation and azimuth angles of incidence for horizontal polarization. For vertical polarization, the response increases with decreasing azimuth angle.

Summary

In any actual assessment of power systems, the use of the worst-case electric field (magnitude and waveform) may lead to over pessimistic results. The response of a conductor is a strong function of the

assumed electric field and its characteristic. Care should be taken in specifying the electric field environment in order to have realistic results. Different points in the power system have greatly differing responses for the same HEMP event. This fact should not be overlooked in assessments.

3.3 Antenna Coupling Models

Antennas and antenna-like structures are found throughout the power system. By virtue of their designed function, "deliberate" antennas are found in the communications subsystems which serve to transmit voice or digital data for the operation of the system. In addition, "inadvertent" antennas exist which interact with the incident EMP in the same manner as does a deliberate antenna, and hence may be analyzed in the same manner as an antenna. Examples of such inadvertent antennas are the short vertical conductors connecting power equipment to a transmission or distribution line and short horizontal conductors in a switch assembly. In both of these cases, either a transmission line model or an antenna model could be used for estimating the EMP response.

3.3.1 Description of Antenna Types

There are many different types of antennas, and some are more susceptible to EMP excitation than are others. An antenna may be viewed as a simple matching transformer which transforms the impedance of the final stage of a transmitter or receiver to the impedance of free space, so as to maximize the efficiency of energy transmission.

Because electromagnetic radiation is possible over a wide range of frequencies, as illustrated in Table 6, there are many different designs for antennas. Those antennas designed to operate in the MF and HF frequency ranges are usually most affected by EMP, since their operating frequencies occur in a band where the EMP signal has a strong spectral content. However, in an assessment of a system, all energy gathering

antennas should be examined for possible adverse effects. Examples of antennas commonly used for the various frequency bands are contained in Appendix E.

3.3.2 Analysis of EMP Excitation of Antennas

In attempting to determine the effect of EMP on an antenna and its related communication gear, an approach similar to that used for understanding the transmission line response to EMP is used. A simple Thevenin equivalent circuit as shown in Fig. 42 is developed to represent the open circuit voltage and the antenna input impedance as seen at the terminals of the antenna. These electrical quantities are then used to excite the load circuitry to determine the overall system response.

Electrically Small Antennas

For monopole type antennas which are electrically small compared to the wavelengths contained in the EMP signal, it is possible to develop a relatively simple expression for the EMP excitation [27]. Figure 43 shows the geometry for this antenna, which could represent a typical blade antenna on a vehicle. As discussed in [1] the open circuit Thevenin voltage for this class of antennas can be represented through an equivalent electrical height as:

$$V_{oc}(\omega) = h_e \, E_n(\omega) \tag{135}$$

and the input impedance is expressed as:

$$Z_{in}(\omega) \quad \frac{1}{j\omega C_a} \tag{136}$$

where C_a is the effective capacitance of the antenna, and may be easily calculated or measured. The effective height h is expressed as:

Table 6

FREQUENCY BANDS

Band Number	Frequency Range		Metric Subdivision		Frequency Nomenclature
4	3-	30 kHz	Myriametric waves	VLF	Very-low frequency
5	30-	300 kHz	Kilometric waves	LF	Low frequency
6	300-	3,000 kHz	Hectometric waves	MF	Medium frequency
7	3,000-	30,000 kHz	Decametric waves	HF	High frequency
8	30-	300 MHz	Metric waves	VHF	Very-high frequency
9	300-	3,000 MHz	Decimetric waves	UHF	Ultra-high frequency
10	3,000-	30,000 MHz	Centimetric waves	SHF	Super-high frequency
11	30,000-	300,000 MHz	Millimetric waves	EHF	Extremely-high frequency
12	300,000-3,000,000 MHz		Decimillimetric waves	---	---
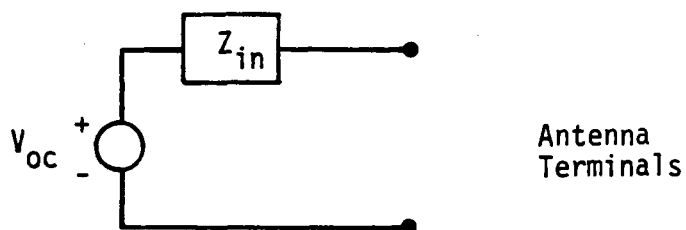
Fig. 42. Thevenin equivalent circuit for an antenna.
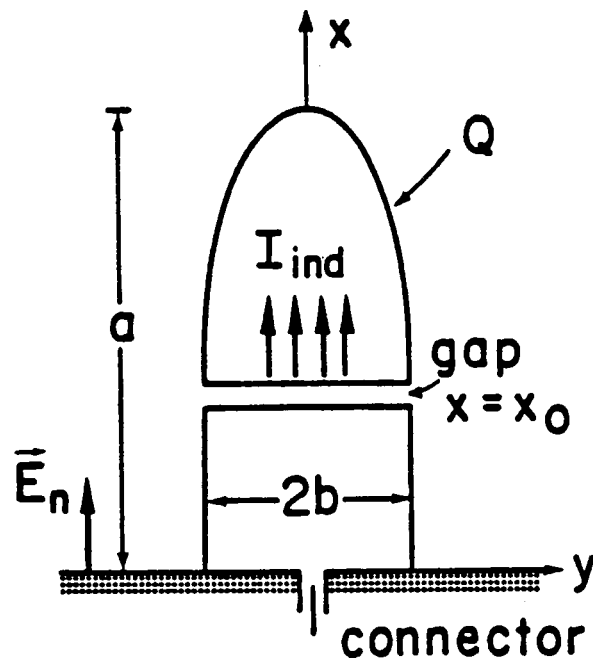
Fig. 43. Illustration of a typical monopole antenna.

$$h_e = \frac{\varepsilon_o A_{eq}}{C_a} = \frac{\varepsilon_o}{C_a} \frac{\pi abm}{(1-m)} \frac{(1-x_o^2/a^2)}{K(m)-E(m)} \tag{137}$$

where $m = (1 - b^2/a^2)$, and $K(m)$ and $E(m)$ are the complete elliptical integrals.

At times, such simple looking blade antennas can be deceptive, due to complicated internal impedance matching circuitry. For example, Fig. 44a shows a real UHF communications antenna with the internal structure indicated. Figure 44b presents the equivalent electrical circuit as seen at the antenna terminals. Note that the admittance element Y_a and the current source I_{ind} are directly related to the open circuit voltage and external impedance through a Thevenin to Norton transformation. The resulting input impedance and effective height of this antenna are illustrated in Fig. 45. Note that in the 0 to 100 MHz frequency range where the EMP spectral content is the greatest, the equivalent height of this antenna is small, indicating that this small antenna is not highly excited.

Due to the diversity of this class of antennas, it is difficult to give one simple equation which is valid for all electrically small antennas. However, the concept discussed above of developing an input capacitance and an equivalent height is generally valid for all such antennas. Details of the analysis, however, need to be worked out on a case-by-case basis for the individual antennas found in the power system.

Resonant Antennas

For antennas whose size is on the order of the wavelengths contained in the EMP portion of the spectrum, a different modeling approach for the EMP response has been developed. This applies to antennas having characteristic linear dimensions on the order of 3 meters or so, such as the HF antennas described previously.

(a)

metal

dielectric

8.7

22.9

stub

A

B

all dimensions
in centimeters

(b)

A ⊢1.5⊣ ←——3.7——→ ⊢1.5→ C_e

$\epsilon_r = 2.55$ $\epsilon_r = 2.55$ $\epsilon_r = 2.55$
50.0 Ω   85.2 Ω   27.8 Ω

L C_p Y_a I_{ind}

B

L = 27.6 nH, C_p = 1.5 pF, C_e = 18.2 pF
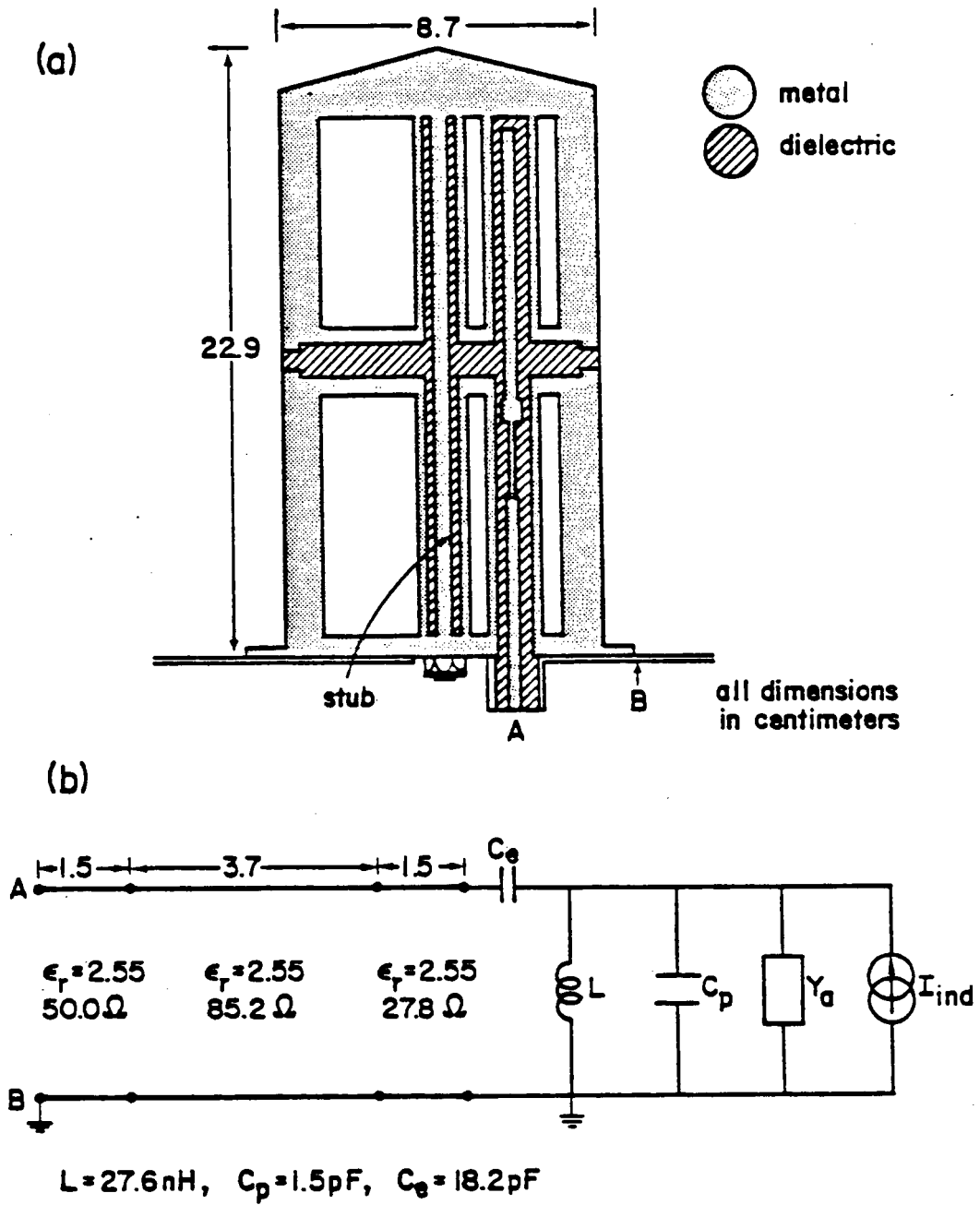
Fig. 44. Schematic diagram and equivalent circuit of
the UHF Communication Antenna.
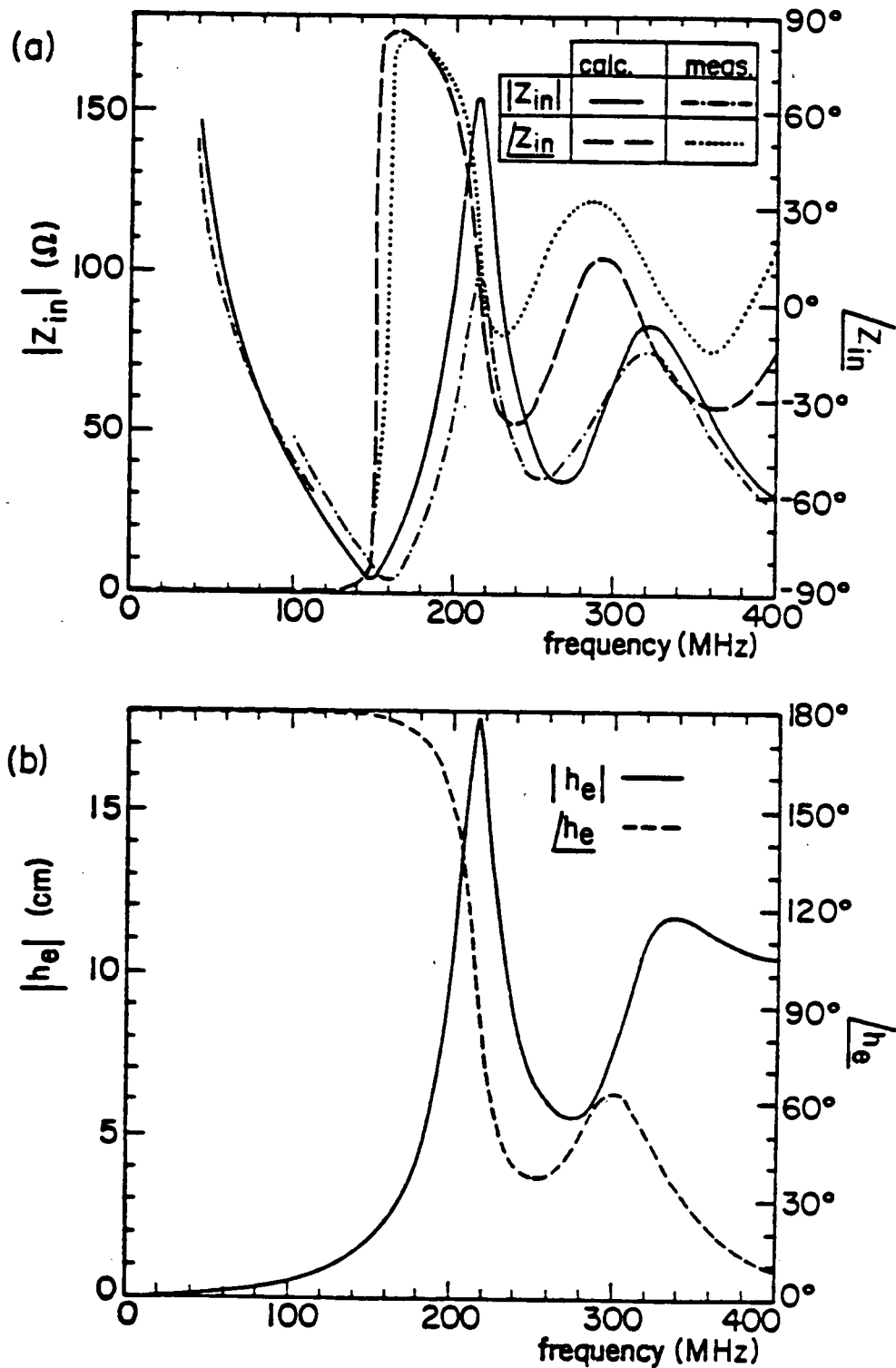
Fig. 45. Input impedance and effective height of the UHF Communication Antenna (225 - 400 MHz).

Figure 46 shows two simple models used for estimating the EMP-induced open circuit voltage for a wide variety of practical antennas. Using analysis concepts developed from the Singularity Expansion Method (SEM) [28], [29], simple expressions for the frequency domain short circuit current and input admittance at a point x on the dipole can be written as [30].

$$I_{sc}(s,x) = \sum_{\alpha} \frac{s\beta_{\alpha} \ \eta_{\alpha}^{(s)} \ M_{\alpha}(x)}{s_{\alpha}(s_{\alpha} - s_{\alpha})} \tag{138}$$

and

$$Y_{in}(s,x) = \sum_{\alpha} \frac{s\beta_{\alpha} \ \eta_{\alpha}^{(a)} \ M_{\alpha}(x)}{s_{\alpha}(s_{\alpha} - s_{\alpha})} \tag{139}$$

In these expressions, the following terms are defined:

s = $j\omega$ = complex frequency

α = $\pm 1 \to \pm\infty$ = summation index

s_{α} = $j\omega\pi L/c$ = natural frequencies

$M_{\alpha}(x)$ = $\sin(\alpha\pi x/L)$ = natural modes

β_{α} $\dfrac{4\pi C}{Z_0 L\Omega}$ = normalization constant (independent of α)

Ω = $2\ln(sh/a)$ = antenna factor

$\eta_{\alpha}^{(a)}$ = $\sin(\alpha\pi x/L)$

$$\eta_{\alpha}^{(s)} = \frac{E_0 \sin\theta_i \ cs_{\alpha}}{j(s^2 \cos^2 \theta_i - s_{\alpha}^2)} \left[1 - (-1)^{\alpha} \ e^{\frac{sL}{c} \cos\theta_i} \right]$$

The term $\eta_{\alpha}^{(s)}$ is referred to as a coupling coefficient for the coupling problem, and $\eta_{\alpha}^{(a)}$ is the corresponding coupling coefficient for the driven antenna problem, providing the input impedance.

Once these Norton equivalent circuit elements have been defined, the Thevenin equivalent voltage may be defined as:

$$V_{oc}(s) = I_{sc}(s)/Y_{in}(s) \qquad (140)$$

and the input impedance as:

$$Z_{in}(s) = 1/Y_{in}(s) \qquad (141)$$

To illustrate a typical response of an antenna to HEMP, consider the case of a center-fed dipole antenna of the type shown in Fig. 46a having a total length of 10 meters, and a radius of 1 cm. This antenna is assumed to be excited by the Bell Waveform described in Section 2, with an angle of incidence of 45 degrees. The application of the above expressions to the calculation of the input admittance and the short circuit current spectrum provide the results shown in Fig. 47. Note that the input admittance varies with frequency in a manner similar to that of a transmission line. The time domain response for the short circuit current is obtained by taking the inverse Fourier transform of the data in Fig. 47b, and this is shown in Fig. 48. Note that the peak current is on the order of 500 amps with a rise time of about 0.03 microseconds. The equivalent Thevenin quantities can be calculated using Equations (140) and (141) above.

In the case of the monopole antenna located above a lossy earth, the excitation field E_{tan}^{inc} (x) used to compute the coupling coefficient consists of the incident field plus a ground-reflected field. This reflected field can be computed using the plane-wave reflection coefficients in order to evaluate the antenna response in this case.

Microwave Antennas

The final antenna category to be discussed in relation to the EMP coupling process is the microwave antenna. A commonly used antenna

a. Isolated dipole
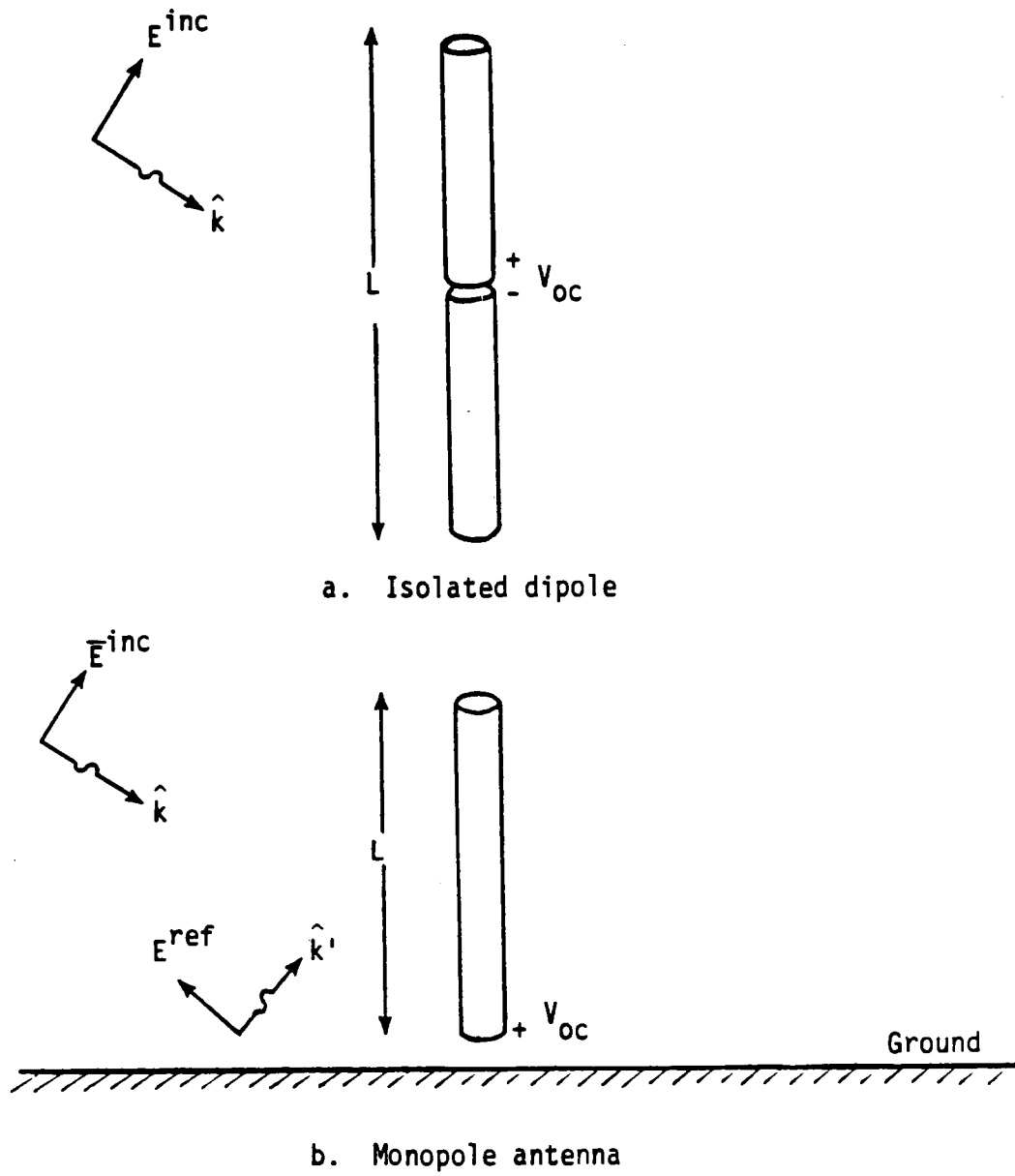
b. Monopole antenna

Fig. 46. Simplified models for resonant antennas.
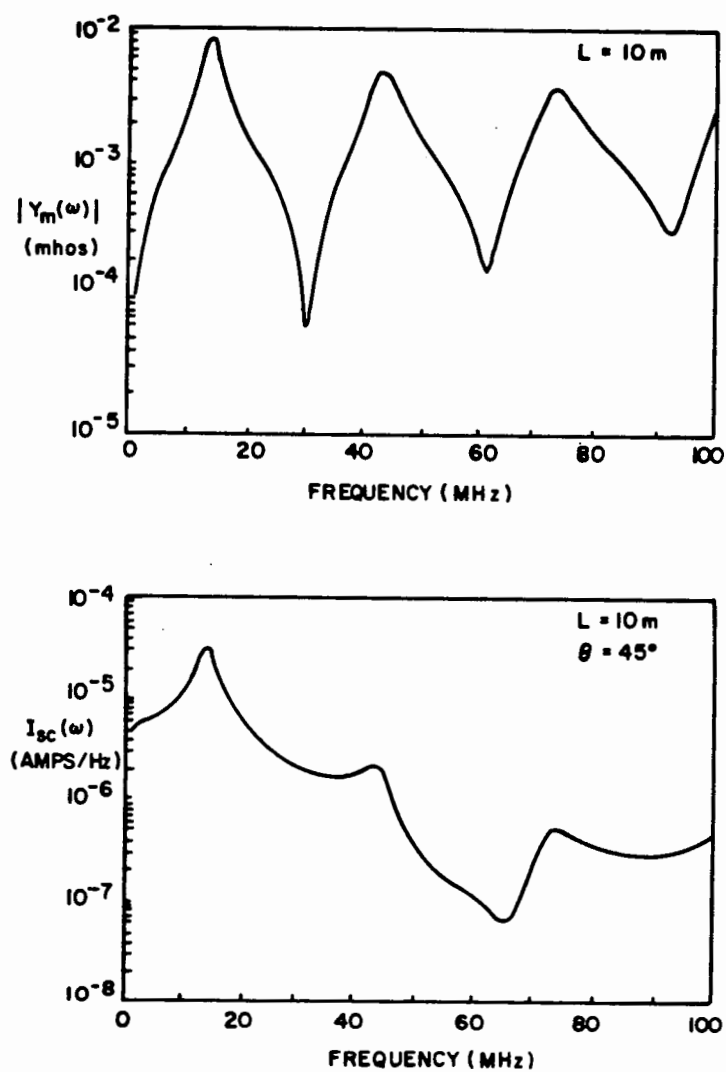
Fig. 47. Input admittance (a) and short circuit current
spectrum (b) of a center-fed dipole antenna or radius
a = .01 m and length L = 10 m.
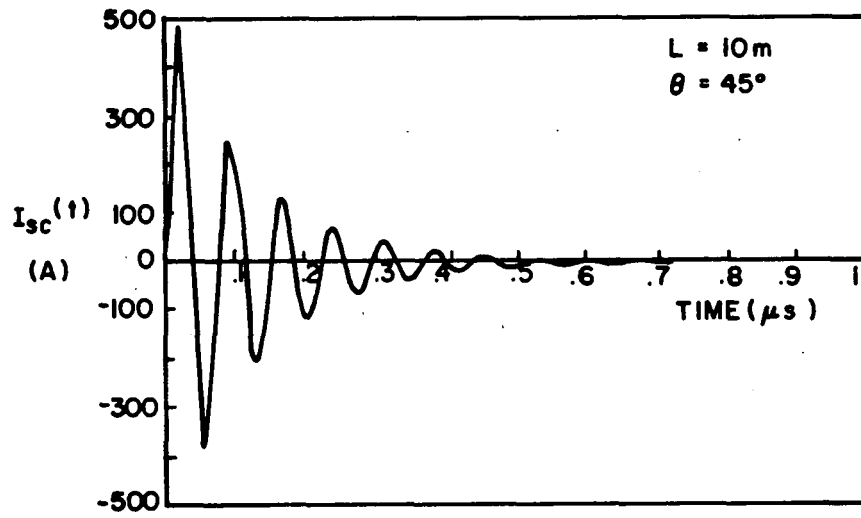
Fig. 48. HEMP-induced short circuit current at center of dipole antenna.

feeding mechanism is through the use of a waveguide which transmits energy from the antenna to the receiver or transmitter. Fortunately, from an EMP protection standpoint, this type of system is self-protecting, since the waveguide naturally attenuates all energy at frequencies below a cutoff frequency given by:

$$f_c = c/2a \qquad (142)$$

where c is the speed of light and a is the largest cross sectional dimension of the waveguide. For a waveguide having a 2" width, the corresponding cutoff frequency is around 3 GHz, well above the EMP spectrum. Since the attenuation of energy below cutoff occurs exponentially as a function of distance down the guide, EMP excitation of waveguide-fed antennas seldom pose a problem to the system.

3.4 Aperture Coupling Models

A significant amount of past work has been conducted into the determination of the penetration of EMP energy into apertures. Generally, apertures are electrically small compared with the EMP pulse, implying that low frequency models of the aperture penetration are applicable. Reference [1] summarizes many of the aperture modeling techniques which are useful for performing an assessment of a system illuminated by EMP.

Consider a simple aperture in the skin of a shielded enclosure as shown in Fig. 49a. The incident field induces surface currents and charges on the exterior of the system and in the vicinity of an aperture, these distributions are perturbed from that normally occuring on the surface. This perturbation of the surface currents and charges causes magnetic and electric fields to penetrate through the aperture and enter into the shielded region, as illustrated in Fig. 49b.

As originally described by Bethe and discussed in [31], the effective penetration of the fields through the aperture can be described through effective dipole moments located at the aperture
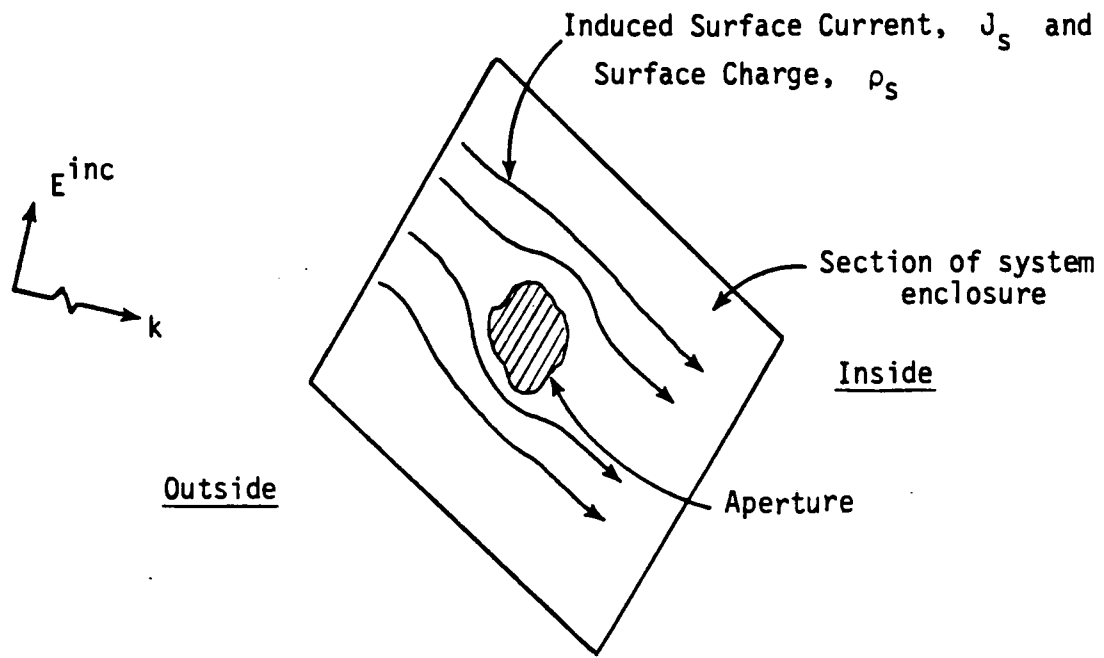
a) Perspective view
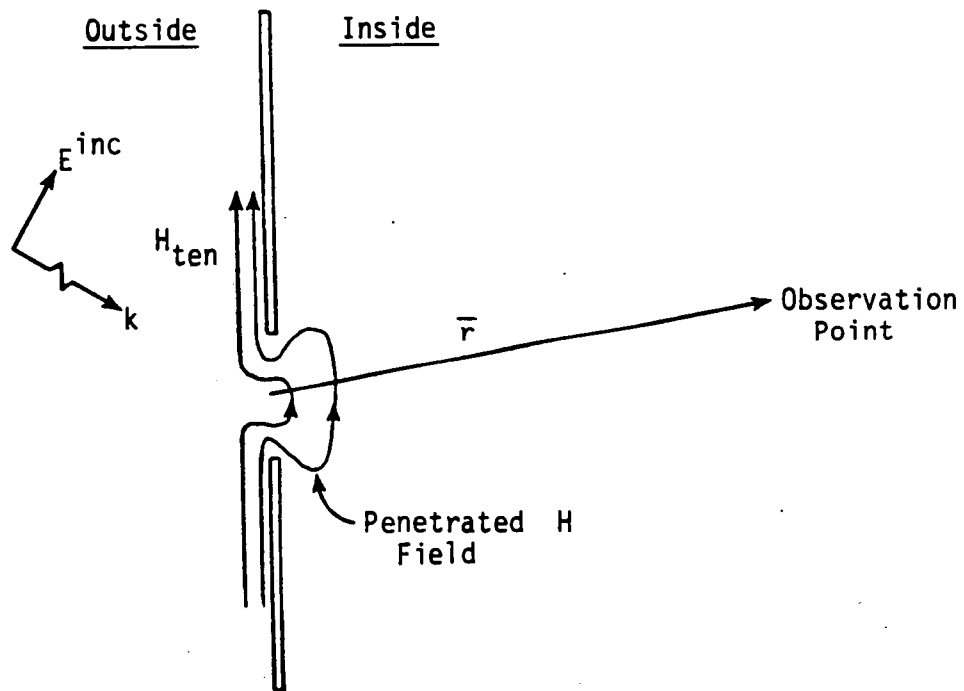
b) Cross Sectional view

Fig. 49. Aperture located in a conducting plane.

location, with the aperture short circuited as shown in Fig. 50. These equivalent electric and magnetic dipoles can in turn be related to the short circuit current and charge which exists over the aperture on the outside region when the aperture is filled in and is illuminated by the EMP.

In this manner, the electric and magnetic fields at point r inside the shield can be expressed as:

$$\vec{E}^d(\vec{r},s) = -\frac{1}{\varepsilon}\ \nabla \times [\vec{p}_a(s) \times \nabla G(\vec{r},s)] + s\mu\ \vec{m}_a(s) \times \nabla G(\vec{r},s) \quad (143)$$

and

$$\vec{H}^d(\vec{r},s) = -s\ \vec{p}_a(s) \times \nabla G(\vec{r},s) - \nabla \times [\vec{m}_a(s) \times \nabla G(\vec{r},s)] \quad (144)$$

in the frequency domain where the parameter s is the generalized complex frequency variable, and $G(\vec{r},s) = e^{-\gamma r}/(4\pi r)$. These expressions are:

$$\vec{E}^d(\vec{r},t) = \frac{1}{4\pi\varepsilon} \nabla \times \left[\frac{1}{r^2} P_a(t)\vec{1}_z \times \vec{1}_r\right] - \frac{\mu}{4\pi}\ \frac{1}{r^2} \dot{\vec{m}}_a(t) \times \vec{1}_r \quad (145)$$

and

$$\vec{H}^d(\vec{r},t) = \frac{1}{4\pi}\ \frac{1}{r^2} \dot{P}_a(t)\vec{1}_z \times \vec{1}_r + \frac{1}{4\pi} \nabla \times \left[\frac{1}{r^2} \vec{m}_a(t) \times \vec{1}_r\right] \quad (146)$$

in the time domain.

In the above expressions, the symbols $\overline{P}_a$ and $\overline{m}_a$ represent the equivalent electric and magnetic dipole moments respectively, and are given by the expressions:

$$\overline{P}_a = 2\varepsilon\ \overline{\overline{\alpha}}_e \cdot \overline{E}_{sc} \quad (147)$$

and

$$\overline{m}_a = -2\ \overline{\overline{\alpha}}_m \cdot \overline{H}_{sc} \quad (148)$$

Outside   Inside

Observation
Point

r_o

$\overline{P}_m$

$\overline{P}_e$

Shorted
aperture

equivalent dipole
moments
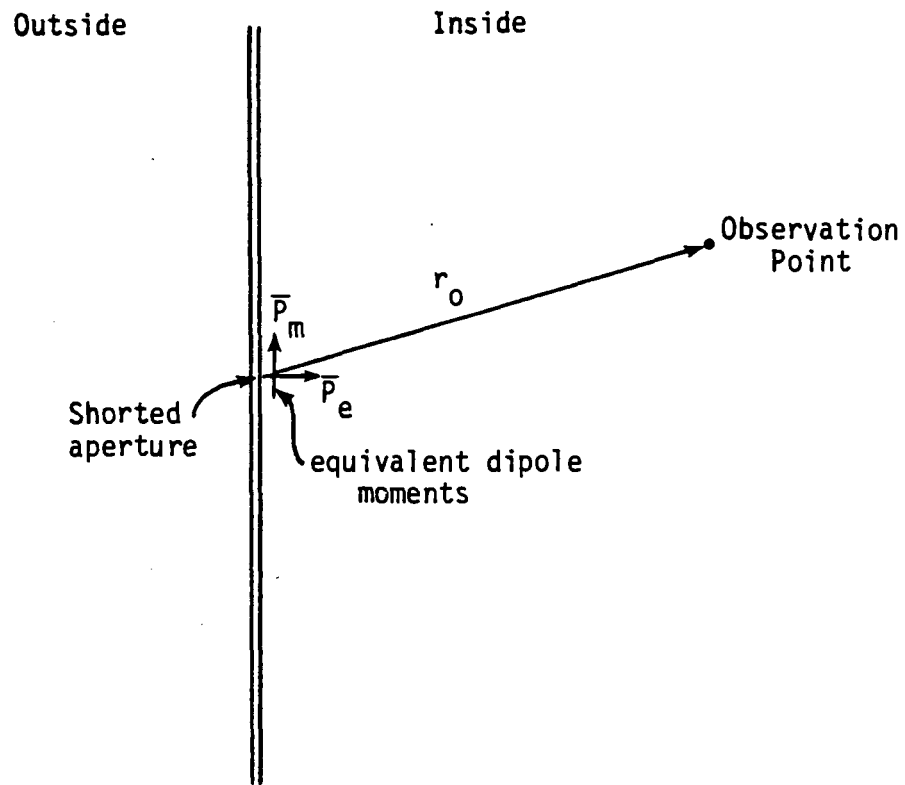
Fig. 50. Representation of aperture penetration by equivalent electric and magnetic dipole moments.

where $\bar{E}_{sc}$ is the normal electric field and $\bar{H}_{sc}$ is the tangential magnetic field over the aperture with the aperture short circuited.

In these last relations, the parameters $\bar{\alpha}_e$ and $\bar{\alpha}_m$ are referred to as the electrical and magnetic polarizibilities of the aperture, and are functions of only the aperture size and shape. They are not functions of the incident field. Note that the polarizibilities are actually tensor quantities, but with the proper choice of a coordinate system, these quantities may be simplified to have only one component for the $\bar{\bar{\alpha}}_e$ and two components for $\bar{\bar{\alpha}}_m$.

For apertures having very simple shapes, these polarizibilities may be calculated analytically. For more complicated shapes, numerical procedures must be used in order to determine the values. In Ref. [1] various polarizabilities are presented. Table 7 presents the analytically derived polarizabilities for elliptical apertures. Figures 51 through 54 present the electrical and magnetic polarizibilities for more complex aperture shapes.

In addition to simple apertures as discussed above, it is possible to have apertures in the form of slits around doors or other hatch closures as shown in Fig. 55. The penetration of EMP fields through these apertures may also be described in terms of equivalent dipole moments, and the pertinent aperture polarizibilities are expressed in [1] as indicated in Table 8.

At times, the apertures in the hatches and doors of Fig. 55 are filled with a conducting material in the form of a seal or gasket, for the express purpose of eliminating the EMP penetration. Mathematical models for the effect of such gaskets have been developed, and Table 9 summarizes resulting aperture polarizibilities. Note that these quantities are now frequency dependent.

Table 7

APERTURE POLARIZIBILITIES

Shape	$\alpha_{e,zz}$	$\alpha_{m,xx}$	$\alpha_{m,yy}$
Circle (d = Diameter)	$\dfrac{1}{12}\,d^3$	$\dfrac{1}{6}\,d^3$	$\dfrac{1}{6}\,d^3$
Ellipse*	$\dfrac{\pi}{24}\,\dfrac{w^2\ell}{E(m)}$	$\dfrac{\pi}{24}\,\dfrac{\ell^3 m}{K(m)\;-\;E(m)}$	$\dfrac{\pi}{24}\,\dfrac{\ell^3 m}{(\ell/w)^2 E(m)\;-\;K(m)}$
Narrow Ellipse (w >> ℓ)	$\dfrac{\pi}{24}\,w^2\ell$	$\dfrac{\pi}{24}\,\dfrac{\ell^3}{\ell n(4\ell/w)\;-\;1}$	$\dfrac{\pi}{24}\,w^2\ell$
Narrow Slit (w >> ℓ)	$\dfrac{\pi}{16}\,w^2\ell$	$\dfrac{\pi}{24}\,\dfrac{\ell^3}{\ell n(4\ell/w)\;-\;1}$	$\dfrac{\pi}{16}\,w^2\ell$

*Ellipse eccentricity $e = 1 - (w/\ell)^2$,
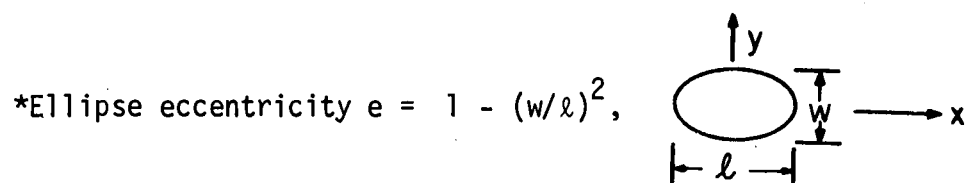
K and E are the complete elliptic integrals of the first and second kind, $m = e^2$.

Table 8

POLARIZIBILITIES OF HATCH APERTURES

Aperture	α_e	$\alpha_{m,xx}$	$\alpha_{m,yy}$
Fig. 55a	$\dfrac{\pi^2}{32}\dfrac{d^3}{\ln(16\,d/g) - 2}$	$\pi^2\dfrac{d^3}{\ln(16\,d/g) - 2}$	$\pi^2\dfrac{d^3}{\ln(16\,d/g) - 2}$
Fig. 55b	$\dfrac{\pi^2 d^3}{16\Omega}\dfrac{s^2\mu\epsilon}{s^2\mu\epsilon + 128h/(\pi\Omega dg^2)}$	$\dfrac{\pi^2 d^3}{8\Omega}\left[1 - \dfrac{8/\pi^2}{1 + \Omega g^2/(8\pi dh)}\right]$	$\dfrac{\pi^2}{16}\dfrac{d^3}{\ln(16\,d/g) - 2}$
Fig. 55c	$\dfrac{\pi^2 d^3}{16\Omega}\dfrac{s^2\mu\epsilon}{s^2\mu\epsilon + 192h/(\pi\Omega dg^2)}$	$\dfrac{\pi^2 d^3}{8\Omega}\left[1 - \dfrac{27/(4\pi^2)}{1 + \Omega g^2/(64\pi dh)}\right]$	$\dfrac{\pi^2 d^3}{8\Omega}\left[1 - \dfrac{27/(4\pi^2)}{1 + \Omega g^2/(64\pi dh)}\right]$
Fig. 55d	$\dfrac{\pi}{4}\dfrac{\ell^2 w}{(1 + \ell/w)\ln[4(\ell + w)/g]}$	$\dfrac{\pi}{12}\dfrac{\ell^3[1 + 3(w/\ell)]}{\ln[4(\ell + w)/g]}$	$\dfrac{\pi}{12}\dfrac{w^3[1 + 3(\ell/w)]}{\ln[4(\ell + w)/g]}$
Fig. 55e	$\dfrac{\pi}{4}\dfrac{\ell^2 w}{(1 + \ell/2)\ln[4(\ell + w)/g]}$	$\dfrac{\pi}{24}\dfrac{\ell^3[8/3 + 7(w/\ell) + 2(w/\ell)^2]}{\ln[4(\ell + w)/g]}$	$\dfrac{\pi}{12}\dfrac{w^3[1 + 3(\ell/w)]}{\ln[4(\ell + w)/g]}$

NOTE: $\Omega = 2[\ln(16d/g) - 2]$

Table 9

POLARIZIBILITIES OF GASKET-SEALED HATCH APERTURES

Aperture	$\alpha_e(s)$	$\alpha_{m,xx}(s)$	$\alpha_{m,yy}(s)$
Fig. 55a	$\dfrac{\pi^2 s\epsilon}{16}\dfrac{d^4}{2G_c + sC_c}$	$\dfrac{\pi^2}{4}\cdot\dfrac{2}{1/L_c + sG_c}$	$\dfrac{\pi^2}{4\mu}\cdot\dfrac{2}{1/L_c + sG_c}$
Fig. 55b	$\dfrac{\pi^2 s\epsilon}{16}\cdot\dfrac{d^4}{2G_c + sC_c + 2/sL_h}$		$\dfrac{\pi^2}{4\mu}\cdot\dfrac{d^2}{1/L_c + sG_c}$
Fig. 55c	$\dfrac{\pi^2 s\epsilon}{16}\cdot\dfrac{d^4}{2G_c + sC_c + 3/sL_h}$		
Fig. 55d	$\dfrac{s\epsilon\ell^2 w^2}{G + sC}$	$\dfrac{1}{1 + sL_x G_x}\,\alpha_{m,xx}(0)$	$\dfrac{1}{1 + sL_y G_y}\,\alpha_{m,yy}(0)$
Fig. 55e	$\dfrac{s\epsilon\ell^2 w^2}{G + sC}$	$\dfrac{1}{1 + s(L_x + L_a)G_x'}\,\alpha_{m,xx}(0)$	$\dfrac{1}{1 + sL_y G_y}\,\alpha_{m,yy}(0)$

Notes:
(i) Δ = gasket thickness; σ = gasket conductivity.

(ii) The static polarizabilities $\alpha_{m,xx}(0)$ and $\alpha_{m,yy}(0)$ in the table entries are those of the corresponding hatch aperture without gasket found in Table 8.

(iii) Constants: $G = 2\sigma\Delta(\ell+w)/g$; $C = 2\epsilon\Omega(\ell+w)/\pi$; $\Omega_x = 2\ell n[4(\ell+w)/g]$; $L = \mu\pi\ell(1+2w/\ell)/8\Omega$;

$L_y = \mu\pi w(1+2\ell/w)/8\Omega$; $G_x = \sigma\Delta\ell/g$; $G_x' = G_x/(1+w/3\ell)$; $L_a = (\pi\mu\ell/24\Omega)w^2/\ell^2$;

$G_y = \sigma\Delta w/g$; $G_c = \pi\sigma\Delta d/2g$; $L_c = \mu d/[4\ell n(16d/g)-8]$; $L_h = \mu\pi g^2/(64h)$;

$C_c = 2\epsilon d[\ell n(16d/g)-2]$.

135
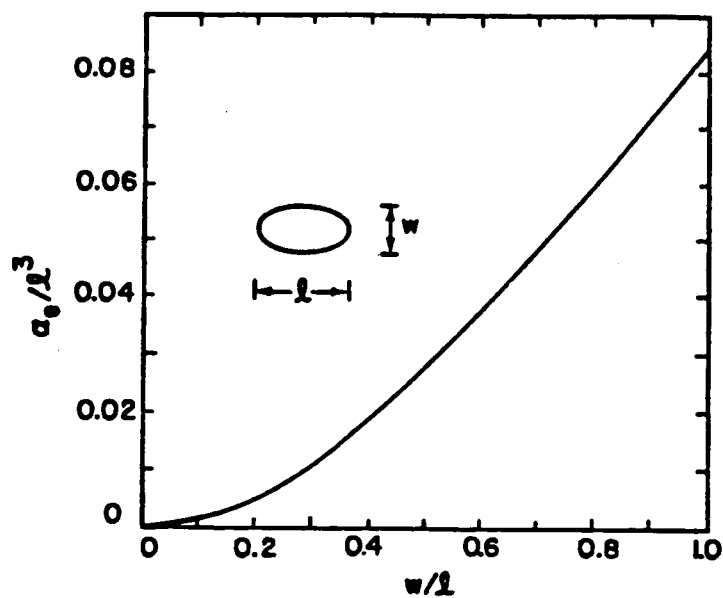
Fig. 51. Normalized electric (imaged) polarizability
of an elliptical aperture.
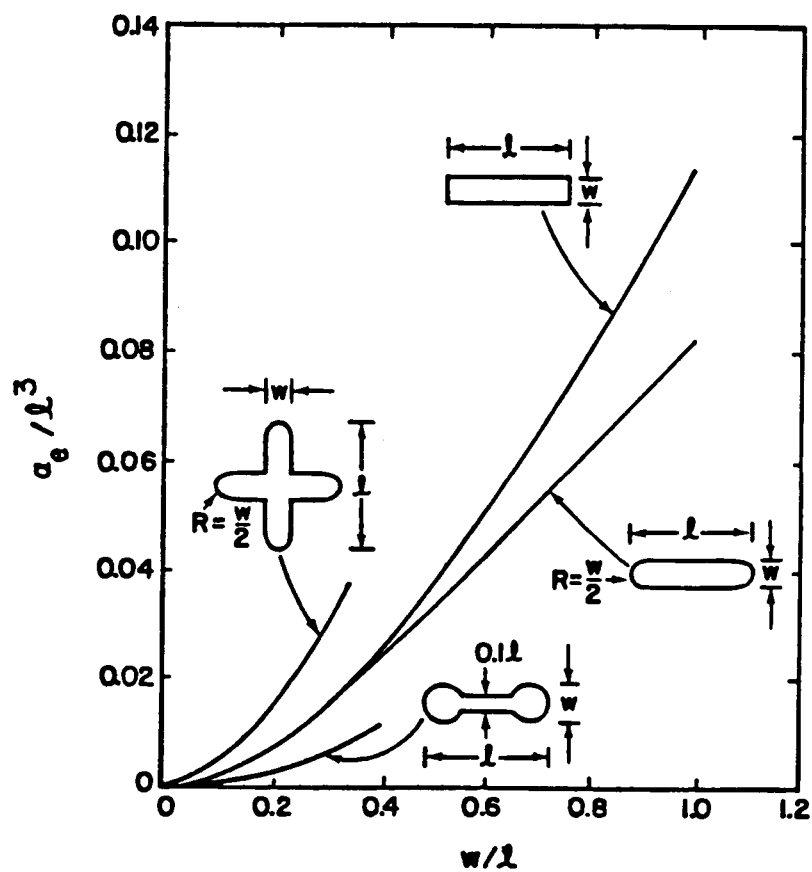
Fig. 52. Normalized electric (imaged) polarizabilities
for four aperture shapes.
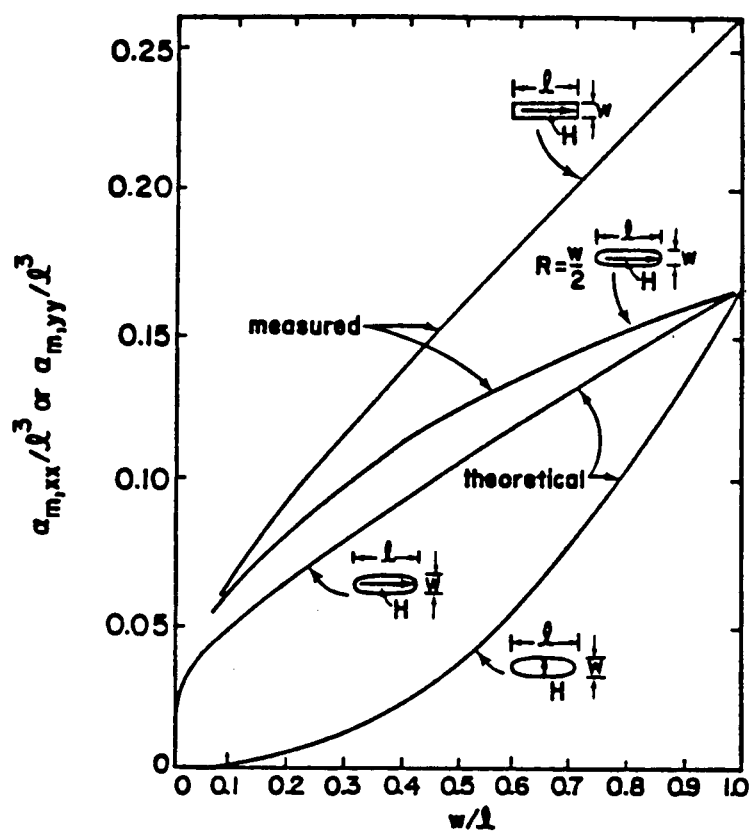
Fig. 53. Normalized magnetic (imaged) polarizabilities for elliptical, rectangular, and rounded rectangular apertures.
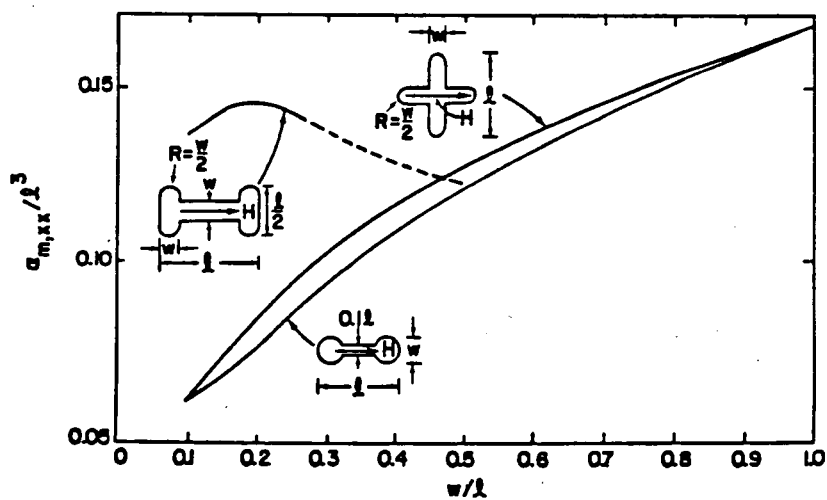
Fig. 54. Normalized magnetic (imaged) polarizabilities for three aperture shapes.
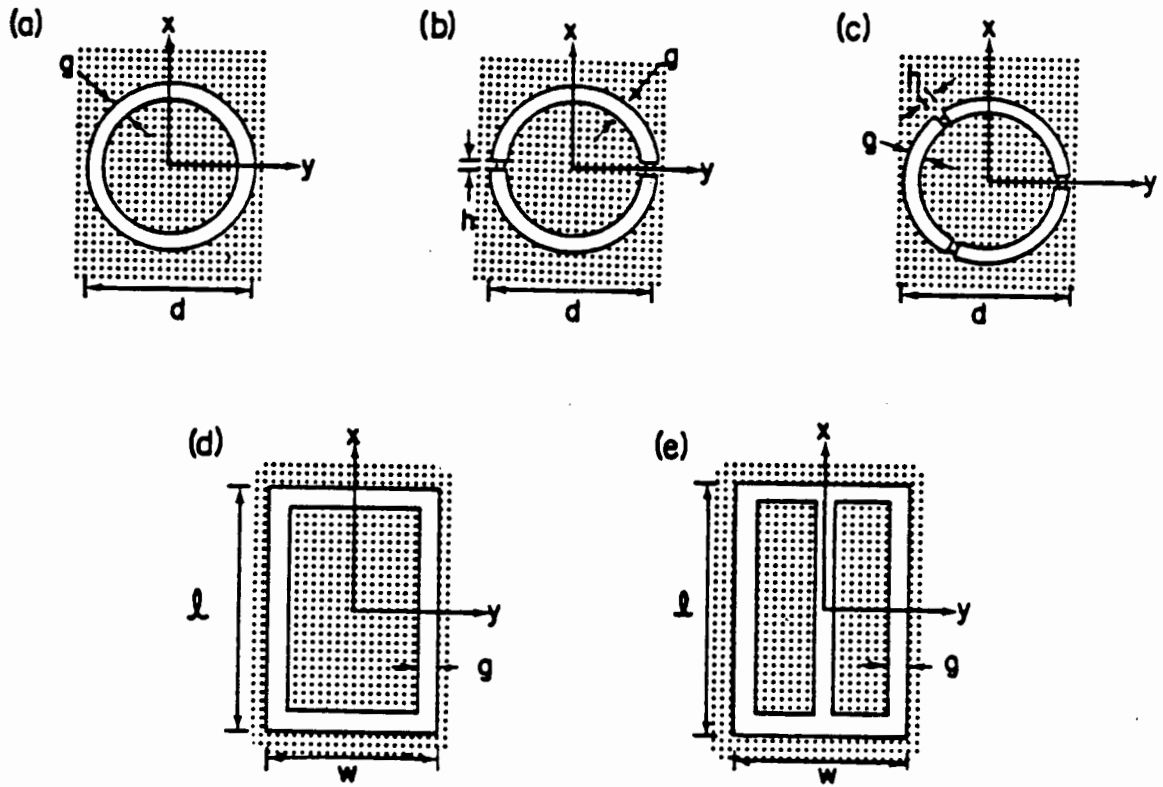
Fig. 55. Hatch apertures.

Often, the determination of the electric and magnetic fields inside of a shielded region does not provide the ultimate system response used in a system assessment. These fields usually couple the EMP energy to internal conductors, and this is propagated to other points within the system. In order to estimate the effects of an aperture excitation on a nearby conductor as shown in Fig. 56a, a simple transmission line model shown in Fig. 56c may be used. Overall, the wire is assumed to be represented by a transmission line model having distributed inductance and capacitance. The effect of the aperture is to induce an additional lumped inductance and capacitance in the line at the aperture location, as well as a lumped voltage and current source. The relationship of these to the aperture polarizibilities is given in Ref. [1].

Often, it is found that the correction of the line inductance and capacitance is insignificant, so that only the lumped excitation sources need to be considered in estimating the line response. Once these sources are determined, the transmission line coupling methods described in the above may be utilized to infer the induced line current and voltage.

Diffusion Interaction Models

The final and usually least important EMP penetration mechanism is that of field diffusion into a shielded facility or subsystem. Electromagnetic field diffusion comes about because the electrical conductivity of the shield surrounding the system is not infinite. At low frequencies for which the wall thickness is less than the electrical penetration depth (skin depth), the diffusion mechanism is known to be an effective means for penetration by the magnetic field, while penetration by the electrical field is negligibly small. At higher frequencies where the wall thickness is larger than the skin depth, most of the incident magnetic field is shielded due to reflections at the surface, and attenuation losses in the wall. Hence, this phenomenon deals mainly with low frequency (late-time) magnetic fields.
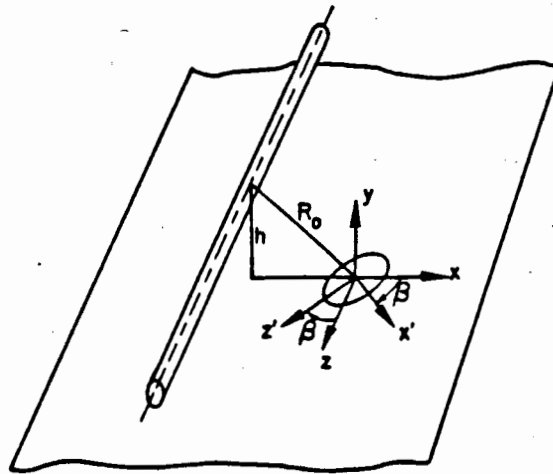
a) Perspective view
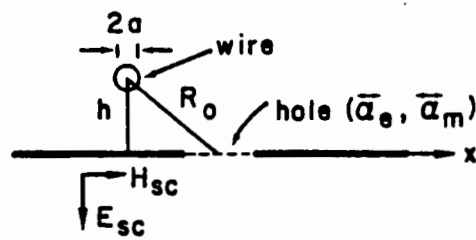
b) Cross Sectional view
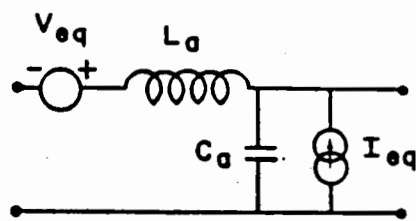
c) Equivalent circuit

Fig. 56. Aperture coupling to nearby conductor.

An example of this effect is shown in Fig. 57 where a volume is enclosed by a thin shell of thickness Δ having constitutive parameters σ and μ. An incident EMP falls on the body, and some of this pulse is able to penetrate into the interior.

As in the case of the aperture penetration models, it is possible to develop some simple expressions for the penetrated fields for the canonical bodies shown in Fig. 58. Reference [1] defines a transfer function for the magnetic fields T_m as:

$$T_m(s) = \frac{H^{in}(s)}{H^{ex}(s)} = \frac{\text{magnetic field inside cavity}}{\text{magnetic field incident on the cavity}} \quad (149)$$

For an assumed uniform incident magnetic field, the frequency dependent transfer functions for the shield geometries shown in Fig. 58a are given as:

$$T_p(p) = \frac{1}{\cosh p + kp \sinh p} \quad (150)$$

for the parallel plate geometry of Fig. 58a:

$$T_c(p) = \frac{1}{\cosh p + \frac{1}{2} kp \sinh p} \quad (151)$$

for the cylindrical shell having longitudinal excitation as in Fig. 58b:

$$T_c^{(t)}(p) = \frac{1}{\cosh p + \frac{1}{2} (kp + \frac{1}{kp}) \sinh p} \quad (152)$$
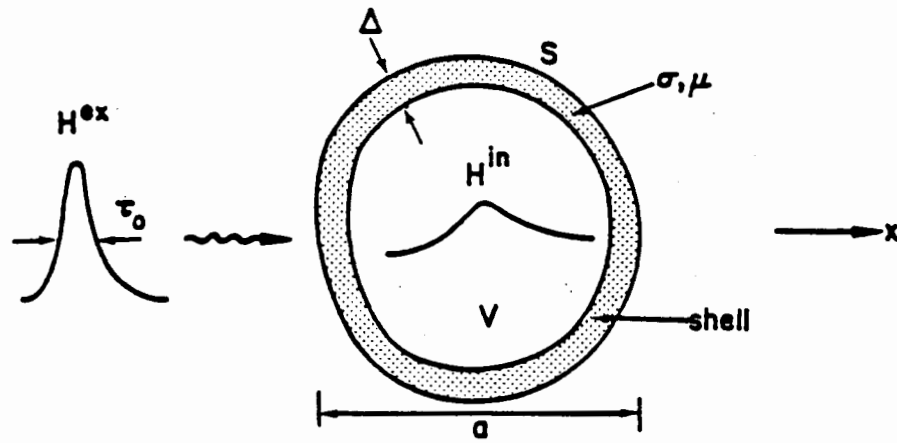
Fig. 57. Geometry of shield for magnetic field attenuation.
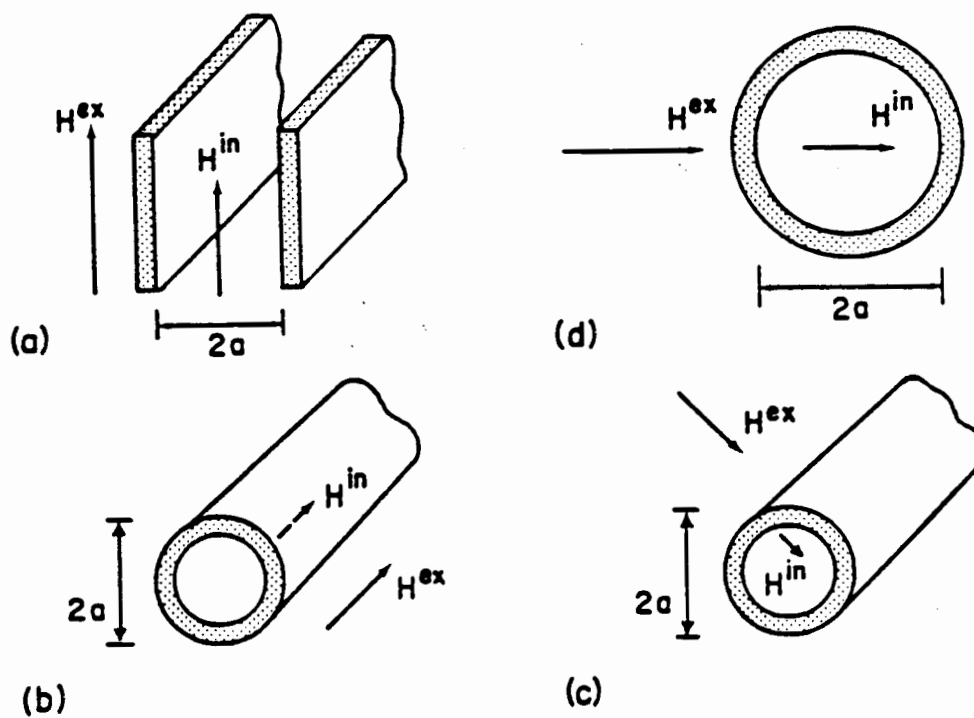
Fig. 58. Several magnetic field shielding geometries:
a) parallel plates, b) cylinder excited by longitudinal
field, c) cylinder excited by transverse field, d) sphere.

for the cylinder with transverse excitation as in Fig. 58c, and:

$$T_s(p) = \frac{1}{\cosh p + \frac{1}{3}(kp + \frac{2}{kp}) \sinh p} \tag{153}$$

for the spherical shell shown in Fig. 58d. In these expressions, s is the complex angular frequency and:

$$k = \frac{\mu_0 a}{\mu \Delta}$$

$$p = s\tau_d$$

$$t = \mu \sigma \Delta^2$$

For a non-ferrous shield, such as aluminum, Fig. 59 shows the frequency dependent transfer function in magnitude and phase for the canonical bodies. Given a particular body geometry, the K factor in Equations (151) to (153) may be calculated and used to define ξ in Fig. 59 depending on the body type. As may be noted from the figure, the low frequency attenuation of the field approaches zero.

For electrically thin shields, where the skin depth $\delta << \Delta$, it is possible to simplify the shield transfer functions:

$$T_p(s) = \frac{1}{1 + s\mu_0 \sigma \Delta a} \tag{154}$$

$$T_c^{(t)}(s) = T_c^{(\ell)}(s) = \frac{1}{1 + s\mu_0 \sigma \Delta a/2} \tag{155}$$

$$T_s(s) = \frac{1}{1 + s\mu_0 \sigma \Delta a/3} \tag{156}$$
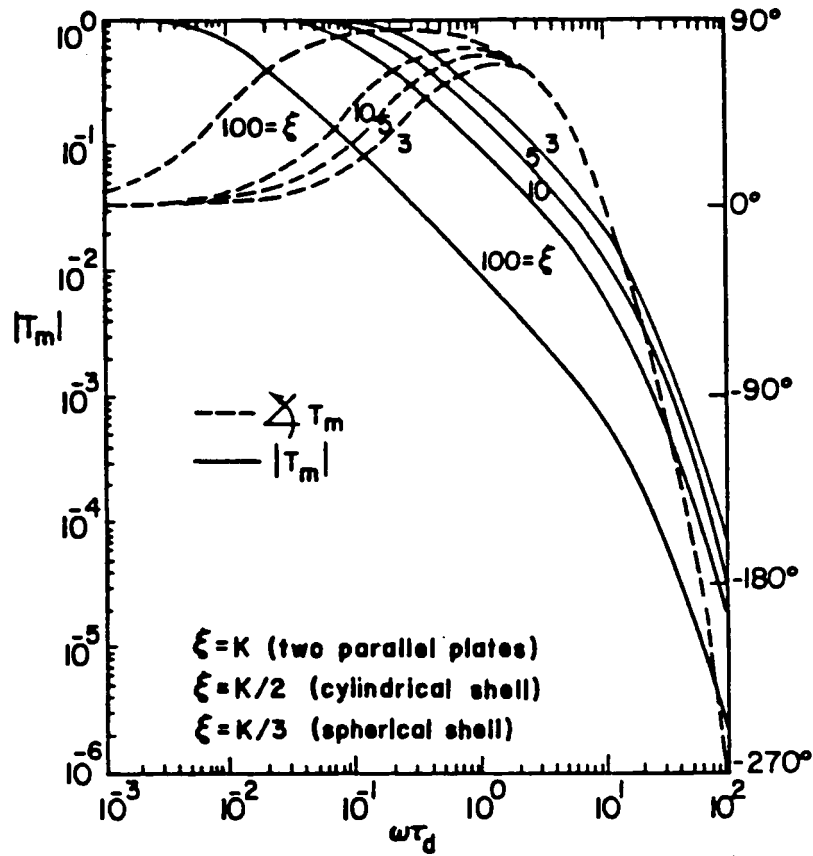
Fig. 59. Magnitude and phase of frequency domain magnetic field transfer function for a non-magnetic shield. $((\tau_d = \mu\sigma\Delta^2)$, $k = a/\Delta)$

It is important to be able to compute the time history of the internal magnetic field, given the transient behavior of the incident field. One approach is to use purely numerical methods for inferring the frequency domain spectrum of the internal field. An alternate approach is to develop an approximate expression, based on the assumption that the incident magnetic field is a delta function in time as:

$$H^{ex}(t,x) = H_o \delta(t-x/c) \tag{157}$$

where H_o is the time integral of the incident magnetic field. That this is a useful approximation is due to the fact that the diffusion process tends to blur out the fine details of the incident field since its time constant is much slower than that of the incident field.

With this approximation to the incident field, the inverse Laplace transform of the internal H field can be approximated as:

$$\dot{H}^{in}(t) \simeq \frac{2H_o}{\sqrt{\pi \xi \tau_d}} \ \frac{\tau_d}{t} \ e^{-\tau_d/(4t)} \ , \ \text{for } t/\tau_d \leq 0.1 \tag{158}$$

for early times, and by:

$$\dot{H}^{in}(t) \simeq \frac{H_o}{\xi \tau_d} \ e^{-\xi^{-1}t/\tau_d} - 2e^{-\pi^2 t/\tau_d} + 2e^{-4\pi^2 t/\tau_d} \ , \ \text{for } t/\tau_d \geq 0.1 \tag{159}$$

for late times. Figure 60 presents the normalized internal magnetic field as a function of normalized time for several different values of the parameter ξ.
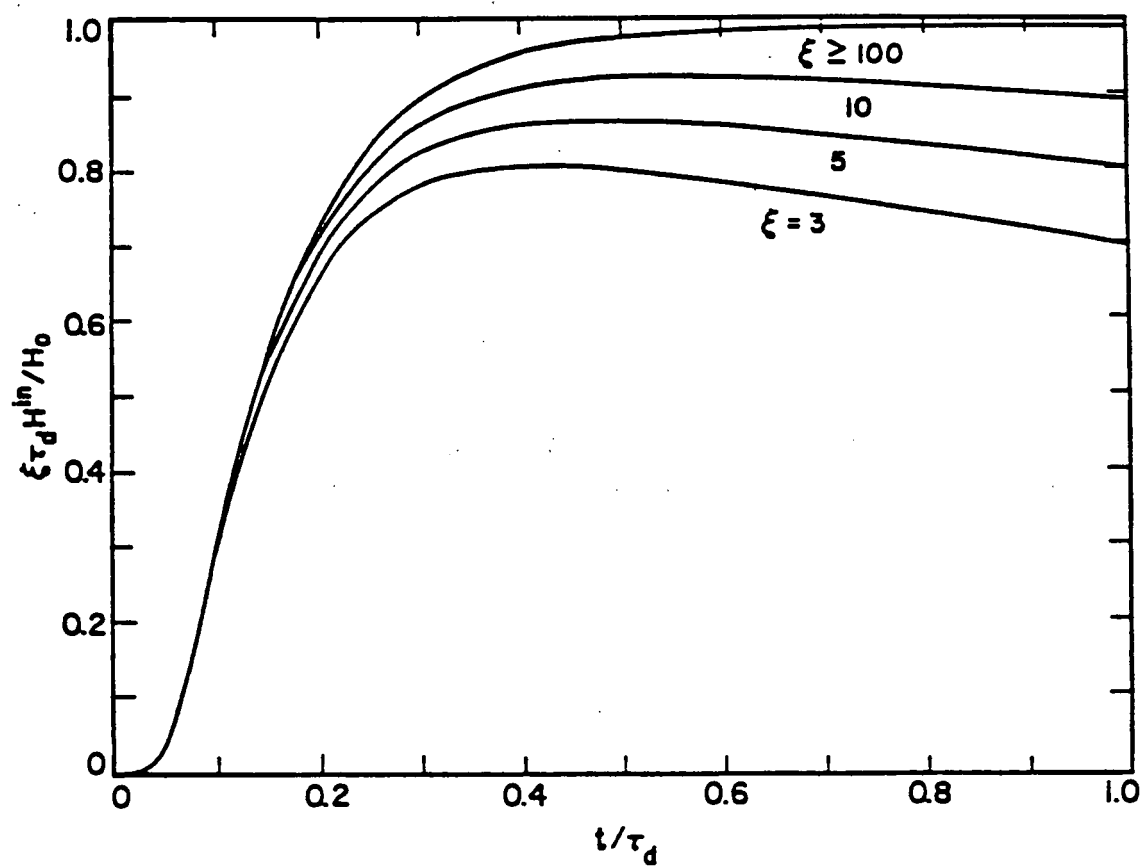
Fig. 60. Time domain variation of the normalized penetrated EMP magnetic field within a shielded enclosure. $(\tau_d = \mu\sigma\Delta^2)$

3.5 Conclusions

The calculational models described in this section may all be used in the process of assessing the behavior of power system components excited by EMP, as will be outlined in the next section. Clearly, all of the interaction models involve some degree of simplification, either with regard to the geometry or to the detail that the physics is incorporated in the solution. In all cases, more accurate calculational models are possible, but it is important to keep in mind the concept of balanced accuracy in the overall problem. What is desired is the simplest solution for the EMP interaction problem which is consistent with the accuracy of the incident EMP environment and the degree to which the EMP susceptibility of components in known.

4. ASSESSMENT METHODOLOGY

4.1 Introduction

This section summarizes a structured methodology that can be used to assess the effects of HEMP on a civilian electric power or network. The methodology assesses the effects from the time of the formation of a source region by a detonation of a high altitude nuclear weapon to two seconds after this formation. After two seconds the power system comes under the influence of the MHD-EMP effects, which are discussed in another report [32]. The time sequence of events following a high-altitude weapon burst is shown in Fig. 61. The HEMP environment has been divided into three relative time periods: early time, intermediate time, and late time or MHD-EMP periods. This figure places the HEMP environment of such a burst in time relationship to the power system reaction to this environment. The assessment for the effects of MHD-EMP are covered in the above referenced report.

The power system network (or utility network) is that group of equipment which, taken together, generates, transmits, and delivers energy to its assigned customer load areas, and the communication and control necessary for this process. Figure 62 illustrates a representative utility network [33] and shows two major systems within the network: a power-delivery system and a communication/control system. These two systems support the mission of the power network to control and delivery energy ("power") to certain geographically-located customers through facilities at specific locations determined by terrain and resources.

In many cases today, different utilities share common generating facilities. They may also be interconnected at various voltage levels at a number of contiguous borders of their individual territories. In some cases, transmission facilities may be functionally shared by a number of utilities although owned by one. Such a circumstance occurs when energy is "wheeled" from one utility over to another area through the facilities of a third utility.

EVENT
10^{-9} 10^{-6} 10^{-3} 10^0 10^3   SECONDS

HIGH-ALTITUDE WEAPON BURST

PROMPT HEMP ENVIRONMENT

MICROSECONDS

INTERMEDIATE HEMP ENVIRONMENT

MILLISECONDS

SYSTEM HEMP RESPONSE(S)

· SECONDS

MHD-EMP ENVIRONMENT

TENS OF SECONDS

SYSTEM MHD-EMP RESPONSE(S)

TENS OF SECONDS
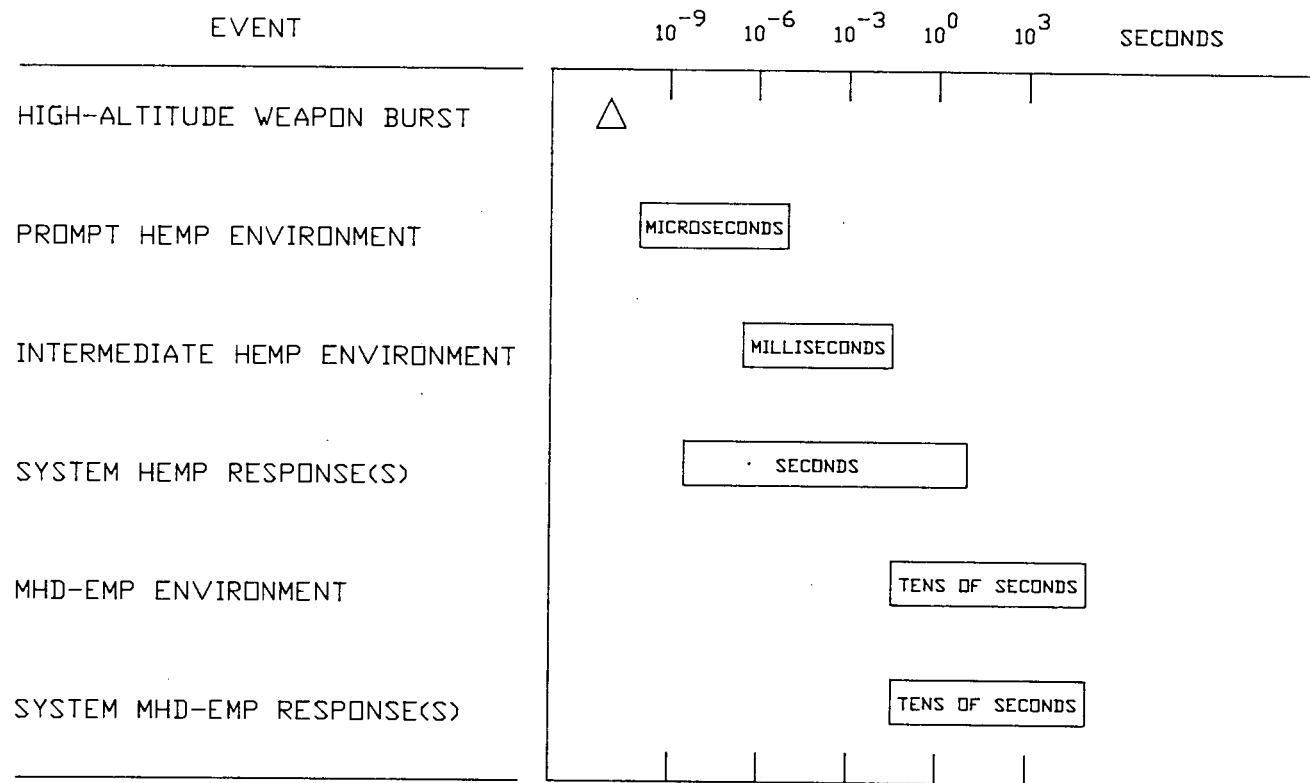
Fig. 61. Time-sequence of events following a high-altitude
weapon burst [32].

150
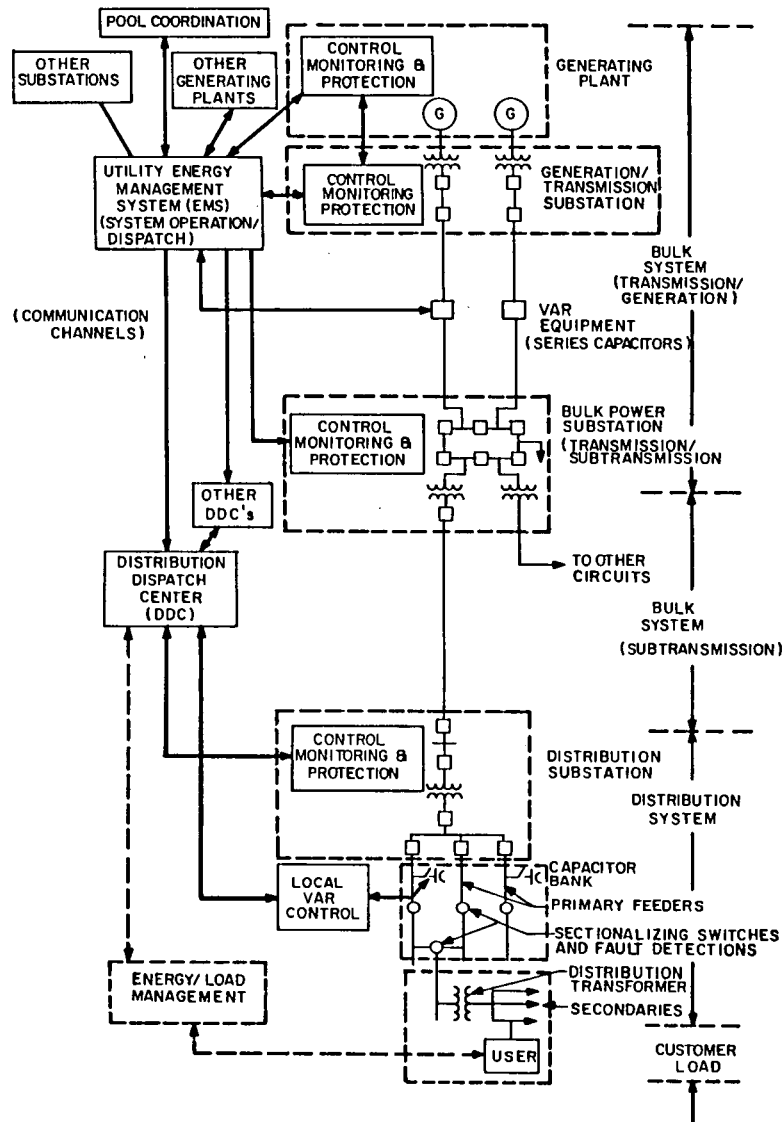
Fig. 62. Representative electric utility network.

Likewise, common communication facilities may be operated to provide communication and common system control between various close-knit utilities. By this communication the requirement can be met that each individual network operates in concert with the others to which it is interconnected; i.e., to operate on the same frequency or in "synchronism."

For the purposes of this methodology, this power-delivery or communication/control system is considered to be made up of a number of subsystems (Fig. 63). The subsystems are the large groups of equipment which are considered to be illuminated with the same HEMP field strength. These subsystems are the generating plants, substations, power lines between substations, centers for control, etc., and communication centers and communication links that are considered under the operation and control of a specific utility.

The equipment within a subsystem can be grouped according to the function they perform. Each functional group of equipment may be assessed separately in many instances on the basis that within the EMP illumination time none of the functional groups can interact. Ultimately, however, their individual viability or proper functioning can be affected by the functioning of the others, and must be taken into account. The major functional groups are:

- Power-delivery group, such as in generation plants and in substations, made up of generators (in the case of generation plants), power transformers, circuit breakers, bus conductors, etc.

- Protection, instrumentation or control groups, such as overcurrent and overvoltage protective relays on transformers, capacitor banks, and power lines, SCADA systems, etc.

- Communication group, such as transmitters and receivers, power line carrier systems, microwave systems, telephone lines, etc., in control or communication centers.
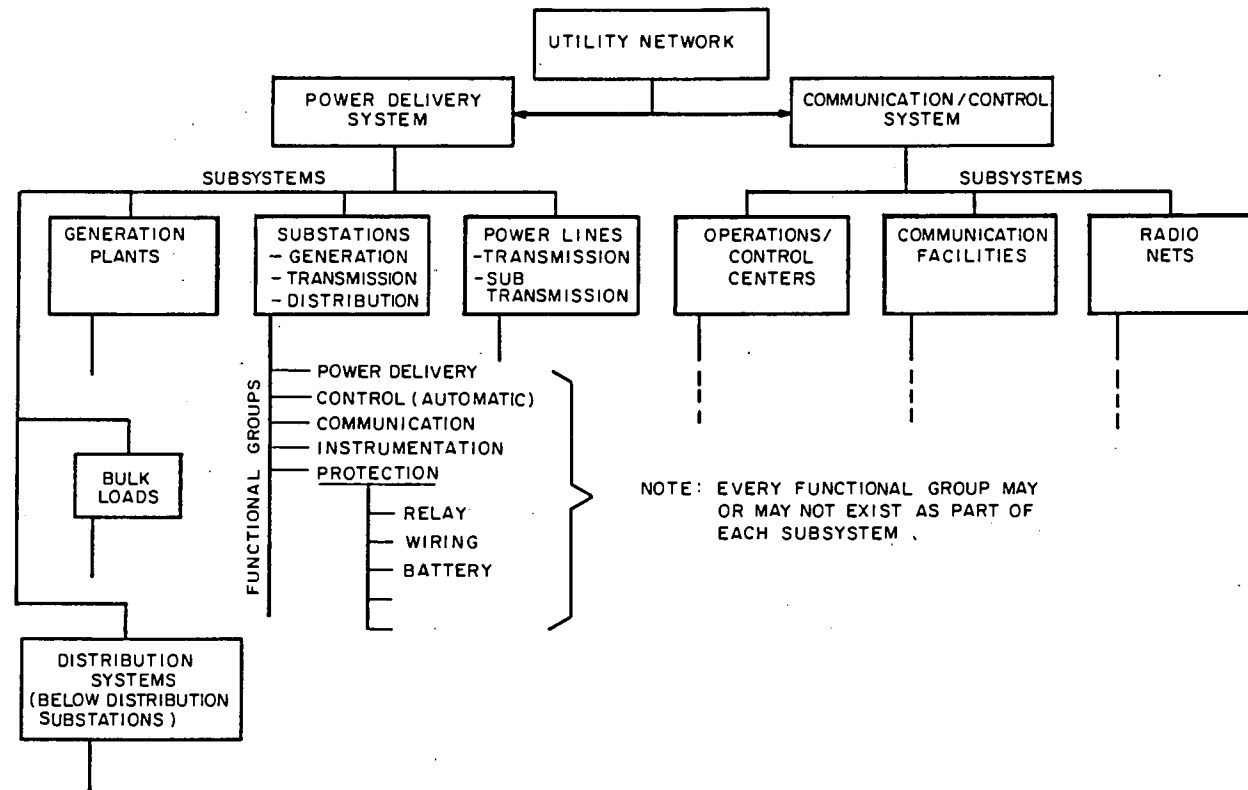
Fig. 63. Hierarchy of elements of electric utility network.

152

A transmission, or power line is a special-type of subsystem in that its major functional group is the power-delivery group, made up simply of conductors. However, the phase conductors also can serve as a circuit in a communications and protection functional group by their providing the means of transmitting the signal for power-line carrier.

A functional group is made up of <u>circuits and devices</u>. For the purpose of this methodology, a circuit is a conductor or system of conductors through which an electric current is intended to flow [34], together with its associated shielding and splicing, etc. In this context, the communication link through air may be called the "circuit" of a communication functional group. A device is an assembly of components to serve a specific purpose [34], such as, in the protection-functional group, relays, current and/or potential transformers, battery supplies, annunciators, switches, operating coils and mechanisms on breakers, and terminal blocks. The device or circuit is the smallest entity considered by this methodology.

Figure 64 illustrates the elemental divisions of the utility network used in this methodology. The states of circuits and devices in a functional group determine the state of that functional group. The states of the functional groups within the subsystem determine the state of the subsystem. The states of the subsystems within the power or communication/control system determine its state. Figure 65 illustrates an overview of the stages or levels of assessments that are discussed later in this section.

One of the reasons for approaching the structure of the methodology in this manner is to provide the vehicle for assessments of major individual subsystems and/or circuits or devices within the functional group or functional groups within a subsystem by different, appropriate, experts. The results of these individual assessments become part of the performance data base (Section 4.3) of the element being assessed. As a result of the assessments at lower levels, certain questions are answered for assessments of the states of the next level of the divisions of the utility network.

CONTIGUOUS BORDERS

UTILITY NETWORK
INTERCONNECTED

UTILITY NETWORK BEING ASSESSED

UTILITY NETWORK
INTERCONNECTED

POWER LINE

INTERCONNECTIONS

SUBSYSTEM

SUBSYSTEM

INTERCONNECTIONS

FUNCTIONAL
GROUPS

FUNCTIONAL
GROUP
INTERACTIONS

CIRCUITS

DEVICES
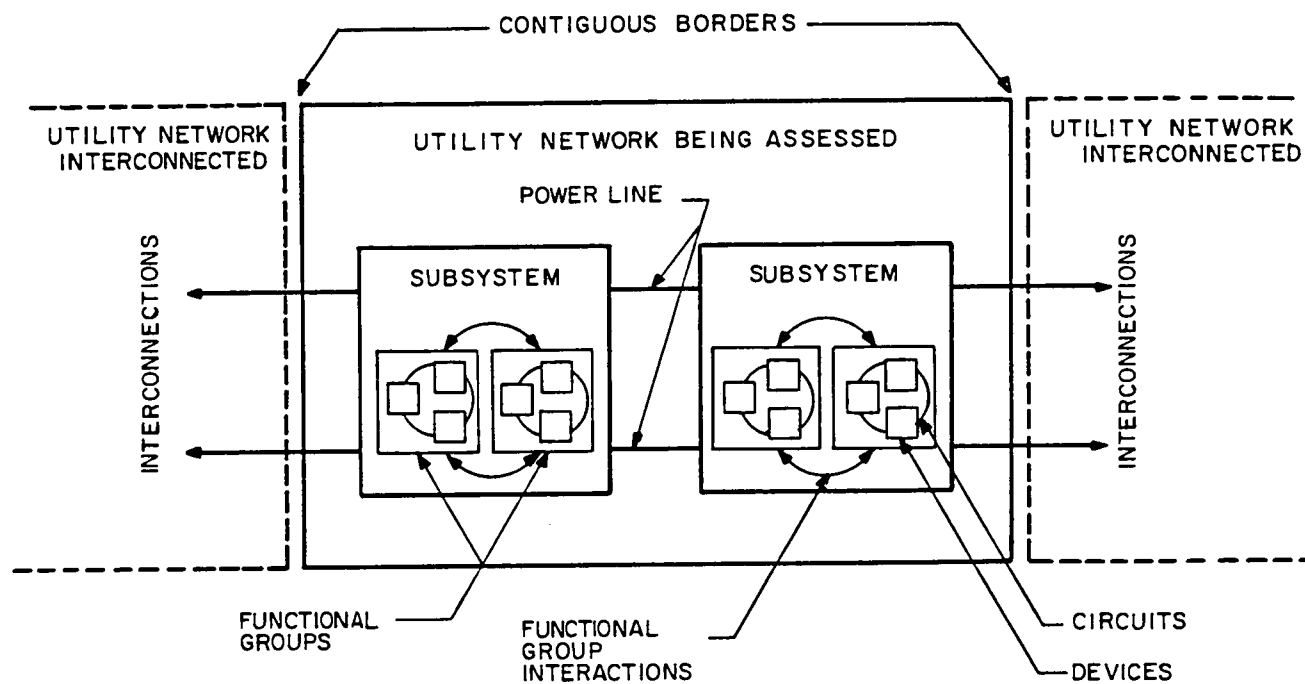
Fig. 64. Elemental division of power system.

```
┌─────────────────────┐
│  WEAPON LOCATION    │
│     AND TIME        │
└─────────────────────┘
           │
           ▼
┌─────────────────────┐
│   SOURCE REGION     │
│  HEMP ENVIRONMENT   │
└─────────────────────┘
           │
           ▼
┌─────────────────────┐
│     HEMP LOCAL      │
│   TO SUBSYSTEM      │
└─────────────────────┘
```
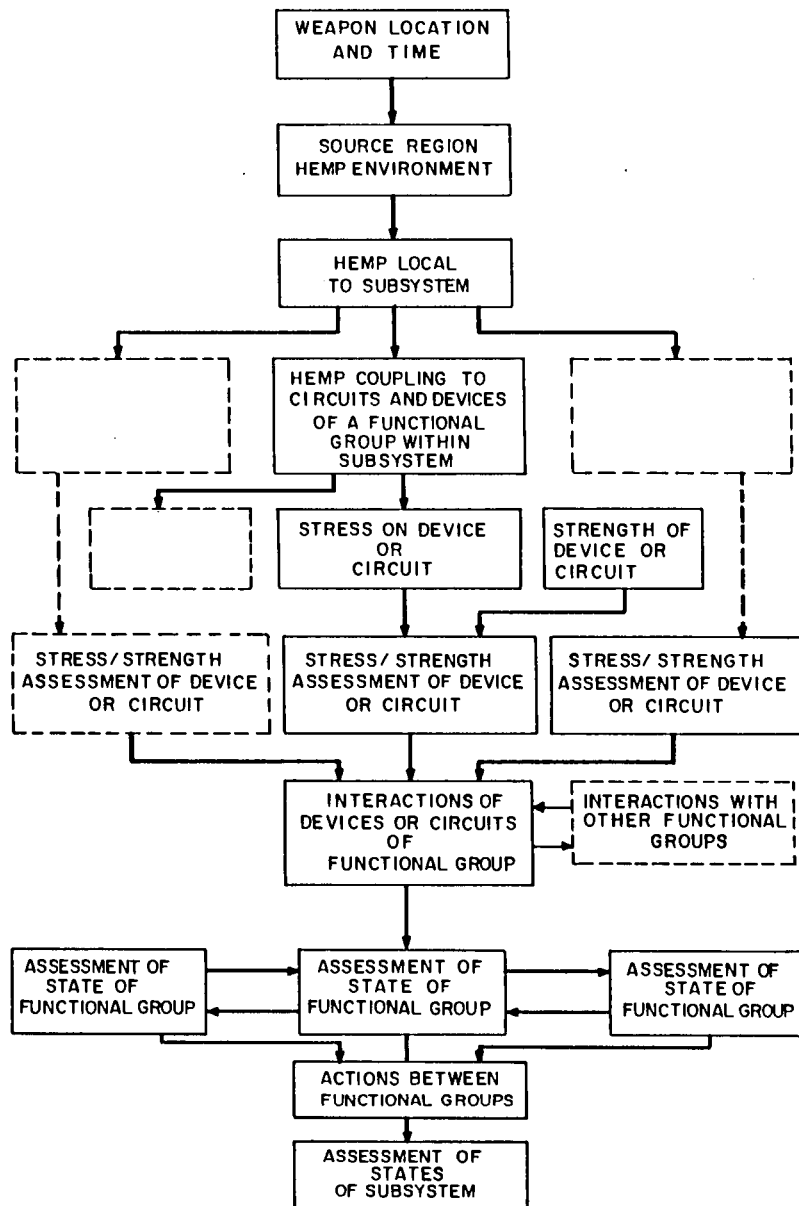

Fig. 65. Flowchart and overview of assessment methodology to level of subsystem.

In an initial period of time to be considered following the HEMP environment (Fig. 61) there can begin to be stress effects in the circuits and devices in the functional groups, such as potential flashovers, upsets, etc.

Each functional group can be initially assessed separately from the others based on the premise that failures and upsets of devices and circuits take place in a very short period of time within a group. (Damaged or upset devices or circuits are stored in a data base of the functional group.) Within the confines of this definition, fault trees of failures and upsets of devices and circuits, for risk assessment of failure, and of upset of the functional group may be developed, with the objective of identifying the potential for the total functional-group failing; based on damage or upsets of individual devices or circuits. If the potential is high for failure of one functional group, then this conclusion may negate the necessity for further analysis or assessment of certain other functional groups within the subsystem. This approach assumes the other functional groups to be "perfect" during the analysis of the one being examined as to its "imperfectness" up to the point where interactions between functional groups come into play. (One failed functional group resulting in an inoperable subsystem may eliminate the need for further analysis at a higher level of assessment.)

For this point in the assessment, interaction sequence diagrams, or "fault trees," may also be utilized to analyze the interplay of failures or upsets between circuits and devices within the functional group.

At this level each decision-tree provides a means to answer specific sets of questions; such questions to be answered as: has the relay-current measuring circuit received the overcurrent signal from the current transformer? Has a relay responded properly? Can the circuit-breaker receive the signal to trip? Is its operating mechanism capable of tripping?

At the next level the approach leads to several additional "fault tree" thought-processes, embodying the concert of the decision "test" points of the individual functional groups but now considering a later period of time. Each of these decision trees provides a means to answer a specific global question, such as with the scenario of a flashover in the power-delivery group when, in the course of time-events, is the protection (relay) functional group now calling for a circuit breaker trip? Can the circuit breaker, in the power-delivery group, trip and clear the fault? Are other actions taking place in time that change the answer to the question being addressed? Is the information available as to what faulted power lines can or cannot be tripped by their respective breakers, or by backup breaker systems?

On a still higher level, can and does an operational control center know the functional status of a substation? Does this affect the operation of the power network to deliver energy?

In the normal operation of power systems the need to answer the above questions may be negated by the failure or upset of one or a few devices. As a result of the EMP environment, the operational state of all devices or circuits involved in obtaining an answer must be assessed in some manner in a structured procedure, including state decisions in a time frame. In some cases, these decisions must be based on engineering judgment. The sequence of events, beginning at the time of the interaction of the functional groups, becomes the "initial conditions," and state changes that are utilized in the time simulation of the power system response; that is, in the load flow, short circuit and transient stability studies. The processes to be simulated in these studies are subject to the status of these functional groups and subsystems. For example, part of the code in the transient stability program at a certain point in time may simulate a relay-trip operation, calling for a circuit breaker opening. If the relay protection functional group, or the circuit breaker as part of the power-delivery functional group, can not perform the required function (opening the breaker), then the simulation in the transient stability program must reflect this condition or "state."

The concept of levels of action within the power system and the reduction of analysis to functional groups within each subsystem allows tests and assessments to proceed in time to the different status. For example, such a concept allows for the HEMP assessment of multiple-bursts of weapons at various states of the power system existing at the time following a previous burst. Following the initial weapon detonation the changes in states of functional groups are assessed over a period of time up to that at which interactions are taking place between subsystems in the power system to produce state changes in the power system as an entity. These states or changes in state then become the "initial conditions" for the overlaying of the effects of the succeeding definitions. That is, the states are, in a sense, "frozen" in time while the effects of the succeeding detonations are assessed.

It is to be noted that certain states may be finalized prior to the succeeding detonation, whereas other states may be in the process of changing when the succeeding detonations occurs. For example, circuit breakers may be opening (or closing) and system voltages and currents maybe changing in magnitudes and angles as determined by stability studies.

An overview of the first stage of the methodology, the assessment of the states of a given subsystem, is shown in Fig. 65. The top three blocks define the HEMP environment (fields) to the local HEMP in which the subsystem and its functional groups lie. This local environment, utilizing models and codes for coupling to individual circuits and devices, is used to determine the stress (voltage, current, or energy) produced in these circuits and devices within the functional group by the HEMP local wave. The stress on a particular circuit or device is compared through its stress/strength models to the strength of the device (or circuit). Available data bases of such strengths are used to perform an assessment of failure or upset of this device. Where stress models or data bases of strengths are not available, calculations and engineering evaluations are made, or experiments performed, to supply this information. Similar assessments are performed for other devices
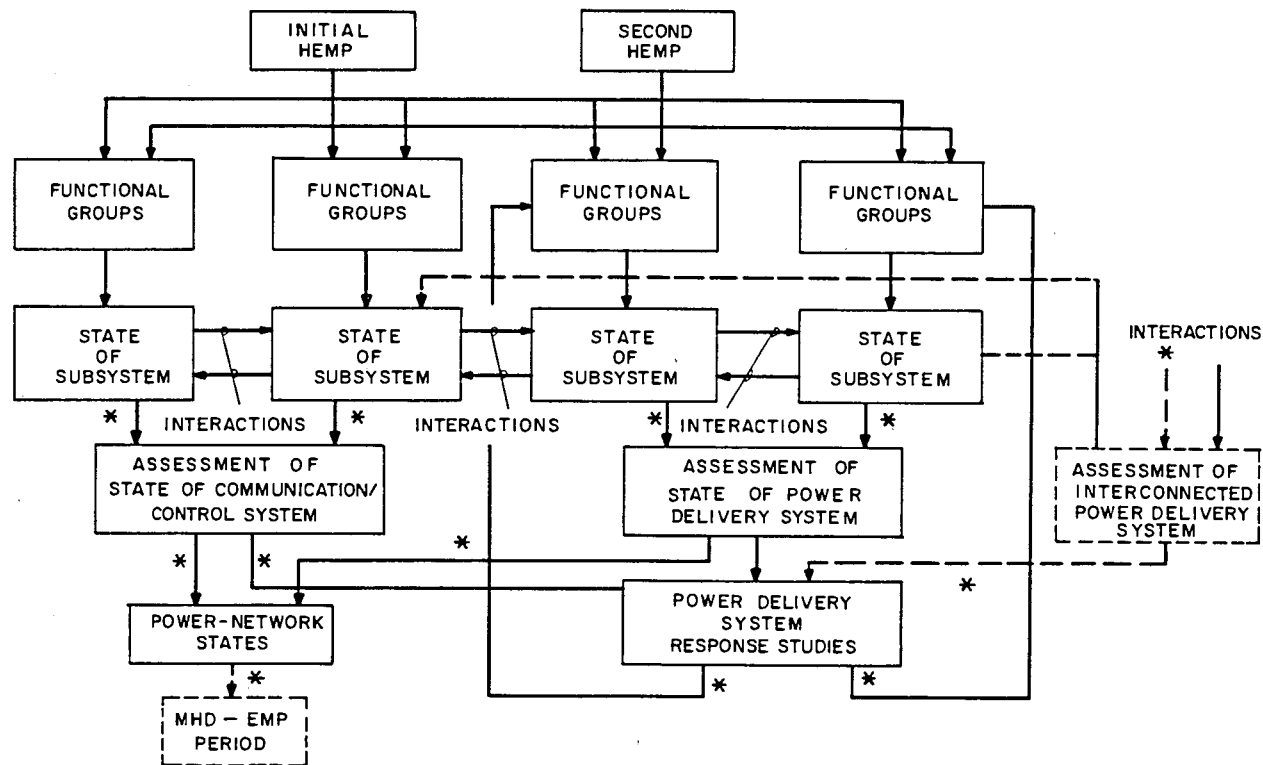
Fig. 66. Flowchart of power network assessment (*possible points of human intervention).

159

and circuits making up the functional group. Through interaction-sequence, fault-tree, or connection diagrams of such failures within the functional group, an assessment is made to determine their effects on changes of states of the functional group. At this time, the effects of possible interactions between functional groups must also be included in the assessment of individual functional groups. For example, stresses produced in the power-delivery functional group of a substation by connected transmission lines may be transferred by instrument transformers into the protection functional group of the substation.

At the next stage of the analysis, the assessed change in states of the functional groups of a subsystem are utilized to provide an assessment of the change in state of the subsystem. The change of states of all subsystems are then assessed individually as to the effects on the initial change of state within the complete power system network (Fig. 66). Because of a given utility power-delivery and communication interconnections between the power system networks of individual utilities it may be necessary at this initial time, to include an additional level of assessment which takes into account the interactions, at certain levels in the hierarchy of assessments described above, of changes in state of the individual power network. A prime example of this may be the loss of a communication functional group in an entity that communicates operation control intelligence to a communication functional group in another utility. It may be necessary to mirror the loss of the one functional group in a change-of-state indicator in the supporting data base of the other functional group.

Another property of the power system that is different from other systems that have been assessed, and which must be considered in its assessment, is its property to attempt to maintain dynamic equilibrium. That is, the initial synchronism of rotating machines within the power system, to each other and to the loads, is such that energy generated within the systems are totally dispersed among system losses and loads such that essential constant speed of rotating machines and consistent system frequency is established and maintained. Disturbances in the

system, such as faults and sudden loss of loads, upset this equilibrium. Faults and loss of loads result in shifts in the flows of real power as well as reactive power throughout the power networks. These changes for real power lead to attempts to regain equilibrium by some machines being accelerated while others may decelerate. Shifts in reactive power lead to changes in voltage levels within the network, and control circuits attempting to reestablish voltage levels will begin to respond.

As the rotating machines change speed, frequency changes take place in different parts of the system. As fast as the protective relay systems and circuit breakers can respond, the faults are isolated from the system, and other changes in real power and VAR flow and other acceleration or deceleration occur.

Other considerations that may become important are drastic changes in voltages in certain parts of the network due to loss of load or to other circuit-breaker operations. Overvoltages of significant magnitude may occur some cycles after those circuit-breaker operations, leading to further failures of circuits and devices in the power network. The subsequent power system reaction to these step changes in the states of the subsystems can be determined by performing system transient stability analyses. There are certain available proprietary codes that perform system stability analysis also taking into account changes that are occurring with time as a result of faults in protection and control functional groups, and of the operation of circuit breakers. These codes also have the facility of simulating a large number of faults, either simultaneously applied or spaced in time, and the resulting machine accelerations with accompanying operations, spaced in time, of particular relay schemes and circuit breakers.

Other codes may be used to do analysis of subsequent changes in state of individual devices within functional groups, such as fuses in the power-delivery functional group, due to, say, transient faults. Alternatively, other analyses can look individually at a condition leading to an overvoltage condition, providing data for an assessment of subsequent circuit or device failures.

It is anticipated that intervention of the engineer at various stages of the assessment levels may be required, especially at an early point in the refinement of the methodology and because of the present scarcity of information for the data bases.

For example, it will probably be more efficient to stop the program within initial network analysis codes in the stability program (or elsewhere) after solving for currents due to multiple faults. Engineering evaluations can be made as to what relay schemes, that are still operable following illumination, will call for a trip current in the circuit breaker operating coils. This judgment of what is still operable is influenced by the result of querying the data bases giving the status for the appropriate functional groups.

With the relay and circuit-breaker operations defined, the stability program is restarted with these operations appropriately simulated in time in the system data file for the stability program. Results of the stability program are monitored in time, for further possible changes in states of protection, or power-delivery, functional groups and, in turn, status of subsystems. These changes are again reflected into the appropriate data bases.

At this stage, depending on the available code, the assessment may become an iterative process, with continuous monitoring by the engineer. Or the stability code may be run out continuously in time with the program automatically performing pre-defined circuit breaker operations as pre-defined relay schemes call for these operations.

Within the two-second period before the MHD-EMP assessment methodology becomes of consideration, it may be necessary to determine the states of the system at given times and restart the process where automatic actions may be taking place toward system recovery. For example, if certain parts of the power network have separated, or interconnections between various utilities have opened, each individual part or utility may require study and additional stability assessment on an individual basis.

The general approach of this methodology, then, is to choose a size of weapon detonation at a given place in space and at a given time, (Fig. 65) recognizing that the impact of the source region buildup following the detonation will vary across the confines of the power system being assessed.

The power network is divided into physical blocks, located geographically of such size that can be analyzed separately in determining the stress effects of HEMP illumination (Fig. 64).

From the detonation location and time the EMP environment is defined at spatial locations throughout the power system with the appropriate environmental characteristics of the early- and intermediate-time periods. Then, utilizing the coupling characteristics of circuit and devices within functional groups within a subsystem of the power system network at a specific place and time, the voltage, current or energy stresses are determined within the functional groups. Here the assumption is made that the entire power system (i.e., all its subsystems, and functional groups, circuits and devices within the subsystem) are "swept" or are affected by the HEMP, in magnitude and instants of time varying with location tc the source region. However, interaction between subsystems, and where appropriate at lower assessment levels, are neglected in the first phase of the assessment; since illumination time is short compared to the inherent time constants of the power network. That is, in early-time quasi-decoupling between subsystems at different locations under the initial illumination is assumed.

The stresses (electrical or thermal) are then compared with the strengths of the selected circuits and devices under consideration to establish a probability of failure, i.e., damage, flashover, or upset, of a certain circuit or device within a functional group.

Following this point in the assessment, interaction sequence diagrams or fault trees may be utilized to analyze the interplay of failures or upsets between circuits and devices within the functional

group. At this level and time, interactions between different functional groups within the subsystem may require consideration.

At the next level, the probability of performance of each functional group within the subsystem is used to assess the changes in operational state of the subsystem. In a later time, interactions take place between subsystems, affecting the performance of the power system and finally between interconnected power networks, if appropriate.

The power network reactions, in time to the changes in states, are determined by performing transient stability analyses incorporating the assessed changes in state of its subsystems (Fig. 66). From these studies any subsequent changes in the power network are further incorporated into additional transient stability analyses.

The analysis can give insight into the transient stability limits of the system, that is, the restrictions on levels of load that certain circuits can carry following the above disturbances, leading to other considerations in the assessment.

The results of this assessment are: what parts of the power system (functional groups and subsystems) will remain in operation, what loads can be supplied, and what changes in state are still taking place in the power system at the end of the period preceding the MHD-EMP period.

The increased complexity of the early-time HEMP environment, and the unknowns associated with this and the intermediate time environment emphasize that the methodology and assessment must recognize that there will be, at least initially, inadequacies in the analysis. Data for many levels of this assessment are difficult to obtain and other available data are of questionable quality. Validity of the assessment process is influenced more by the quality of the data than the process itself.

Results based on the limited data augmented with additional small-scale experimentations must be viewed with some caution. As more data becomes available and further analyses are done, with validation, more confidence will be gained in the data and techniques used in the assessment procedures.

4.2 Methodology Structure

By definition, methodology is a system of principles, practices and procedures applied to a set of knowledge to achieve a specified objective. The process is structured; it can be considered as a series of interrelated tasks. Each task may take the form of: (1) information gathering, the establishment of required data bases, (2) information transformation, the modeling and simulation of systems by analytical techniques, or (3) assessment, the comparison of two or more data bases or models in an attempt to quantify cause and effect relationships. The HEMP assessment methodology has been developed within the context of this definition.

For the purpose of this report, the complete set of tasks which constitute the methodology process has been partitioned under several major groups which address specific aspects of the power system network. These major groups are defined as:

● Definition of HEMP event (Section 4.2.1).

● Delineation of electric power network's power-delivery and communications systems to be assessed (Section 4.2.2).

● Description of subsystems, and devices and circuits of functional groups within subsystems (Section 4.2.3)

● HEMP coupling codes and response models for circuits and devices of functional groups within subsystems (Section 4.3.4).

● Interaction of circuits and devices within functional group (Section 4.2.5).

● Stress/strength assessment of damage or upsets of circuits and devices within the functional group (Section 4.2.6).

● Effect of failures upon functioning state of the functional group (Section 4.2.7).

● Interaction between functional groups as they affect the status of the subsystem (Section 4.2.8).

- Effect of status of the subsystem upon the states of the power network system (Section 4.2.9).

- Response states of the power network over time (Section 4.2.10).

4.2.1 Definitions of the HEMP Event

The methodology must of necessity begin with a definition of the event and of the electric power system of interest. As described in Section 2, HEMP Environmental Description, the nuclear high-altitude burst environment is specified as follows:

- Location in space of the event (burst origin and altitude), which establishes location of the source region.

- Temporal and spatial characteristics of the total HEMP environment produced by the event.

- Temporal and spatial definition of the local environment field "sweeping" the elemental area under consideration of the power system.

4.2.2 The Power Network

The power network as defined in this methodology by:

- A physical description connected with grid-coordinate locations defining systems configuration. This definition includes geographical locations of subsystems, such as substations and communication facilities, as "nodes" of transmission lines and of radio/microwave communication links. It also includes information giving the direction or orientation of the transmission lines.

- Subsystems, circuits and devices at a particular location under initial illumination and the functional relationships between them.

- Initial subsystem operating conditions at the particular location and of the overall power system before the event.

These characteristics of the power network systems may take the form of data bases or coded descriptions. The area of the systems must, therefore, be defined in terms of spatial coordinates to the event based on certain limiting criteria. These criteria might be spatial invariance of the EMP field over the confines of the area, or a size as determined on the basis of the concept of critical line length (Section 3.2.1.3). Because of the large geographical dispersion of the systems, the definition of the elemental area may take the form of longitudinal and latitudinal grid lines such as in Fig. 67. This figure, however, may show grid lines of too large a definition to be useful to the limiting criterion; therefore, smaller incremental areas meeting the limiting criteria may be used.

The methodology then defines what devices and circuits, functional groups of devices and circuits, and subsystems are within the elemental area with regard to a smaller grid system. Through this grid system, information can be provided about orientation and connections between these elements, etc.

4.2.2.1 Data Base: Power Network

In this task, a data base is established for the systems of the network exposed to the electric field. The data base must include the following information:

- "State" of the electric power-delivery system in terms of 60-Hz electric dynamic parameters, including implied "states" of subsystems and functional groups.

- "State" of the communication/control system.

- Spatial location of the major subsystems including interconnection data.

- Functional groups of circuits and devices within each subsystem.

Fig. 67. Definition of location of elements of utility network.

4.2.2.2 Model: Spatial Coordinate or Map System of Reference for Power Network Power-Delivery System

In this task, a frame of reference is selected to place in position the major subsystems of the power network power-delivery system under assessment, and the spatial relationship of the source region to each of the subsystems. This can, simply, take the form of map coordinates similar to Fig. 67.

4.2.2.3 Model: Spatial Coordinate or Map System of Reference for Power Network Communication System

This task is very similar to 4.2.2.2 but is described by subsystems with network communication functions.

4.2.3. Subsystems and Functional Groups

Data bases, keyed to the coordinate system, are then used to define the subsystems, circuits, and devices lying in each elemental grid area. Data bases then link the type of circuits and devices, etc., in the elemental area to their respective coupling codes and to other characteristics. Section 4.3 describes the hierarchy of data bases to support the methodology.

Major subsystems within a power network can include [33]:

- Generation plants, or separate generator subsystems within a plant
- Generation substations
- Transmission/subtransmission substations
- Transmission/subtransmission power lines
- Distribution substations
- Primary and secondary distribution systems
- Operation centers, administrative offices, field offices, etc.
- Communication facilities.

Figure 62 has illustrated a representative utility system.

Generation consists of the generating facilities of the power system. In addition to the power generation and main transformer(s), this subsystem includes the associated protection, control, instrumentation, and auxiliary equipment of the respective facility.

Substations include the transmission (ac and dc) and distribution substations, as well as the switchyards of the generating facilities. In addition to the equipment associated directly with the power delivery function, the equipment necessary for the protection and control of the power system and for the communication with control centers located at the substation are included. Series capacitors in the center of a line with their associated control are considered in this methodology to be substation subsystems.

Transmission lines consist of those power delivery lines which connect the substations, which may be classified as transmission or subtransmission. DC transmission lines, less their terminals, which are substation subsystems, are also included in this type of subsystem. Transmission-line subsystems may be replaced with equivalent "driver" networks as part of other subsystems.

Distribution power circuits subsystem includes the distribution line, distribution transformers, and protective equipment out in the line, as removed from the distribution substation. The distribution subsystem may also include the load, or the size or characteristic of the load may predicate a separate subsystem. A distribution line is defined as that which is connected to the primary of a distribution transformer to supply utilization voltage to the utilities' customers.

Operation and control centers consist of the utilities' control and dispatch centers. These operation centers can control, among other things, the generation output and the switching functions of the substations.

Communication and other equipment in the communication/control system, affecting power transfer facilities and links, provide communications between different physical locations. Examples of

communication links include radio, telephone, and power-line carrier communication equipment. Local communication at a physical site are included in the analysis of that site as a subsystem.

As indicated, common to each major subsystem are some or all of the following functional groups of circuits and devices:

- Power-delivery function
- Protective function
- Control function
- Instrumentation function
- Communication function

Each functional group in a given subsystem is assumed decoupled from the other groups in the initial time of illumination by the HEMP field. The relatively longer response times of the functional groups provide a justification for this assumption.

Analysis of malfunction or upset of the power-delivery function can be segmented into tasks based on the coupling and stress models for devices and circuits supporting the function. The following are examples of tasks that may or may not be common to various subsystems.

    Power Line, bus, or cable analysis
    Power and auxiliary transformer analysis
    Shunt reactor analysis
    Instrument transformers analysis
    Circuit-breaker analysis
    Power fuse/current-limiter analysis
    Surge protection analysis
    Series capacitor analysis
    Turbine-generator analysis
    Excitation system devices and circuits analysis
    Line-trap analysis
    Motor analysis
    Series capacitor protection relay analysis
    Distribution secondary and connected loads

Analysis of upset of the protective, control and instrumentation functions can be segmented into, among others, the following analysis tasks based on the devices and circuits supporting this function:

    Relaying devices
    Battery supply circuits
    Instrument transformers
    Circuit-breaker operating mechanisms
    Interconnection wiring and cable
    Shielding means
    Grounding means
    Instruments
    Panel Switches
    Annunciators

Analysis of the upset of the communication function includes analysis of, among others:

    Power supplies
    Transmitters
    Receivers
    Coupling devices (such as HV coupling capacitors for
      power-line carrier)
    Antenna
    Interconnection wiring and cable

4.2.3.1 Data Base: Characteristics of Circuits and Devices within Functional Groups

This task addresses gathering the following data on selected circuits and devices of critical functional groups within each subsystem to be assessed for their effect on the state of the subsystem.

- ● Individual circuit parameters and equipment and device characteristics (including electrical parameters and dielectric and thermal strengths; where appropriate) within each functional group, such as the following examples:

    - tower configurations (if overhead), length, orientation in reference grid, resistance, capacitance and reactance of conductors [35].

- relaying or control circuit lengths and orientation in reference grid.

- location, ratings and type for power transformer and shunt reactor banks contained within a power-delivery functional group.

- series capacitor characteristics and control.

- generator electrical and dielectric parameters for generation plant.

- auxiliary motor electrical and dielectric parameters.

- relay types, settings, operating characteristics

- Antenna parameters (if communication functional group within power system).

● Interaction data of circuits and devices within each functional group (such as, connection diagrams) [36].

Since it is impossible to assess small components in a device from the device assessment itself, the device with all its components will be treated as a "black box" with terminals or input-output "ports." It should be noted that normally output terminals from a device may, in the EMP threat, become input terminals to the device for the EMP stress.

4.2.3.2 Utility Communication/Control Systems

Utility communication/control systems can include a wide variety of methods for information transfer. These may be voice, analog or digital signals in form corresponding to the telemetry, control and/or protective system functions required. For HEMP assessment, communications can be considered as two general categories.

● Radio communication systems including point-to-point microwave and base station/mobile radio equipment.

- Wire-based communication systems which use "links" of the form of (1) power line carrier, (2) shielded wire, (3) utility owned twisted pair and coaxial circuits, and (4) leased telephone line with associated transceiver terminal equipment.

In the case of wire communications, the HEMP environment is identical to that previously discussed for the power system grid.

4.2.3.3 Data Base: Radio Communications Operation

In preparation for assessment of utility radio communications in an HEMP environment, the systems are categorized by (1) the frequency of the carrier, (2) the normal signal to noise ratio and, (3) type of function and/or information content. Data in the functional groups in terminals supporting the communications are gathered.

The additional tasks entail quantifying operational, strength, and coupling characteristics of the remaining devices and circuits in the communicational functional group, and the connections between them.

4.2.3.4 Data Base: System Line Communication

This task has a number of subtasks, one of which is detailing the spatial location and orientation, characteristics of the communication line or link. In the case of power line carrier systems, this part of the data base is included in that for the power line as part of the power defining functional group.

4.2.4 HEMP Coupling Codes and Response Models

A coupling code or model is a means by which relatively simple cause-effect relationships can be derived between stresses and the effects of these stresses. Two models may be required for individual circuits and devices: one giving the effect of stress on failure of the device and the other translating the effect of stress on the device into output quantities utilized for further assessment. A simple example of the latter is the model for a current transformer, translating the surge

in its high-voltage primary to the output signal at its secondary terminals. Due to the complexity and diversity of the EMP interaction problem, it may be required to perform some analyses to have several different models available. Examples of other models are:

Transmission-line coupling models.

Models for predicting EMP penetration through apertures in shielded enclosures.

Models for predicting EMP interaction with antennas.

Transfer-function models for voltage or current transfer

Voltage-stress response models

A power-line of considerable length entering a substation may be replaced with an equivalent "driver" model of a voltage source behind the characteristic impedance of the conductor system. The concept of "critical line length" (Refer to Section 3.2.1.3) is a basis for this model. The use of a "critical line length" model effectively moves the boundaries of the substation subsystem out the distance of the critical line length.

Depending on the grazing angle of the HEMP field "critical line lengths" of conductors may be relatively short compared to the size of the substation. In this case partitioning of the power-delivery functional group may be based on this length.

HEMP energy can be coupled into a shielded system through antennas, direct penetration through shields, through windows and on conductors penetrating the outside structure of the system. The coupling modes are examined to determine which is the most critical for the circuit or device under consideration. The determination of the most critical HEMP coupling can be done in some cases by visual inspection of the system/facility.

The approach taken in the stress/strength assessment, for example, for a control center block is to characterize the shielding effectiveness for the HEMP wave of the building for the locations of

interest inside the building and to characterize the attenuation of HEMP induced voltage and current transients on conductors (power lines, signal cables, antenna lines, etc.) entering the structure.

Included in the models for HEMP penetration are the effects of shieldings, field diffusion and conduction into the space occupied by the device under assessment. Sequence interaction diagrams could be used at this stage in the assessment to evaluate the effects of field stress. However, in order to reach an initial decision about the susceptibility of individual circuits and devices in the power-delivery system to damage or upset from direct HEMP, the assessment can neglect effects on shielding or field strength of all enclosures, except the intermediate enclosure or next level to the internal components of the device. However, each situation must be judged individually.

In this task group, the localized field may be "coupled" to a device "driver" model using a "coupling" model. From this model are derived output quantities to be used as stress "drivers" in assessing interaction upon other devices in the same functional group (See Section 5). Each stress "driver" model is defined at a point of concern (connection or coupling point) to the "equivalent" strength model of the device being assessed. Devices selected for assessment are those critical to the operation of the functional group.

Similar techniques are utilized for stress effects of other circuits and devices connected to the input and output terminals of the critical devices being assessed.

It is to be noted that device equivalent circuits as well as the "driver" equivalents may be different for each form of stress to be considered. Figure 68 illustrates interactions of models at the device level for effects of fields on the device and for the device as a "driver."
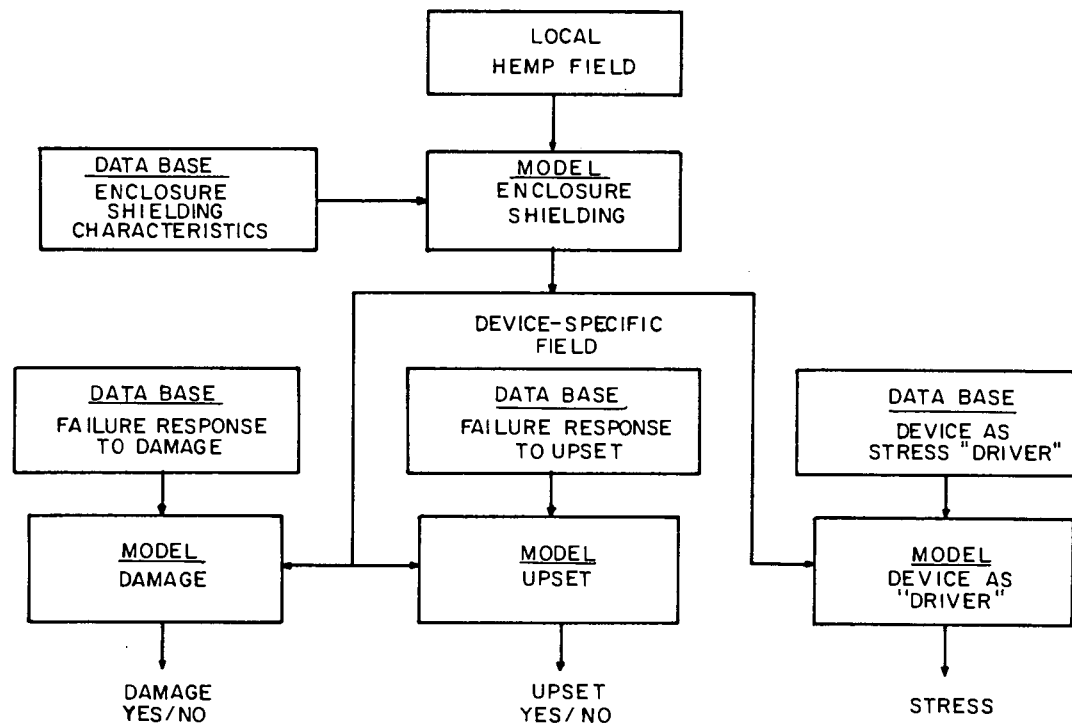
Fig. 68. Interrelation of data bases and models at device-level assessment with effects of field.

177

4.2.4.1 Assessment: Selection of Critical Devices to Operation of Functional Group

Establish criteria for selection of devices critical to operation of functional group. Identify potentially critical devices. As Fig. 69 indicates this may be an iterative process through tasks described later.

4.2.4.2 Data Base: Shielding Characteristics of Enclosures

When shielding effects can not be neglected, nor derived from calculation or engineering methods, test data is obtained on selected types of enclosures and environments.

4.2.4.3 Model: Shielding Characteristics

Relationships are derived to modify the coupling of localized fields at devices or on circuits. Effect of EMP penetration through apertures and by conduction is approximated in this model.

4.2.4.4 Data Base: Failure Response Characteristics for Damage Analysis of Individual Device or Circuit

Where models can not be developed from calculation or engineering methods, test data is obtained on selected devices or types of devices to relate stress into coupled voltages or currents.

4.2.4.5 Model: Damage Response for Device or Circuit

Based on calculations or test, cause-effect coupling relationships are derived for damage modes for the devices from fields and from conductive coupling.

4.2.4.6 Data Base: Failure Response Characteristics for Upset Analysis of Individual Device

The approach to this task is similar to 4.2.4.4.
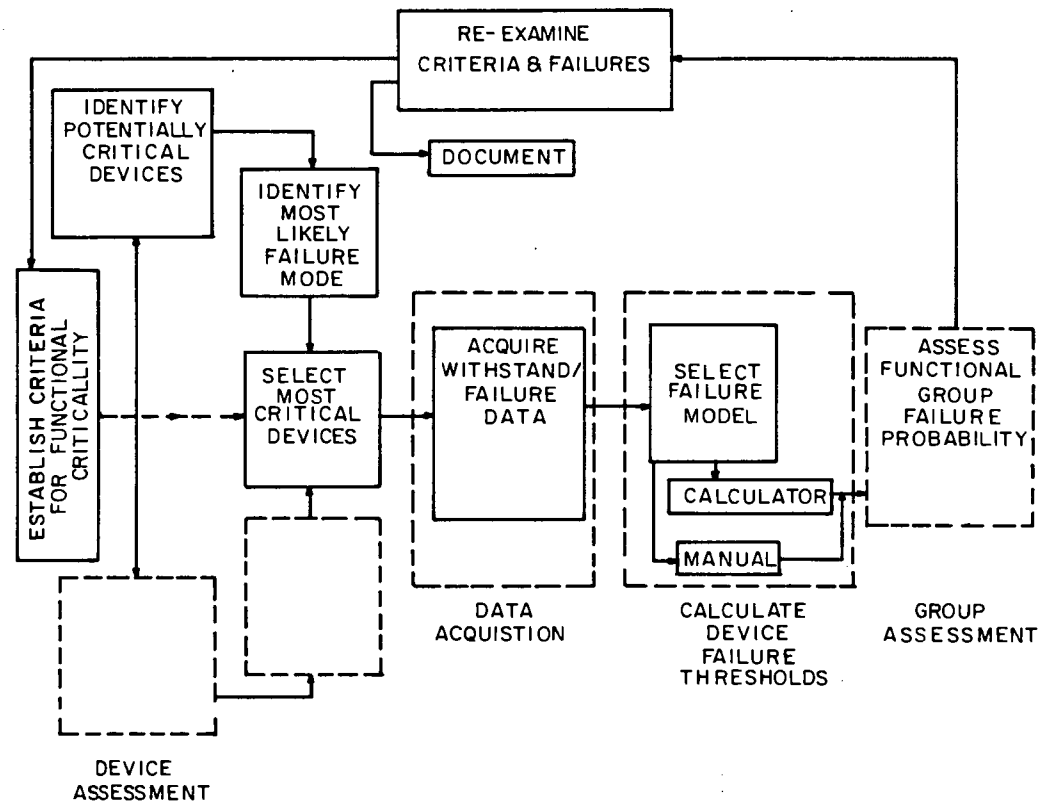
Fig. 69. Flowchart for selection of critical devices [36].

4.2.4.7 Model: Upset Response for Device

Cause-effect "coupling" relationships are derived between stress and upset modes of the device from fields and from conductive coupling.

4.2.4.8 Data Base: The Device or Current as a "Driver"

This is similar in approach to 4.2.4.4.

4.2.4.9 Model: "Driver" Model of Device

The device is reduced to an equivalent "driver" circuit as defined by its use at connection or coupling points in the functional group.

4.2.4.10 Models: Communication Line Response

Based on the information gathered in the previous task group and the specified electric field environment, an equivalent "driver" network is simulated for the communication line, in the form of either a Thevenin or Norton equivalent for estimating stress.

With coupling models for the devices and circuits and the specified electric field environment, similarly, "driver" outputs are also derived for stress analysis.

4.2.5 Interaction of Circuits and Devices within Functional Group

Failures of many devices or circuits in power networks are more likely to occur due to stresses produced by other devices or circuits on the device being assessed for failure. The connection-location diagrams of functional groups within a subsystem (Fig. 70) give an indication of where one form of interactions between functional groups may be possible [35], and the possible stress mode of a specific device or circuit in a functional group. In a sense, the coupling or direct interaction of stress from one functional group into another is another "driver" acting on appropriate terminals of devices or circuits being assessed. Fig. 71, for example, illustrates that the relay of its
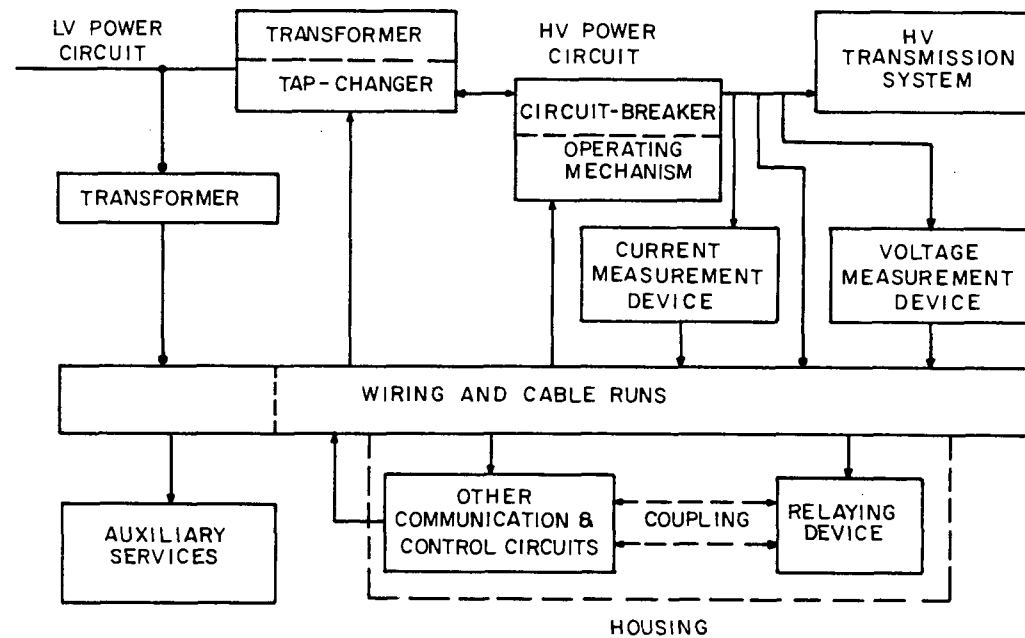
Fig. 70.   Connection-location diagrams.
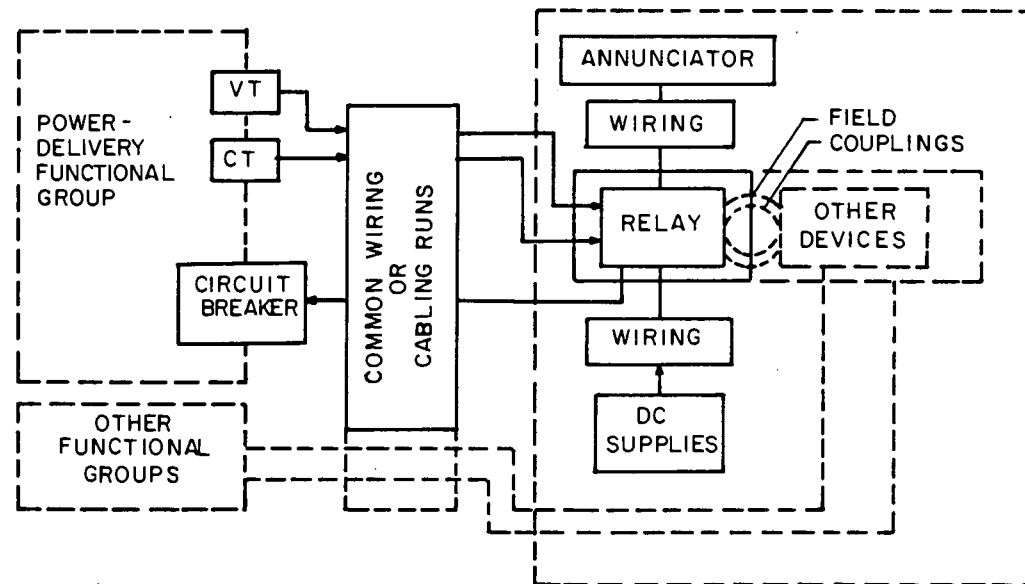
Fig. 71. Simplified physical interconnections of circuits
devices with attention given to relay.

functional group can be influenced by the power-delivery functional group through the voltage and current transformers that provide the current and voltage signals from the power-delivery functional group to the relay functional group, specifically to the relays or circuits in this group. Wiring and cable runs may be common to a number of functional groups, and therefore provide possible coupled paths between these groups. Relay devices may be "housed" in the same confines as provide possible coupled paths between these groups. Relay devices may be "housed" in the same confines as other circuits, such as for communication and control. Proximity effects may lead to "coupling" to the relays.

In this group of tasks physical interconnections of circuits and devices within one functional group and potential coupling interactions are derived from a study of the connection and layout (location) diagrams from data obtained in Section 4.2.3, as illustrated in Fig. 70 and 71, with attention given to each device critical to the performance of the functional group, Fig. 71.

Based on the "driver" circuit equivalents of Section 4.2.4 and the interconnection diagrams, interaction diagrams can be constructed for each critical device or circuit (Fig. 72).

As mentioned previously, the "driver circuit" equivalents and the configuration of the interconnection diagram will vary with the type of stress applied and susceptibility being assessed.

4.2.5.1 Data Base: Interconnection/Location Diagrams

These data are derived from data in Section 4.2.3 (Fig. 70).

4.2.5.2 Model: Device-Specific Interconnection Diagram

Similar to Fig. 71, this is derived from the previous data base.
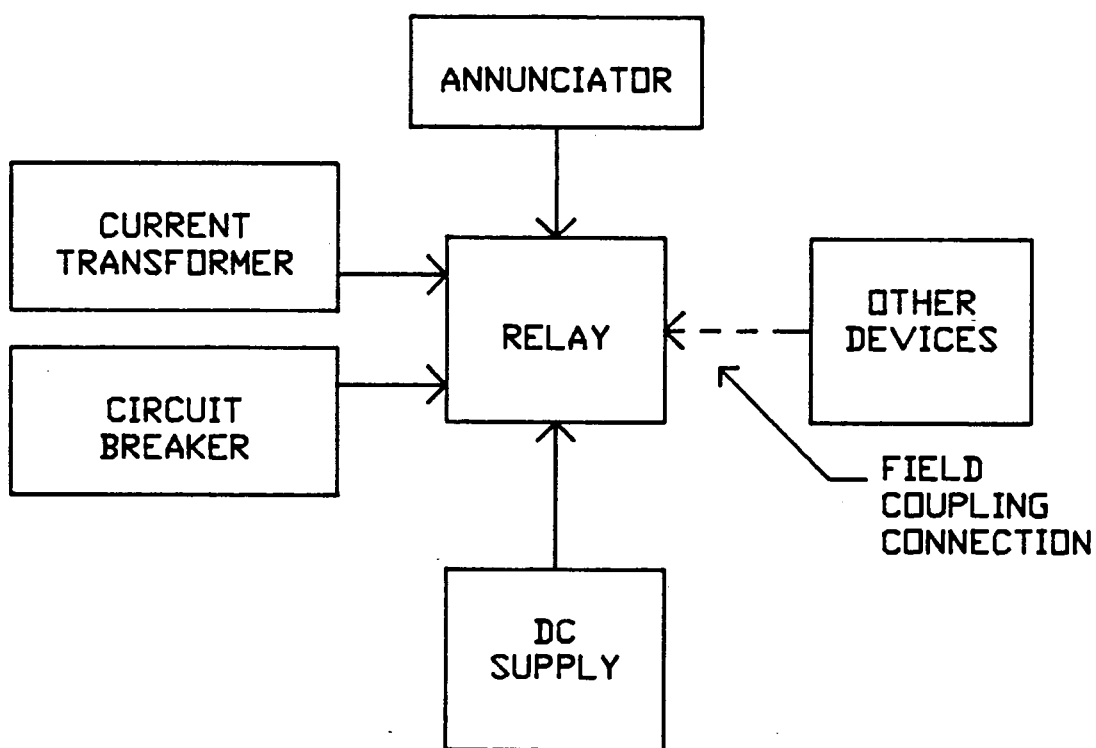
Fig. 72. Illustration of interaction diagram of "driver" models connected for strength assessment of a relay device.

4.2.5.3 Model: Device-Specific Interaction Diagrams

This task is the summation of the previous sets of tasks, leading to diagrams similar to Fig. 72 for each model of stress-failure assessment to be made.

4.2.6 Stress/Strength Assessment of Damage or Upsets of Circuits and Devices within The Functional Group

The two issues to be addressed under this set of tasks are the stress that appears in a circuit or device within a functional group, and the strength of the circuit or device to this stress; that is, the susceptibility of the device or circuit to either failure due to damage or to upset (Fig. 73).

4.2.6.1 Stress

In the context of the power system network assessment, the term "stress" can mean either the voltage appearing on a device or circuit, or the current flowing into the terminals of the device or circuit (or circulating internally).

The voltage or current may be due either to the field illumination directly on the device or circuit, or to connections or couplings with other devices or circuits to the device of consideration (Fig. 70 and 72).

While equations and computer codes are available or can be developed to calculate the voltages and currents produced by the HEMP event at all locations in a power system and the strength could be determined for these locations, it is not practical to do so unless unlimited resources are available. For studies with limited resources, engineering judgment must be used to determine the critical points or devices in critical functional groups at which the stress/strength comparisons are to be made (Fig. 69).

When the rise time of HEMP stress is less than the usual inter-connecting cable or wire length divided by the speed of light, both
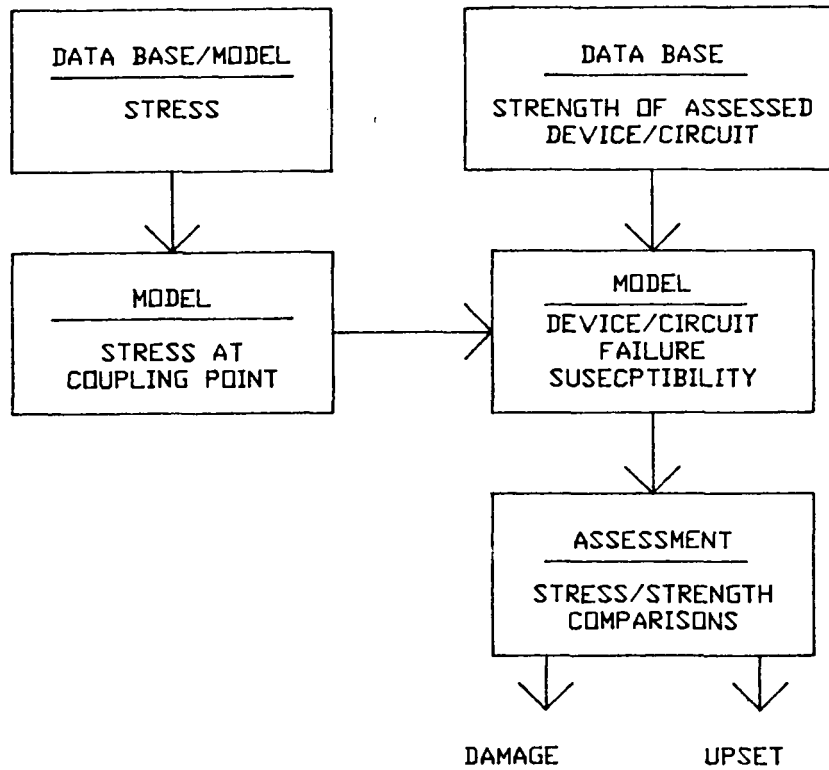
Fig. 73. Flowchart for stress/strength assessment of device or circuit.

EMP-induced stress and system stress inside a confine could exhibit standing waves. Therefore, determining the dominance of system-generated stress at one point within the confines taken, will not insure its dominance everywhere in the same confines [37].

With an HEMP rise time of 10 nanoseconds, if the length limitation criteria, L, is defined as:

$$10 \times 10^{-3} \text{ microsec} > 2L/1000 \text{ ft/per microsec}$$

then if L is less than 5 feet:

1. Standing wave effects are not significant.
2. System-generated stresses can be utilized for a base comparison for HEMP susceptibility.
3. HEMP-induced stress can be represented as a Thevenin equivalent voltage source with appropriate series impedances or a Norton-equivalent current source.

If the maximum frequency to be considered in the assessment is 10 megaHertz, having a wave length of 100 feet, then the limiting distance, L, can be somewhat larger, perhaps 10 feet.

Many circuits and device configurations within the functional group have dimensions that fall within the limiting length criterion. Therefore, these can be treated within the three guidelines stated above.

In the case of devices in the power-delivery functional group, dielectric or insulation withstand test results are available in the form of basic insulation levels (See Appendix F). Surge voltages of several different waveshapes are applied by test sets to the terminals of the power equipment to determine withstand levels of the insulation at these terminals. For example, Basic Impulse Insulation Levels (BIL or BIIL) and switching surge withstand levels (BSL) are available for each voltage class of power transformer. These data can become part of the withstand strength data base for power-deliverable devices.

4.2.6.2 Strength

Because of the variety of devices and circuits to be found in the functional groups of a power network, a number of different measures are used for "susceptibility" to failure. These can be identified with respect to dielectric failure, to thermal failure, and to functional mis-operation, or "upset."

Flashovers are one form of "failure" due to overvoltages in power networks. For transmission and distribution lines suspended from towers or poles, the lowest strength (flashover) values would normally be obtained at the insulators on the towers or poles. Line-to-line flashovers would be unlikely since the HEMP excitation is common mode and the line-to-line stress would normally be quite low. Since the stress on a line should normally be rather uniform, the stress/strength comparisons should be made at the insulators on the towers or poles, especially at points of discontinuity where the stress might be increased.

Surge arresters of different ratings and size are commonly used on both the power-delivery lines and (in much smaller sizes) in electronic equipment used in the control centers and for the instrumentation, control, and protective functions. Thus, in some circumstances physical damage of a device or circuit due to overvoltage is not a consideration because of surge protection at a terminal by the use of capacitors and surge arresters. Under this circumstance, thermal stress may be of more concern as it may affect the devices being used for the surge-voltage protection. This may also be the situation, for example, in the consideration of certain control-functional devices or communication-function devices.

Ambient stress levels can be high in substations and in control rooms in power systems because of energy levels associated with power-delivery switching functions. For example, it is well known that operation of high-voltage disconnect switches in substations generate high-frequency current surges in buses and lines whose fields can be coupled into control wiring if measures are not taken to suppress them.

Similarly, high-frequency currents flowing in ground conductors during switching of large shunt capacitor banks can also create voltages of several thousand volts in control wiring and low voltage power circuits.

This then establishes a "system-generated" or base environment threshold to which can be compared the stresses produced by HEMP. Such threshold data are available in the literature from tests made in the field. But it is to be noted that system-generated stresses from switching operations, in general, excite different points of the network in different manner, whereas HEMP excites all points essentially simultaneously.

In other instances, failure either from overvoltage or thermal considerations is not a concern, but rather the malfunction or functional "upset" of the device or circuit. This can be the situation for control or communication devices or circuits.

Two categories of "upset" have been defined [38]:

- Upset involving precipitous actions, such as tripping of a generator plant, "caused by erroneous states induced by the stress of electromagnetic pulse (EMP) in logic or other electronic or electromechanical elements of a system or subsystem. This category can be characterized by the instantaneous or nearly instantaneous consequences of temporary EMP disturbances. After the EMP has passed, the disturbed electronic or electromechanical elements are assumed to resume completely normal operation; but some significant undesirable action has occurred because of the disturbance caused during the EMP event."

- Upset leading to storage of erroneous information in an electronic or other memory that will result in an undesirable action at a future time.

It is presumed, a priori, that in the power system the latter category of upset is of secondary concern since devices that store information will be well shielded when used in the power system environment. However, this is another area which may need investigation in the assessment.

Section 5 discusses further concepts of strength and of strength data bases and models.

4.2.6.3 Responses and Stresses within Individual Circuits and Devices

The analysis must assess interactions between devices or circuits in producing stress in or on the individual device or circuit in a functional group. Each device, group of devices, or circuit connected to the assessed device is reduced to an appropriate equivalent "driver" circuit based on the field and coupling code to the connected devices and circuits (Section 4.2.4.8).

The "driver" equivalents and the device models having been derived, the next step is to apply each "driver" to the appropriate points of entry into the strength model equivalent of the device being assessed to calculate the stresses that develop at that application point by the specific "driver" (Fig. 72).

Stress can also be produced on a device by the HEMP field coupled to the device. The HEMP environment inside the control center building is defined for a given external environment in terms of a localized field strength at critical device locations, and/or in terms of voltage or current surges appearing on unfiltered incoming lines and cables.

Through tests or available data bases for a device such as (for example), a solid-state relay, the strength to damage or upset is compared to the localized field strength on the device at the frequencies of most significance (Fig. 68). The localized field strength is obtained by modifying the geographically-located field on the total enclosure of the relay by the shielding effects of major and minor enclosures and circuits between this field and the internal components of the device. In most cases, the effects will be to reduce the field strength at any given voltage.

The localized field strength as modified is then coupled to the internal components of the device by stress coupling models for the

device as an entity. (The entity may include a case normally used to enclose the internal components of the device.)

Where the field strength stress is comparable to the damage or upset strength of the device, a probability of failure is assumed. The result of this device assessment is entered into the "fault" tree that is later used to determine the state for this functional group of which this device and others are a part. In some cases failure of a device, a prior, means "failure" of the functional group, and is so noted at the level of assessment of the functional group. Figure 74 summarizes the above process and the following tasks.

4.2.6.4 Definition of Tasks for Stress/Strength Assessment

In this set of tasks, a stress/strength assessment for either damage or upset is performed on selected device or circuits within functional groups of concern. When appropriate to the assessment of the functional group, the output of assessment of a device or circuit can be expressed as the probability of failure (damage or upset) of the device or circuit. In many cases these data must be determined by test from a generic group, by calculation, or by judgment. With the strength characteristics of the devices and circuits established, the output of the assessment of functionability of the specific functional group can be in terms of probabilities through use of fault tree techniques as described in the next section.

Data are presently scarce in this area. Since uncertainties are attached to this process, small scale tests and large-scale simulations may be required for this analysis and to validate the assessment procedure. It may be necessary to iterate the process of analysis and test as more data become available until satisfactory assessment is obtained.

4.2.6.4.1 Assessment: Select Critical Functional Groups

This selection is predicated on the importance of the functional group performance to that of the subsystem. Generally, yard lighting
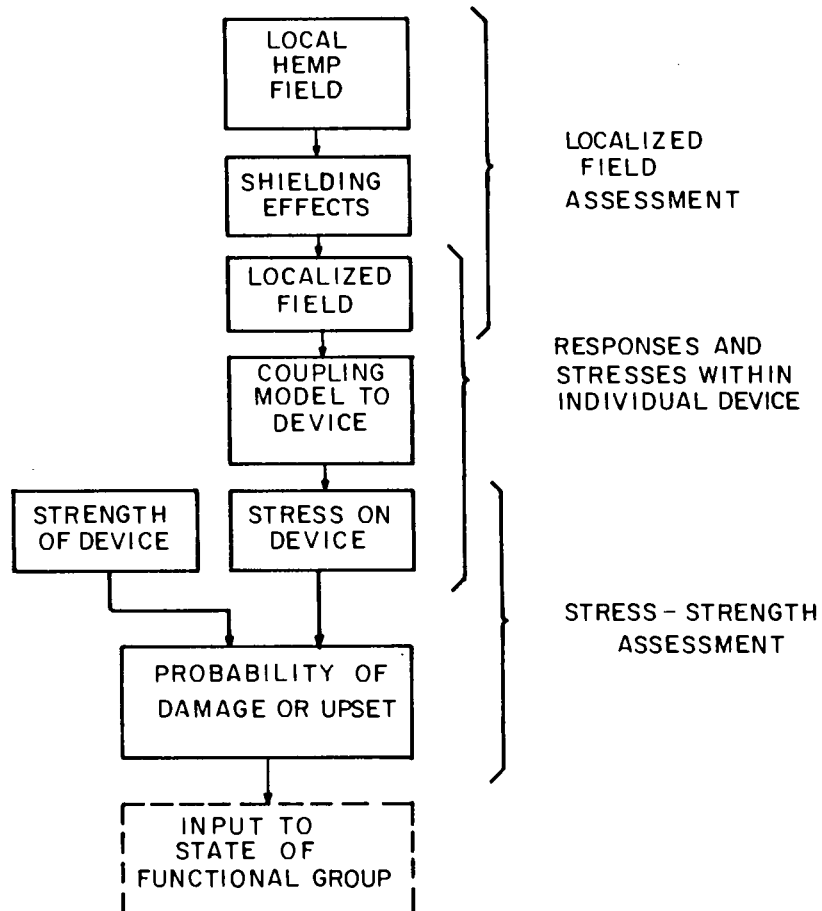
Fig. 74. Flowchart of stress-strength assessment of device due to field effects.

systems, for example, may not be critical; whereas, relaying functional groups may be critical to the functioning of substation subsystems.

The operational state of the functional group at the time immediately preceding the HEMP event affects this selection and is obtained from the initial system state data base. For example, for a power delivery functional group, this state may include the status (closed or open) of all switches or circuit breakers, the position of transformer taps and voltage regulators, the load flows through the various power delivery elements, etc. If the circuit breakers or switches are open, for example, "out of service" then, obviously, this power-delivery functional group is initially not critical to the functioning of the substation subsystem. However, it is important to know whether the state of this functional group is such that it can be used in later time for power network restoration. The state data base for this functional group would reflect the two conditions, i.e., not in service but capable of being put into service.

4.2.6.4.2 Data Bases: Characteristics of Devices and Circuits

Strengths should be defined with respect to terminals of devices. Data bases of withstand strengths may be given in terms of certain characteristics (i.e., pulse width, wave shapes, magnitudes) as derived from test results available or to be obtained by test. For example, surge withstand capability tests (SWC) of a given magnitude and waveshape are applied to certain relay systems. These data are available and could be part of the withstand data base for these relays.

The physical characteristics of the devices or circuits are obtained from the physical description data base, while the parameters to use in equivalent circuits are obtained from the equivalent circuit parameter data base. The locations of these devices or circuits are defined within the functional group by connection diagrams.

Data bases of strengths for some devices or circuits may not be available at the time of the assessment, and must be estimated based on characteristics of similar equipment. Data bases of "upset" strengths may be even less available, and engineering judgment also may be necessary to estimate these characteristics.

4.2.6.4.3 Assessment: Select Critical Device or Circuit within Functional Group

Identify from the data bases of all devices or circuits and the connection diagram what is the weakest device or circuit functional group from a damage and from an upset standpoint.

One basis for the selection of the critical devices is to perform a series of preliminary stress/strength calculations at representative points to identify the most likely failure mode. From the trend of the stress/strength comparisons, the most critical devices can be determined.

Some of the points for which preliminary calculations should be made can be selected in advance through a consideration of the parameters affecting the stress/strength relationship.

The strength relationships for the control room devices and circuits may be defined in terms of the maximum allowable electric field strength and the transient voltage and current levels on incoming lines for the various classes of equipment.

4.2.6.4.4 Assessment: Calculation of Stress

In this task the stress is determined for the terminal or points of entry of the strength models or equivalents at which comparisons between the strength and stress are going to be made. Depending on the device or circuit involved, the stress may be defined in terms of voltage or current waveshape or energy.

The stresses (either of voltage or of thermal concern) are approximated by the use of the "driver" equivalents acting on the device

stress/strength models. The stresses are compared to data bases of withstand strength levels or upset levels for the model of the particular device or circuit to determine the potential for physical failure of the device under consideration, or its functional upset (i.e. functional malfunction).

Given the time dependent magnitude of the "driver" voltages, the increase in rise and/or threshold of circuit or device upset is assessed. For high enough stress levels, potential damage due primarily to thermal failure is assessed using thermal strength models for the devices.

By the use of a decision "fault tree" or by risk analysis, assume the potential problem has been reduced to, say, a comparison of overvoltage levels to a consideration of potential "upset." The HEMP "noise" level as represented first by its magnitude would be compared to the upset level of the device or to the normal ambient noise level experienced by the device. If the HEMP "noise" does not fall within a selected margin of the ambient, or of the upset withstand level of the device then the analysis proceeds to other assessments. If the HEMP "noise" level is within this margin or higher, then the duration or frequency of the noise must be evaluated against allowable values to estimate potential of upset of the device under consideration.

The results of these failure assessment for a device is entered into the overall fault tree assessment of the state of the functional group of which the device is a part.

The following is an example of an assessment of a specific device in the relay or control functional group.

Analysis of Instrument Transformer as an Equivalent "Driver"

Knowledge of the steady state and transient performance of instrument transformers is of critical importance for instrumentation and protective relay system assessment. The simultaneous ac and dc excitation due to fault current offset will result in transformer

operation closer to or in the saturation state. The partial or full saturation can cause the secondary voltage or current waveform to deviate from the primary waveform. For transient fault conditions, a dc offset in the fault current of the same polarity can substantially reduce the time to saturation.

Data Base: Instrument Transformers

The data base should contain the following information (1) bus location of the instrument transformer, (2) operating characteristics including saturation curves and time to saturation characteristics, (3) configuration of secondary connection, (4) connected ratio, and (5) burden. This information is used in conjunction with the branch fault current data base to quantify operational performance in terms of the modified nature of the secondary waveforms.

Assessment: Current Transformer (CT) Operation

Based on the magnitude and time history of the fault current exciting the current transformer, in conjunction with ac excitation, the percent error of CT response will be calculated and secondary waveforms investigated as they may affect proper relay or instrument operation. An analysis may be made of the possible magnitude of CT remanant flux for later assessments in MHD-EMP.

The following are examples of specific device assessments in the power-delivery functional group.

Analysis of Power Fuse

The combination of normal power frequency current and the fault contribution as a result of faults due to the HEMP event may result in power fuse misoperation during the two-second HEMP assessment time. This potential risk assumes increasing importance since the fuse is a single operation device. A "blown" power fuse requires manual replacement which can increase the time required for electrical service

restoration. A fuse may also be damaged by an initial fault but not "blown" until an additional current surge.

Data Base: Power Fuses

This data base consists of fuse operating curves which depict the relationship between time and rms total current. (See Fig. 24 of MHD-EMP report [32] for a typical set of curves.)

Assessment: Fuse Operation

The power fuse data bases will be compared to the expected values of 60 Hz power frequency rms current combined with the fault-current value, to ascertain the probability of fuse operation.

Analysis of Power Transformers

It is known that high magnitudes of surge voltage applied to the terminals of a transformers can result in:

- Possible insulation deterioration or damage due to failure of major insulation to ground or turn-to-turn insulation.

- Transfer of voltage components inductively and capacitively to other terminals [39].

It is common practice to protect the major insulation to ground by utilizing surge arresters connected to ground at the terminals of the transformer. Rarely are surge arresters connected phase-to-phase except for transformers in some DC installations. Although the surge arresters tend to reduce the voltage components if the surge is above the protective level of the surge arrester, voltage components below this level are transferred through the transformer to other circuits. This leads to the consideration of data bases and models directed toward two regimes for assessment: strength and transfer characteristics. It is assumed that, except at winding terminals and based on the inherent shielding of the steel transformer tank, coupling of HEMP fields into internal parts are insignificant in the assessment procedures.

Data Base: Power Transformer Strength

Strength of windings of transformers are defined by standard withstand levels, termed chopped wave, basic impulse insulation level, basic switching impulse insulation level and rarely, front-of-wave (see power definitions, Appendix F). The first and last levels mainly test turn-to-turn insulation. Depending on the insulation class, values for these withstand levels are tabulated against the insulation class for factory test. A multiplier is applied to these tabulated levels to reflect strength of the transformer after being in service. Tests of older equipment in field service for some time are generally given withstand tests at 75% of the factory tests. This provides a qualitative margin for failure in field installations. These withstand levels are utilized for strength assessments.

Data Base: Transformer Transfer Characteristics

These data imply sufficient details of the inductances and capacitances of the transformer windings are obtained so that simple transfer models can be derived, sufficient for the frequencies of interest in the surge impinging on the terminals of the transformer.

Model: Transformer Strength

Because the high frequency equivalent of a transformer consisting of inductances and capacitances, the shape and magnitude of an impulse surge on the terminals of a transformer are changed. A model for this effect is needed that relates open-circuit voltage on a line to that voltage resulting across the terminals for the proper assessment of transformer strength.

Model: Transformer Voltage/Current Transfer

Based on the data base associated with this task, a "transfer-function" model is developed. This model may be frequency specific.

Assessment: Transformer Insulation Damage

To assess the possibility of insulation damage, impinging surge voltages, after modification by the transformer surge model, are compared to the most appropriate of the available withstand voltage levels for estimating failure.

4.2.7 Effect of Failures Upon Functioning of The Functional Group

Fault trees are developed from the functional relationships and connection diagrams as a basis for assessment of the probable states of each functional group [36]. For example, a fault tree can simplify determination of the circuit breaker operational state as part of the functional group assessment. "Fault tree analysis is a systematic method of tracing the effects of failures at lower levels of system upon its higher levels" [38]. The method can be used to estimate probability of survival for complex systems and to compare various hardening approaches.

"A fault tree analysis will yield a probability distribution of the probability of system survival conditional upon the level of confidence associated with the assigned probabilities" [38].

Data bases have been established under Task Group 4.2.3 that contains the functional relationships between the devices and circuits of a power delivery functional group. Examples of the functional relationships contained in this data base are the relay scheme used to control power circuit breakers, and a control scheme for a generator.

At least two "trees" of failure probability are required, one to define the probability of damage in the functional group (preventing the group from performing its specific function) and the other to define the probability of upset leading to an incorrect indication of its purpose. For example, a protection-functional group, could be made up of a current transformer signalling through wiring or cable to a relay. Two dc power supplies are provided; only one is necessary for proper functioning of group. The relay and one or both power supplies may in

turn be connected to the operating coil of a circuit breaker. The failure of any one of these devices or circuits can cause failure or upset of the group and cause the circuit breaker to trip. Fig. 75 shows a simple "fault tree" representing this functional group.

Some of these devices, due to their high reliability, or low probability of failure or of upset may be eliminated from the "fault tree". Due to lack of data, some engineering judgment of failure probabilities may be necessary in the assessment for other devices.

It is expected that a generic form for one or both types of analysis, damage or upset, can be developed that will fit any specific type of functional group. This approach will simplify code development for fault trees. Codes are presently available to create appropriate fault or decision trees.

The approach to be taken is to develop a minimum of generic fault-tree models for each type of functional group. Generic models enable representative assessment of HEMP effects. A unique fault tree model need not be developed for each individual functional group of every subsystem. Consequently, assessment of HEMP effects can be accomplished for all generic models and any subsystem can be uniquely modeled by a representative combination of these models.

The following is an example of an assessment of two specific functional groups.

4.2.7.1 Analysis of Instrumentation, Control and Relay Functional Group

Subsequent to the assessment of current and voltage transformer operation in an HEMP environment, this information must be integrated into the analysis of instrumentation, control and protective relay schemes. For instrumentation, the assessment should consist of the quantification of measurement error introduced by the modified secondary waveforms of the instrument transformer as determined under Task Group 4.2.6. Control system operation must be investigated to ascertain
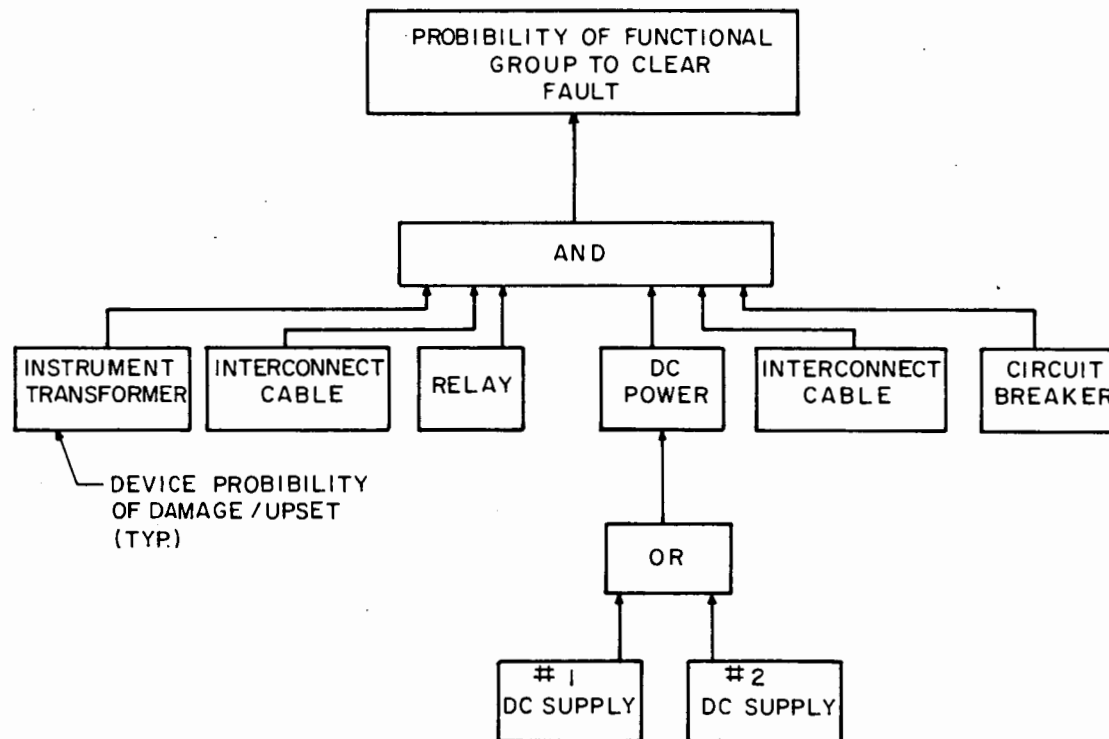
Fig. 75. Simplified example of fault tree analysis of effect of device probabilities upon state of functional group.

the impact of misleading input information. Protective relay schemes must be investigated in the context of relay security and operational dependability.

Data bases, as established in Task Group 4.2.3, would contain the operating characteristics of measurement instrumentation including transducers and metering systems. Measured system parameters for assessment are voltage, current, frequency, real and reactive power. The control system data bases would include the operating characteristics for systems such as automatic generation control, local frequency and local voltage control schemes.

4.2.7.2 Assessment: Instrumentation and Control System Operation

The assessment will quantify the amount of measurement error contained in the output of instrumentation systems. The total error will be the combination of the ratio and phase angle error of the instrument transformers in conjunction with the modified uncertainty of transducers and metering systems. Control system operational assessment is based upon the ability of these systems to perform their intended functions given distorted power system parameter input data. (The ability of control systems to filter "bad" data would be included in this documentation.)

The resulting assessments would be reflected in the state data base for this control functional group.

4.2.7.3 Assessment: Protective Relay Scheme Operation

The assessment will consist of the quantification of relay scheme security and relay scheme dependability. A loss of security is defined as an undesired relay operation in the absence of those conditions for which the relay must perform its intended function. The loss of relay scheme dependability is defined as the failure to operate, or, operation with excessive delay for abnormal conditions. For example, dependent on relay design, the primary effect of current transformer secondary distortion may be zero-crossing shift, peak reduction, rms value reduc-

tion or harmonic content. Relay schemes of particular interest include current-differential protection, overcurrent protection, undervoltage schemes and distance relaying applications based on line impedance parameters.

The resulting assessments are reflected into the state data base and fault tree for this protective relay functional group.

4.2.8 Interaction Between Functional Groups as They Affect The Status of The Subsystem

The outputs of the stress/strength assessments, for functional groups, as reflected in their states data base and fault trees can be used as the basis for determining the reaction of the subsystem to the HEMP event. Damage and/or misoperation of some of the functional groups may have little or no short term effect on the operation of the subsystem. For example, misoperation of the instrumentation functional group due to damage of panel meters would have no effect in the interval following initiation of the event since human intervention would be required to initiate a change based on the faulty information. Similarly, loss of communications would have little immediate effect except for communications used in protective relaying schemes. (However, in a later assessment, loss of communications could make the power system more difficult to control and the restoration of power after a power outage slower.)

At this level, engineering decisions, that is, human intervention, through a thought process based on the various states of the individual functional groups may be required for assessing the status of the subsystem made up of these functional groups and ultimately the power network (Fig. 76). In future refinements in the methodology, this thought process might be supported by "expert systems" or "artificial intelligence systems."

Proper assessment, however, requires that all relevant modes of failure can be identified, including such factors as human error. Also, the relationship of various parts of the subsystem must be understood
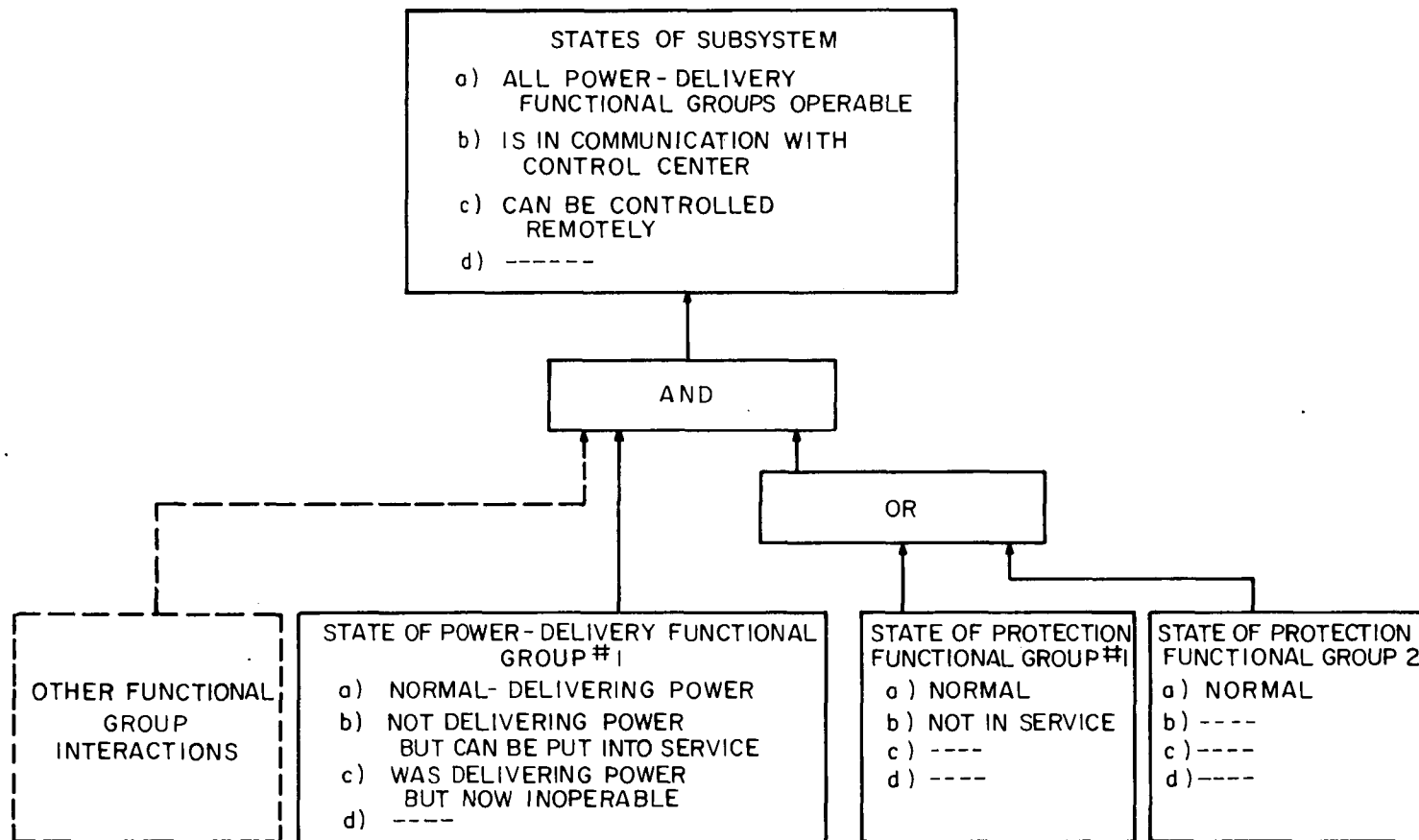
Fig. 76. Simplified "fault tree" questions for deciding states of subsystem.

well enough as to "model" them appropriately. In these assessments, it may be necessary to estimate a number of the probabilities, tempering these estimates with engineering knowledge of the viability or the subsystem dependence upon certain functional groups, and the devices within these groups.

4.2.8.1 Data Base: Critical Questions Bearing on
Subsystem's Ability to Support Power-Delivery Mission of Network

In these tasks questions are formulated that are critical to the subsystem operation, similar to the questions in Fig. 76, but of specific form.

4.2.8.2 Data Base: States of All Functional Groups in Subsystem

These tasks entail identifying which functional groups are in operation before and after the HEMP event; which are not in service (performing function) or can be put into service in a future action; which have failed while in service and extent of failure (damage or upset) and why failure has taken place; and which have failed so as to inhibit future actions. As an example, Fig. 77 illustrates part of the thought process in identifying functional groups and their effect on answering a critical question "can the generation subsystem in a generator plant continue to deliver power into the network." (Because of the long time required to bring a generator up to speed and on line delivering power, the question of whether an out-of-service generator can be brought on line is academic in the HEMP assessment time.)

Model: Decision Tree for Answering Question

A decision tree in answer to each critical question is built, similar to Fig. 77, down to levels of assessment in sufficient detail to identify blocks significant to the answer to the question and to relate to the tasks of Section 4.2.7.
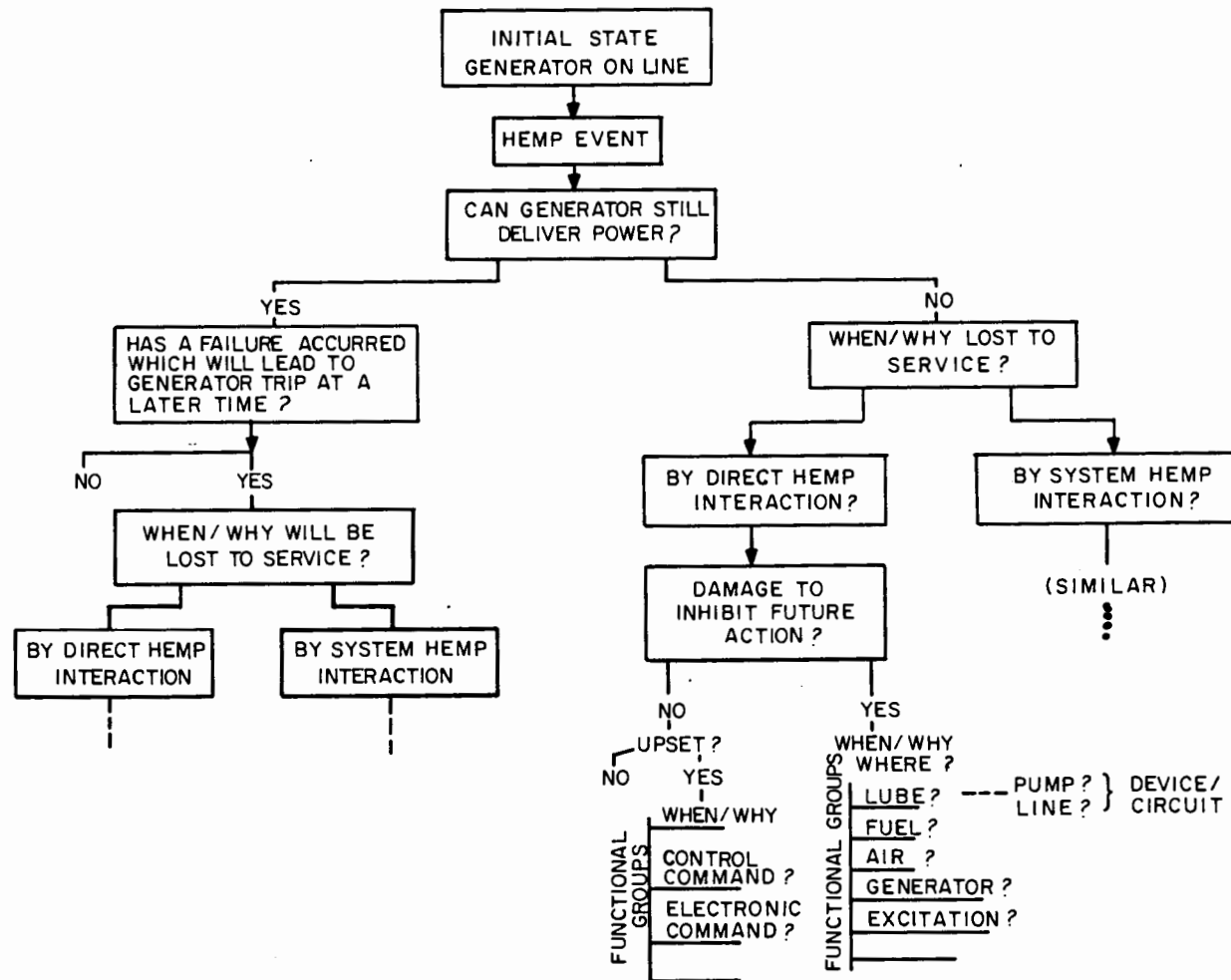
Fig. 77. Illustration of analysis of question, "Can generator still deliver power?"

4.2.9 Effect of States of Subsystems Upon Status of The Power System Network

The primary mission of the the power network is the delivery of power, and this mission is supported by the functions of subsystems in both the power-delivery system and the communication and control systems. Therefore, the emphasis of this level of assessment is on this power-delivery mission.

The purpose of this set of tasks is to utilize data bases of the initial and subsequent states of the subsystems, as imposed by their functional groups, to formulate the conditions at given points in time as input to the codes used to study the response of the power network. It can be anticipated that the states of certain subsystems will be influenced or changed at later times in the assessment by the results of changes in states of other subsystems at the time of the HEMP illumination, and as the power network responds dynamically to the initial changes in states.

Fig. 78 illustrates the major power-delivery subsystems of a small power network for the purpose of this discussion. This figure shows also assumed communication links in the form of radio nets, microwave channels, and leased telephone lines. Because of the short pulse-width of the HEMP it is not expected that other than leased lines, will be affected by HEMP. However, these are "subsystems" that become of concern during the MHD-EMP assessment. (In contrast, of course, functional groups at the terminals of these lines can be affected by the HEMP illumination.)

A basic assumption throughout this methodology is that all of a given subsystem (with perhaps the exception of very long transmission lines which may be handled in a special manner) is illuminated by HEMP at the same instant. With the HEMP fields moving at no less than the speed of light, substation subsystems, for example, separated by several hundred miles in the direction of the movement of the field, would experience the HEMP at a time difference of a very few milliseconds.
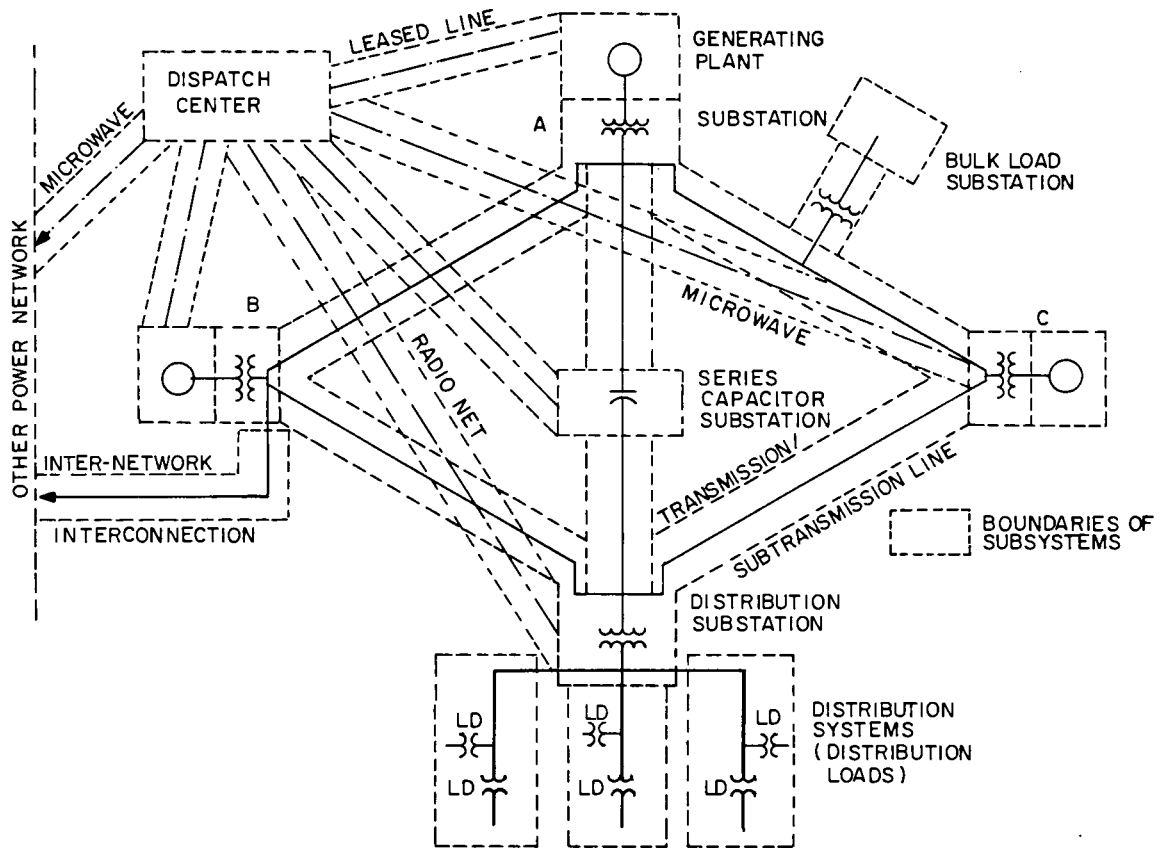
Fig. 78. Illustration of a small power network
with single interconnection to another power network.

For example, with the HEMP wave coming in at the top of Fig. 78, the generating plant A and its substation would experience HEMP before generating plants B & C, (which would receive illumination at the same time).

With the relatively long response times of power changes in a power network (cycles of the system frequency), a reasonable assumption, however, is that the total power network is illuminated essentially at the same time. This means, then, for the purpose of assessment that flashovers and other changes that occur in the power system as a result of the HEMP occur essentially at the same time.

Generally, the power-delivery functional groups of many subsystems are interactive through circuit breakers or switches with their associated supporting protective relaying functional groups, Fig. 79. Because of physical location, circuit breakers are considered in this methodology as part of substation subsystem; however, the circuit breakers at line terminals and their supporting relaying functional groups, could be considered as part of their respective power-line subsystems. Thus, the overlapping function of a circuit breaker provides the basis for the interactive states of the substation and associated power lines. Fig. 79 illustrates these details.

The results of the previous groups of tasks are used in the assessment to the level of interactions between subsystems. As is discussed earlier in this section, it can be anticipated that the states of certain subsystems will be influenced or changed, at later times, by the results of changes in status of other subsystems at the time of HEMP illumination.

For example, one state for a power line is whether the line is faulted by flashover due to HEMP or not faulted, and if faulted the data base for this set includes a measure of where the flashover has occurred. Since these data are to be used for short-circuit studies in the next group of tests, this latter piece of data can be the impedance
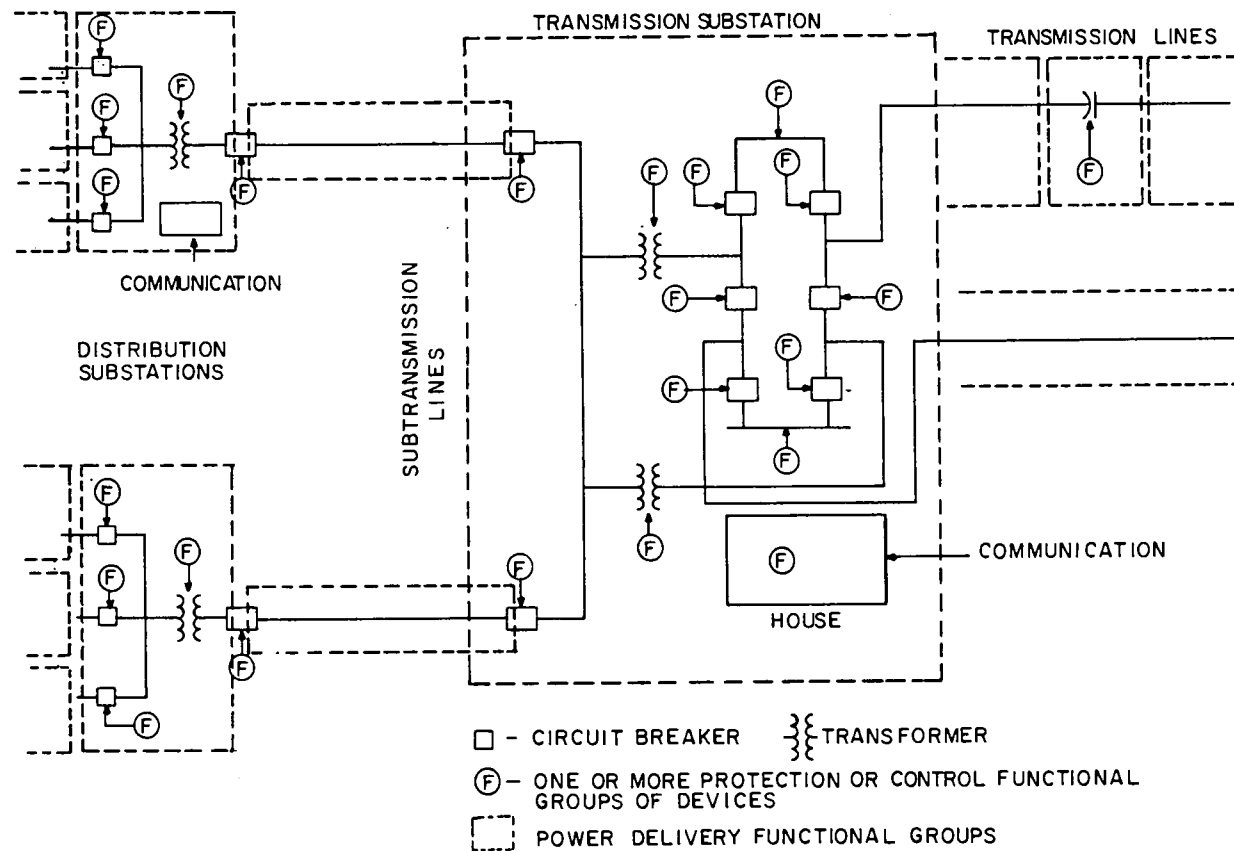
Fig. 79. Subsystems details illustrating overlapping interconnections of subsystems through circuit breakers and their associated supporting functional groups.

from the terminals of the power line to the fault location. Likewise, the operability of other devices in the power-delivery network is in question.

Levels of load demanded and generation available following the HEMP event are identified with their locations within the power network. The status of the transmission lines and substations are determined as to what lines have flashed over due to the HEMP event and what states a substation is in as to power deliverability or to control.

Assessment interactions of the subsystems in a power network is an iterative process, as illustrated by Fig. 66 through response of functional groups from results of the power network studies. The power network response studies introduce the element of the time constants associated with the power network. Initial assessments of the power network are made which become "initial" conditions for the first pass through the response studies. The results of these studies impact, for example, on relaying functional groups which, through causing operations of circuit breakers, cause interaction between subsystems, such as generation and load. These interactions result in new conditions in the response studies which, in turn, can result in additional changes in state.

Concurrently, characteristics of other interconnected power networks, and results of state changes in these other interconnected power networks, may become part of the data for the power network response studies.

The following data base tasks are based on the initial assessment tasks of previous sections as reflected into performance data bases.

4.2.9.1 Data Base: Operation of Generation Subsystems

Identify the generation plants and associated generators that are still operable.

Establish allowable levels of real and reactive power generation for plant, data to be used in load flow studies.

Establish composite impedances of operating generation, in conjunction with generating plant substation subsystem, data to be used in short-circuit and transient stability studies.

4.2.9.2 Data Base: Interconnection Power Network

Identify if flashovers have occurred on interconnecting power lines.

Establish location in terms of impedance to flashover fault for short circuit study.

If no flashover (faults), establish what power level can be delivered over interconnection.

Establish transient stability study equivalents for interconnected power networks based on other assessments of these interconnected power networks.

4.2.9.3 Data Base: Substation Subsystem Operation

Identify what major power-delivery functional groups within the subsystem are still in operation from a previous assessment of the power-delivery functional groups and their associated supporting functional groups in previous sections. This entails identifying from previous data bases which power delivery functional groups or their supporting groups:

- are operable
- have become inoperable due to EMP event

- will become inoperable at a later time due to interaction between functional groups one or more of which have become inoperable due to EMP event.

4.2.9.4 Data Base: Power Line Subsystem Flashover

Identify on which power lines flashover due to EMP have occurred.

Establish location in terms of impedance to fault location (flashover) from each terminal of power line.

4.2.9.5 Data Base: Bulk Load Equivalents

Identify status of bulk loads following HEMP event.

Establish levels of load in terms of real and reactive power.

Establish characteristics of rotating machines still operating in bulk load.

4.2.9.6 Data Base: Operation of Distribution Subsystem

Identify what failures have taken place in the distribution subsystem initially due to HEMP; i.e., flashovers, insulation damage of equipment and in later time following short circuit studies, fuse blowings, overloads, etc.

Establish allowable power levels through subsystem.

Establish composite impedances from distribution substation to fault locations.

Establish load level remaining following HEMP of distribution subsystem in terms of real and reactive power.

4.2.10 System State Analysis in Response to Subsystem State Changes

The impact of changes in states in subsystems on the change in "state" over time of the power system network must be assessed from the following aspects:

- Initial system load flow as starting base-case conditions for the short-circuit and transient stability analysis.

- Changes in system current flows following power-delivery device or circuit failures, either as output from the first stage in the network analysis portion of the transient stability code, or utilizing other network analysis codes.

- System switching overvoltages which may result in subsequent power-delivery or circuit failures due to circuit-breaker operations.

Base case steady-state conditions for the power network prior to the HEMP event must be specified. Short-circuit studies give magnitudes of fault current for analysis of what relaying schemes and circuit breakers should operate, if still functional following the HEMP. Stability studies are concerned with the movement of angles of internal voltages of synchronous machines away from states of equilibrium required to balance energy of existing loads and losses against the energy of electrical generation within the power network. Disturbances occurring within the system that create an imbalance in these energy levels lead to angular swings of machines which are reflected in voltage and current angles throughout the system. Opening of circuit breakers, dropping significant loads, can result in system overvoltages, leading to other equipment damage.

4.2.10.1 Data Base: Fault Impedances and Source Voltages

This data base, derived in an earlier set of tasks, supports the study of currents within the power system due to faults.

4.2.10.2 Model: Short-Circuit Studies

The system is set up in sufficient detail using the previous data base that fault currents in various power-delivery functional groups can be calculated.

4.2.10.3 Assessment: Relay-Scheme and Circuit-Breaker Operations

Fault currents are compared to trip settings of relaying schemes that are still functional. Where tripping of associated circuit breakers are called for, tripping times are decided for those that are still operable.

4.2.10.4 Data Base: System Load Flow and Stability

This data base establishes the base case steady state condition of the system prior to the introduction of HEMP effects. The type of data required is consistent with that usually given for conventional system studies.

4.2.10.5 Model: Load Flow

The required load flow models are identical to those contained in typical existing load flow digital programs. The output of the simulation will reveal the following system assessment summaries.

4.2.10.6 Assessment: Results of Load Flow

The following are typical outputs of load flow studies:

- Real and reactive power flows into or out of designated buses

- Voltage levels at these buses

- Real and reactive power from generators

- Line losses
- Regulated bus data (transformer taps, etc.)

4.2.10.7 Model: System Stability

In addition to the quantification of the new steady-state load flow caused by the HEMP environment, the effects on system stability as it moves from state to state of power equilibrium must also be considered. The load flow defines the initial steady-state conditions. The stability program represents the dynamic models of generation, load, and reactive power compensation. The system is disturbed by the effects of HEMP. The program output quantifies the dynamic response of the system, such as generator swing angles as a function of time and flows over still-operable lines. In addition, the effects of load-shedding schemes and line tripping are considered.

The effects of overvoltages on long-line de-energization, (i.e., quasi-steady-state 60 Hz voltages), can be investigated using existing analysis techniques in the transient-stability program.

4.2.10.8 Assessment: System Response

"Swing" curves for major generation, still operable following the HEMP, are obtained over time. The effect of relay and circuit breaker operations are examined as to load dropping, subsystem "islanding," etc. The effect of bypassing and reinsertion of series capacitors on load flows and stability are determined.

4.2.10.9 Assessment: Change of System State

The combination of load flow, short-circuit and stability studies caused by and in the presence of an HEMP environment will lead to an understanding of complete system operational response and system state up to the MHD-EMP, Fig. 80. Probability of equipment (devices and circuits) damages and upsets subsequent to HEMP is evaluated for reiteration in the assessment process.
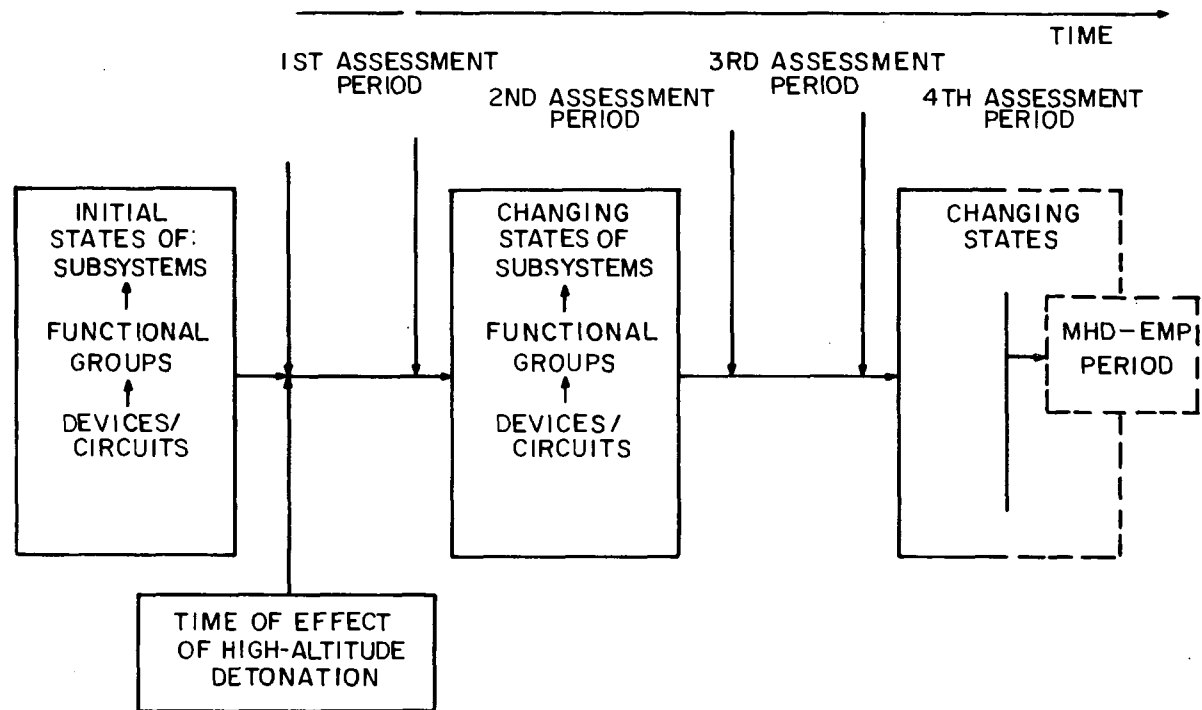
TIME

1ST ASSESSMENT
PERIOD

3RD ASSESSMENT
PERIOD

2ND ASSESSMENT
PERIOD

4TH ASSESSMENT
PERIOD

INITIAL
STATES OF:
SUBSYSTEMS
↑
FUNCTIONAL
GROUPS
↑
DEVICES/
CIRCUITS

CHANGING
STATES OF
SUBSYSTEMS
↑
FUNCTIONAL
GROUPS
↑
DEVICES/
CIRCUITS

CHANGING
STATES

MHD–EMP
PERIOD

TIME OF EFFECT
OF HIGH-ALTITUDE
DETONATION

Fig. 80. Response of states of power network over time.

4.3 Hierarchy of Data Bases

Figure 81 illustrates the hierarchy of data bases supporting the various levels of assessment within the power system that have been discussed in previous sections.

The initial and subsequent interaction to the effects of HEMP at the functional-group level predicates data bases being available for models of specific circuits and devices making up each functional group and their initial states (Fig. 82), (E2) with interactive (connection diagrams) relationships defined (E1). Data bases for circuits and devices may include physical models on transfer functions, models of potential failure modes including probabilities of dielectric or thermal failures (flashover and burn-up) and malfunctions or upset without permanent damage (E3).

For each functional group there is an initial state of the group as an entity (D1), which will be reflected in a separate data base for use in assessment. Data in such a base are subject to change in time, with the states of the individual circuits and devices (E2) making up the functional group. This data base, with similar ones for other functional groups, provides a "test point" in time to relate states of functional groups (Fig. 83) for the assessment at the subsystem level. Thus, data bases for a specific functional group includes information about, first, the initial state of one functional group (D2), changed to succeeding states with time as appropriate, as well as a listing of the circuits and devices making up the functional group with the measure of its performance state as a functional group (D3).

In addition, in order to tie the field environment definition in a space to the functional group in the space, are information about the spatial location of the functional group (D1). This information can be similar, in part, if not the same, as the information describing the spatial location of the subsystem in which the group functions (C1).
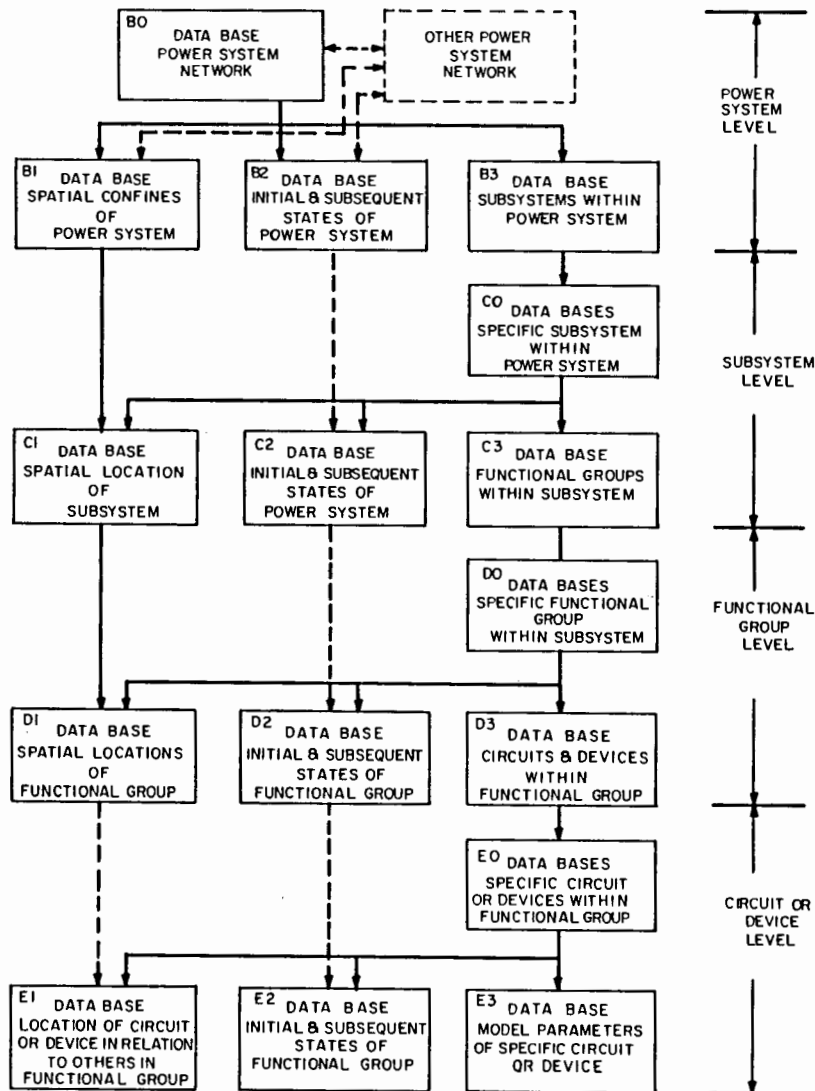
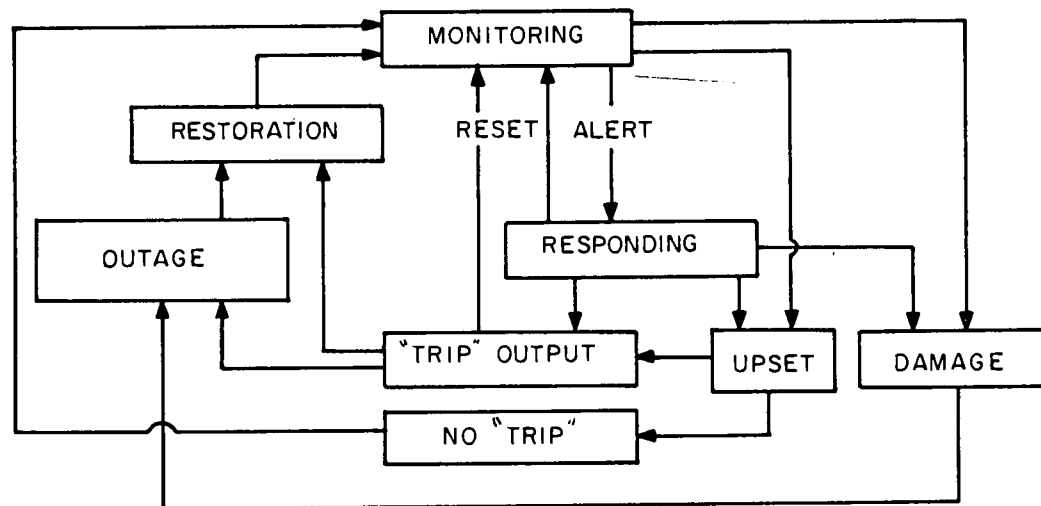Fig. 81. Hierarchy of data bases for levels of power system assessment.
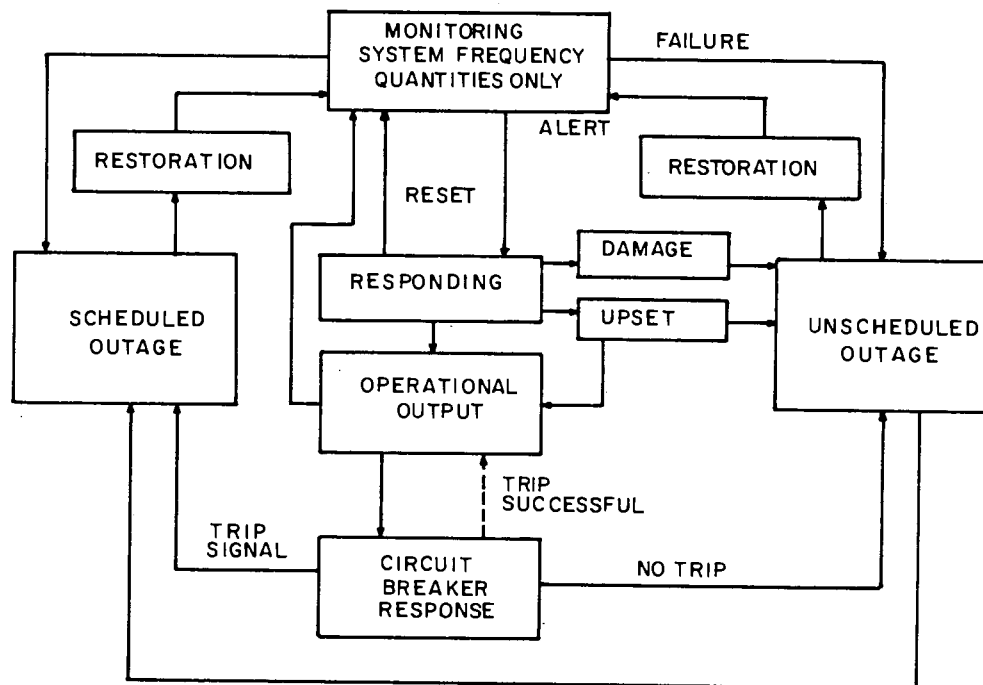
Fig. 82. States of relaying device.

Fig. 83.   States of protective functional group.

It is anticipated that data bases for these circuits and devices within the functional groups may be site-specific as well as subsystem specific. A spatial location data base for a functional group (D1) may include information about the effects of shielding of enclosures common to all or part of the functional group. Information on the effects of enclosure shielding are derived from models as discussed in Section 5. Shielding affects on the individual devices, because of their own cases or enclosures, becomes part of the coupling code data base of the model for the device itself (E3). Broadening data bases can be anticipated as more data is obtained by experiment or calculation on individual circuits and devices and enclosure shielding and functional group performance. A complete data base for level E∅, for example, would include all types of devices and circuits that could or would be used in a specific functional group, together with other data bases defining their possible state (E2), characteristics, and parameters (E3) and how they connect or interact with other devices or circuits in their functional group (E1). Where important, information in this data base may be required that links one functional group to another (E1) through a common device. For example, a current transformer provides a link between the power-delivery functional group and the protection and control functional group.

Data bases for specific functional groups (D∅ and below) then become subsets of information describing a large part of the subsystem. Listing of functional groups and overall performance data of a functional group are such a subset (C3) of the data bases defining the subsystem. In conjunction with this data base are those describing the initial state of the subsystem, and subject to change with time during the assessment (C2), and information about the spatial location of the subsystem (C1) providing the link to the field equations on an aggregate standpoint. As mentioned previously, the spatial data base (D1) may be the same as, or similar, to (C1). Data base C2 provides a link in time, a "test point," with states of other subsystems for the assessment at the power network level.

At the level of the complete power system are additional data bases defining its boundaries and contain information about electrical interconnections and communication links within its confines and with other power system networks (B1), initial and subsequent operational states of the power system as "test points" to other power systems through information across interconnections and communication links (B2), and the listing and performance data of subsystems making up the power system of interest (B3). Figure 84 illustrates typical operational states of the power network.

4.4 Summary

The HEMP assessment methodology presented herein begins with a defined high-altitude burst scenario, and a defined power network configuration and set of initial conditions. This assessment concludes at an elapsed time of two seconds after the burst event with an assessment of the probable new state of the systems under evaluation. This output states of the systems serve as the new set of initial conditions for the associated MHD-EMP methodology described in Volume 3 of this report series. The above break between the initial HEMP assessment and the subsequent MHD-EMP analysis is necessitated by the change in system response models from those applicable for high-frequency modeling to those models directed towards very-low frequency analysis.

The methodology is structured on the basis of a hierarchy of elements of the power network: systems, subsystems, functional groups, devices and circuits. The concept of "critical line length," introduced in Section 3 of this report, combined with a knowledge of power system time constants, effectively limits the topological extent of various subsystems to be assessed during the time of local HEMP illumination.

This structure provides the vehicle for data for assessment at several levels of the partitioning of the power network, or the assessment itself, to be generated by different groups of experts. The
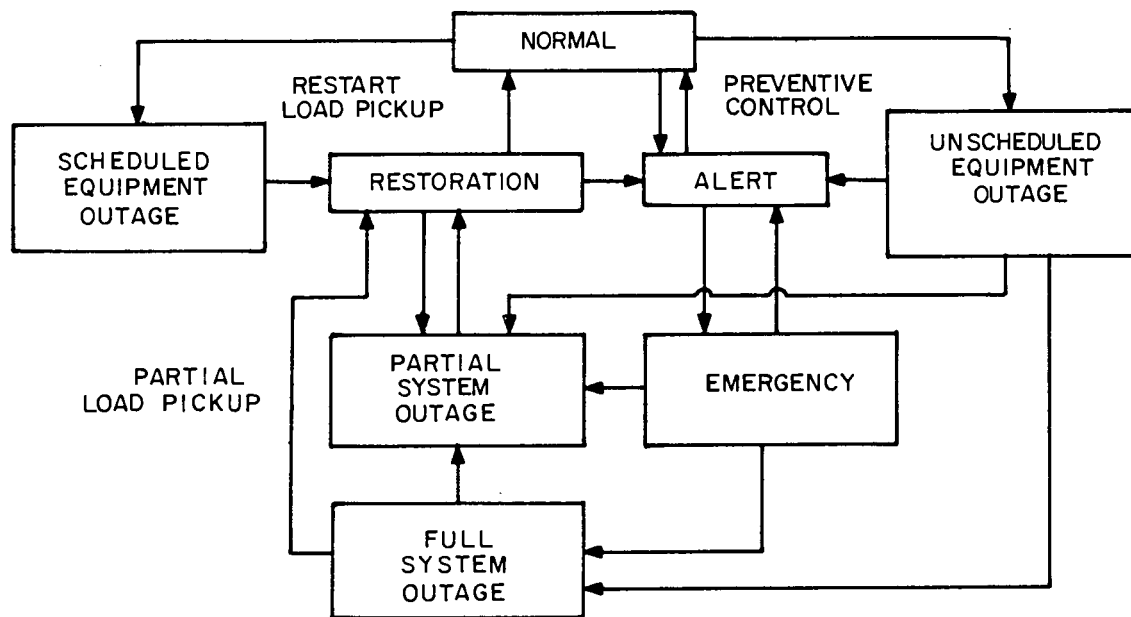
Fig. 84. Power network operational states [33].

proven techniques of fault-tree assessment have been incorporated as part of the methodology in order to explicity relate cause and effect. The development of individual fault trees at the subsystem/functional group/circuits and devices levels is a system-specific task required by the methodology as part of the assessment process. This development naturally leads to a definition of specific questions about functional interactions at the various levels. The examples of functional interaction offered in this section should not be considered as an exhaustive list of the important questions to be addressed in the assessment.

It is important to note that the HEMP assessment methodology has been intentionally developed as to remain "transparent" to the quality of the data. This approach places the uncertainty of the assessment results as a function of the uncertainty of the "stress and strength" data and not of the assessment process.

5. HEMP CODES, MODELS AND EXPERIMENTS

5.1 Introduction

This section briefly discusses technical issues concerning: 1) feasibility of digital code development, 2) power system device and apparatus models, and 3) an experimental program to support model development of HEMP interaction with civilian electric utility systems.

The digital code development is presented as a series of code modules operating within the assessment methodology. The individual codes are used in conjunction with human analysis and evaluation.

The principles of device and apparatus modeling are discussed in terms of "external" models: the device is replaced in the model circuit by the relevant lumped parameter elements. In the case of power apparatus, the effects of equivalent shunt capacitance at the device terminals are explored in order to understand the relationship between open-circuit voltage and applied terminal voltage. The subsection also discusses the attributes of various "strength" models for equipment.

The subsections conclude with a discussion of the types of experiments required to verify the external models and/or determine the nature of device failure under HEMP environments.

5.2 Digital Code Development

The assessment methodology, presented in Section 4 of this report, anticipates the development and/or use of several digital codes in support of the assessment process. It is not intended that the total methodology should, or can be accomplished as a single, unified simulation code. The methodology incorporates specific code modules as analysis tools to explore the interaction of HEMP and the power system.

The digital codes incorporated within the methodology can be divided into three categories:

- HEMP Environment Code
- HEMP Interaction and Device Response Codes
- Functional Group, Subsystem and Power System Response Codes

The HEMP Environment Code translates a given high-altitude nuclear burst at a known location to the corresponding spatially local HEMP environments experienced at subsystem geographic locations within the area of direct illumination. The HEMP interaction codes translate the local incident field into a corresponding set of transient stresses experienced by the functional groups/devices within each subsystem. Device response is then obtained by stress/strength comparison of relevant data files. Power system response at later times employs a set of functional groups, subsystem and system-level response codes. These response codes are recursive in time and yield the prospective state of the system necessary to begin the MHD-EMP methodology. Attributes of the digital code development are discussed in the following subsections.

5.2.1 HEMP Environment Code

The local HEMP environment code is necessary at the start of the HEMP assessment. The code requires, as an input, information concerning the geographic location of the nuclear burst (X-Y spatial coordinate and height of burst) and the spatial coordinate locations of the subsystems at which the local HEMP environment is required in the assessment. The code computes each local environment and creates an output file containing the following descriptions for the local incident fields at the specified locations:

- Waveform
- Angle of Incidence
- Fractions of Polarization

The above descriptions are discussed in Section 2 of this report. It is anticipated that the code will be valid for the continental United States. For assessments requiring sensitivity analysis of incident field parameters or a single "threat" environment, the output file can be directly constructed. An elementary flowchart for this code module is shown as Fig. 85.

5.2.2 HEMP Interaction and Device Response Codes

The next series of codes required to support the methodology operate on the local HEMP incident field environment at a subsystem of interest to calculate the expected stress and/or local fields experienced by devices within functional groups. These coupling and interaction codes will be developed from the formulas presented in Section 3 of this report. The conducted stress at the device terminals of interest are formatted in terms of appropriate voltage/current transient drivers.

The calculated device stress is then compared to the appropriate device strength and device state files to estimate probable device responses. These assessment comparison codes allow for the translation of stress and/or strength data to a common base for comparison. The output files of this set of code modules are the time-dependent device responses. An elementary flowchart of these code modules is shown as Fig. 86. It is planned that existing computer codes used as part of the Phase I research will form the basis of this portion of the Phase II code development.

5.2.3 System Response Codes

The code modules required in this portion of the methodology accept, as input data files, the device response data and the system set of initial conditions. The devices responses are entered into a fault tree assessment code to estimate the functional group response within any subsystem. Additional code modules examine the interaction between subsystems in order to estimate total system response as a function of
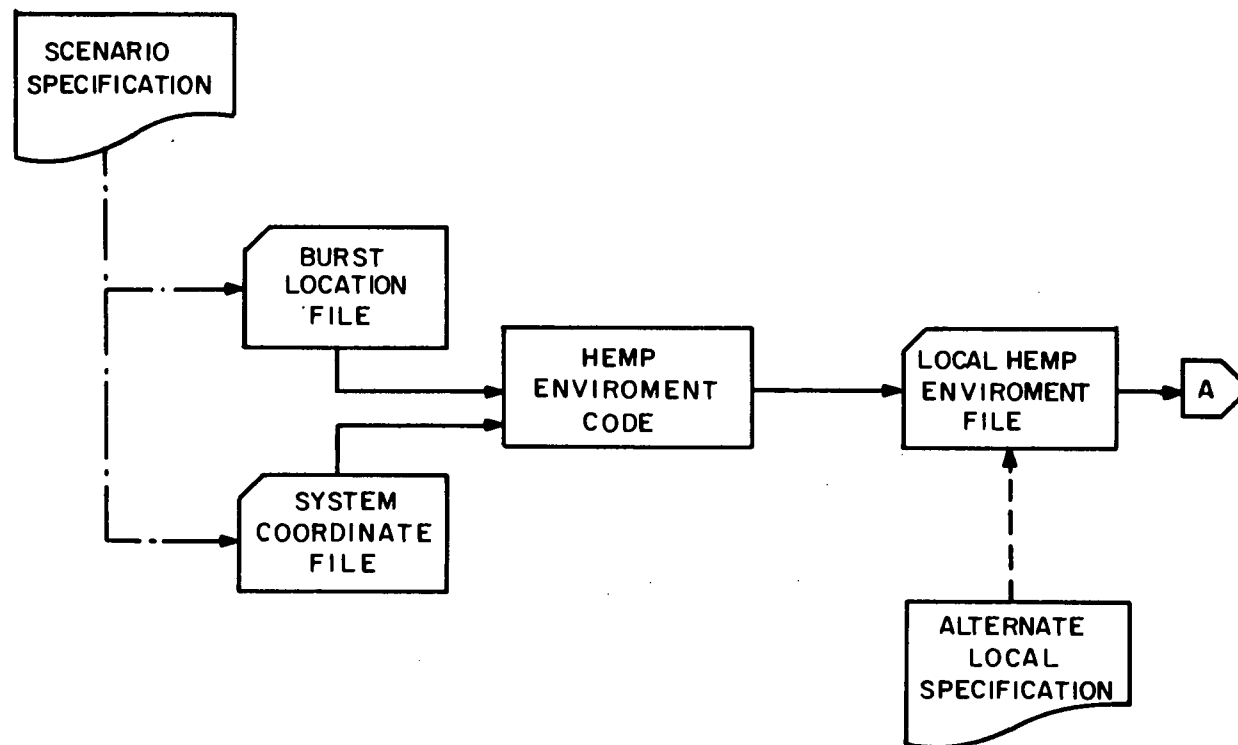
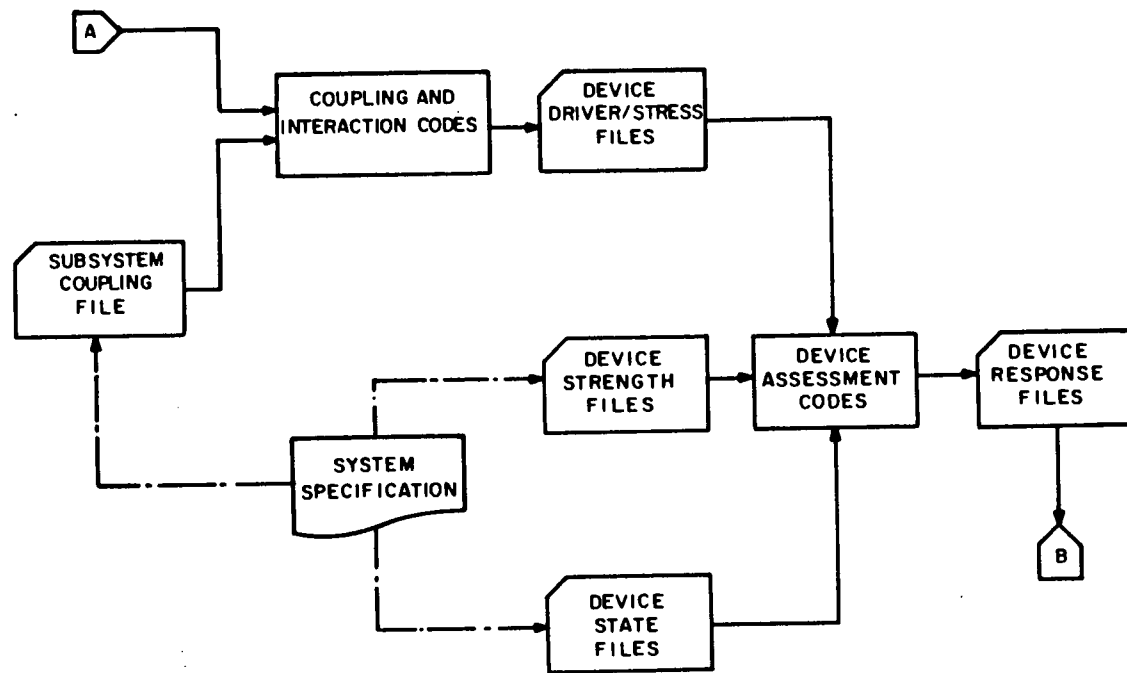Fig. 85. Local HEMP environment code flowchart.

Fig. 86. Device response code flowchart.

time. An elementary flowchart for this set of code modules is shown in Fig. 87.

The system response codes will not require extensive original code development. Existing fault-tree solution codes developed for nuclear power plant risk assessment are applicable to functional group analysis. In addition, system response codes for load flow, short-circuit and system stability can be adapted from existing software.

5.3 Equipment Models

The complexity of early-time HEMP equipment models is a function of: 1) the spectra of the surge and 2) the level of the assessment. For a system level assessment, equipment can be represented by an equivalent "external" network of lumped elements. Such external models may take the form of a single, shunt capacitance, an R-L-C equivalent network or the appropriate surge impedance. For example, in lightning studies, rotating machines have been successfully modeled as surge impedances.

This subsection discusses the implications of external model representation, in particular shunt capacitance, as a modifier of HEMP voltage stress at the equipment terminals. The subsection continues with an example of the development of internal, distributed models applicable to power transformers. The subsection concludes with a general discussion of equipment performance criteria for HEMP stress.

5.3.1 External Models

In Section 3 of this report, the HEMP induced surge at a location of interest has been presented in terms of a calculated open-circuit voltage or short-circuit current. The presence of shunt capacitance at this location of interest will reduce the value of the actual terminal voltage impressed across the equipment from the HEMP open-circuit calculation.
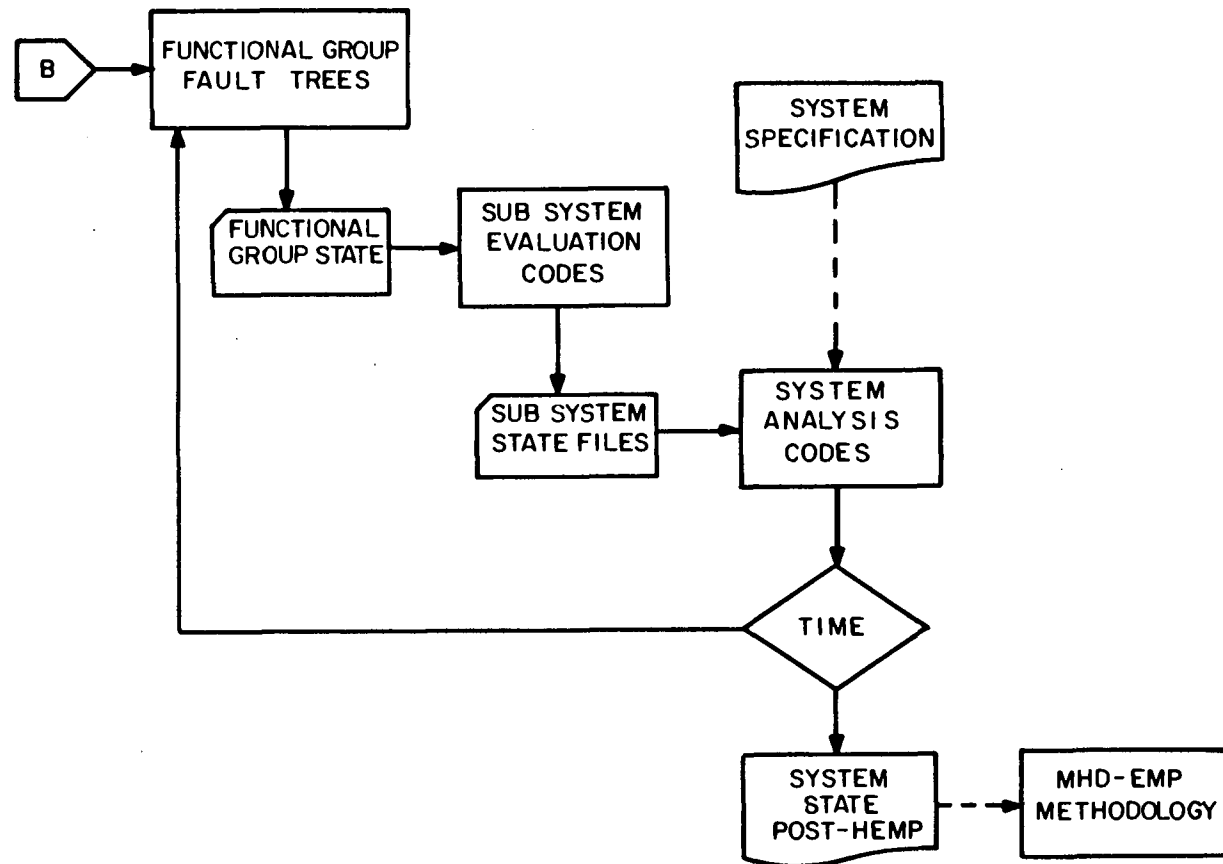
Fig. 87. System Response Code Flowchart.

An example of this effect is shown in Fig. 88. This figure compares the voltage variation for HEMP and 1.2x50 μs standard lightning surge at the end of a 241 meter transmission line as a function of shunt capacitance. Figure 89 shows the complete HEMP voltage waveforms for select values of shunt capacitance. For a given value of capacitance the reduction of voltage magnitude is more pronounced for HEMP waveform due to the higher spectral content when compared to standard lightning.

More complex external, equivalent models for equipments include inductive and resistive elements as well as shunt capacitance. Neglecting any resistive element, the examples shown in Fig. 89 have been expanded to include series inductance in the model. Figure 90 shows the variation of terminal voltage for different values of inductance assumed in series with 100 pf of shunt capacitance. The voltage waveform is seen to be a strong function of the LC combination.

In the absence of specific, measured data for power delivery equipment, estimates of lumped, equivalent capacitance can be obtained from Industry Standards such as ANSI/IEEE Standard C37.011 (1979) [41]. These representative values are the result of a survey of manufactures by the IEEE Power Circuit Subcommittee, Working Group on Transient Recovery Voltages. It should be noted that the values contained in the above ANSI Standard are based on power frequency measurements. Additional investigation is required to determine what correction factor may be necessary to adjust this data to the frequencies of interest. An example of such capacitance data for power transformers is shown in Fig. 91 [41].

5.3.2 Distributed Models

Distributed models for power equipment at HEMP frequencies are concerned with the modeling of the internal, distributed shunt and series capacitive elements within the equipment. This subsection presents the example of the power transformer.
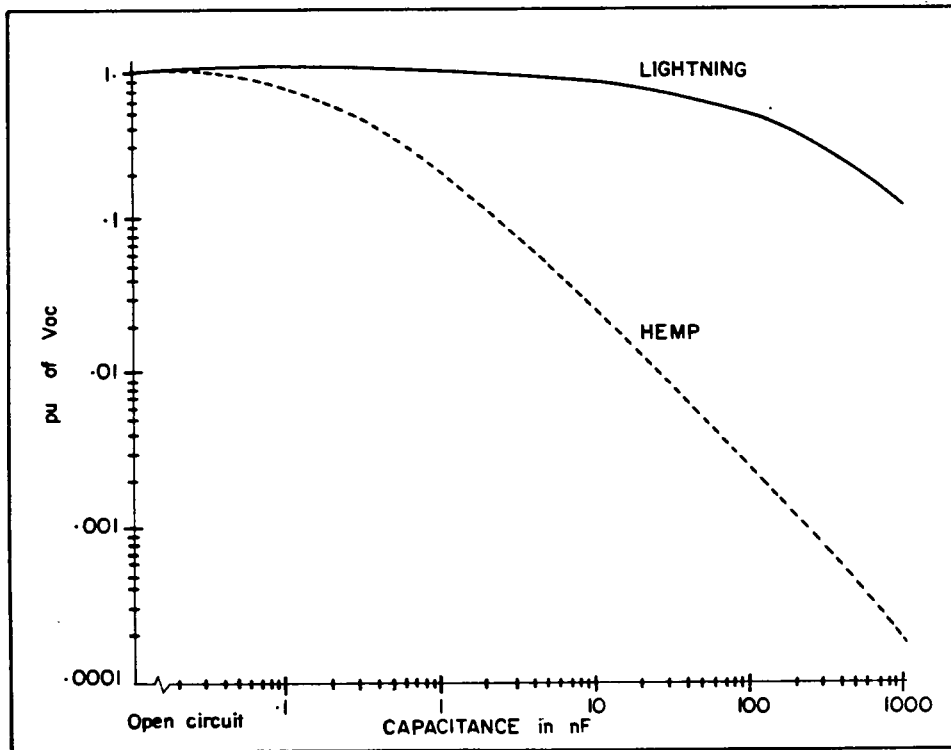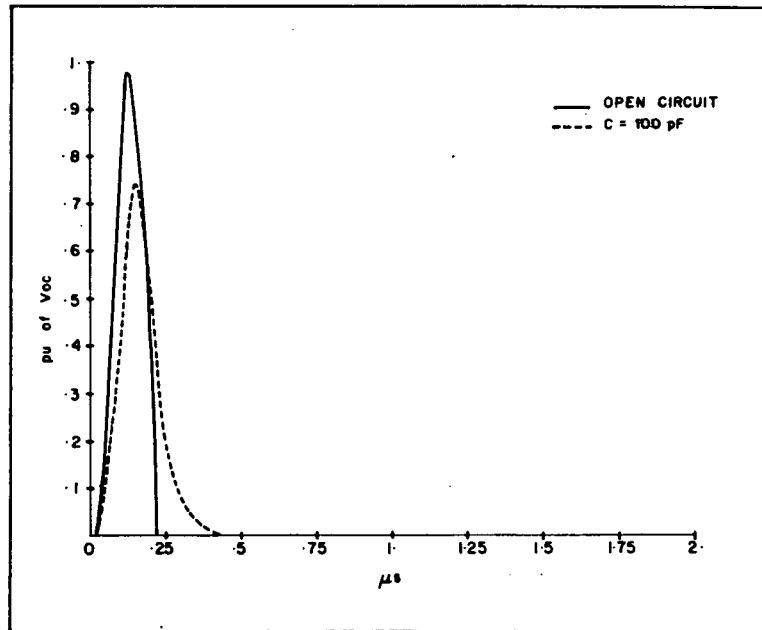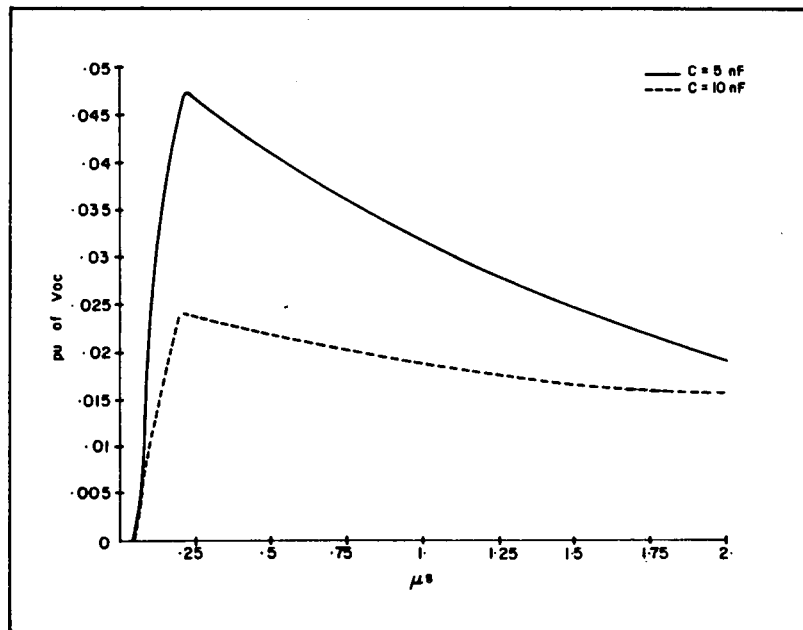
Fig. 88. The induced voltage at the end of a 241m long conductor 12.3m above ground due to a) HEMP ($\Psi=30°,\phi=0°$, vertical polarization), b) 1.2x50 µs standard lightning wave.
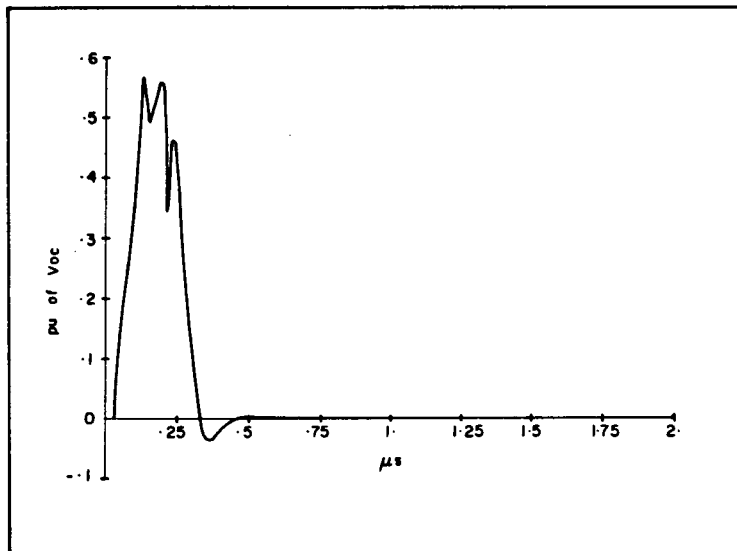
a)

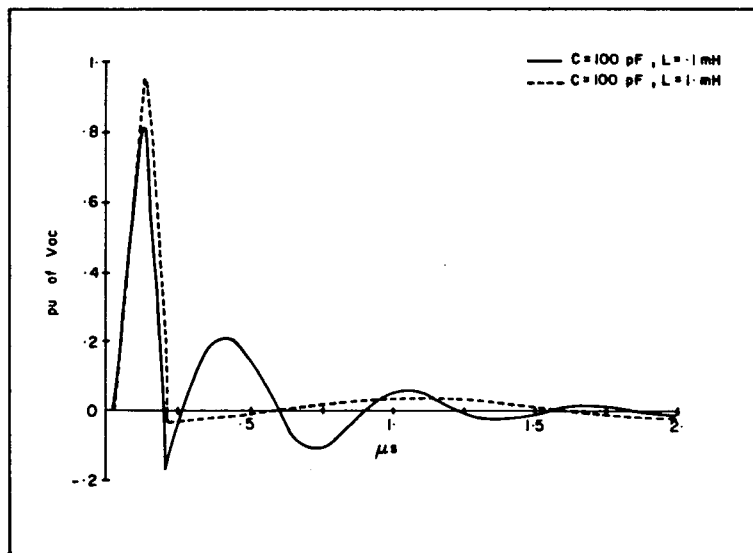b)

Fig. 89. HEMP induced voltage at the end of the 241m conductor for different terminal capacitance to ground.

a) L=.01 mH, C=100 pF

b) L=1. and 0.1 mH, C=100 pF

Fig. 90. HEMP induced voltage at the end of the 241m conductor for different value inductance in series with a 100 pF capacitor.
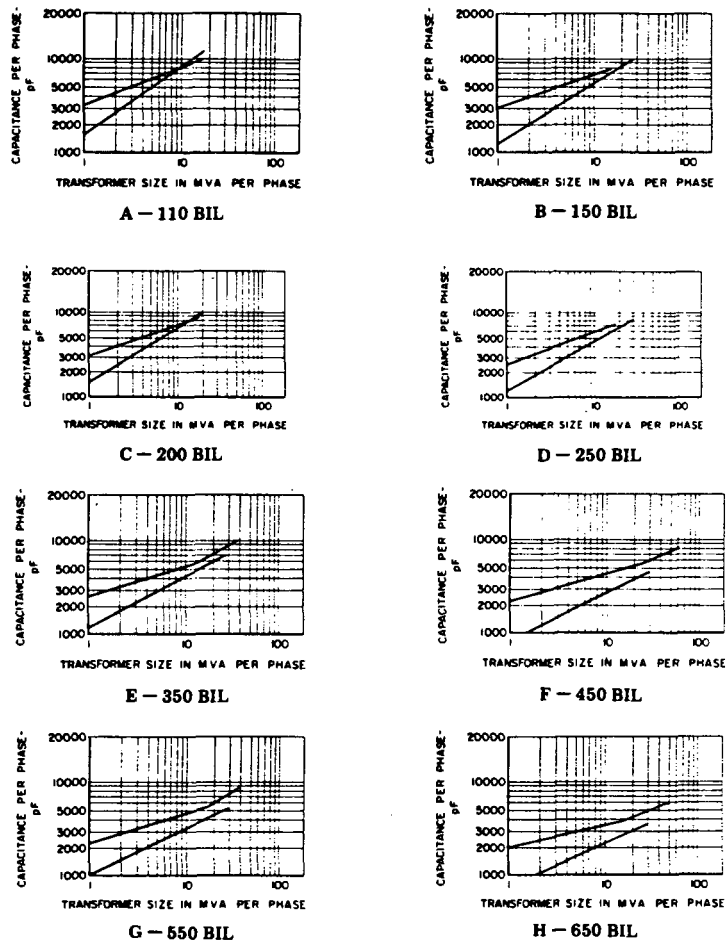
237

Fig. 91. Transformer winding capacitance to ground range of values for various BIL of highest voltage winding; (a) 110 kV BIL, (b) 150 kV BIL, (c) 200 kV BIL, (d) 250 kV BIL, (e) 350 kV BIL, (f) 450 kV BIL, (g) 550 kV BIL, (h) 650 kV BIL [41].

For many power transformers, the capacitive network can be represented by the ladder network for a winding divided into n segments, as shown in Fig. 92, where:

C_{HS} is the total interwinding capacitance of the HV winding,
C_{LS} is the total interwinding capacitance of the LV winding,
C_{HG} is the total capacitance of the HV winding to ground,
C_{LG} is the total capacitance of the LV winding to ground, and
C_{HL} is the total capacitance of the high voltage winding to the LV winding.

The ladder network can be simplified to the approximate equivalent circuit shown in Fig. 93, where:

$$\alpha_H = \frac{C_{HG}+C_{HL}}{C_{HS}} \tag{160}$$

$$\alpha_L = \frac{C_{LG}+C_{HL}}{C_{LS}} \tag{161}$$

$$\alpha_L = \frac{C_{LG}+C_{HL}}{C_{LS}} \tag{162}$$

$$C_{HSE} = \frac{C_{HG}+C_{HL}}{\sinh \alpha_H} \, C_{HS} \tag{163}$$

$$C_{LSE} = \frac{C_{LG}+C_{HL}}{\sinh \alpha_L} \, C_{LS} \tag{164}$$

$$C_{HGE} = C_{HG} \left[\frac{C_{HS}}{C_{HG}+C_{HL}} \right]^{1/2} \frac{\cosh \alpha_H - 1}{\sinh \alpha_H} \tag{165}$$

$$C_{HLE} = C_{HL} \left[\frac{C_{HS}}{C_{HG}+C_{HL}} \right]^{1/2} \frac{\cosh \alpha_H - 1}{\sinh \alpha_H} \tag{166}$$
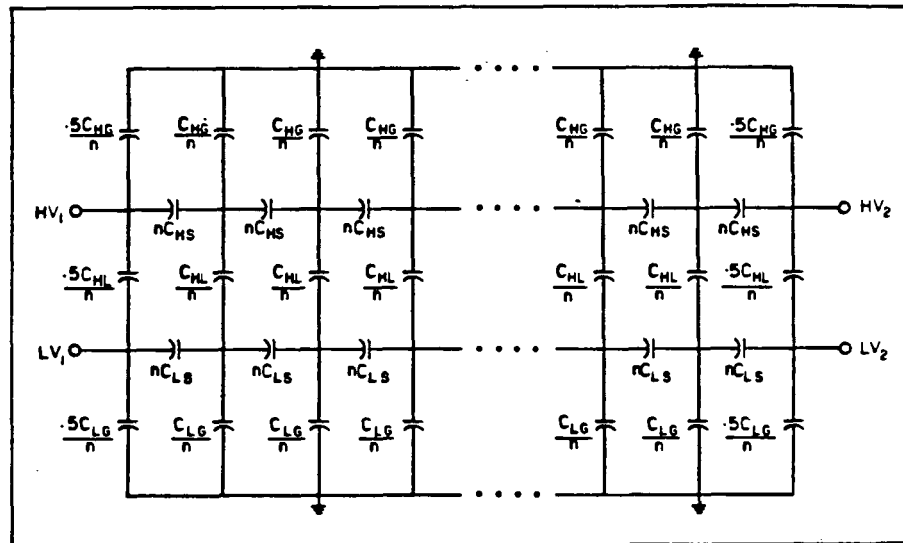
Fig. 92. Equivalent high frequency circuit of a
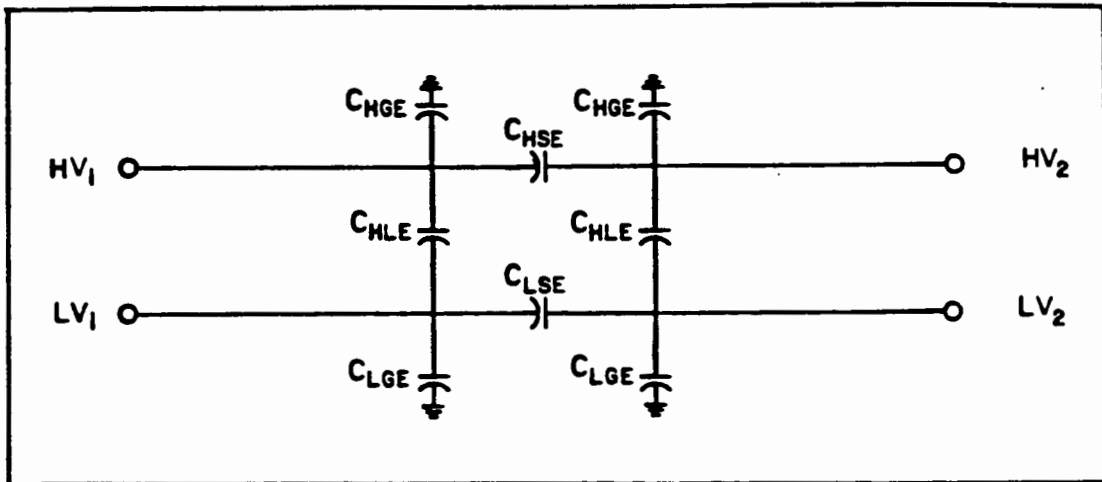two winding transformer (HV and LV).

Fig. 93. Approximate high frequency equivalent
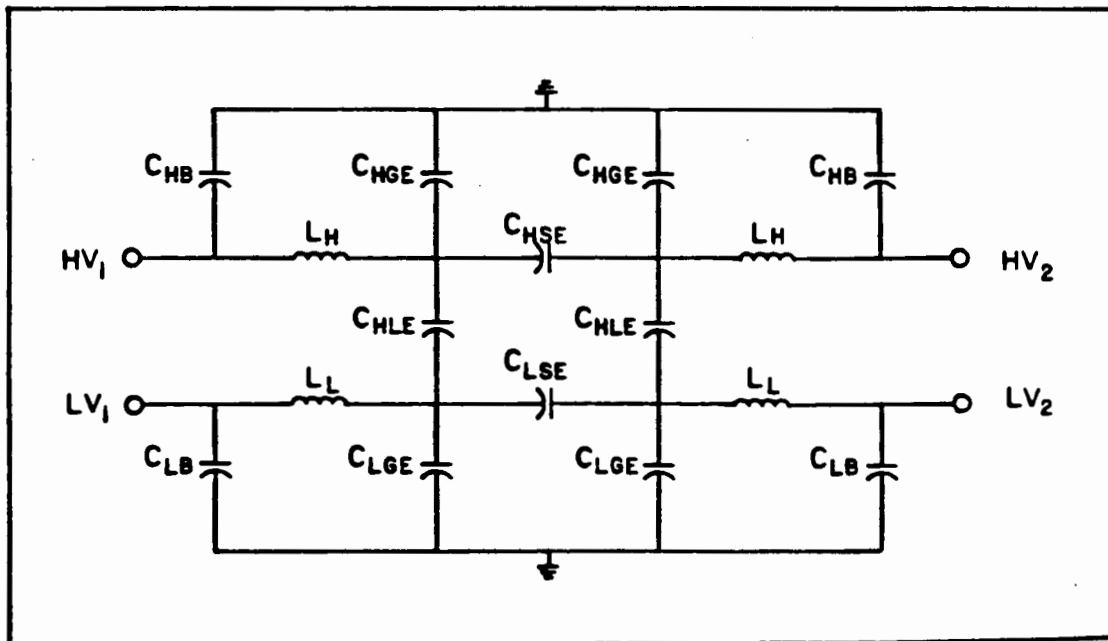circuit for two winding transformers.

Fig. 94. Approximate high frequency equivalent circuit
for two winding transformer including leads and bushings.

$$C_{LGE} = C_{LG} \left[\frac{C_{LS}}{C_{LG}+C_{HL}} \right]^{1/2} \frac{\cosh \alpha_L - 1}{\sinh \alpha_L} \tag{167}$$

The use of α_H in Equations (165) and (166) is appropriate for determining the effect of a voltage source applied at the HV terminals.

Similar simplified high frequency equivalent circuits can be developed for most power transformer geometries for which the equivalent capacitance network shown in Fig. 92 does not apply.

The equivalent circuit for one phase of a two winding transformer is shown in Fig. 94 where the lead inductances, L_H and L_L, of the high voltage and low voltage loads, and the bushing capacitances, C_{HB} and C_{LB}, of the high voltage and low voltage bushings have been added to the equivalent circuit of the windings shown in Fig. 93.

The inductances and capacitances shown in Fig. 93 and 94 may be calculated from the transformer test data and geometry data which might be available from the manufacturer.

5.3.3 Model Tests

There are two types of tests that can be performed to help determine and/or validate the appropriate electrical models required by the assessment. These tests are: 1) repetitive pulse tests and 2) frequency response tests. Both kinds of tests are designed to be non-destructive to the equipment under evaluation.

Under the repetitive pulse test a constant, low voltage surge is applied via a repetitive pulse generator and the terminal response is measured for different prospective waveforms. The variation of the front and tail of the surge yields information as to the external model of the equipment at frequencies of interest.

The frequency response test is an injected CW experiment designed to investigate the transfer function characteristics of circuits and equipment. A constant voltage (current) input is progressively injected

through the frequency bandwidth of interest. The output signal is compared to the input using a spectrum analyzer to obtain both gain and phase relationships. The tests also give an indication of the natural resonance frequencies for the circuit or equipment under investigation.

It is anticipated that the Phase II research will include a select number of repetitive pulse and frequency response experiments for generic types of power equipment as part of the development and validation of circuit and equipment models.

5.3.4 Equipment Failure Models

A very important aspect of the assessment process is a knowledge of how devices might fail due to HEMP interaction with the utility system. For the purpose of this report, device failure is defined as a device change of state due to damage and/or misoperation which results in an immediate or time-delayed undesired response on the power system. This device change of state may be permanent or temporary in duration.

As discussed by Vance and Morgan [42] the threshold of device failure is related to the HEMP associated electromagnetic stress that produces such unacceptable performance. The specification of a threshold for any devices requires: 1) the definition of unacceptable performance, 2) the physical location where the threshold stress is defined and compared to device strength, and 3) definition of the appropriate stress parameters.

For power system devices and circuits, with the exception of self-restoring insulation systems, the actual threshold of failure is rarely determined by experimentation. Device design and testing is based on the specification of some "withstand" capability; a standardization stress applied in a prescribed manner for which no unacceptable change of state is observed. An example of standard power system definitions concerning electrical insulation strengths are documented in Appendix F of this report. Existing Surge Withstand Capability (SWC) criteria for protective relay systems are documented in

ANSI/IEEE C37.90 [43]. By definition, the stress withstand capability for any equipment is less than the failure threshold. The margin between withstand and failure threshold is usually unknown.

An important task in the Phase II research is anticipated to involve the correlation of existing device withstand criteria to the dielectric, thermal and/or noise stress produced by HEMP. In the case of self-restoring insulation systems, the HEMP breakdown voltage stress may be investigated by direct experimentation subject to the limitations of the generation and measurement of surges having nanosecond fronts. It is anticipated that the prospective waveshape and magnitude for such experiments will be developed as part of a HEMP parametric study task of the Phase II research. A limited, possibly destructive set of experiments for select equipment may be necessary to correlate existing withstand performance to prospective HEMP stress.

6. CONCLUSIONS AND RECOMMENDATIONS

Phase I research to investigate the effects of HEMP on civilian electric utility systems indicates that the HEMP environment may interact with all aspects of the system. In preparation for Phase II preliminary risk assessment, a methodology applicable to electric power systems has been developed. This methodology anticipates the necessary environmental and power system data bases, system response mechanisms and power system analysis techniques necessary to conduct quantitative assessments.

In the areas of HEMP environmental definitions, power system responses, methodology development, and systems analysis, the following conclusions are presented:

1. In electric utility, system-level analysis, the environmental description of early-time HEMP incident fields should retain the spatial variation of: 1) waveform, 2) angle of incidence and 3) polarization as functions of burst location. The methodology supports sensitivity analysis of the above parameters on the major subsystem level.

2. The existing, unclassified data for intermediate-time HEMP incident fields are <u>not sufficient</u> to develop a system-level environmental <u>description</u> to the same confidence level as early-time HEMP. Section 2 of this report presents an initial effort by the authors to represent intermediate-time HEMP within the methodology. The description contained herein has not been critically examined for credibility.

3. For power system assessment, HEMP excitation of electrically-long lines and conductors can be quantified by TEM transmission line techniques in lieu of scattering theory. This conclusion is based upon the comparisons offered in Section 3 of this report.

4. The nature and time-duration of initial power system response to HEMP excitation is such that major-subsystems can be initially assessed as a parallel set of tasks. The concept of "critical line length" combined with power system time constants supports this conclusion.

5. A major uncertainty in the assessment of power system functional groups, circuits and devices is caused by the lack of existing "strength" data bases on power system equipment to allow direct comparison to HEMP stress. A major effort is required in Phase II of the research effort to develop such data bases. The methodology presented herein has been developed so to be "transparent" to the quality of the data.

6. The use of "fault-tree" assessment techniques provides an existing, structured methodology to examine the interaction of functional groups, devices and circuits. Fault-tree development requires the interactive participation of cognizant power system engineers.

7. A significant digital code development effort is required to efficiently incorporate the coupling techniques and environmental parameters, discussed in Section 2 and 3 of this report as part of the methodology.

8. Existing power system analysis codes for: 1) short-circuit studies, 2) load flow studies, and 3) stability studies can be, with modification, directly incorporated into the HEMP assessment methodology.

Phase I investigation of HEMP interaction with civilian electric power systems has revealed several areas of additional research necessary to better limit the assessment uncertainty. The recommendations are beyond the anticipated scope of work for Phase II research.

The recommendation for additional research are:

1. Additional investigation as to the effects of corona on early-time HEMP interaction with overhead lines. This effort should incorporate experimental validation of analytical results.

2. Specification and implementation of a test program to illuminate power system facilities, or components, using free-field HEMP simulators.

3. Detailed development of an unclassified, unified HEMP environmental definition, incorporating intermediate-time HEMP, applicable for power system assessment.

4. Development of integrated EMP environmental descriptions applicable to investigations which consider simultaneous or time-spaced, joint high-altitude and surface burst events.

7. BIBLIOGRAPHY

1. Lee, K. S. H., ed., EMP INTERACTION: PRINCIPLES, TECHNIQUES, AND REFERENCE DATA-EMP Interaction 2-1, AFWL-TR-80-402, December, 1980.

2. Longmire, C. L., "On the Electromagnetic Pulse Produced by Nuclear Explosions," IEEE Trans. Antennas and Propagation, Vol. AP-26, No. 1, Jan., 1978.

3. Karzas, W. J. and R. Latter, "Detection of Electromagnetic Radiation from a Nuclear Explosion in Space," PHYSICAL REVIEW, Vol. 137, No. 58, March 8, 1964.

4. Ricketts, L. W., J. E. Bridges, J. Miletta, EMP RADIATION AND PROTECTIVE TECHNIQUES, John Wiley and Sons, New York, 1976.

5. EMP ENGINEERING AND DESIGN PRINCIPLES, Bell Laboratories Publication, Whippany, NJ, 1975.

6. ELECTROMAGNETIC PULSE HANDBOOK FOR MISSILES AND AIRCRAFT IN FLIGHT, EMP Interaction 1-1, AFWL-TR-73-68, September, 1972.

7. Ghose, R. N., EMP ENVIRONMENT AND SYSTEM HARDNESS DESIGN, Don White Consultants, Pub., January, 1984.

8. Barnes, P. R., Oak Ridge National Laboratory, Private Correspondence to J. R. Legro, Westinghouse, August 28, 1984.

9. King, R. W. P., Electromagnetic Theory, Dover.

10. Lee, K. S. H., F. C. Young, N. Enqheta, "Interaction of High-Altitude Electromagnetic Pulse (HEMP) with Transmission Lines: An Early-Time Consideration," AFWL EMP Interaction Note 435, December, 1983.

11. R. W. P. King, et. al., Transmission Lines, Antennas, and Waveguides, Dover, 1965.

12. Sunde, E. D., Earth Conduction Effects in Transmission Systems, D. Van Nostrand Co., New York, 1949.

13. Vance, E. F., Coupling to Shielded Cables, Wiley Interscience, New York, 1978.

14. Fontaine, J. M., et. al., "Ground Effects in the Response of a Single-Wire Transmission Line Illuminated by an EMP," Electromagnetics, Vol. 2, No. 1, January-March, 1982.

BIBLIOGRAPHY (Cont'd)

15. Tesche, F. M., and T. K. Liu, "Recent Developments in Electromagnetic Field Coupling to Transmission Lines," Proceedings of the 1981 EMC Conference, Zurich, Switzerland, March 10-12, 1981.

16. Agrawal, A. K., et al., "Time Domain Analysis of Multiconductor Transmission Lines with Branches in Inhomogenious Media," AFWL EMP Interaction Note, February, 1978.

17. Tesche, F. M., and T. K. Liu, "Selected Topics in Transmission Line Theory for EMP Internal Interaction Problems," AFWL EMP Interaction Note 318, August, 1977.

18. Baum, C. E., T. K. Liu and F. M. Tesche, "On the General Analysis of Multiconductor Transmission Line Networks, "AFWL EMP Interaction Notes, Note 130, November, 1978.

19. Ianovici, M., and F. M. Tesche, "Use of General Multiconductor Transmission Line Analysis Code for the Study of EMP Effects in HV Networks," presented at the 1984 Nuclear EMP Meeting (NEM), Baltimore, MD., July, 1984.

20. Tesche, F. M., and T. K. Liu, "User Manual and Code Description for QV7TA: AFWL Multiconductor Transmission-Line Analysis Program.

21. Vance, E. F., "Electromagnetic Pulse Handbook for Electric Power Systems," DNA Report No. 3466F, February 4, 1975.

22. Schelkunoff, S. A., "The Electromagnetic Theory of Coaxial Transmission Lines and Cylindrical Shields," Bell System Tech. Journal, Vol. 13, pp. 532-579, October, 1934.

23. Liu, T. K., "Transient Analysis of TEM Transmission Lines," Proc. IEEE, Vol. 56, pp. 1090-1092, June, 1968.

24. Agrawal, W. K., et al., "Time Domain Analysis of Multiconductor Transmission Lines with Branches in Inhomogenious Media," AFWL EMP Interaction Note, February, 1978.

25. Scharfman, W. E., and E. F. Vance, "EMP Coupling and Propagation to Power Lines: Theory and Experiments," AFWL-TR-73-287, Contract F29601-69-C-0127, Air Force Weapons Laboratory, Kirtland Air Force Base, New Mexico, May, 1973.

26. Flammer, C. and H. E. Singhaus, "The Interaction of Electromagnetic Pulses with an Infinitely Long Conducting Cylinder Above a Perfectly Conducting Ground," Interaction Note 144, Air Force Weapons Laboratory, Kirtland Air Force Base, N.M., July, 1973.

BIBLIOGRAPHY (Cont'd)

27. Liu, T. K., K. S. H. Lee, and L. Marin, "Broadband Responses of Deliberate Aircraft Antennas," AFWL EMP Interaction Note in 228, May, 1975.

28. Baum, C. E., "The Singularity Expansion Method," in Transient Electromagnetic Fields, L. B. Felsen, ed., Springer, New York, 1976.

29. Tesche, F. M., "On the Analysis of Scattering and Antenna Problems Using the Singularity Expansion Technique," IEEE Trans on Antennas and Propagation, Vol. Ap-21, pp. 53-62, January, 1973.

30. Tesche, F. M., "User's Manual and Code Description for ANTSCAT," LuTech Report, LTI-84-103, May 31, 1984.

31. Collin, R.E., Field Theory of Guided Waves, McGraw-Hill, New York, 1960.

32. Legro, J. R., N. C. Abi-Samra, F. M. Tesche, "Study to Assess The Effects of Magnetohydrodynamic Electromagnetic Pulse on Electric Power Systems," ORNL Report 83/433741, Volume 3, March, 1985.

33. Barnes, R. P., E. F. Vance, H. W. Askins, Jr., "Nuclear Electromagnetic Pulse (EMP) and Electric Power Systems," Oak Ridge National Laboratory Report, ORNL-6033, April, 1984.

34. IEEE Standard Dictionary of Electrical and Electronic Terms (IEEE Std. 100-1977), Second Edition, published by the Institute of Electrical and Electronics Engineers, Inc., NY, NY.

35. Zainger, H. W., "Electromagnetic Pulse (EMP) Interaction with Electric Power Systems," Oak Ridge National Laboratory Report, ORNL/Sub/82-4X7905/L, August, 1984.

36. "Interaction of Electromagnetic Pulse with Commercial Nuclear Power Plant Systems," Sandia National Laboratories, U.S. Nuclear Regulatory Report, NUREG/CR-3069, February, 1983.

37. Graf, W., J. M. Hamm, E. F. Vance, "Unification of Electromagnetic Specifications and Standards - Part II: Recommendations for Revisions of Existing Practices," EMP Interaction Note 439, 28 February, 1983.

BIBLIOGRAPHY (Cont'd)

38. "Evaluation of Methodologies for Estimating Vulnerability to Electromagnetic Pulse Effects," A Report prepared by the Committee on Electromagnetic Pulse Environment, Energy Engineering Board, Commission on Engineering and Technical Systems, National Research Council, National Academy Press, Washington, DC, 1984.

39. Hileman, A. R., "Surge Transfer Through Three-Phase Transformers," AIEE Transactions, Pt. III, Vol. 77, 1985, pp 1543-51.

40. "National Electric Power Grid Assessment Program - Phase I Final Report," Report D180-20951-3, Boeing Aerospace Company, Seattle, Washington, 30 June 1982.

41. "Application Guide for AC High-Voltage Circuit Breaker Rated on A Symmetrical Current Basis," American National Standard, ANSI/IEEE C37.011-1979.

42. Vance, E. F. and G. E. Morgan, "Options for Defining and Determining Failure Thresholds," Electromagnetic Specifications and Standards Memo No. 1, AFWL Memorandum.

43. "IEEE Standard Relays and Relay Systems Associated with Electric Power Apparatus," American National Standard, ANSI/IEEE C37.90-1978.

APPENDIX A

EMP Excitation of Multi-Wire Transmission Lines

In attempting to perform an assessment of the effects of an electromagnetic pulse (EMP) on a distributed power system, it is convenient to model above-ground power and distribution lines as a single-wire line over a lossy half space, as in Reference [A1]. In most cases, however, the resulting analysis is only approximate, since the real power line usually consists of three or more conductors.

In this appendix, the formal analysis for a field-excited multiconductor line is reviewed. For simplicity, the line is taken to be lossless.

Consider a lossless section of multiconductor transmission line having sources, as shown in Fig. A1. The length of the line is denoted by ℓ and it contains n wires, located over a ground plane which is taken to be the reference conductor. The n wires are required to be parallel, but not necessarily coplanar. For such a line, its electrical properties are determined by a capacitive coefficient matrix, $(C'_{n,m})$, and an inductive coefficient matrix, $(L'_{n,m})$, which depend only on line geometry and dielectric properties around the line. For this line, these matrices are nonsingular matrices of order n.

As discussed in Reference [A2], the voltages and currents on this line without sources must obey a coupled set of partial differential equations as:

$$\frac{\partial}{\partial z} \begin{pmatrix} (V_n(z,s)) \\ (I_n(z,s)) \end{pmatrix} = -s \begin{pmatrix} (0_{n,m}) & (L'_{n,m}) \\ (C'_{n,m}) & (0_{n,m}) \end{pmatrix} \begin{pmatrix} (V_n(z,s)) \\ (I_n(z,s)) \end{pmatrix} \qquad (A1)$$

where the notation (V_n) represents an n-vector for the line voltage between the n conductors and the ground plane, and a similar notation holds for the current. The parameter s is the complex frequency variable, and the prime represents a Laplace transformed quantity.
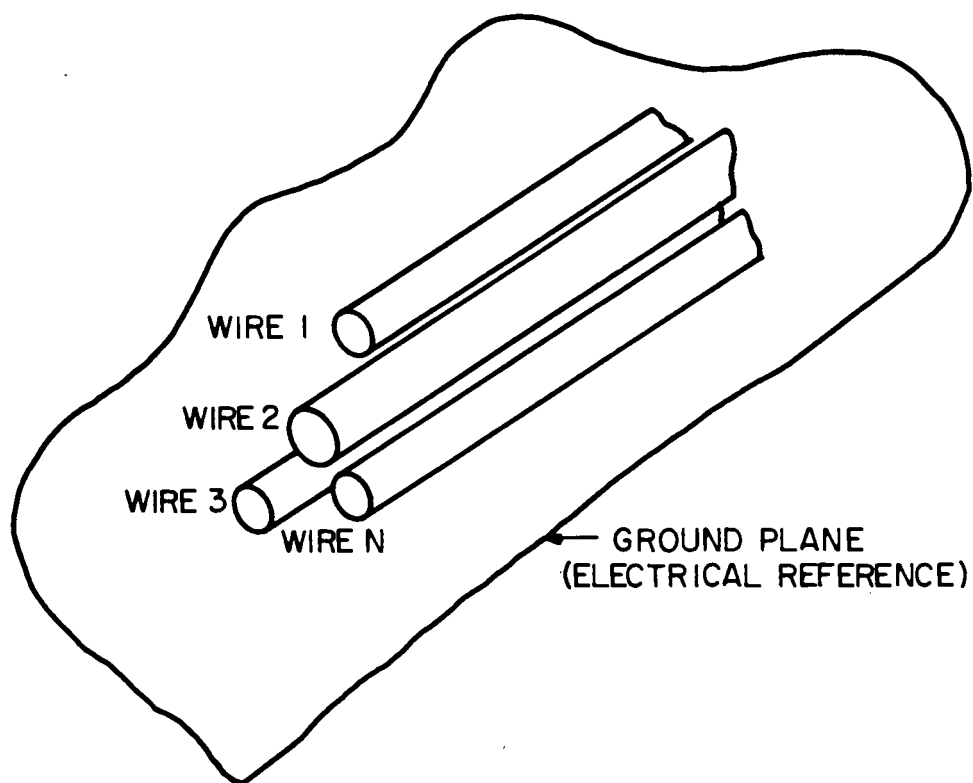
Fig. A1. Section of multiconductor transmission line.

Equation (A1) can be manipulated into two separate equations for voltage and current vectors. The current equation becomes:

$$\frac{\partial^2}{\partial z^2} (I_n(z,s) - s^2(C'_{n,m}) (L'_{n,m}) (I_n(z,s)) = (0_n) \qquad (A2)$$

which is a one-dimensional wave equation for the n-vector current.

For a lossless multiconductor line in a homogeneous region, the matrix product $(C'_{n,m}) (L'_{n,m})$ in Eq. (A2) is diagonal and the individual elements of the curent n-vector are themselves a solution to a simple wave equation:

$$\frac{\partial^2}{\partial z^2} I_n(z,s) - \frac{s^2}{v^2} I_n(z,s) = 0$$

where v is the velocity of wave propagation on the line. Note that this neglects the effects of the lossy ground plane on the wave propagation on the multiconductor line.

A more general line, however, does not have a diagonal result for the $(C'_{n,m}) (L'_{n,m})$ matrix, although it is possible to diagonalize it through the use of a nonsingular nxn transformation matrix, denoted by $(T_{n,m})$, which consists of the current eigenmodes, $(\phi_n)_i$, as columns. The ϕ_n's are solutions to the eigenvalue equation:

$$s^2(C'_{n,m}) (L'_{n,m}) (\phi_n)_i = \gamma_i^2 (\phi_n)_i \qquad (A3)$$

where γ_i^2 is the ith eigenvalue corresponding to the eigenmode $(\phi_n)_i$.

By introducing a change of variables as:

$$(I_n(z,s)) = (T_{n,m}) (i_n(z,s)) \qquad (A4)$$

where $(i_n(z,s))$ represents the modal currents, the wave equation for the modal currents becomes:

$$\frac{\partial^2}{\partial z^2} \; i_n(z,s) \; = \; s^2 (T_{n,m})^{-1} \; (C'_{n,m}) \; (L'_{n,m}) \; (T_{n,m}) \; (i_n)$$

$$\tag{A5}$$

$$= (\gamma_{n,m})^2 \; (i_n)$$

where $(\gamma_{n,m})^2$ is a diagonal matrix containing the γ_i^2 terms as elements.

Since the matrix $(\gamma_{n,m})^2$ in the Eq. (A5) is diagonalized, the solution for the modal currents can be expressed directly as exponential functions of position, and the total solution for the line currents becomes:

$$(I_n(z,s)) = (T_{n,m}) \; \left(e^{-(\gamma_{n,m})z} \; (\alpha_n^t) + e^{(\gamma_{n,m})z} \; (\alpha_n^-) \right) \tag{A6}$$

where (α_n^+) and (α_n^-) are N-vectors which define the amplitudes of each of the propagating modes on the line and which depend on the line termination and excitation. The terms $e^{\pm(\gamma_{n,m})z}$ are diagonal matrices having as elements $e^{\pm\gamma_i z}$, where $\gamma_i = +\sqrt{\gamma_i^2}$.

A similar development for the line voltage $(V_n(z,s))$ can be carried out to determine voltage modes and a propagation equation similar to Eq. (A6). By defining a characteristic impedance matrix as:

$$(Z_{C_{n,m}}) \; = \; s^{-1} (C'_{n,m})^{-1} (T_{n,m}) \; (\gamma_{n,m}) \; (T_{n,m})^{-1} \tag{A7}$$

the line voltage N-vector can be expressed using the same constants (α_n^t) and (α_n^-) as in Eq. (A6):

$$(V_n(z,s)) = (Z_{C_{n,m}}) \; (T_{n,m}) \; \left(e^{-(\gamma_{n,m})z} \; (\alpha_n^t) - e^{(\gamma_{n,m})z} \; (\alpha_n^-) \right) \tag{A8}$$

The unknown constants (α_n^+) and (α_n^-) are determined by taking into account the loads at each end of the line, as well as the excitation. Consider the line shown in Fig. A2, which has lumped voltage and current sources at $z=z_s$, as well as load impedances $(Z_{1n,m})$ and $(Z_{2n,m})$ at $z=0$ and $z=\ell$ respectively. On the section of the line $0 \leq z \leq z_s$ Eqs. (A6) and (A8) are valid, since this section of the line is source-free. Similarly, for $z_s \leq z \leq \ell$ similar equations are valid, but with different constants, $(\hat{\alpha}_n^\pm)$. By relating $(V_n(z,s))$ to $(I_n(z,s))$ at $z=0$, and $z=\ell$ through the load impedance matrices and by relating the discontinuities of $(V_n(z,s))$ and $(I_n(z,s))$ to the voltage and current sources at $z=z_s$, a set of linear equations can be developed with the (α_n) constants for each section of line as unknowns.

Of special interest are the load currents, i.e., $(I_n(0,s))$ and $(I_n(\ell,s))$. Using the solutions for the (α_n) as well as Eq. (A6) for $z=0$ and $z=\ell$, the load currents may be expressed as:

$$
\begin{bmatrix} (I_n(0,s)) \\ (I_n(\ell,s)) \end{bmatrix} = \begin{bmatrix} (\delta_{n,m}) + (\Gamma_{1_{n,m}}) & (0_{n,m}) \\ (0_{n,m}) & (\delta_{n,m}) + (\Gamma_{2_{n,m}}) \end{bmatrix} :
$$

(A9)

$$
\begin{bmatrix} (\Gamma_{1_{n,m}}) & (T_{n,m})\,e^{(\gamma_{n,m})\ell}(T_{n,m})^{-1} \\ (T_{n,m})\,e^{(\gamma_{n,m})\ell}\,(T_{n,m})^{-1} & -(\Gamma_{2_{n,m}}) \end{bmatrix}^{-1} \begin{bmatrix} (I_n^-(s)) \\ (I_n^+(s)) \end{bmatrix}
$$

where $(\delta_{n,m})$ is a diagonal unit matrix and the terms $(I_n^+(z_s,s))$ and $(I_n^-(z_s,s))$ represent the source terms for the positive and negative current traveling waves on the multiconductor line. Those are referred to as combined current sources, since they have the dimension of current
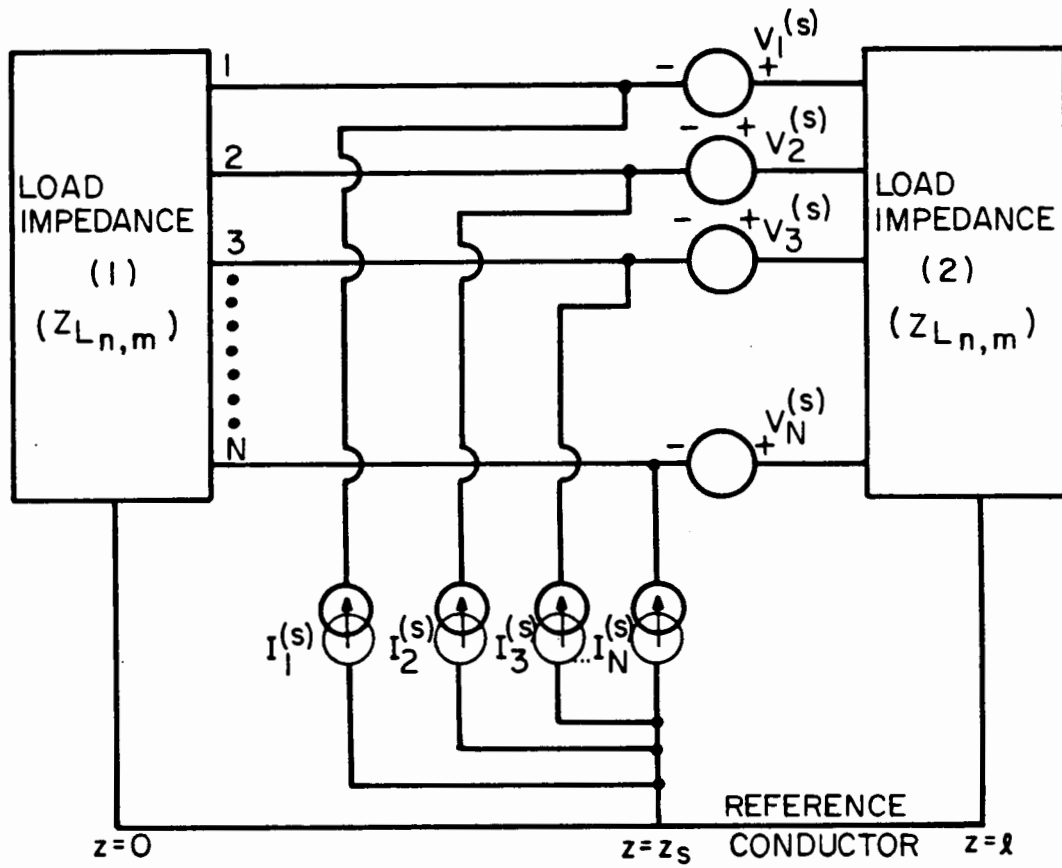
Fig. A2.   Single length of multiconductor transmission
line with loads and lumped sources at $z=z_s$.

but arise from both the applied voltage and current sources at $z=z_s$. In this equation, the terms $(\Gamma_{1n,m})$ and $(\Gamma_{2n,m})$ are generalized current reflection coefficient matrices given by:

$$(\Gamma_{1_{n,m}}) = \left[(Z_{1_{n,m}}) + (Z_{C_{n,m}})\right]^{-1} \cdot \left[(Z_{1_{n,m}}) - (Z_{C_{n,m}})\right] \quad \text{(A10)}$$

for the load at $z=0$, and similarly for $(\Gamma_{2n,m})$ at $z=\ell$ with $(Z_{2n,m})$ as the load impedance. As defined previously, $(Z_{Cn,m})$ is the characteristic impedance matrix of the line.

Notice that the matrix equation in Eq. (A9) has, as its elements, matrices. Thus, it is referred to as a super matrix equation. The double dot operator (:) is used to signify the product between two super matrices by first treating the super matrices as if they were regular matrices and then performing matrix multiplications for each of the individual multiplications of the super matrix product.

The form of the source terms in Eq. (A9) can be shown to be:

$$(I_n^-(s)) = \frac{1}{2} (T_{n,m}) \cdot e^{(\gamma_{n,m})z_s} \cdot (T_{n,m})^{-1} \cdot \left((Z_{C_{n,m}}) \cdot (V_n^{(s)}(z_s,s)) + (I_n^{(s)}(z_s,s)) \right) \quad \text{(A11)}$$

and

$$(I_n^+(s)) = \frac{1}{2} (T_{n,m}) \cdot e^{(\gamma_{n,m})(\ell-z)z_s} \cdot (T_{n,m})^{-1} \cdot \left((Z_{C_{n,m}})^{-1} \cdot (V_n^{(s)}(z_s,s)) - (I_n^{(s)}(z_s,s)) \right) \quad \text{(A12)}$$

With these source terms, the terminal response of the transmission line can be determined for lumped voltage and current sources at $z=z_s$. For field excitation of the transmission line, it is necessary to consider distributed excitation, as opposed to the discrete excitation

discussed above. This can be regarded as a simple extension of Eqs. (A11) and (A12) by integrating over the source terms $(V_n^{(s)})$ and $(I_n^{(s)})$. Doing this, the combined current sources become:

$$(I_n^-(s)) = \frac{1}{2}\int_0^{\ell}\left((T_{n,m})\cdot e^{(\gamma_{n,m})\xi}\cdot(T_{n,m})^{-1}\cdot(Z_{C_{n,m}})^{-1}\cdot(V_n^{\prime(s)}(\xi,s)) + (I_n^{\prime(s)}(\xi,s))\right)d\xi \tag{A13}$$

$$(I_n^+(s)) = \frac{1}{2}\int_0^{\ell}\left((T_{n,m})\cdot e^{(\gamma_{n,m})(\ell-\xi)}\cdot(T_{n,m})^{-1}\cdot(Z_{C_{n,m}})^{-1}\cdot(V_n^{\prime(s)}(\xi,s)) - (I_n^{\prime(s)}(\xi,s))\right)d\xi \tag{A14}$$

which follows directly from superposition. Notice that now the voltage and current sources are per-unit-length quantities, and hence denoted by a prime. These quantities must be determined given a knowledge of the incident electromagnetic field on the line, as well as a knowledge of the transmission line cross-sectional geometry.

The determination of these sources is discussed in detail in Ref. (A3). There, the per-unit-length current and voltage sources on each wire of the multiconductor line are related to electric and magnetic field quantities through the relations:

and

$$\left(I_n^{\prime(s)}(z_s)\right) = -s(C_{n,m}^{\prime})\left(\bar{E}^{tot}(z_s)\cdot\bar{h}_n\right) \tag{A15}$$

$$\left(V_n^{\prime(s)}(z_x)\right) = s\mu_0\left((\bar{h}_n\times\hat{z})\cdot\bar{H}^{tot}(z_s)\right) \tag{A16}$$

where $\bar{E}^{tot}(z_s)$ and $\bar{H}^{tot}(z_s)$ are the total electric and magnetic fields exciting the line. These are determined by removing the multiconductor line and evaluating the sum of the incident and ground-reflected fields in the vicinity of each of the wires in the line. For a perfectly conducting ground plane, these are given as:

$$\mathbf{\overline{E}}^{tot} = \hat{n} \left[2(\mathbf{\overline{E}}^{inc} \cdot \hat{n}) \right] \tag{A17}$$

and

$$\mathbf{\overline{H}}^{tot} = (\hat{k} \times \hat{n}) \left[2(\hat{k} \times \hat{n}) \cdot \mathbf{\overline{H}}^{inc} \right] \tag{A18}$$

where $\hat{n}$ is the unit normal to the ground plane, $\mathbf{\overline{E}}^{inc}$ and $\mathbf{\overline{H}}^{inc}$ are the incident electric and magnetic fields and $\hat{k}$ is the direction of propagation of the incident field. For the case of an imperfectly conducting ground, these last relations must be modified to include the well-known plane-wave reflection coefficients.

The vector $\mathbf{\overline{h}}$ in Eqs. (A15) and (A16) are the "field coupling vectors" as defined in Ref. A3. As shown in Fig. A3, for each wire, n, the parameter $\mathbf{\overline{h}}_n$ is a vector normal to the ground plane and terminating at the geometric center of charge when the nth wire has an arbitrary charge Q placed on it and with all other conductors having zero net charge.

Generally the determination of these field coupling parameters involve solving a set of auxillary quasi-static problems, defined by the geometry shown in Fig. A3. In the case of overhead power lines, however, the conductor radius is always much less than the phase conductor separation and height above the ground, which implies that the field coupling parameters are simply the wire height above the ground plane.
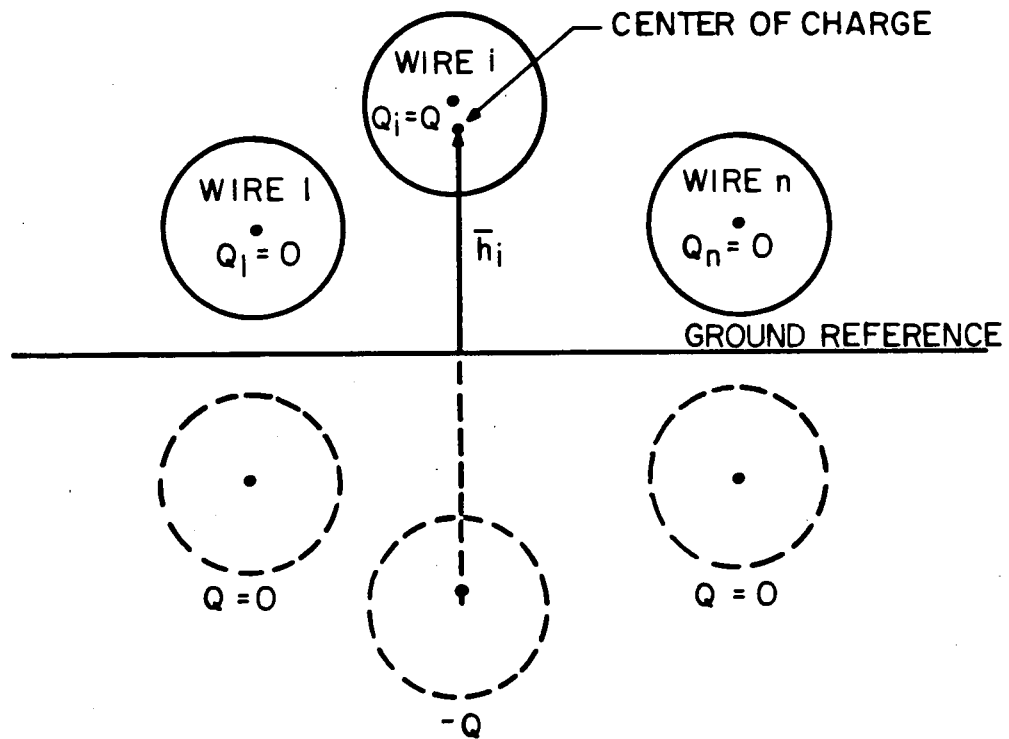
Fig. A3. Field coupling vector for Wire i of multiconductor line over a ground plane.

BIBLIOGRAPHY

A1. Tesche, F. M., "On the HAEMP Response of Above-Ground Electrical
      Transmission Lines," PSA Memo - Memo 2, April 5, 1984.

A2. Baum, C. E., T. K. Liu and F. M. Tesche, "On the General Analysis
      of Multiconductor Transmission Line Networks," AFWL EMP
      Interaction Notes, Note 130, November 1978.

A3. Tesche, F. M. and T. K. Liu, "Field Excitation of Multiconductor
      Transmission Lines," AFWL EMP Interaction Notes, Note 351,
      September 1978.

APPENDIX B

Numerical Examples Showing The Response
of A Single Line Above Ground to HEMP Fields

B.1 Introduction

This appendix contains numerical solutions of the equations presented in Section 3 for a single line above ground excited by a HEMP field. A vertically polarized HEMP field was used in most of the examples since this polarization generally produces a larger response than horizontal polarization.

The examples contained in Section B.2 show the effect of variations in parameters such as waveshape of the HEMP field, angles of incidence, conductivity of the soil, height of the line, and length of the line on the response of the line.

Section B.3 shows how HEMP fields can be separated into their horizontal and vertically polarized components, the response calculated for the two components separately, and the total response determined by combining the responses for the two components. This approach works if the system is linear.

Section B.4 gives the response of transmission lines at eight different geographic points for a HEMP burst at a specific location. The actual HEMP fields that would be produced at these points per currently available information is used in calculating the responses at these points. The response at one of the points is calculated for an assumed intermediate time HEMP waveform.

In Section B.5 a time domain solution is shown that takes into account the effects of transmission tower flashovers.

B.2 Effect of Variations in Parameters on The Response
to Vertically Polarized HEMP Waves

In this section the effects of variations in parameters such as HEMP waveshape, angles of incidence, conductivity of the soil, and height and length of the line are examined.

Effect of Waveshape of the HEMP Electric Field

The magnitude and waveshape of the induced voltages and currents on conductors depend on the assumed waveshape of the incident HEMP electric field and the characteristic of the ground (lossy or perfect). To illustrate this, consider an incident HEMP electric field plane wave incident at an elevation angle, ψ, of 40 degrees and orientation or azimuth, ϕ, angle of $0°$ on a long conductor, 10 m above ground. Assume that the incident field can be represented by a double exponential waveshape of the form:

$$E^{inc} = E\ (e^{-\alpha t} - e^{-\beta t}) \tag{B1}$$

whereby, E is a constant, kV/m.

    $1/\alpha$ is the fall time constant, in sec.
    $1/\beta$ is the rise time constant, in sec.

Lossy Earth

Figure B1 shows the variation in the peak open circuit voltage (V_{ocp}) at the end of the conductor for seven different fall time constants (different αs) while keeping β constant at 4.76×10^8 $\sec^{-1}$. Figure B2 shows the variation of the tail of open circuit voltage (V_{oc}) (time needed for waveform to reach 50% of the peak) as a function of the tail of the incident field. Figure B3 shows the variation in V_{oc} for seven different rise time constants (different βs) while keeping α constant at 4.00×10^6 $\sec^{-1}$. Figure B4 shows the seven different field
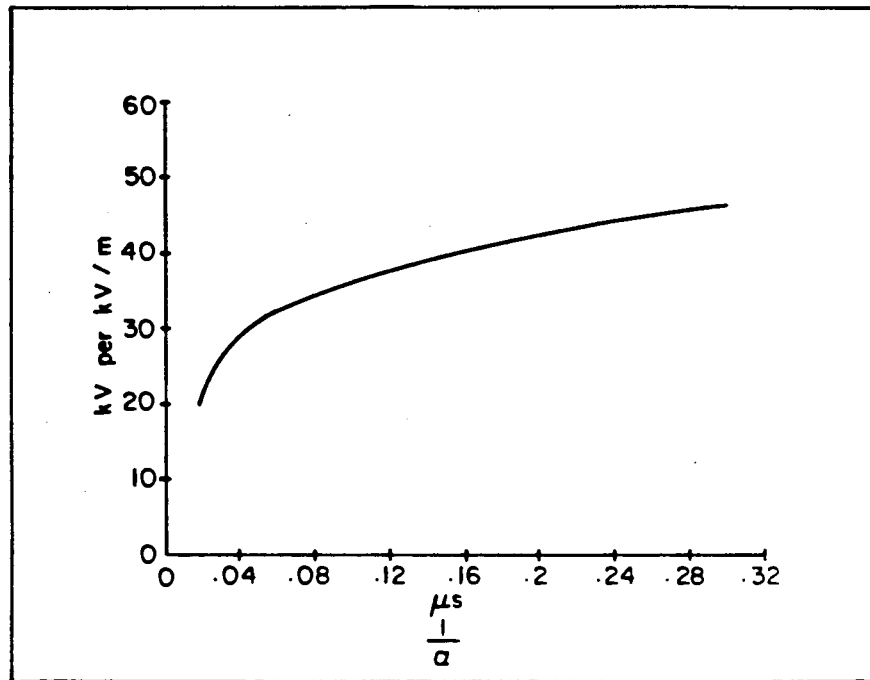
Fig. B1. Normalized variation in the peak open circuit
voltage as a function different fall time constants $\left(\frac{1}{\alpha}\right)$.
β maintained at 4.76×10^8 sec^{-1}.
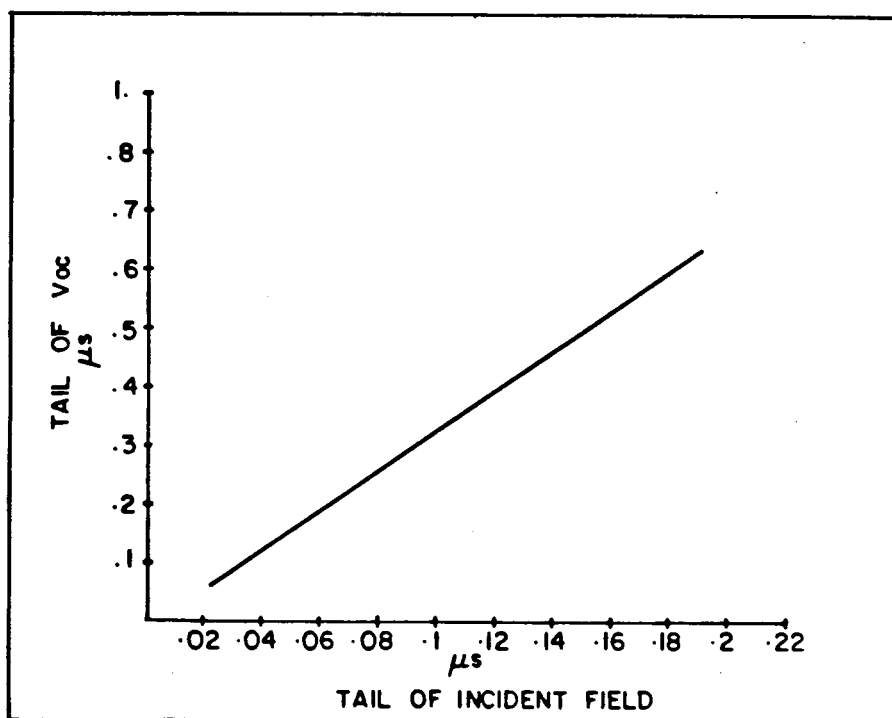
Fig. B2. Variation of the tail of the open circuit voltage V_{oc} as a function of the tail of the incident field.
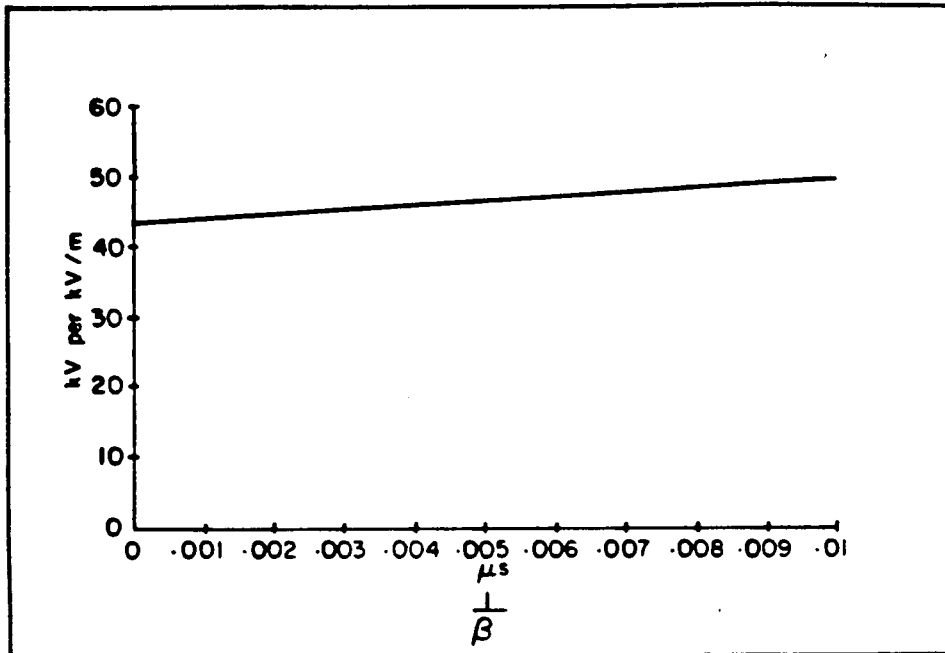
Fig. B3. Normalized variation in the peak open circuit
voltage as a function of different rise time constants $\left(\frac{1}{\beta}\right)$.
α maintained at 4×10^6 sec^{-1}.
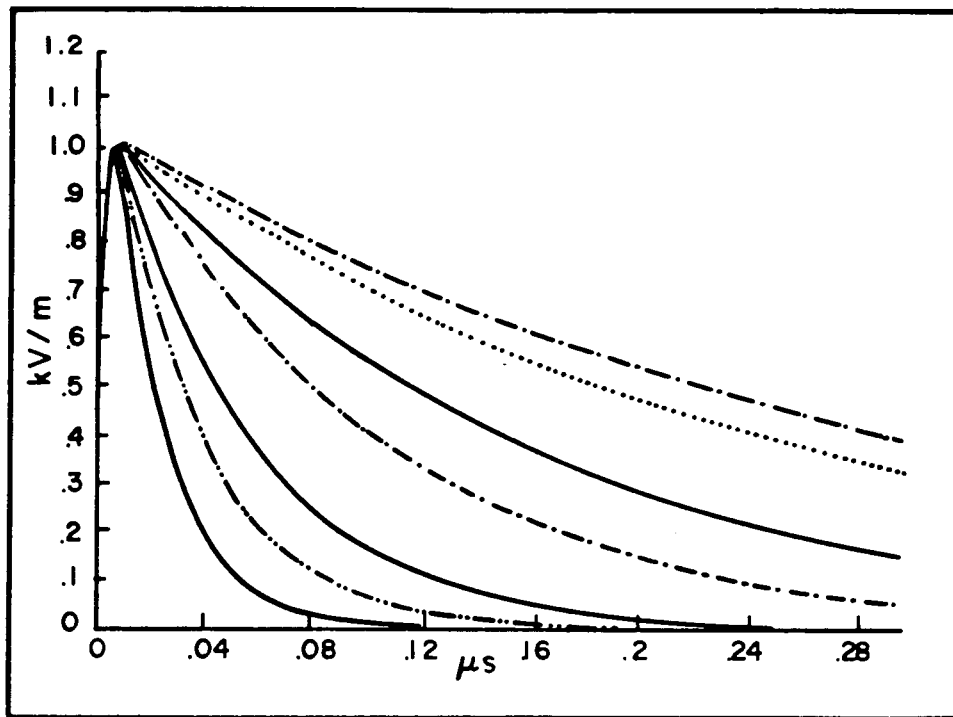
Fig. B4a. Normalized waveshapes of incident
electric fields waveshapes.
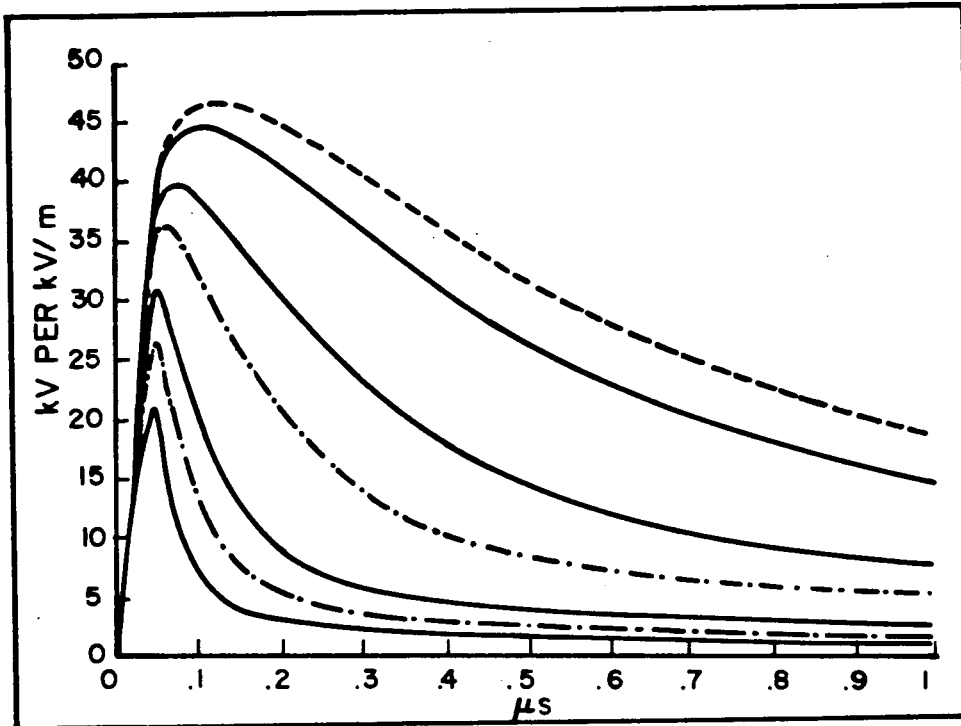
Fig. B4b. Normalized response of a lossy conductor, 10 m
above a .01 mhos/meter conductivity when excited with the
waveforms of Fig. B4a. The incident fields are assumed to
be vertically polarized, with $\psi=40°$, $\phi=0°$.

waveforms and the corresponding complete response for long conductors (responses in Fig. B4b correspond to fields in Fig. B4a). Ground conductivity is considered to be .01 mhos/m.

It is apparent from the above figures that the peak magnitude of the induced voltages on conductors, over lossy earth, is affected strongly by the fall time constant and weakly by the rise time constant. The wider the pulse, the larger the section of conductor near its terminals over which distributed sources add in phase resulting in a larger voltage. To illustrate this numerically, a regression analysis on the peak magnitude of V_{ocp} for the given conductor and polarization of the incident HEMP against the two constants given in the following results:

(B2)

$$V_{ocp} = 66.4 \; \frac{1}{\alpha}^{.277} \qquad \text{kV per kV/m incident electric field}$$

(B3)

$$V_{ocp} = 43.58 + 585.936 \; \frac{1}{\beta} \qquad \text{kV per kV/m incident electric field}$$

whereby, $1/\alpha$ and $1/\beta$ are the time constants expressed in microseconds. V_{ocp} can also be expressed as a function of the tail of the incident wave by the following expression:

(B4)

$$V_{ocp} = 78.37 \; \tau^{.3229} \qquad \text{kV per kV/m incident electric field}$$

τ is the tail of the incident wave in microseconds.

As is expected, the wider the incident wave, the longer it takes to reach peak magnitude, and the longer the tail of the resulting induced voltage on the conductor. This is illustrated in Fig. B4b.

Perfect Earth

For a perfect (lossless) ground, the effect of a wider pulse affects the tail of the induced voltage only, leaving the peak and time to peak unchanged. The effect of changing the rise time constant of the incident wave on the induced voltage over perfect earth is minimal.

Waveform Used In the Illustrations of This Report

Unless otherwise indicated, the waveform labeled as the "Bell Labs" waveform in Table 2 of Section 2.5 will be used for all numerical examples throughout this appendix. The use of the results presented in this section, however, should enable the reader to estimate the responses to an arbitrary waveform. All results are also normalized to 1 kV/m incident electric field strength.

Cross-Reference Between The α and β Parameters and The Front and Tail of Waveshapes

In power analysis it is more customary to represent waveshapes as a function of two different times: The front and tail, as in Fig. B5. To measure the front, a straight line is drawn on the front through two points: the points at which the waveform is equal to 30% and 90% of its crest value. The point of interaction of this line with the time axis is called "Virtual Origin," and all times are measured from this point. The time between the virtual origin and the time defined by the intersection of the straight line and a horizontal line drawn at the crest is defined as the front, T_F. The front can better be defined by simply stating:

$$T_F = 1.67 \ (t_{90} - t_{30}) \tag{B5}$$

The tail, or time to half-value, is the time, T_F, between the point at which the wavehape decreases to half the crest magnitude and the virtual origin. The front and tail are normally written in two ways
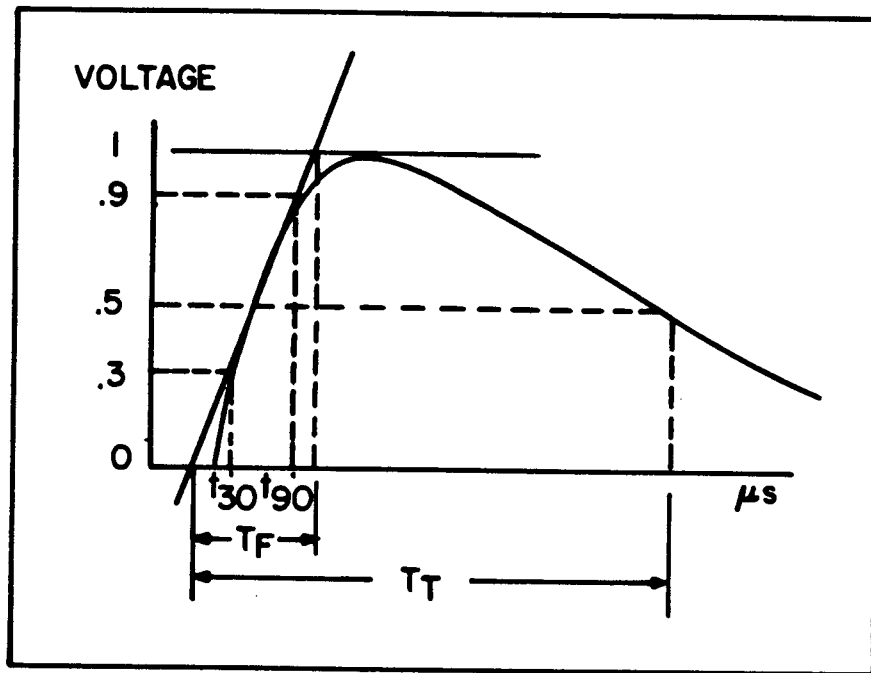
Fig. B5. Definition of front and tail for a waveform.

T_F/T_T or $T_F \times T_T$. The rate-of-rise of the impulse, or more properly the virtual rate-of-rise is defined by the rate-of-rise of the line shown through the 30%-90% values above.

Figure B6 illustrates the dependency of the tail, T_T, on the time constants of a double exponential waveform of the form Equation (B1). In this figure β is maintained constant at 4.76×10^8 sec^{-1} and $1/\alpha$ varied from .02 to .3 microseconds.

A more general idea of how the front and tail vary with α and β is shown in Fig. B7. This figure shows the ratio of tail time, T_T to the front time, T_F as a function of ratio of the two time constants. Bewerly, in Ref. [B1], presents a set of curves and a method to construct a double exponential waveform from T_F, T_T and the peak magnitude, and vice versa. These curves are shown in Fig. B7. The use of Fig. B7 is illustrated through the following two examples.

Examples on The Use of Figure B7

a) T_F, T_F and E_1 specified

Determine a double exponential expression of the form of Equation (B1) to fit a .009/.101 µs waveshape with unity peak magnitude.

For a T_T/T_F = 11.22 Figure B7 gives a $\beta/_\alpha$ = 60

For β/α = 60 , αT_F = .070 and E_1/E = 1.087

Hence $\alpha = 7.78 \times 10^6$ sec^{-1} , $\beta = 467 \times 10^8$ sec^{-1}, E = 1.087
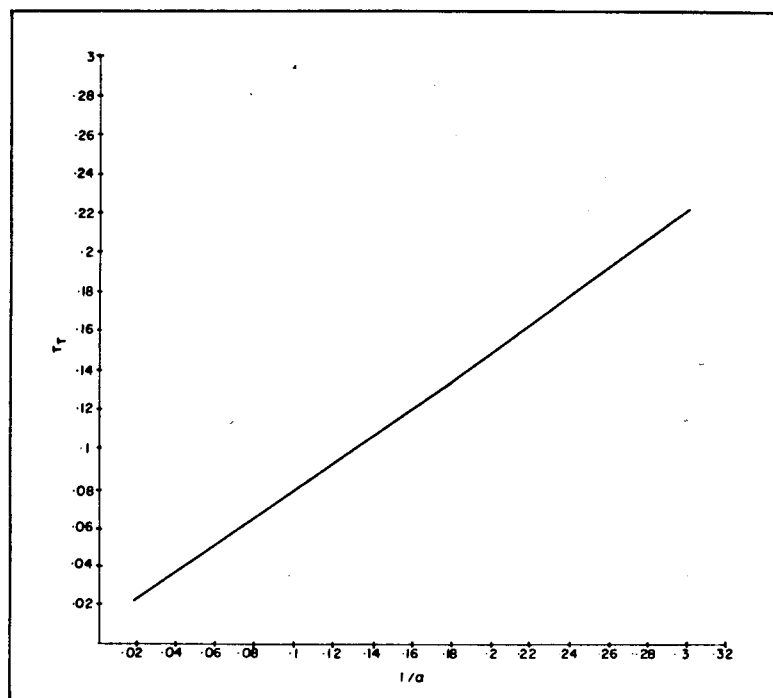
Fig. B6. Dependency of the tail, T_T on $\alpha(\beta=4.76\times10^8 \text{ sec}^{-1})$. T and $1/\alpha$ are in microseconds.
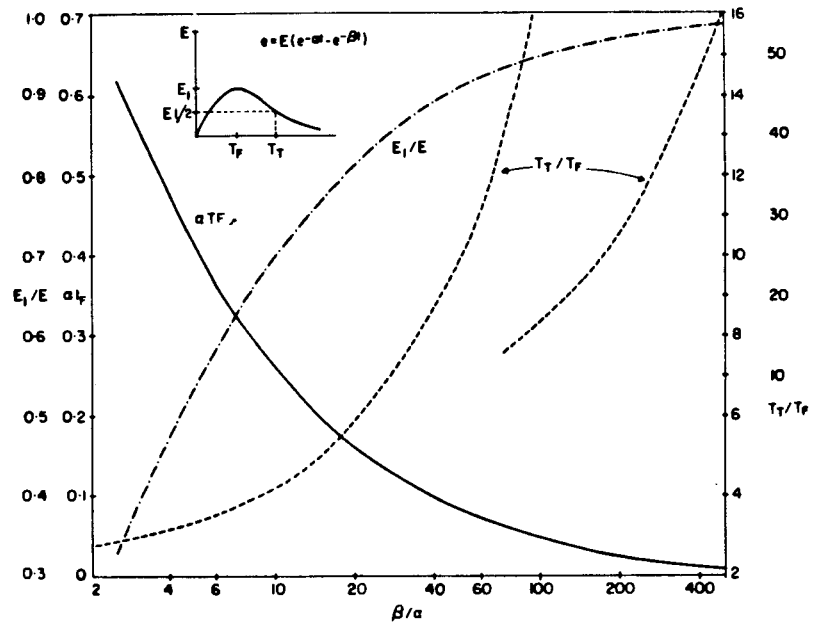
Fig. B7. Cross reference for defining a waveform either by α and β parameters, or T_F and T_T.

b) $\underline{\alpha,\beta \text{ and } E \text{ specified}}$

Let $\alpha = 30 \times 10^6 \text{ sec}^{-1}$ $\beta/\alpha = 15.86$

$\beta = 476 \times 10^6 \text{ sec}^{-1}$

$E = 64.25$

From Figure B7, we get:

$T_T/T_F = 5.2$ $T_F = .0063 \text{ }\mu\text{s}$

$\alpha \text{ } T_F = .158$ $T_T = .032 \text{ }\mu\text{s}$

$E./E = .78$ $E_1 = 50$

Effect of Angles of Incidence

The elevation and orientation angles of incidence of the HEMP plane wave affect the response induced on conductors. As illustrated in Figures B8 and B9, the response of the conductor increases with decreasing elevation and excitation angles of incidence. The results shown in this figure, however, should not be extrapolated for elevation angles much less than 30, for reasons discussed below. Figure B10 shows a typical variation of the tail of the open circuit voltage as a function of the elevation angle.

Case of Grazing Angle of Incidence

If the elevation angle, ψ, approaches 0 degrees, with the HEMP plane wave oriented along the conductor ($\phi=0°$), the response of a semi-infinite line as obtained with the general equations presented in Section 3.2 becomes very high if the magnitude of the HEMP field is assumed to be constant along the line. In fact, for low loss, long lines, both voltage and current can approach infinity.
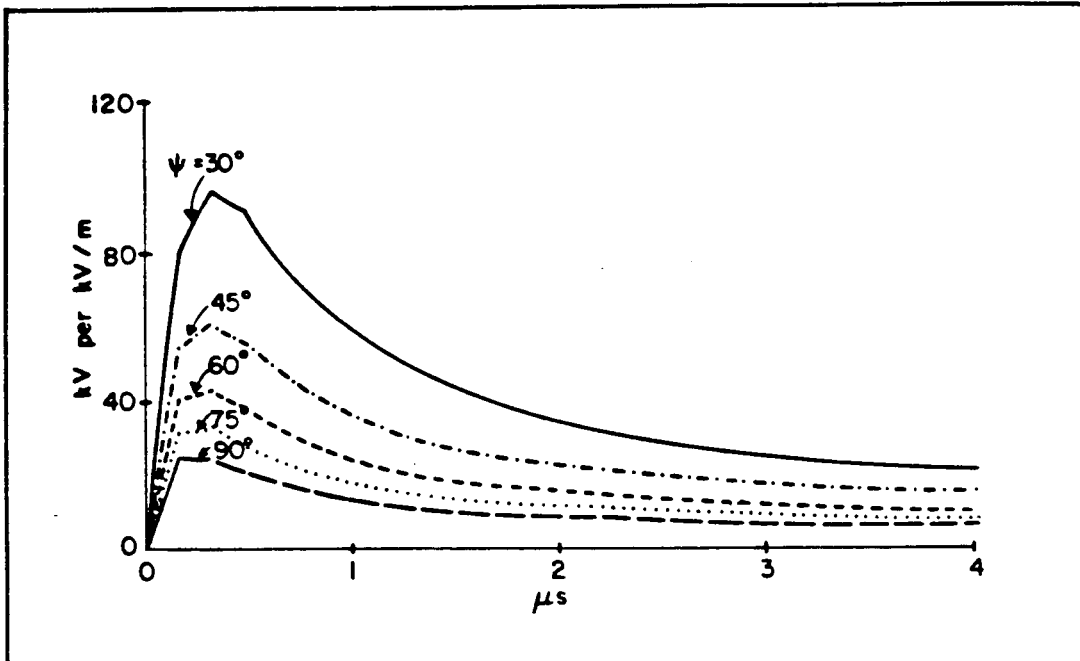
Fig. B8. Normalized open circuit voltage at the end of a long line 10m above a 10^{-3} mhos/meter conductive ground. $\phi=0°$, vertical polarization.
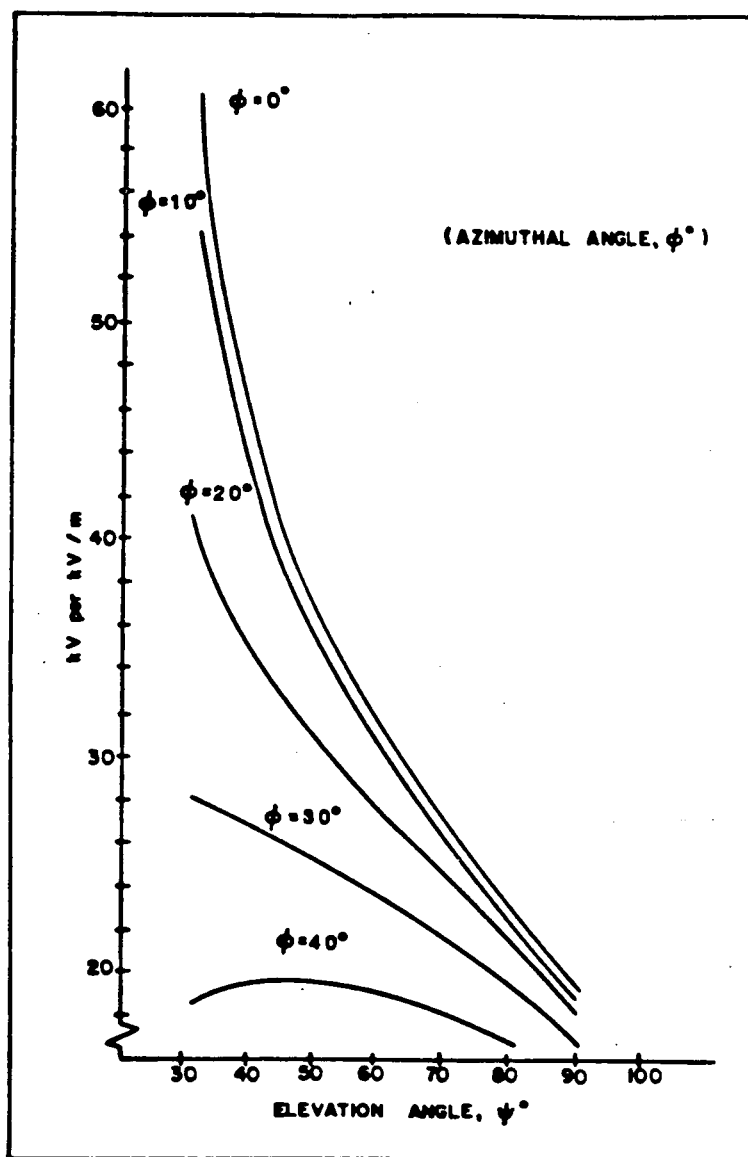
Fig. B9. Effect of elevation and orientation angles on the peak open circuit voltage at the end of long lines of height 10m above ground. Ground conductivity = .01 mhos/meter. Vertical polarization.
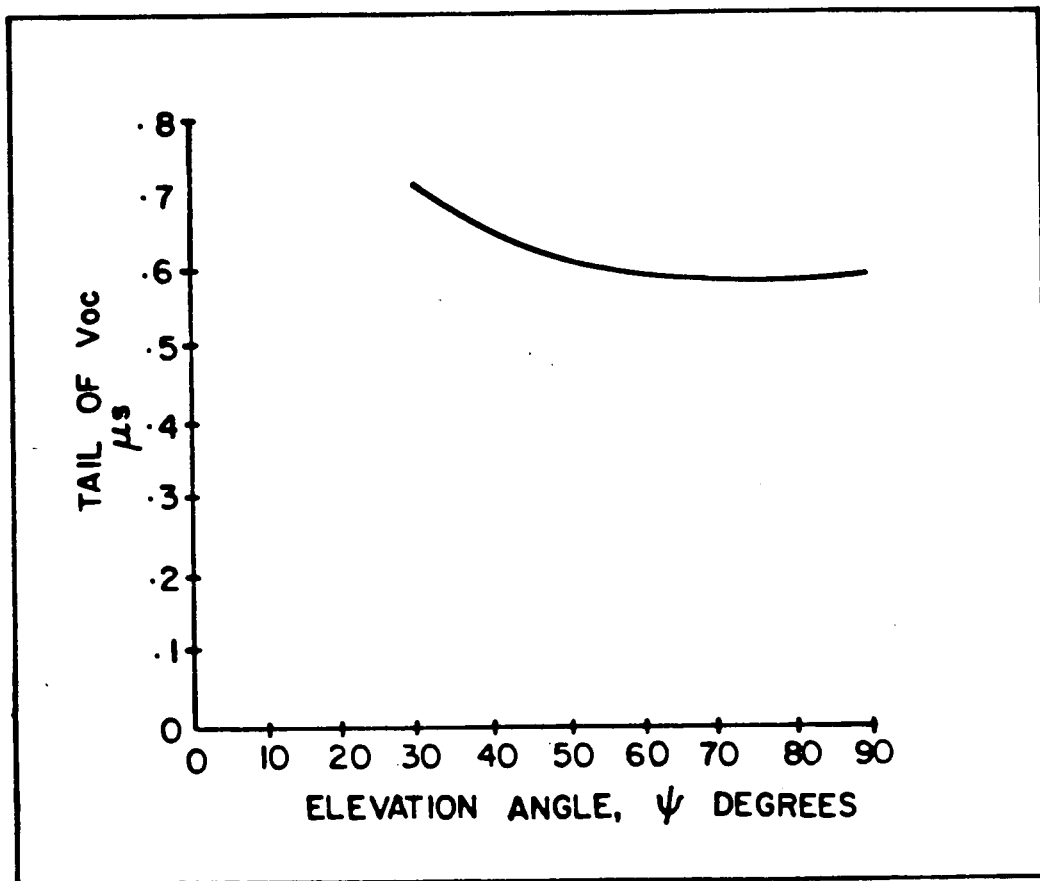
Fig. B10. Typical variation of the tail of the open circuit voltage of a long conductor 10m above .01 mhos/m earth for different elevation angles, ψ. Orientation angle of the conductor is set at 0 degrees. Vertical polarized incident field.

However, when the angles become small, the critical line length becomes large and the assumption that the magnitude of the HEMP field is constant along the entire length of the line becomes questionable. The solution method should be modified to use the actual magnitude of the field along the line.

Effect of Height Above Ground

The height of a conductor above ground affects the voltages and currents induced on it due to HEMP. Figure B11 shows the affect of height on the voltage induced due to vertically polarized HEMP plane wave, for a ground conductivity of .01 mhos/m. Figure B12 shows the variation in the peak magnitude of the induced voltages due to different conductor heights and different ground conductivities.

From the above two figures it can be concluded that:

- Only for perfect (lossless) ground, is the induced voltage zero at ground level.

- The effect of height is more pronounced for more conductive ground, i.e. the incremental increase in voltage due to an incremental increase in height is less for lower ground conductivities. Said in another way, the ground effect is more important than the height effect for less conductive grounds.

- As the height of the conductor above ground increases, the voltages for ground conductivities of .1 mhos/m or more approach those calculated assuming perfect ground.

Effect of Ground Conductivity

The induced response on an aerial conductor is a function of the tangential electric HEMP field (the resultant of the incident and the ground reflected fields). If the ground is considered as a perfect conductor ($\sigma = \infty$ mhos/m or $\rho = 0$ m-ohms), the resultant field is zero. In this case, the peak voltage is reached when the reflection from ground arrives at the conductor given at $t = 2h\sin\psi/c$, where h is the height, ψ is the elevation angle and c the speed of light. As the ground becomes
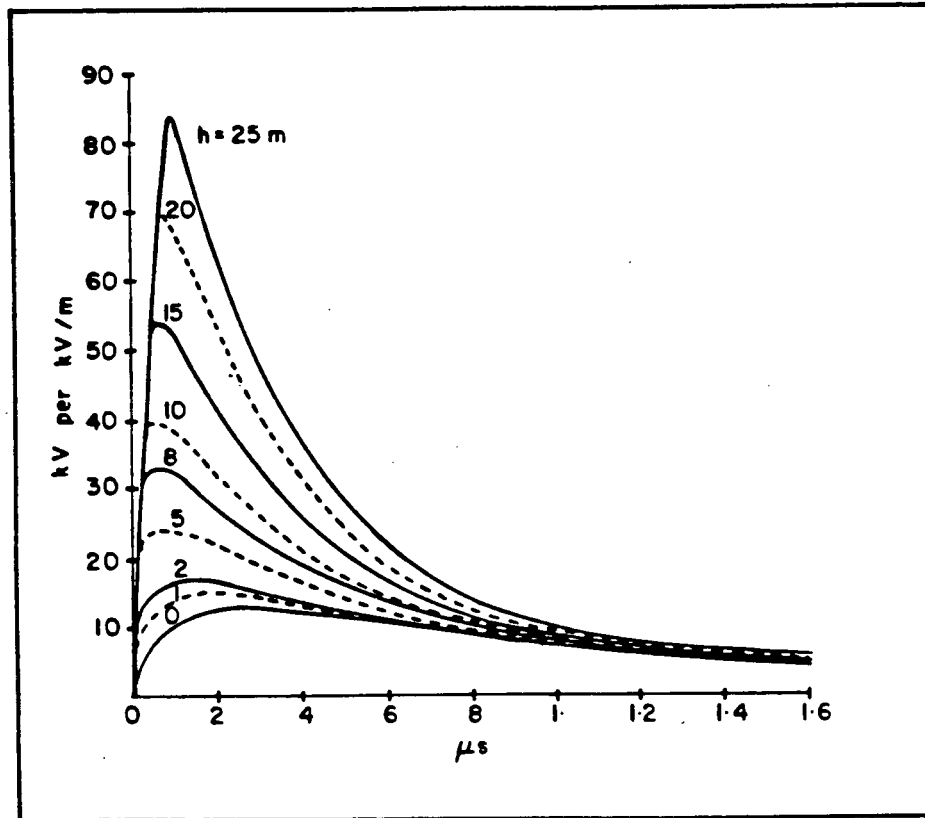
Fig. B11. Normalized open circuit voltage at the end
of a long conductor 10m above a .1 mhos/m conductivity
ground. $\psi=30°$, $\phi=0°$. Vertical polarization.
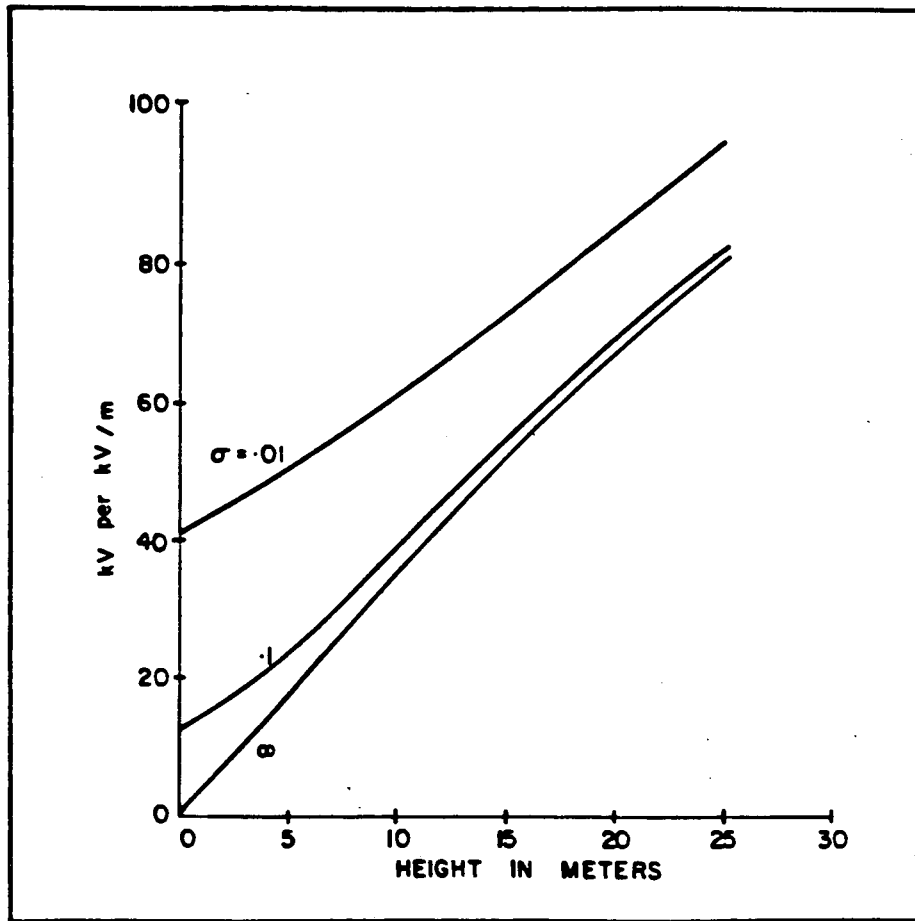
Fig. B12. Normalized open circuit voltages at the end of a long conductor 10m above grounds with different conductivities (.01, .1 and ∞ mhos/m). $\psi=30°$, $\phi=0°$. Vertical polarization.

less and less conductive, the cancellation is less complete and the resultant tangential field increases, increasing with it the peak voltage at the end of the conductor. The time to reach the peak voltage is no longer coincident with the arrival of the ground reflected field. The lower the conductivity, the longer it takes to reach peak voltage, assuming a long conductor. Figure B13 shows the effect of ground on a long conductor due to a vertically polarized HEMP plane wave. Figure B14 shows the effect of ground for horizontally polarized HEMP plane wave. These two figures illustrate that the ground effect coupling to vertical polarization is considerably greater than the coupling to horizontal polarization. Figure B15 shows a typical variation of the open circuit voltage for long lines as a function of ground conductivity for vertical polarization.

Critical Line Length

The concept of the critical line length for a single conductor is presented in Section 3.2.1.3. Formulas for determining the critical line length are given in Equations (64) and (65).

The effects of the line length on the response is illustrated in Figures B16 and B17. As illustrated by these figures, the responses are identical to those for the semi-infinite case up to the time $t=L/C(1-\cos \psi \cos \phi)$.

B.3 Systematic Method to Calculate Response Due to Arbitrarily Polarized HEMP

There are at least two ways to calculate the response to arbitrary HEMP polarization. In the first method, one finds the resultant tangential electric field on the conductor due to the arbitrary polarization by defining a new ground reflection coefficient for the electric field. The resultant field is then integrated along the conductor to find the response. This method leads to the correct response, however, it may be very complex.
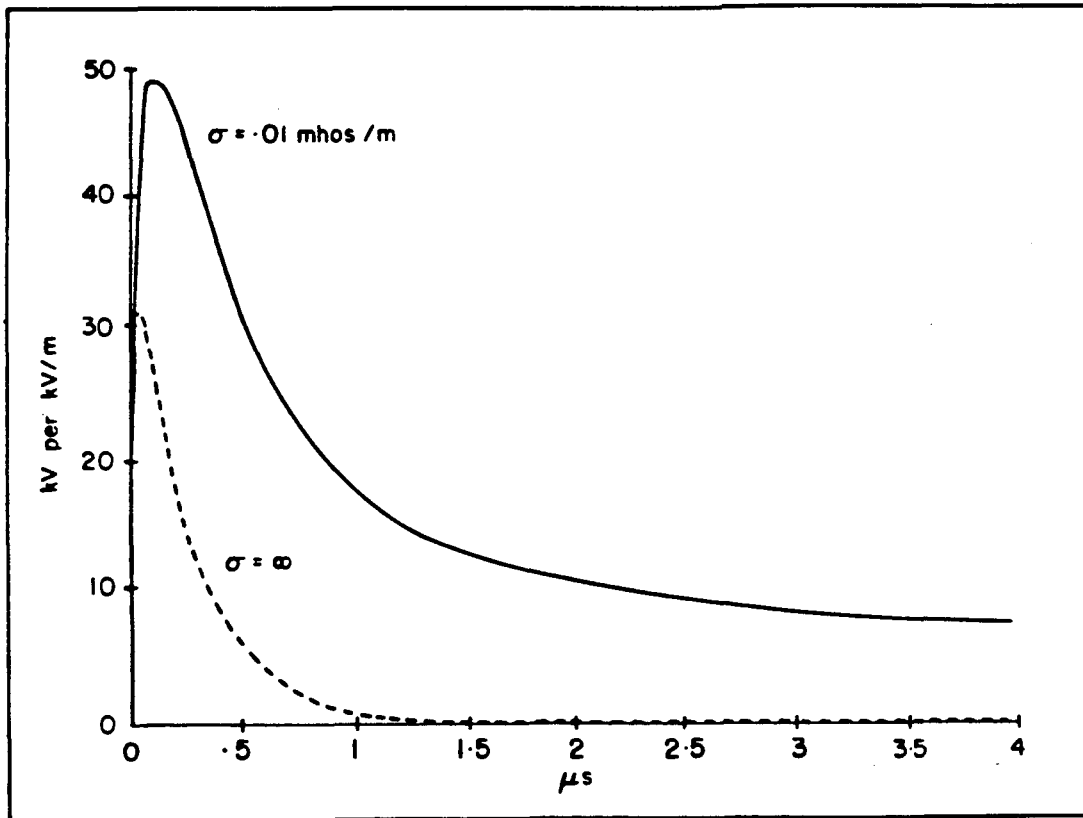
Fig. B13. Normalized open circuit voltage induced on a long conductor 10m above ground. $\psi=36°$, $\phi=0$. Vertical polarization. Solid line, σ = .01 mhos/m. Dashed line, $\sigma = \infty$.

Fig. B14. Normalized open circuit voltage induced on a long line 10m above ground. $\psi=36°$, $\phi=0$. Horizontal polarization. Solid line, $\sigma = .01$ mhos/m. Dashed line, $\sigma = \infty$.
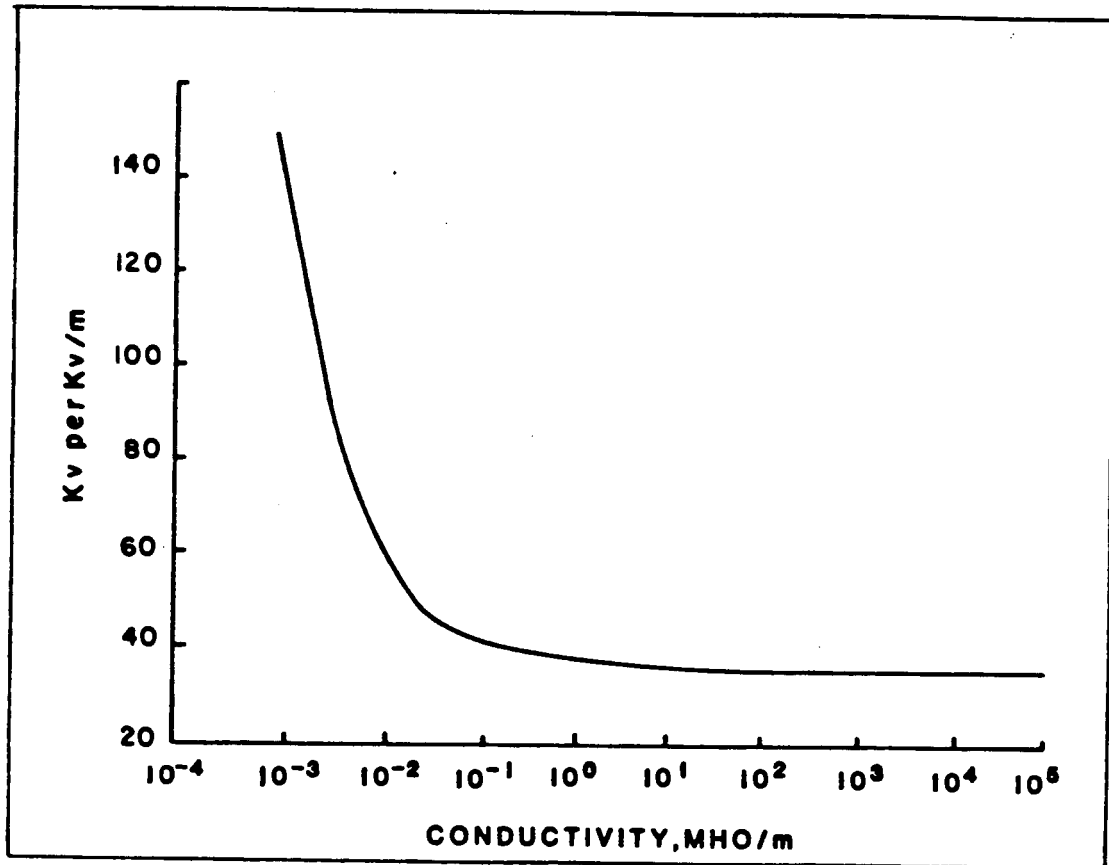
Fig. B15. Effect of ground conductivity on the peak open
circuit voltage at the end of long conductor of height 10m
above ground. $\psi=30°$, $\phi=0°$. Vertical polarization.
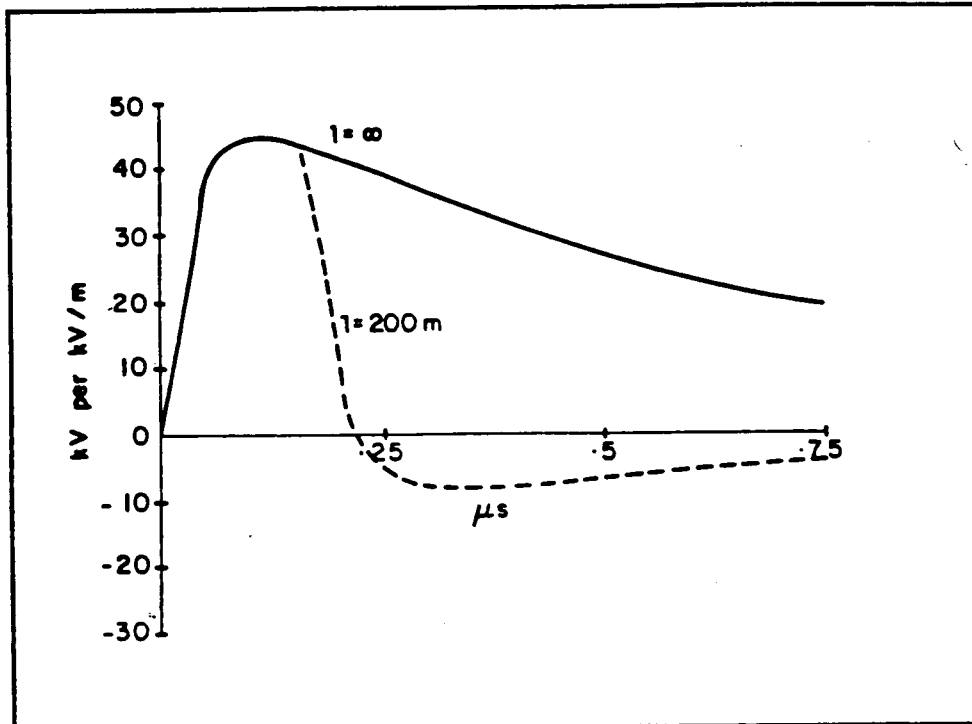
Fig. B16. Normalized HEMP induced open circuit
voltage on conductor 10m above .01 mhos/m earth,
$\psi=40°$, $\phi=0°$, vertically polarized field. $Z_L=Z_0$.
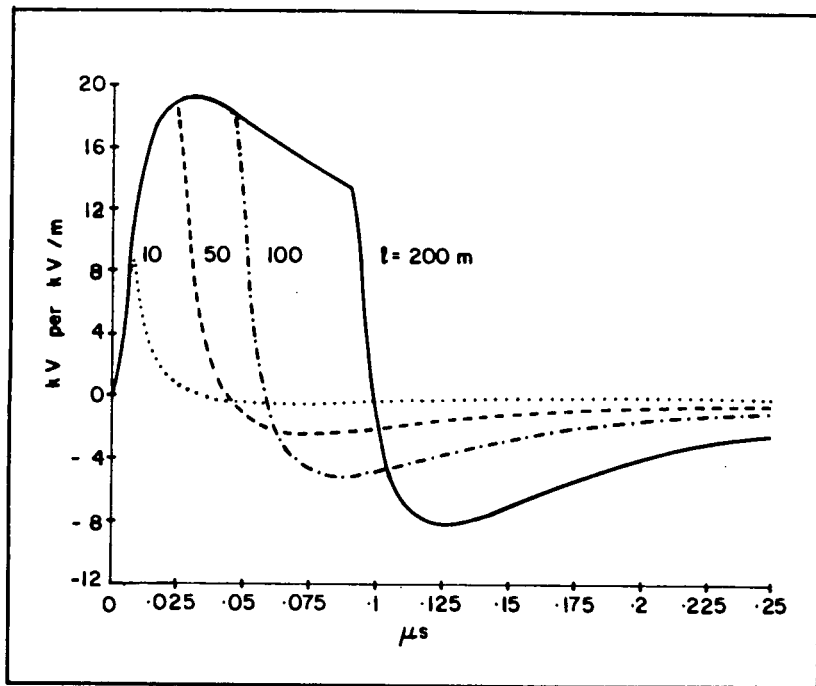
Fig. B17. Normalized HEMP induced responses on conductors of different length, 1 m above .01 mhos/m conductivity earth, $\psi=30°$, $\phi=0°$. Vertical polarization.

An alternative method to do this task is presented here. This method is based on the principle of superposition. This method can be described as follows:

● Break the incident electric field to vertically and horizontally polarized components as determined from Figure 7 and Equations (9) and (10).

● Calculate the response of the conductor to each of the above two components independently.

● Add these two responses together to find the total response.

B.4 Numerical Calculation of HEMP-Induced Responses at Eight Different Locations With Respect to Ground Zero of a High Altitude Burst

Introduction

This section of the report presents numerical examples of the response of eight above-ground lines at eight different locations (observation points) with respect to a ground zero of a high altitude burst. The relationships and principles of Sections 2 and 3.2 are used throughout here. The waveforms of the incident field are estimated from Ref. [B1].

The locations of the selected observation points are shown in Fig. B18. The locations are all given with respect to magnetic north. Point #1 corresponds to a location directly under the burst point. Observation Point #2 is positioned directly south of Point #1 and is located in the region of maximum electric field strength. The incident fields at both of these points are both horizontally polarized.

Point #3 is located near the horizon, directly west of the burst point, and has an incident field waveform of a much longer fall time than the two previous cases. The polarization of the field at this point contains both horizontal and vertical components.

Fig. B18. Locations of observation points on
the earth's surface.

Observation point, Point #4, lies approximately southeast of the burst point, has a waveform similar to that of point #1, but with only a vertical polarization component of the incident field.

Point #5 is located on the horizon (ψ=1°), directly south of the burst point. Points #6, 7, and 8 are also located due south of the burst at distances that give elevation angles, ψ, of 11°, 14°, and 18°, respectively. The HEMP incident fields are entirely horizontally polarized for Points 5 through 8. The polarizations are obtained from Fig. 7.

Definition of the Incident HEMP Electric Fields at the Eight Different Observation Points

Reference [B1] describes the variation of the peak magnitude and time dependency of the electric field as a function of the location of the observation time with respect to ground zero of the burst. The time dependency, according to Ref. [B1], is defined as follows. Near the ground zero, E has a rise time of about 5 ns and a tail of 20 ns. In the region of maximum peak intensity (i.e., south of ground zero), the rise time is just under 10 ns and a tail of about 50 ns. Near the tangent radius due south of the burst, the rise time is somewhat longer than 10 ns and tail is about 200 ns.

The dependency of the peak magnitude on the location is illustrated in Fig. B18.

The maximum field that can be produced by the burst is assumed to be 50 kV/m for this example, hence, Fig. B19 shows the assumed electric field waveforms for the different points. The electric field at each of the different points is assumed to be a plane wave of constant magnitude along the lines at that point.

In the cases to follow, the relative ground permittivity, ε_r is assumed to be 10. The conductor radius is 2.5 cm, corresponding to a characteristic impedance of 400 Ω when the wire is 10 m above a perfectly conducting earth. All lines are considered to be long (semi-infinite) for simplicity.
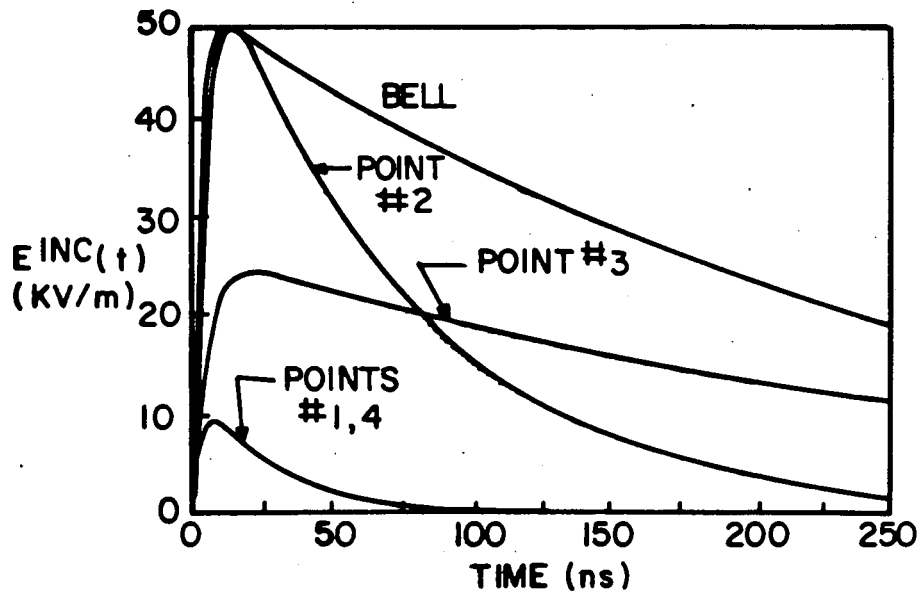
Fig. 19a. Various HEMP waveforms used for estimation of power system responses.
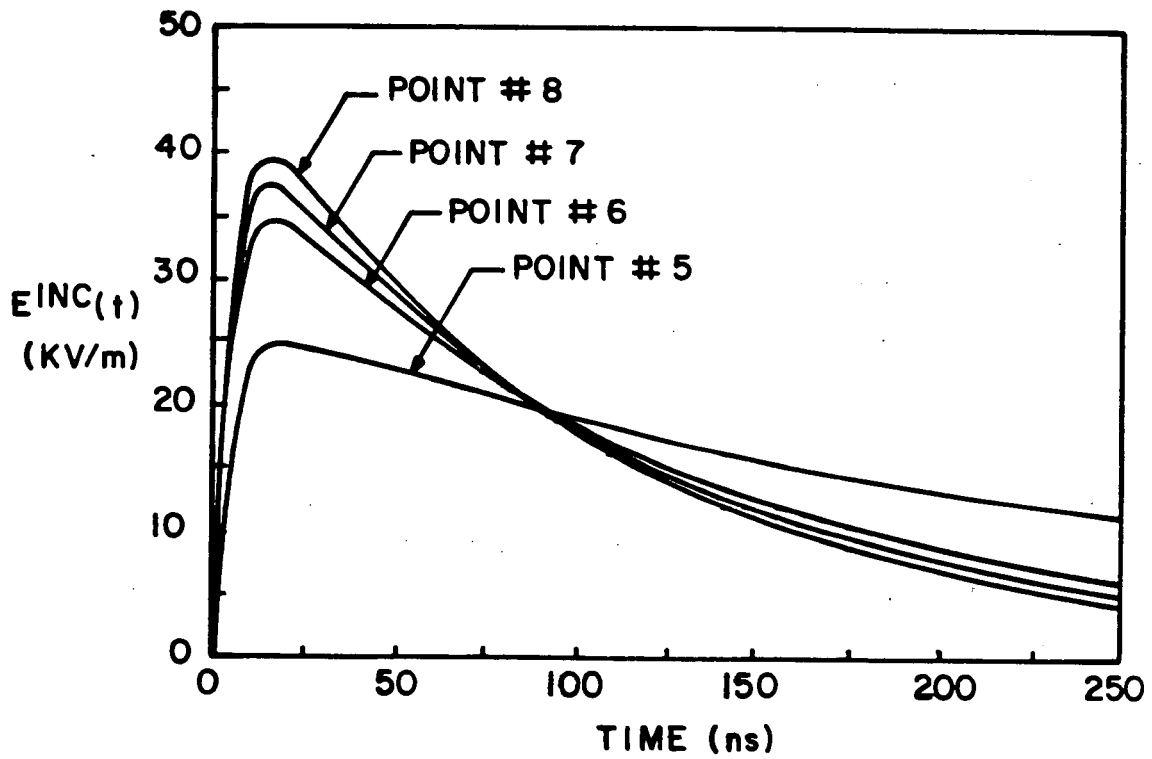
Fig. B19b. Incident HEMP field at observation Points #5-8.

A. Point #1 Responses

For the observation point directly under the burst point, the incident field on the line is horizontally polarized and arrives with an angle $\psi=90°$ and any possible value of ϕ. For this point, the maximum induced response is for the case of $\psi=\phi=90°$, and these values are used in the parametric studies presented in Fig. B20.

In this figure, the open-circuit voltage response for two different line heights of 20 and 10 meters, and for ground conductivities of 0.1, 0.01, and 0.001 mhos/meter are presented.

The effects of the earth conductivity are seen to occur principally for late times in the response. For times earlier than t=2h/c, where c is the speed of light, there is absolutely no effect on the response by the earth's conductivity. This is because the reflected field has not yet had time to effect the line response; only the incident field excites the line in this time. For the angles of incidence used for this observation point, this time occurs at 0.133 and 0.066 for the conductor heights of 20 and 10 meters respectively. This time is clearly noted in Fig. B20.

B. Point #2 Responses

The second observation point lies directly south of the burst point and is in a region of maximum electric field intensity. The field is also horizontally polarized at this point.

As may be noted from Fig. B18, the point of maximum field intensity occurs at a radial distance of about twice the burst height. Assuming a locally flat earth, elementary geometrical relationships indicate that the incident field has an incidence angle of $\psi=26°$. As in the previous case, the line being excited by the incident field can be positioned on an arbitrary angle ϕ, with the maximum response occurring when $\phi=\psi$.
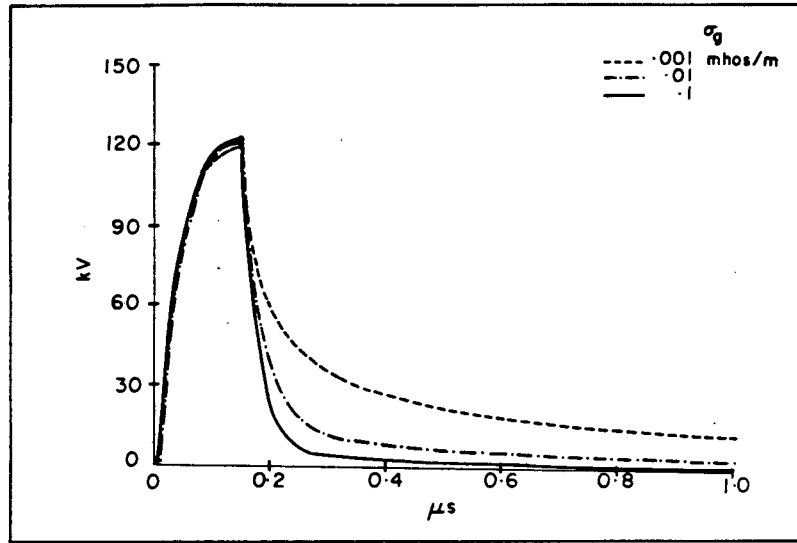
a) Line height = 20 m
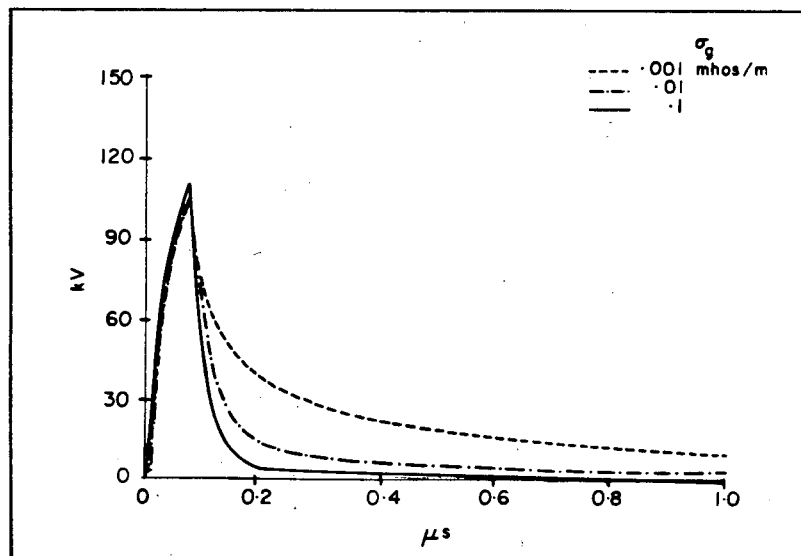
b) Line height = 10 m

Fig. B20. Plots of V_{OC} vs. time at location #1 for two line heights and different ground conductivities.

The calculated open-circuit voltages for the line at this point are presented in Fig. B21, for two line heights and three conductivities. As in the previous case, the peak open-circuit voltage occurs for the largest line height, and the effects of a decreasing conductivity are seen in an increasing late-time response.

C. Point #3 Responses

The calculated open-circuit voltages for a line at Point #3 near the horizontal tangent point of the HEMP on the earth's surface are shown in Figures B22 and B23 for the conductor heights and three ground conductivities. The incident field at this point contains both horizontal and vertical polarization components.

The assumed angle of incidence ψ has been taken to be $10°$, and in each of these figures a parametric variation of the response with the angle ϕ is presented. As may be noted from the form of the solutions for both vertically and horizontally polarized fields in Section 3.2, the vertical response is a symmetric function of the angle ϕ about zero, whereas the horizontally polarized response is an anti-symmetric function. Thus, the composite response of the line to the incident field at Point #3 exhibits no symmetry about the $\phi=0°$ value.

As in the previous cases, the maximum response occurs for the larger line height and for the lowest ground conductivity. Peak open-circuit voltages of 2500 kV are noted for the $\phi=0$ case. In addition, for negative values of the angle ϕ, the waveform is bipolar.

Previous studies of line responses have indicated that for a vertically polarized field, the maximum coupling to the line occurs when the elevation angle becomes small and $\phi=0$, resulting in a marked increase in the line response. For horizontal polarization, this enhancement does not occur. Because the HEMP field at Point #3 has both vertical and horizontal polarization components, it was decided to investigate the effects of changing the angles of incidence. In doing
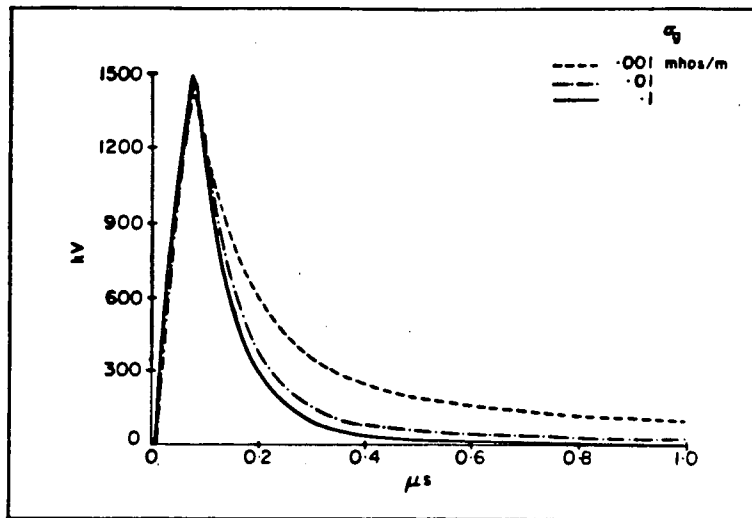
a)
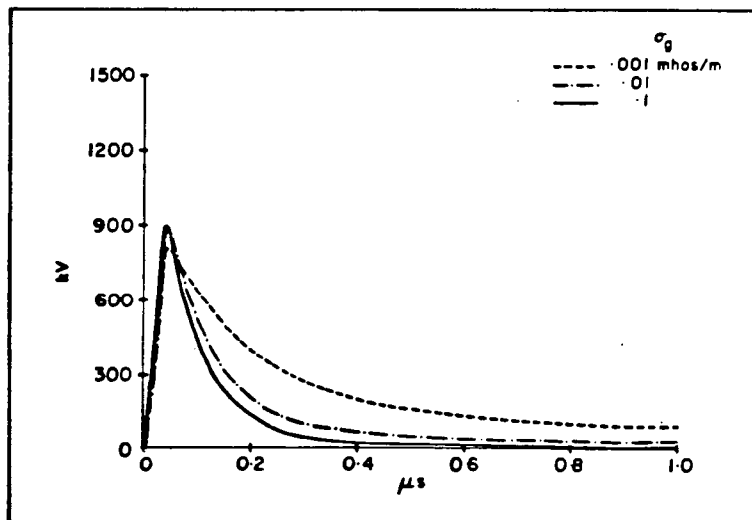
b)

Fig. B21. Plots of V_{oc} vs. time at location #2 for two line heights and three ground conductivities. $\psi=\phi=26°$.
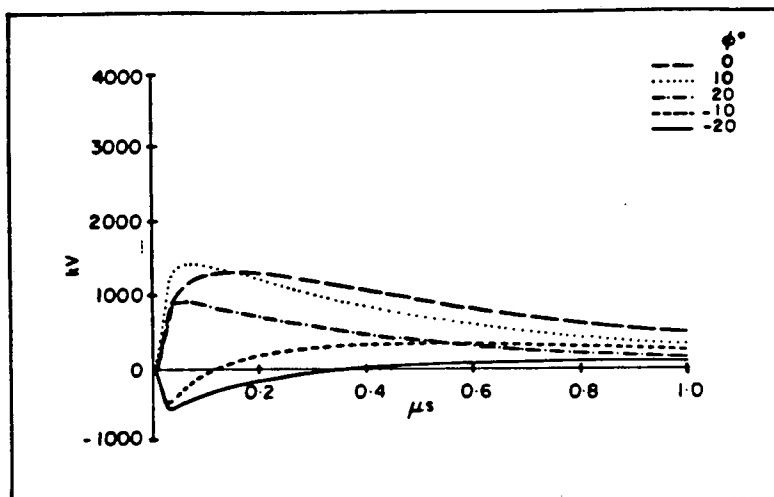
a) σ_g = .1 mhos/m
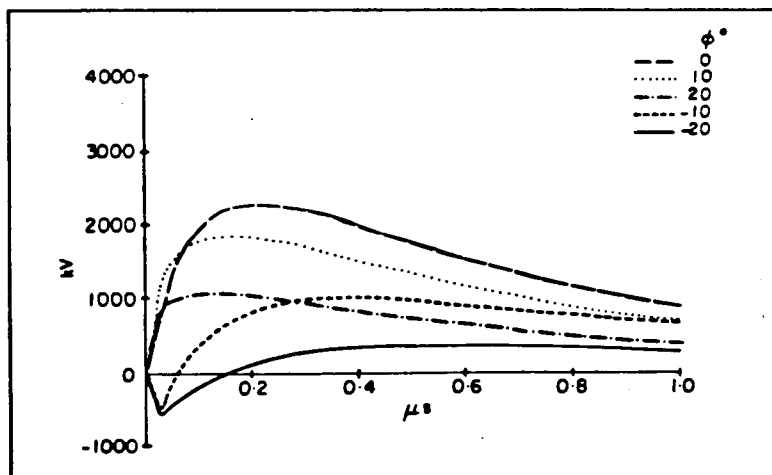
b) σ_g = .01 mhos/m

Fig. B22. Plots of V_{oc} vs. time at location #3 for ground conductivities and line orientation angle, ϕ. Elevation angle ψ=10°, h=20m.
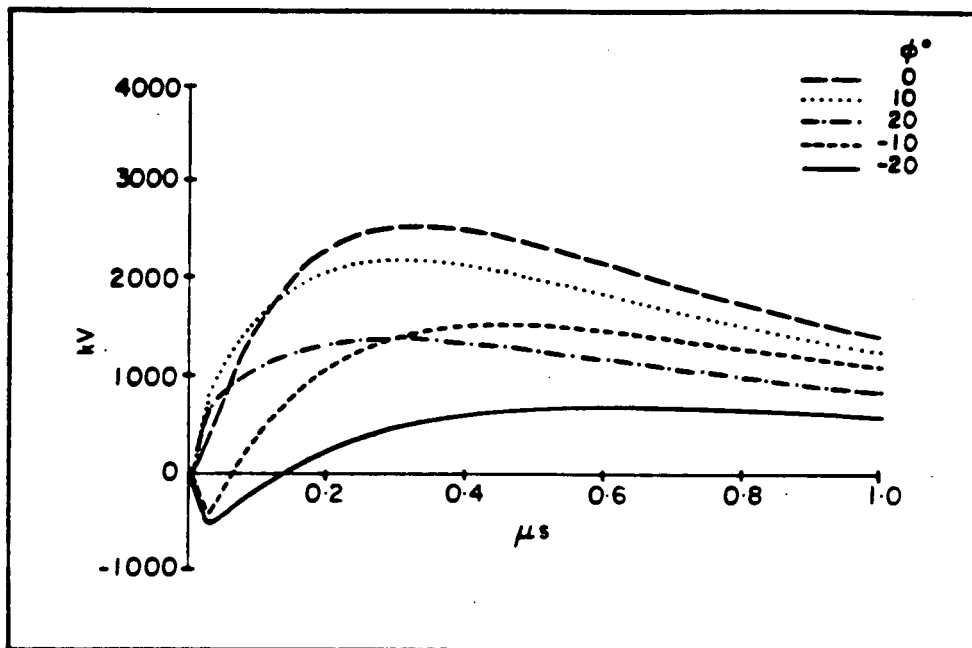
c) $\sigma_g = .001$ mhos/m

Fig. B22. (Continued)
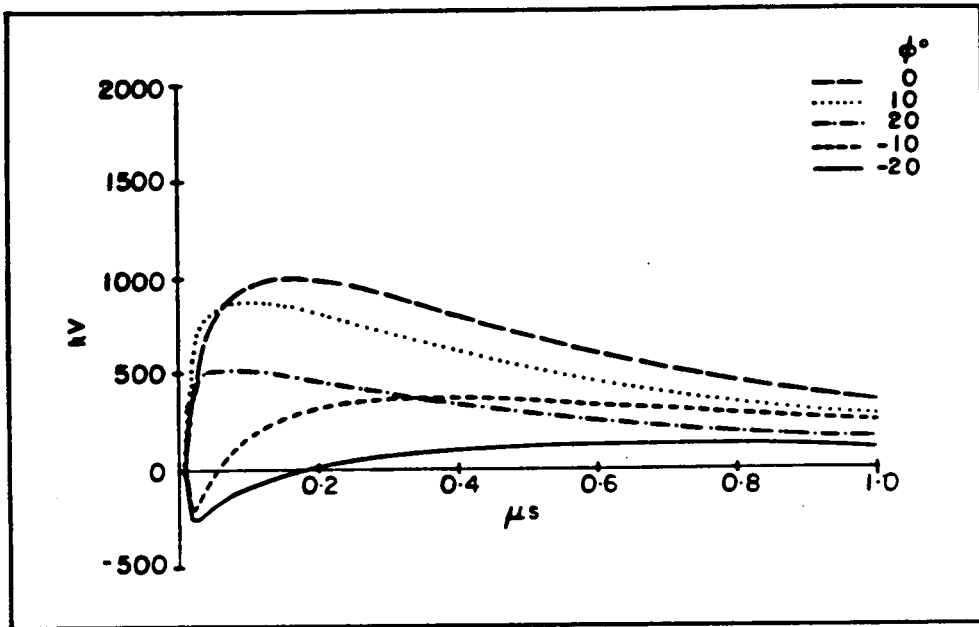
a) σ_g = .1 mhos/m
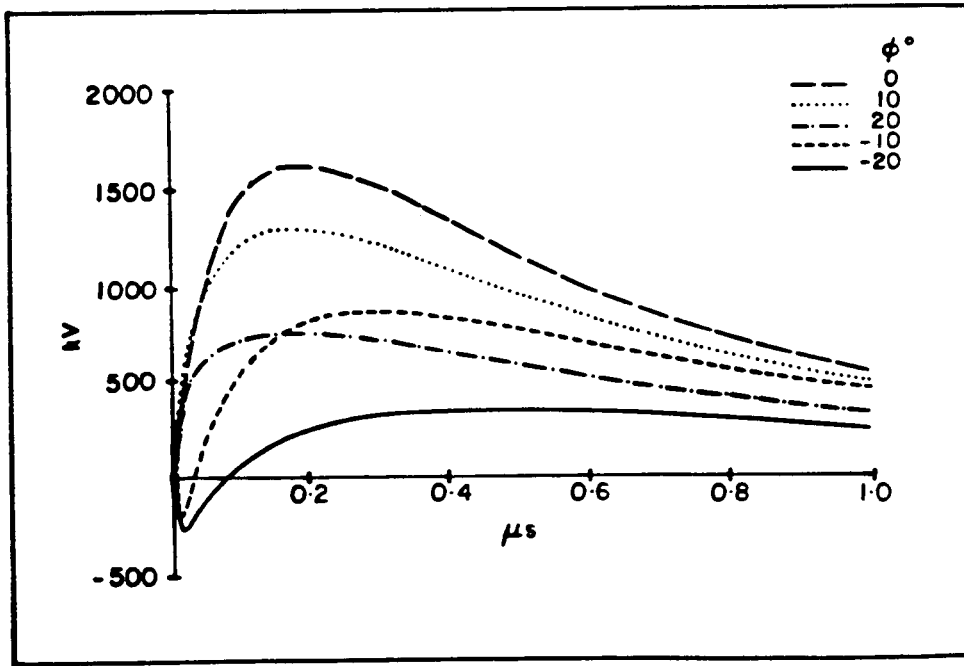
b) σ_g = .01 mhos/m

Fig. B23. Plots of V_{oc} vs. time at location #3 for three ground conductivities and line orientation angle, ϕ. $\psi=10°$, h=10m.
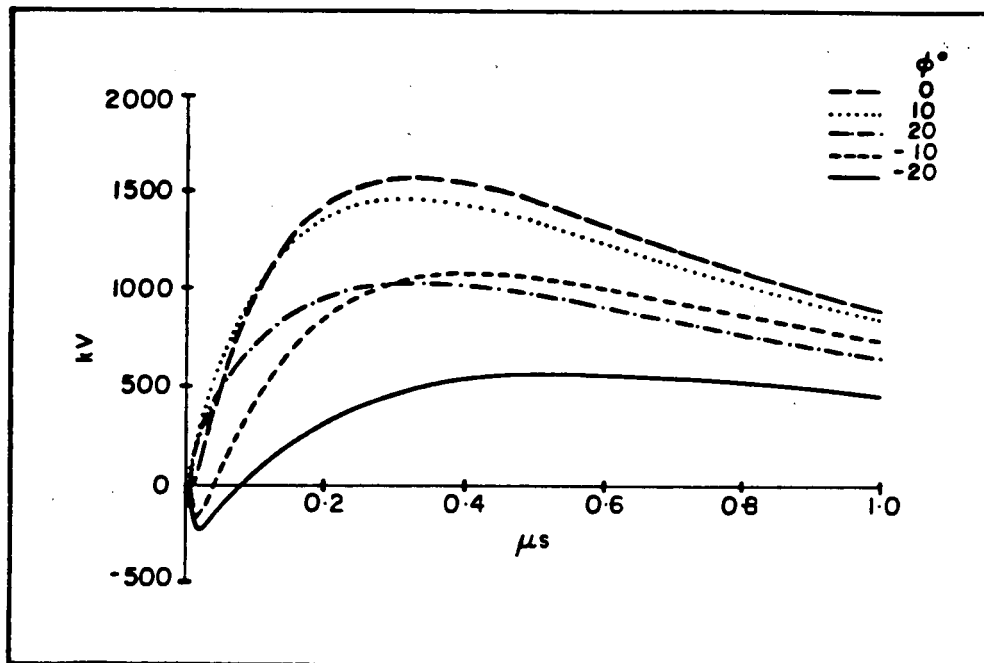
c) σ_g = .001 mhos/m

Fig. B23.   (Continued)

this, it was found that the maximum open circuit voltage on the line at this point did not occur at $\psi=10°$, but at other angles which depend on the conductivity and line height.

Figure B24 presents the early-time responses providing the maximum values of the line open-circuit voltage. These curves have been obtained by sweeping through the angles ψ and ϕ in steps of 1 degree and selecting those angles providing the maximum response. It should be noted that the responses here are substantially larger than those obtained with $\psi=10°$. However, these responses are still considerably lower than those expected if the worst-case excitation involving a vertically polarized Bell Laboratory were to be used. It is interesting to note a trend that as the conductivity becomes smaller, the angle ψ providing the maximum response tends to increase. Also, the value of $\phi=0°$ provides the maximum response.

Response at Point #3 for A HEMP Excitation That
Includes An Intermediate Time Component

Recently, there has been some discussion as to the possibility of an intermediate time "tail" occurring on the HEMP waveform. Thus, instead of the incident HEMP appearing as a simple double exponential there could be an additional component which persists much later in time. Figure B26 shows a version of such a hypothetical waveform. The early-time portion of this waveform is identical to that used previously for Point #3, and an exponential tail having an amplitude of 100 v/m and a fall time of 1 ms. As given in Equation (13) is appended for the late-time excitation. Note that because of the rather extreme ranges of both the time duration and the field amplitude, the data are plotted on a log-log scale.

For the case of a transmission line located 20 m above the ground at Point #3, three separate cases have been considered, each corresponding to one of the three values of earth conductivity. For each case, the open-circuit voltage response for the line excited by the unmodified HEMP waveform as well as by the waveform with the late-time tail has been calculated, and these data are presented in Fig. B27.
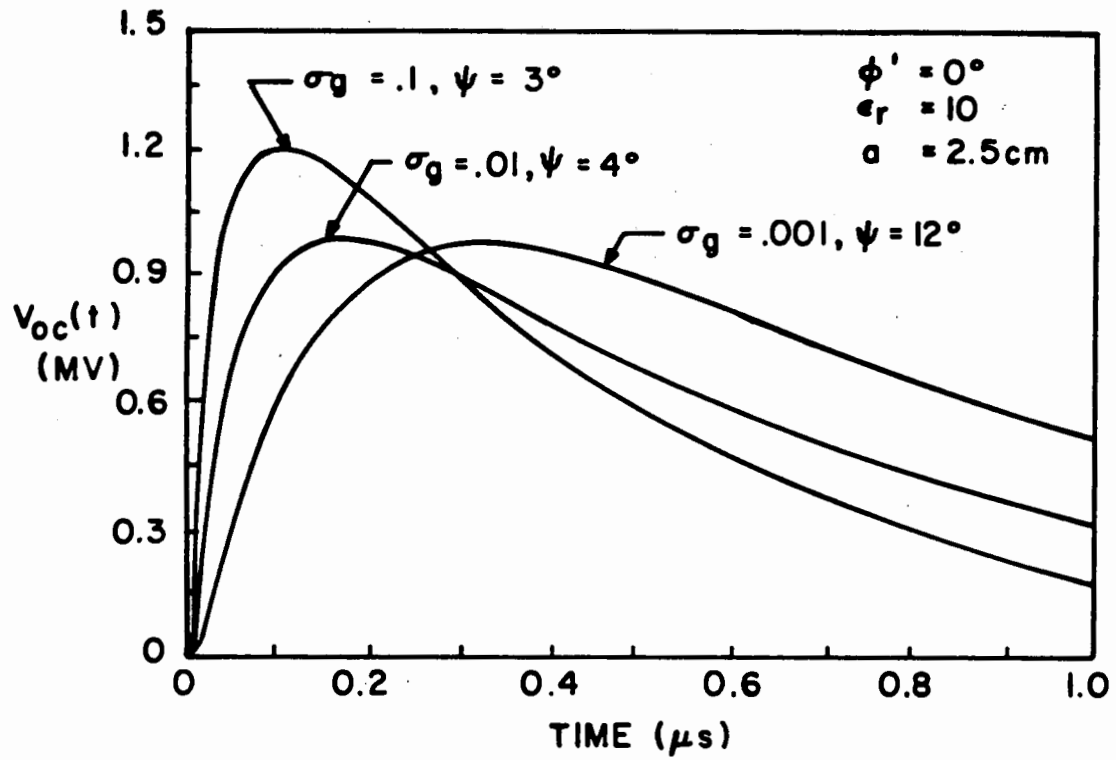
a) h = 5 m

Fig. B24. Plots of early time $V_{oc}(t)\big|_{max}$ for line at Point #3 for h=5, 10, 20 m, and σ= .1, .01, and .001 mhos/m ϕ=0, ϕ=variable.
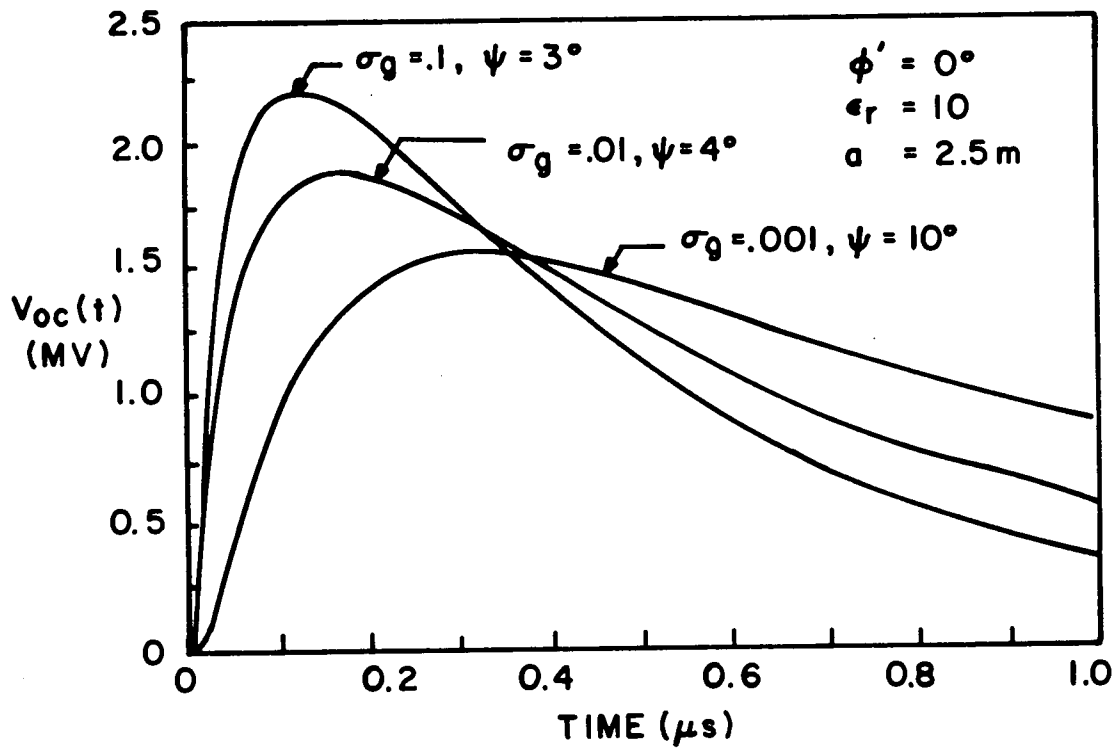
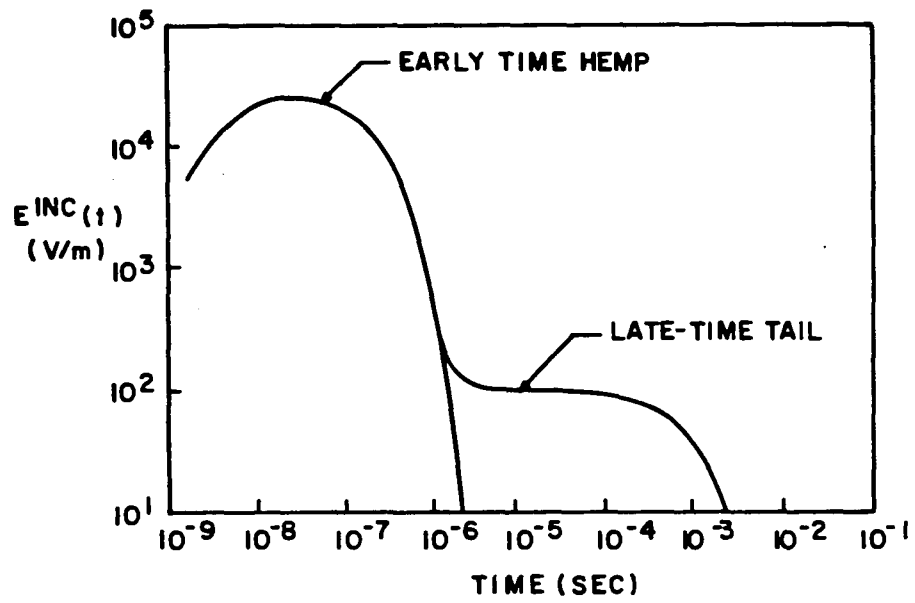b) h = 10 m

Fig. B24. (Continued)
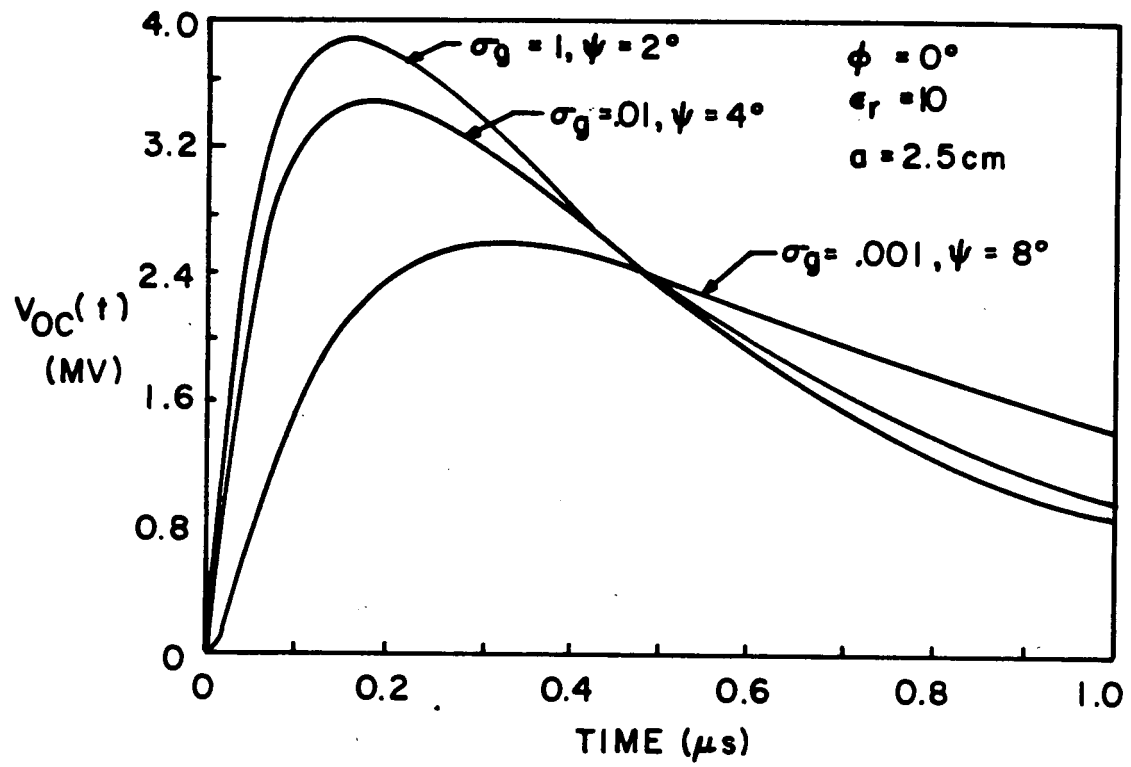
c) h = 20 m

Fig. B24. (Continued)

Fig. B25. Assumed HEMP incident field (with and without a late time tail at Point #3.
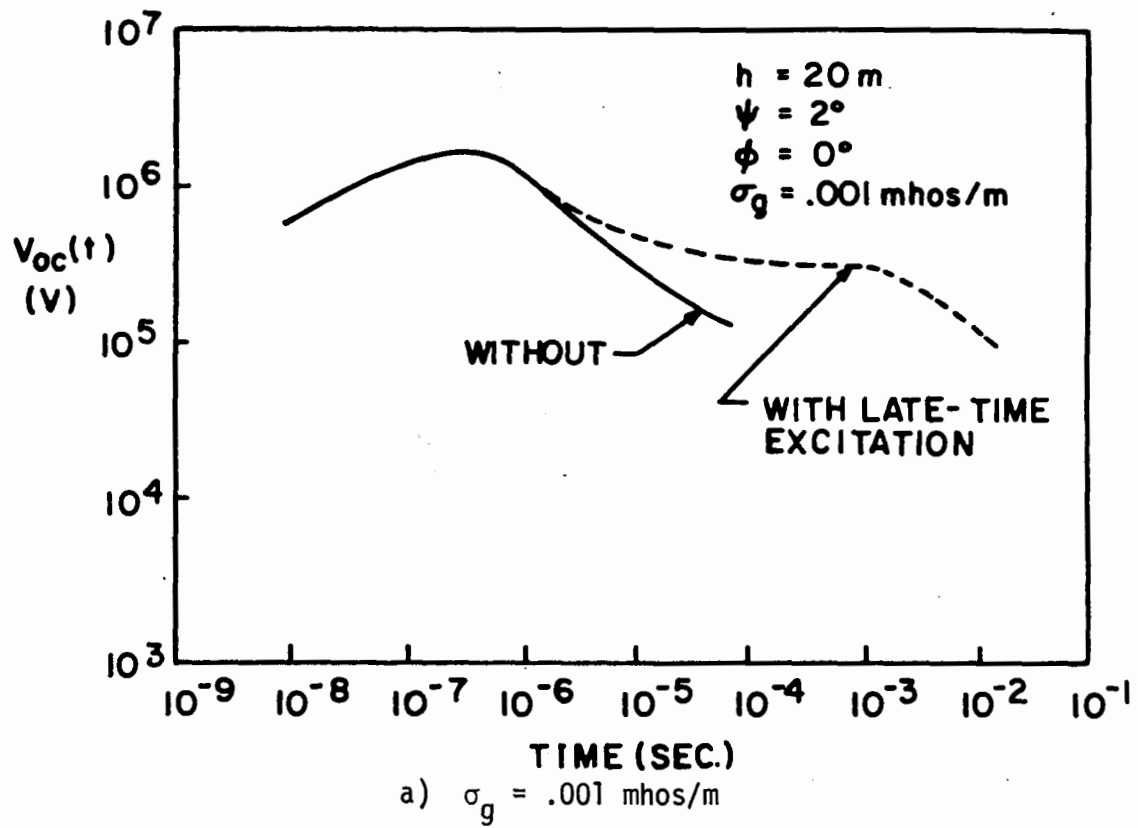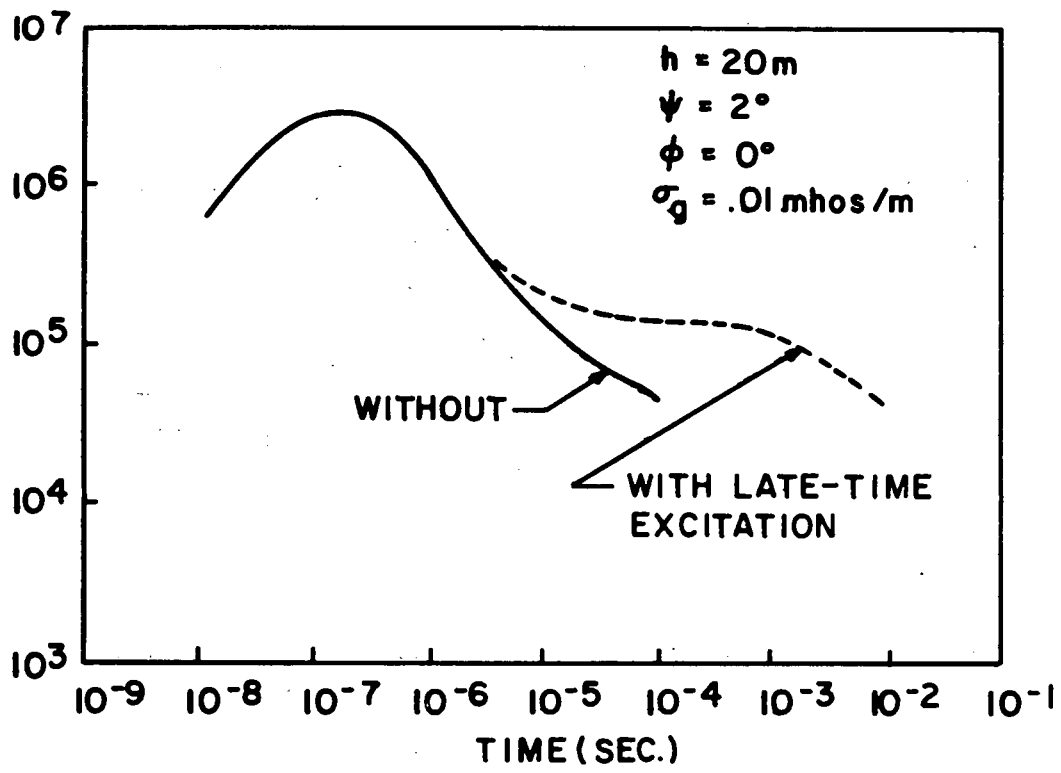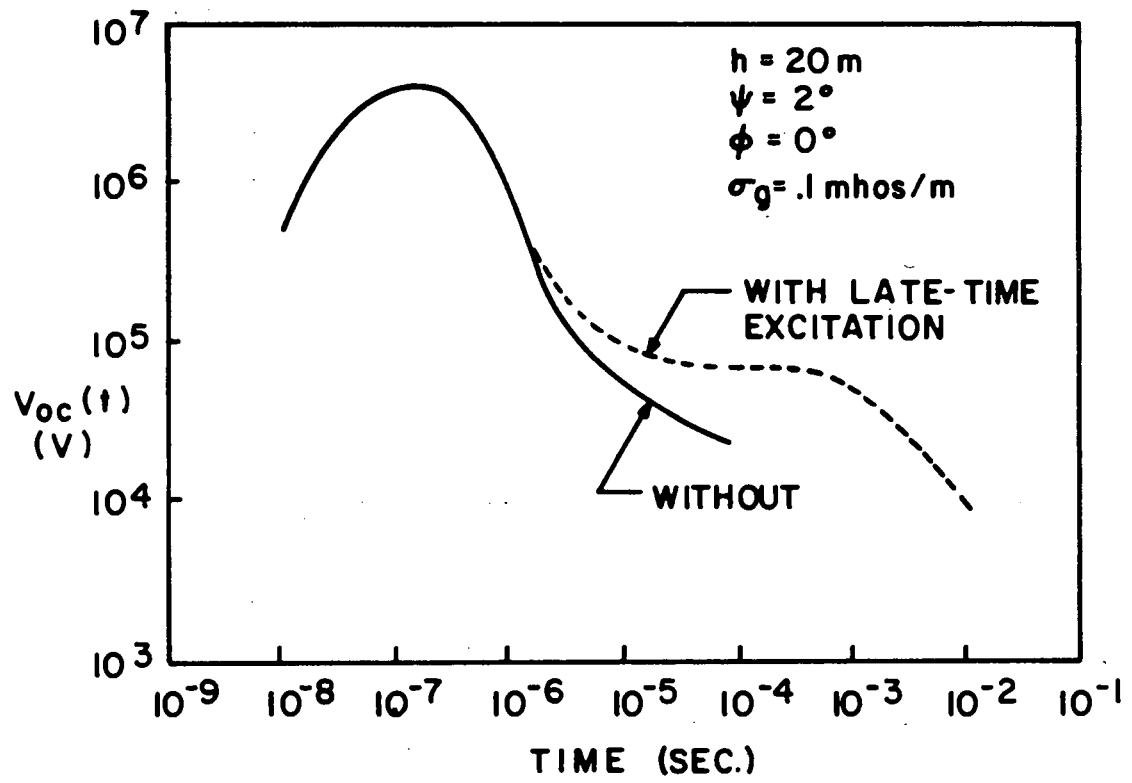
a) σ_g = .001 mhos/m

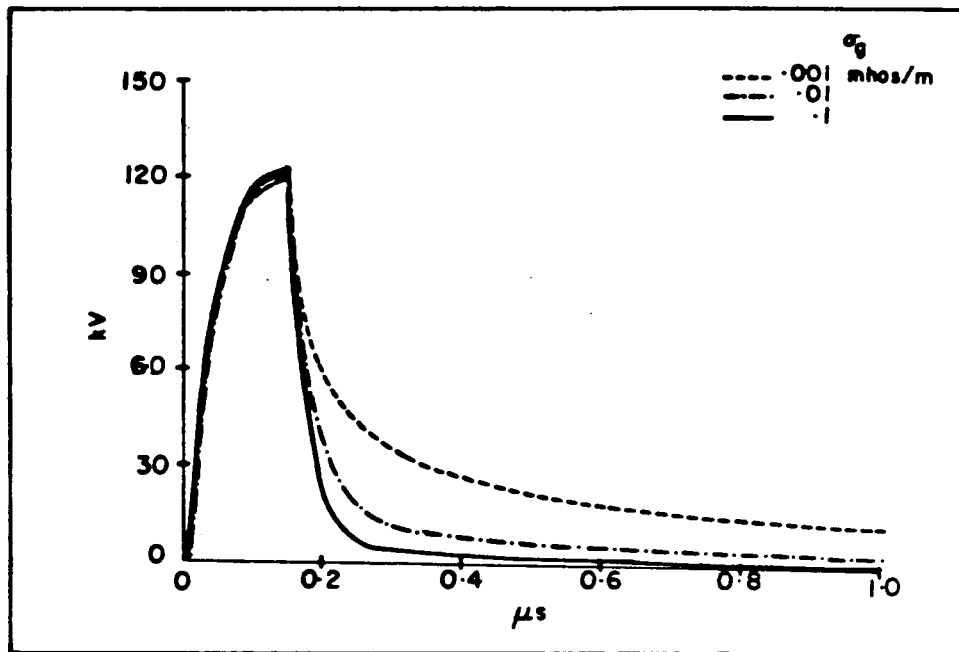Fig. B26. Open circuit voltages for a semi-infinite line excited by an HEMP at Point #3.
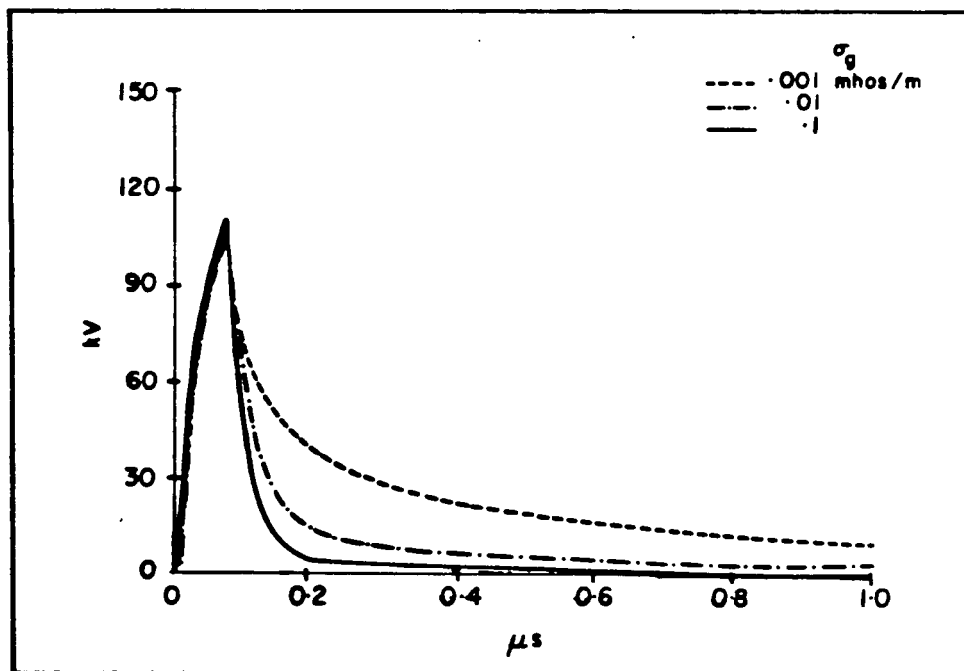
b) σ_g = .01 mhos/m

Fig. B26. (Continued)

c) $\sigma_g = 0.1$ mhos/m

Fig. B26. (Continued)

a) Line height = 20m

b) Line height = 10m

Fig. B27. Plots of V_{oc} vs. time at location #4 for two heights and three ground conductivities.

As expected, the early-time peak in the open circuit voltages is not at all affected by the presence of the late-time tail on the incident field. However, the late time response is considerably modified, retaining its value for several milliseconds. Although the amplitude of this late-time portion of the response is low compared with the peak response (approximately 1 to 2 orders of magnitude lower), there may be a significant amount of energy delivered to a load, due to the long time that this response exists.

D. Point #4 Responses

Point #4 southeast of the burst point with an elevation angle of $\psi=80°$. At this location, the incident field is entirely vertically polarized. Using the same functional form for the waveform as used for Point #1, the resulting open-circuit voltage for this point is shown in Fig. B27. The amplitudes for this location are substantially lower than those for the line on the horizon.

E. Responses for Points #5 Through #8

In order to obtain more information about how the line response varies over the surface of the earth, Points #5 through #8 were defined at various distances to the south of Point #2. These points have incident fields that are entirely horizontally polarized.

Since the polarization of the incident field is entirely horizontal, the maximum of the response occurs when the angle ϕ is equal to ψ, and this case has been considered for the numerical studies for Points #5 through #8. Figures B28 through B31 present the calculated open-circuit voltage on the lines at these observation points for three conductor heights and for three ground conductivities. An important conclusion in examining these data is that the response of the line located at Point #3 is generally larger than those at locations #5 through #8, due to the fact that the vertically polarized component of the incident field tends to dominate the response there.
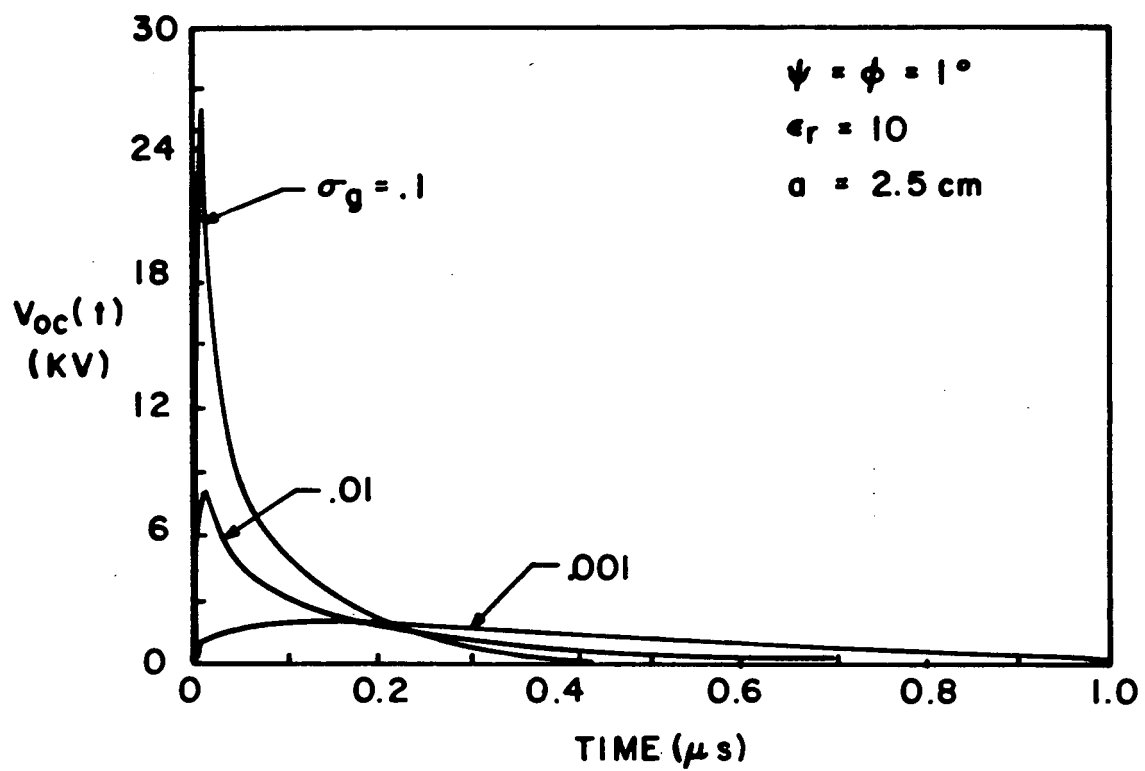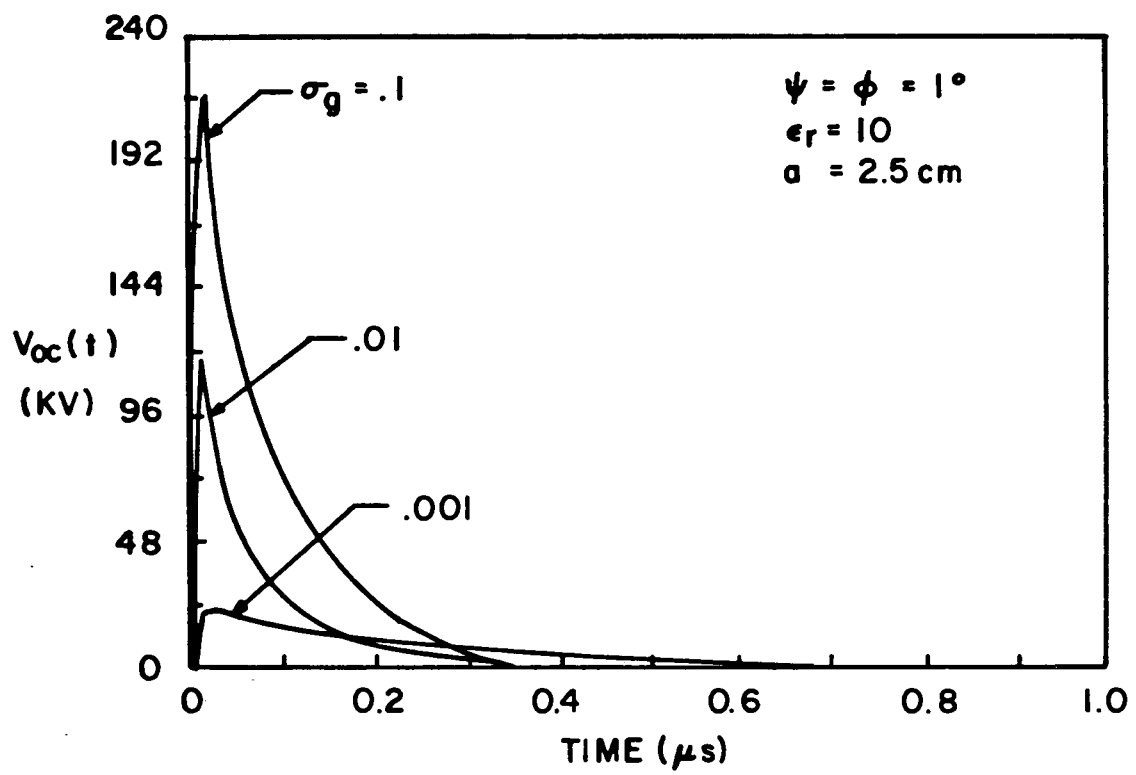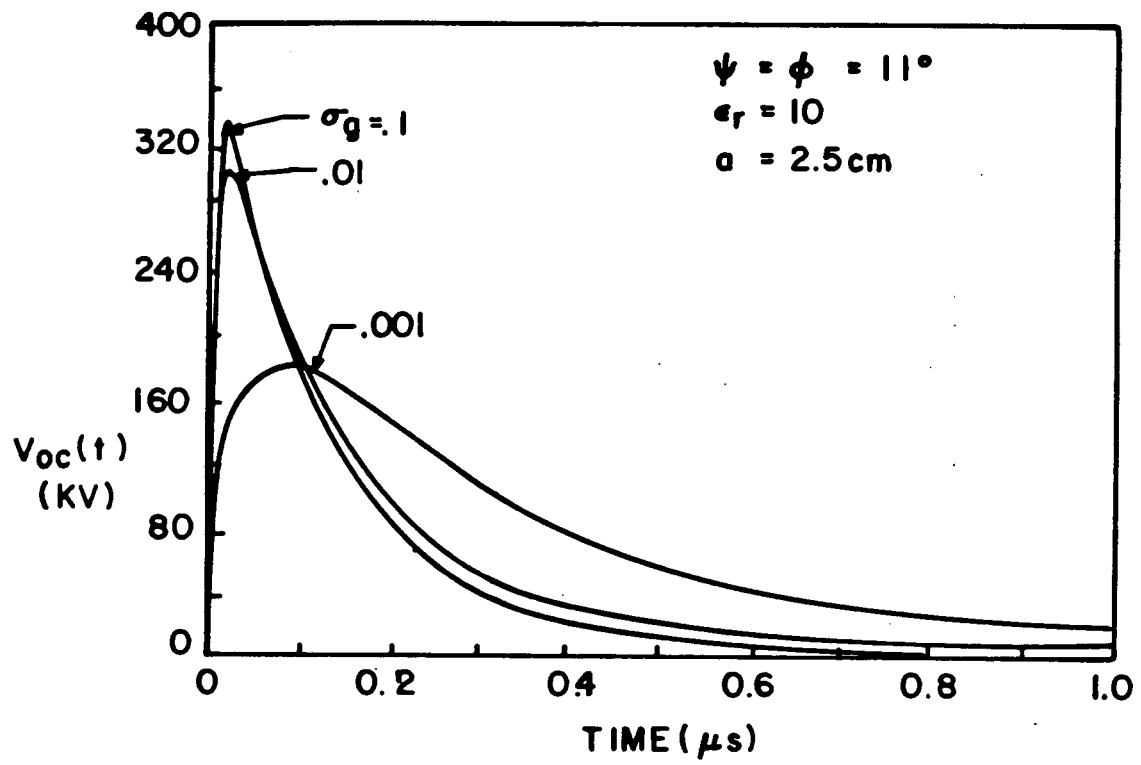
a) h = 5 m

Fig. B28. $V_{oc}(t)$ data for Point #5.
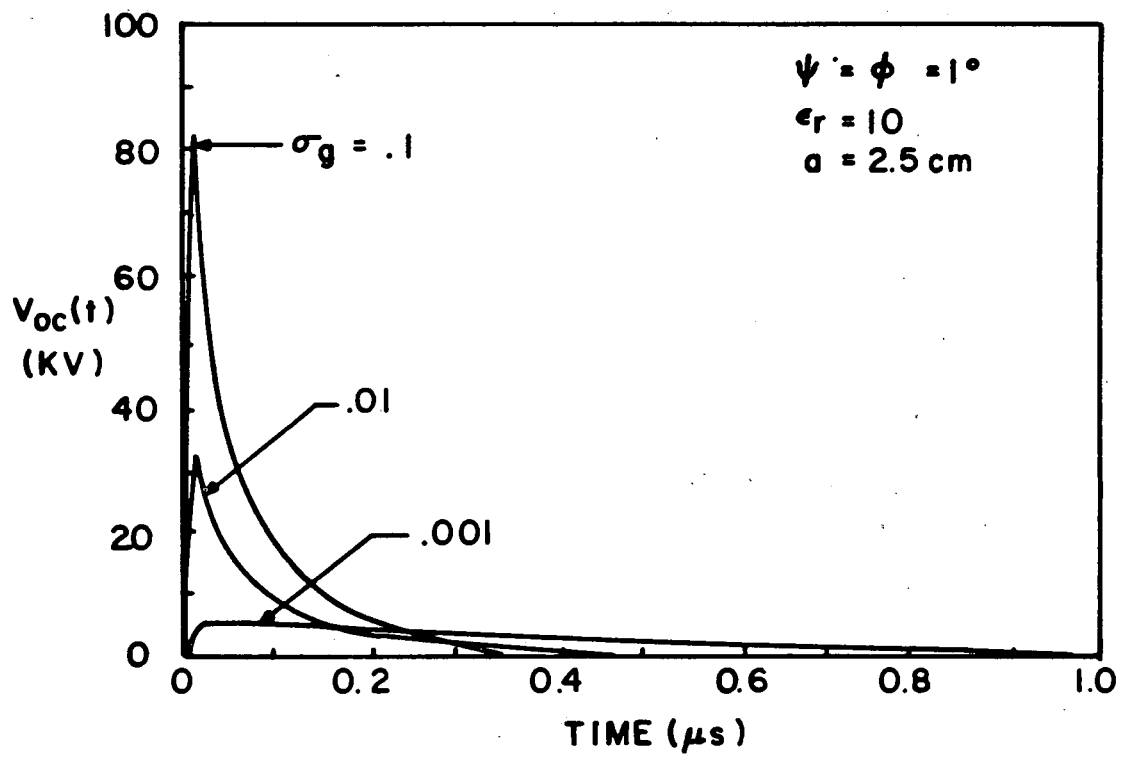
b)   h = 10 m

Fig. B28.   (Continued)

c) h = 20 m
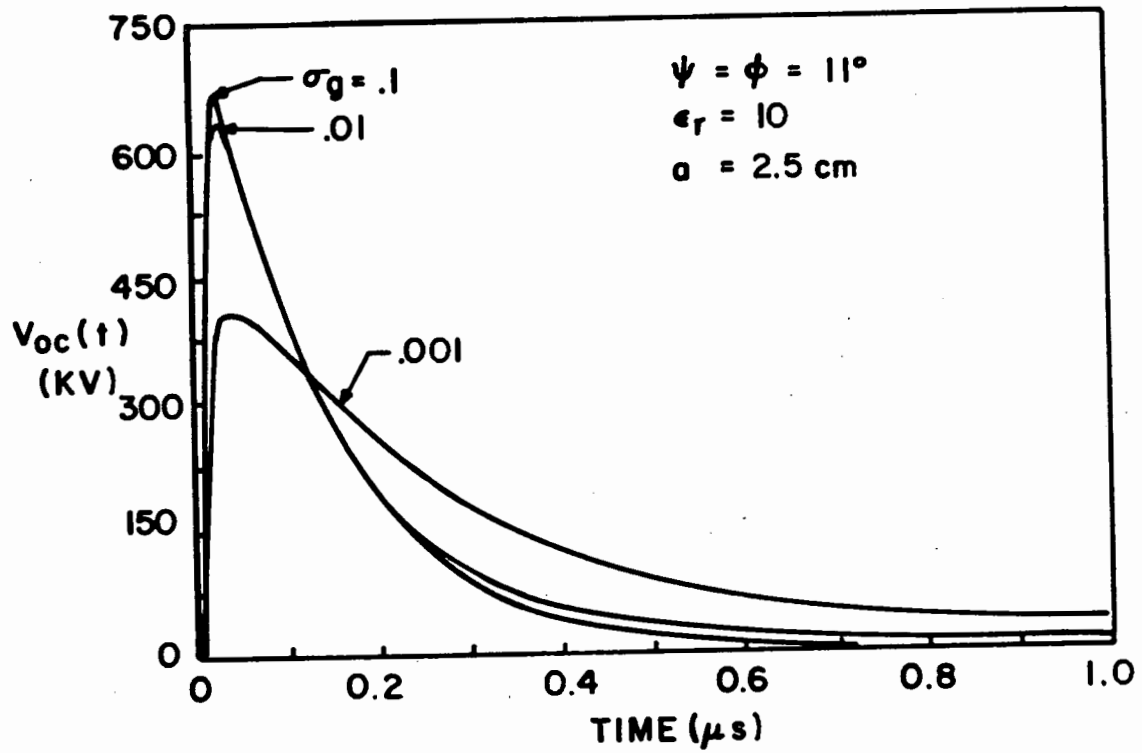
Fig. B28. (Continued)

a) h = 5 m

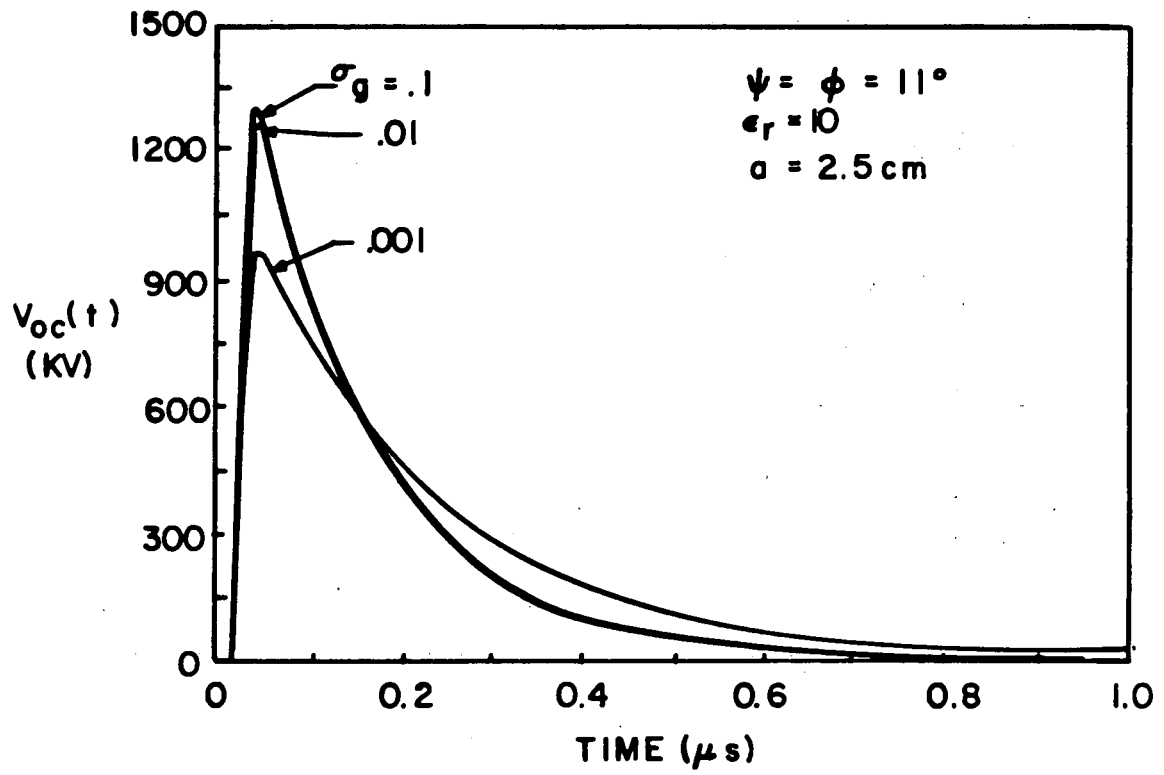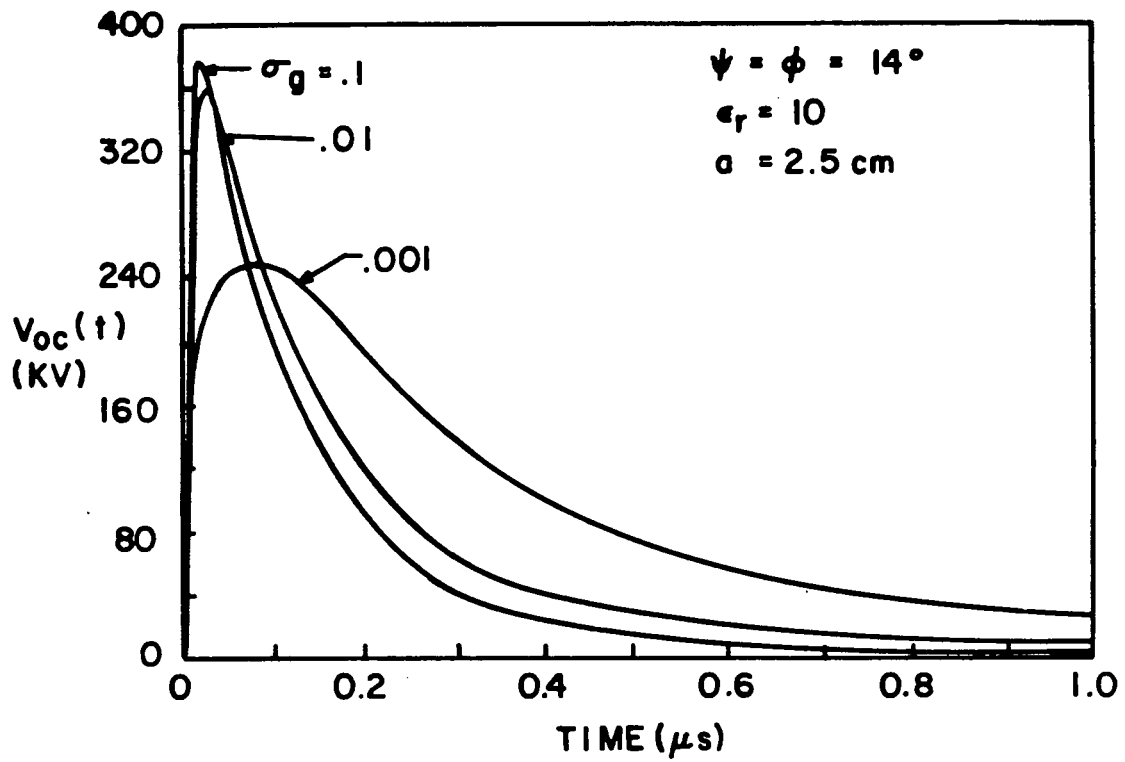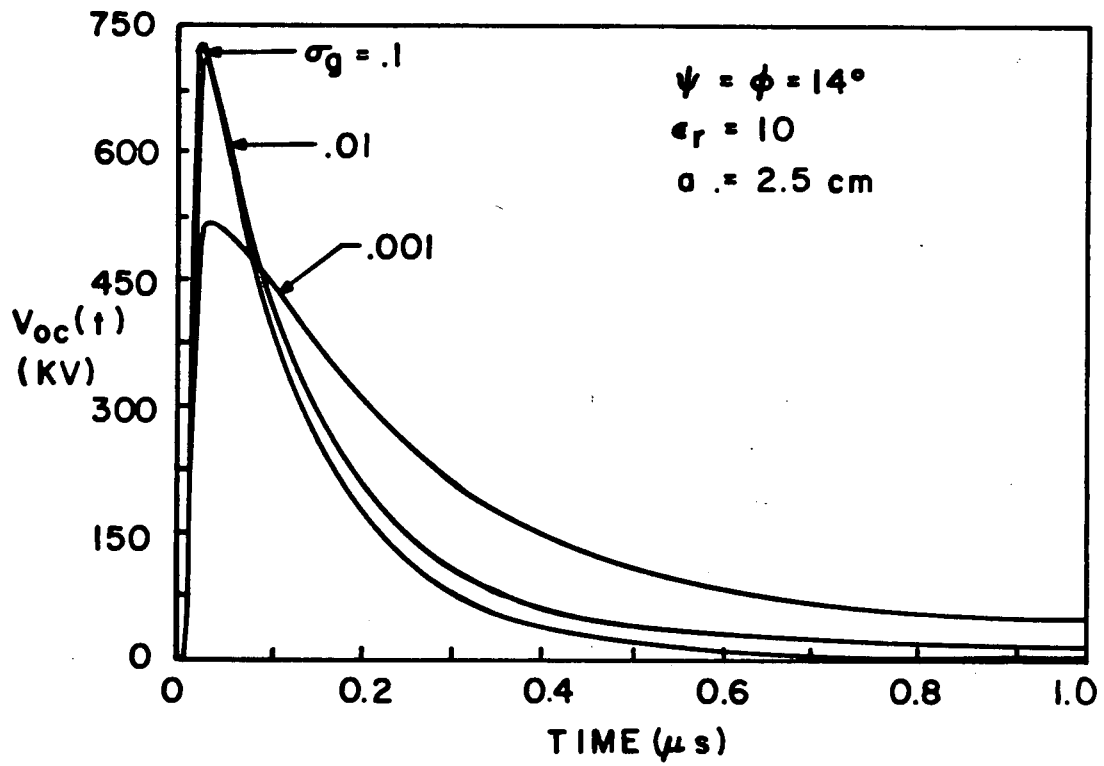Fig. B29. $V_{oc}(t)$ data for Point #6.

b) h = ·10 m

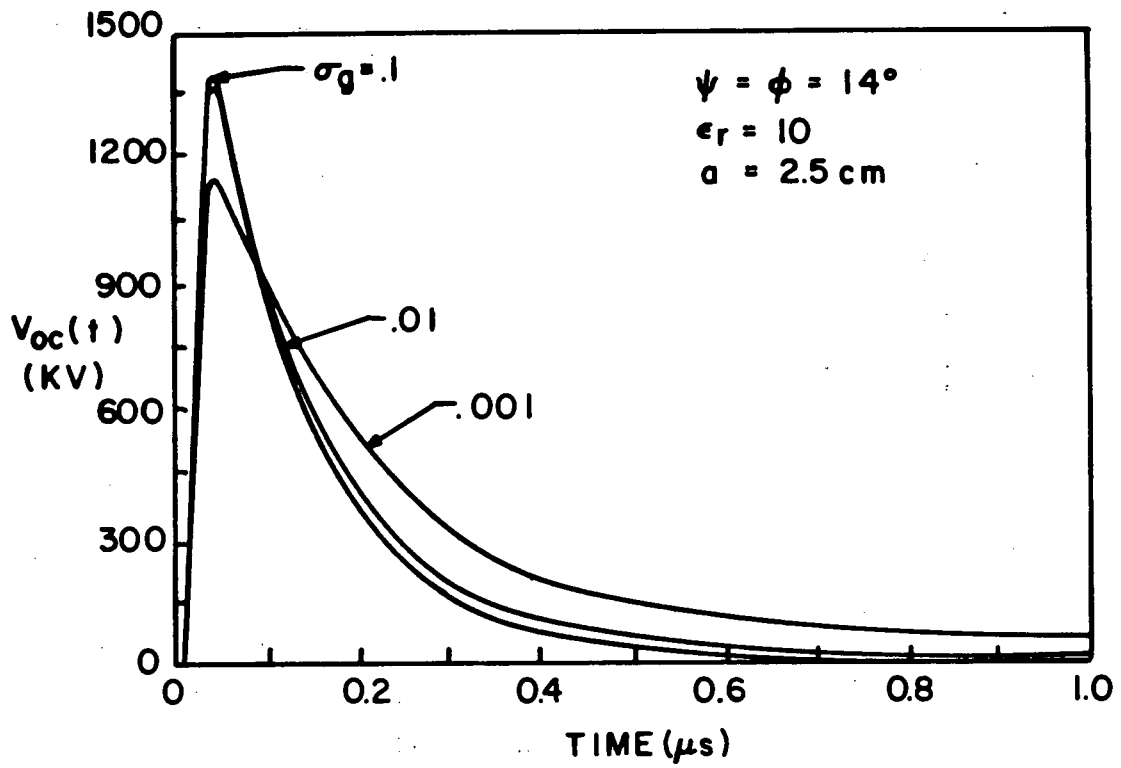Fig. B29. (Continued)

c) h = 20 m

Fig. B29. (Continued)
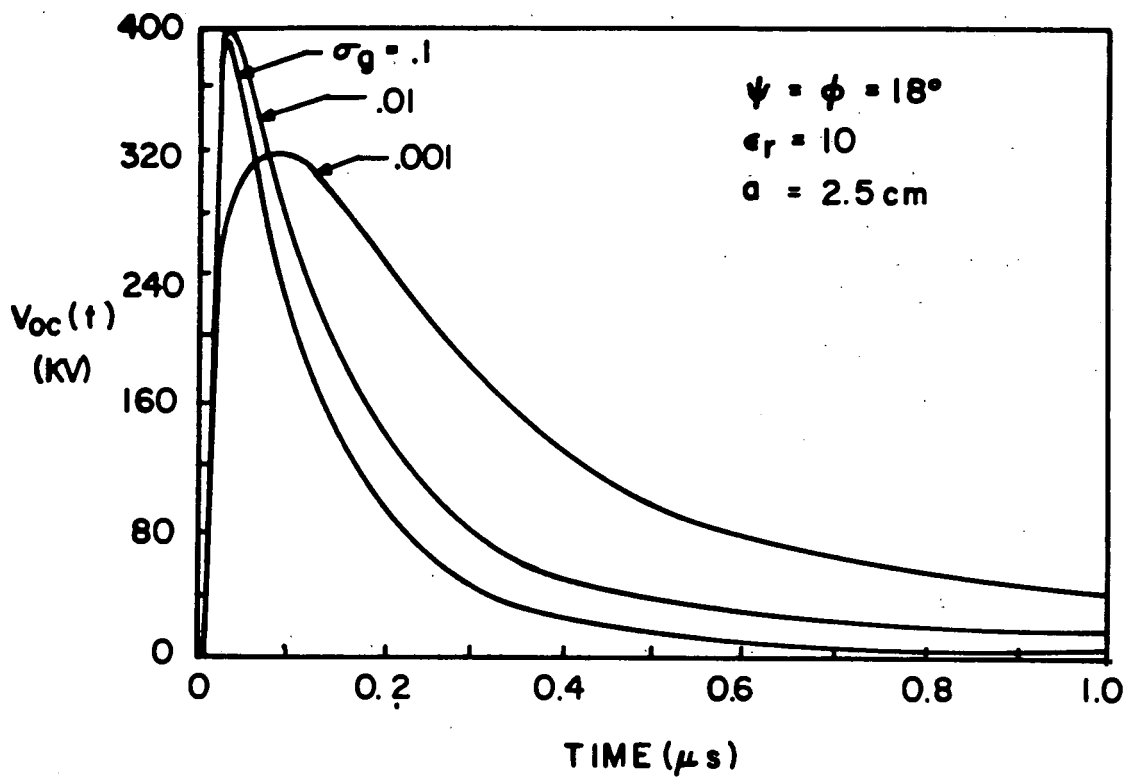
a) h = 5 m

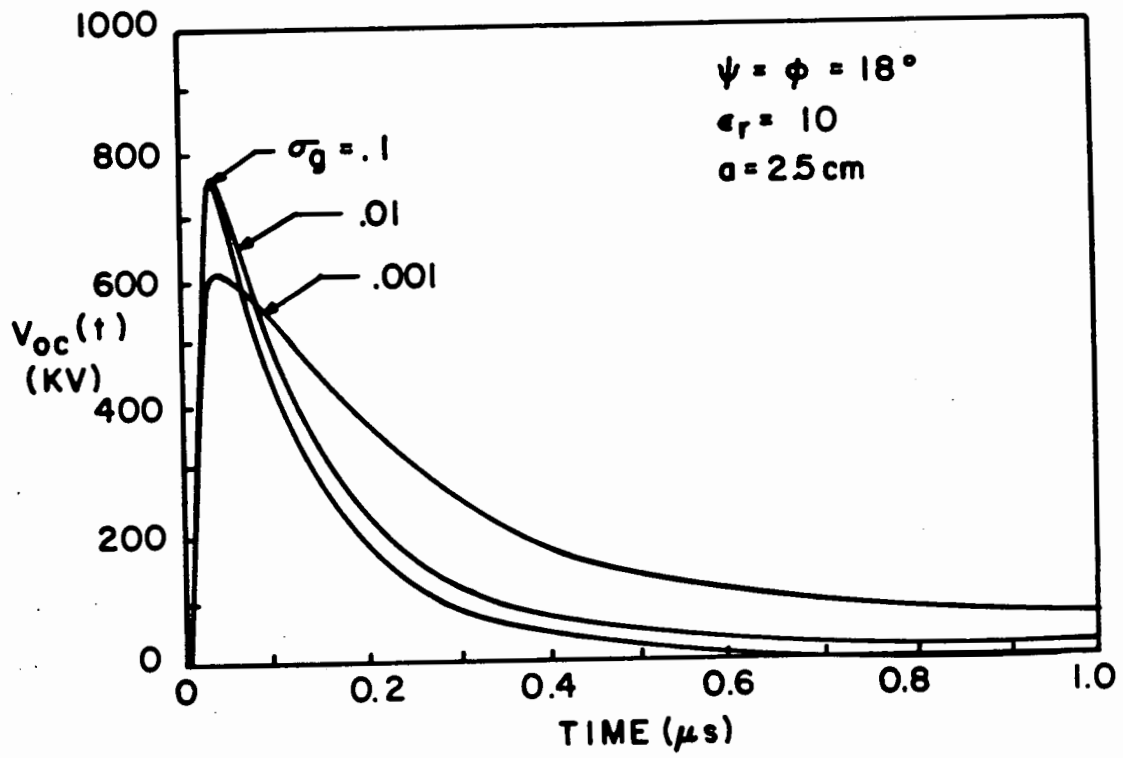Fig. B30. $V_{oc}(t)$ data for Point #7.

b) h = 10 m
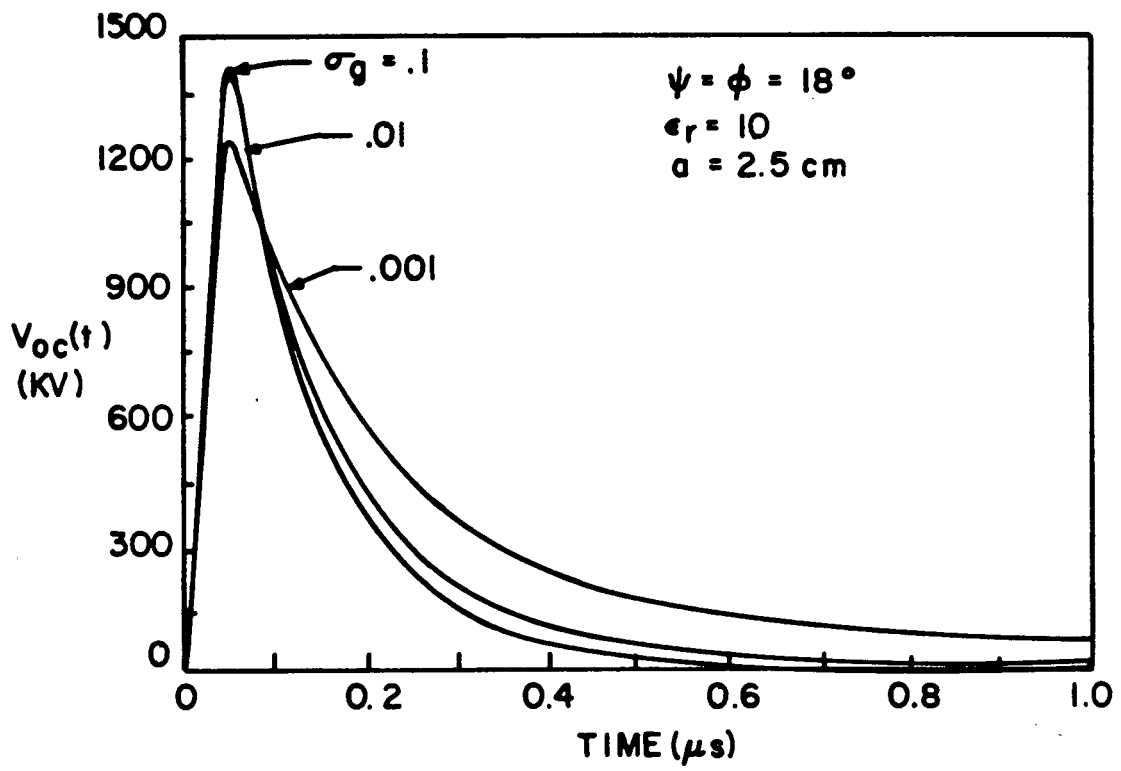
Fig. B30. (Continued)

c)   h. = 20 m

Fig. B30.   (Continued)

a)   h = 5 m

Fig. B31. $V_{oc}(t)$ data for Point #8.

b)   h = 10 m

Fig. B31.   (Continued)

c)   h = 20 m

Fig. B31. (Continued)

B.5 Non-Linear Response Solution In the
Time Domain

In order to illustrate the solution of a problem having a non-linear solution, a numerical solution for a short transmission line similar to the one shown in Fig. 37 was obtained for equations presented in Section 3.2.1.3. The non-linearity involved is that a tower is assumed to flashover instantaneously if the voltage at the tower reaches or exceeds the flashover voltage, V_{fo}.

The 10 meter high transmission line was 3 kilometers long and included 10 towers spaced at 300 meter intervals with a 300 meter distance to the closest tower at the observation point. The footing resistance of each tower was 10 ohms and a value of 400 ohms, the characteristic impedance of the line, was used for Z_L. A vertically polarized incident electric field wave having a waveform of $52,500(e^{-4.0x10^6 t} - e^{-4.76x10^8 t})$ was used.

The first numerical solution was obtained for an infinite tower flashover voltage. The results of the second solution, which was obtained for a tower flashover voltage, V_{FO}, of 1.3 MV, are shown in Fig. B32a. Since these results were identical to those of the first case, which had an infinite flashover voltage, no flashovers occurred. The reason for this is that at an arbitrary point on the line, the EMP-induced voltage consists of two parts: a positive and a negative propagating wave. Only at the open end do the two waves coincide and add to provide the peak observed voltage of 1.6 MV. Elsewhere, the voltage is roughly one-half of this value, and is not enough to trigger the tower flashover. If the transmission line was terminated in its characteristic impedance instead of an open-circuit, the voltage at the observation point would be one-half of the open circuit value (650 kV).

The negative portion of the wave in Fig. B32a is due to the lack of distributed excitation of the line for values of Z<0. From a calculation based on the geometry of the line, the incidence angle of the plane wave, and the propagation velocity of a traveling wave on the transmission line (assumed to be $300x10^6$ m/sec), a traveling wave initiated by the leading edge of the plane wave striking the line at the
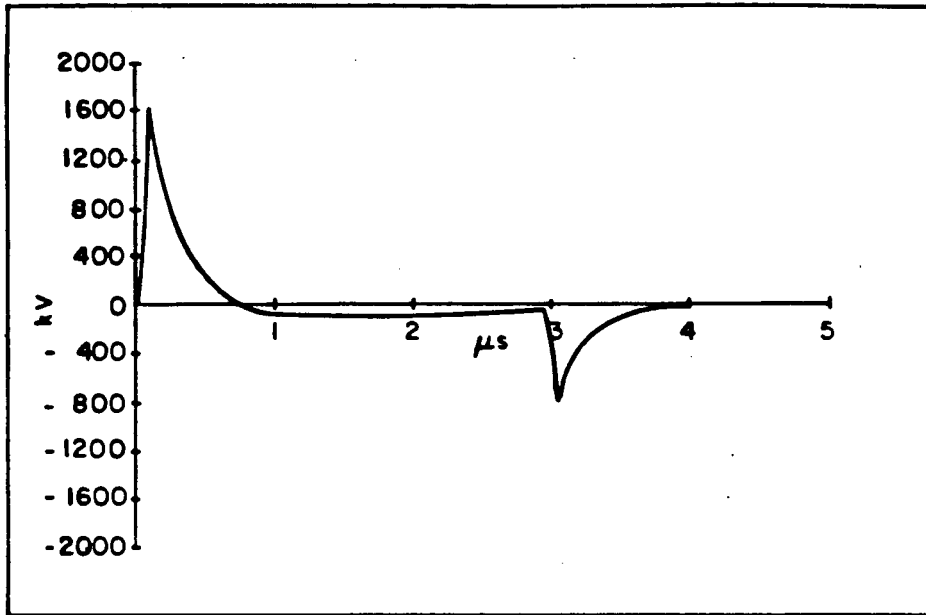
a) High flashover voltage (V_{fo}=1300 kV).
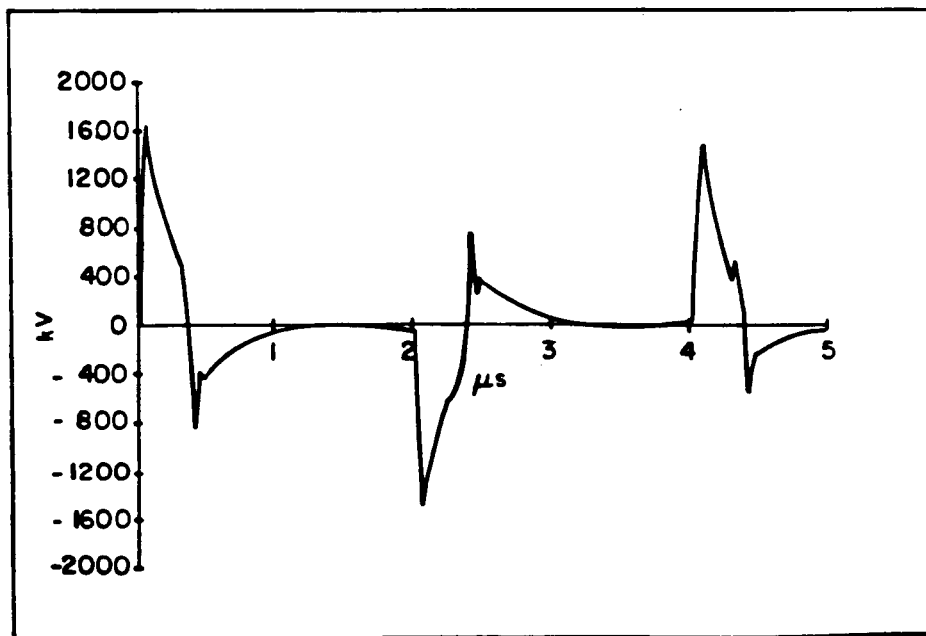
b) Low flashover voltage (V_{fo}=500 kV).

Fig. B32. Plot of HEMP-induced V_{oc} at the end of a matched 3 km line with 10 towers spaced 300 m. ψ=45°, ϕ=0°, h=10m, σ_g=0.01 Ω/m, σ_w=0.25 Ω/m.

point Z=0 will reach the observation point located at Z=3000 meters 3 microseconds after the leading edge of the plane wave strikes the line at the observation point. The negative response between 3 and 4 microseconds is due to the lack of excitation of the line for values of Z<0.

By reducing the assumed tower flashover voltage to 500 kV, a noticeable effect is observed, as seen in Fig. B32b. As noted from the figure, the initial peak in the observed voltage is the same, but there is an influence of the tower on the response occurring at about 0.5 μs which is in the form of a negative pulse. Later at around 2 μs there is a reflected pulse which has traveled one round trip (600 m) on the line.

Figure B33a presents the same data for a longer calculation time. It is instructive to compare this result with the result obtained for the same line shorted at opposite ends but neglecting all the towers, which is illustrated in Fig. B33b. The similarity between the two waveforms is striking. In Fig. B33a, the time scale is 0.1 that of the Fig. B33b, due to the fact that distance between the end of the line and the tower is 300 m as opposed to 3000m.

From the above examples, it is possible to draw a preliminary conclusion regarding the effects of tower flashover on power lines. It appears that the presence of a flashover on a line serves to effectively isolate the line into segments. Because the arc and tower impedance is generally much lower than the characteristic impedance of the line, the flashover at the time appears to be similar to a short circuit to the line. Thus, for an observer at a particular point in a general network where it can be safely assumed that tower arcing will occur, the HEMP response can be estimated by simply putting a short circuit at the closest towers or other flashover points, and treat the resulting coupling problem using linear analysis methods. The validity of this conclusion needs a bit more study before it is acceptable for use in a general power system assessment. For example, the tower flashover is not expected to occur instantaneously as was assumed here, but will occur only after the critical voltage is maintained for a period of time
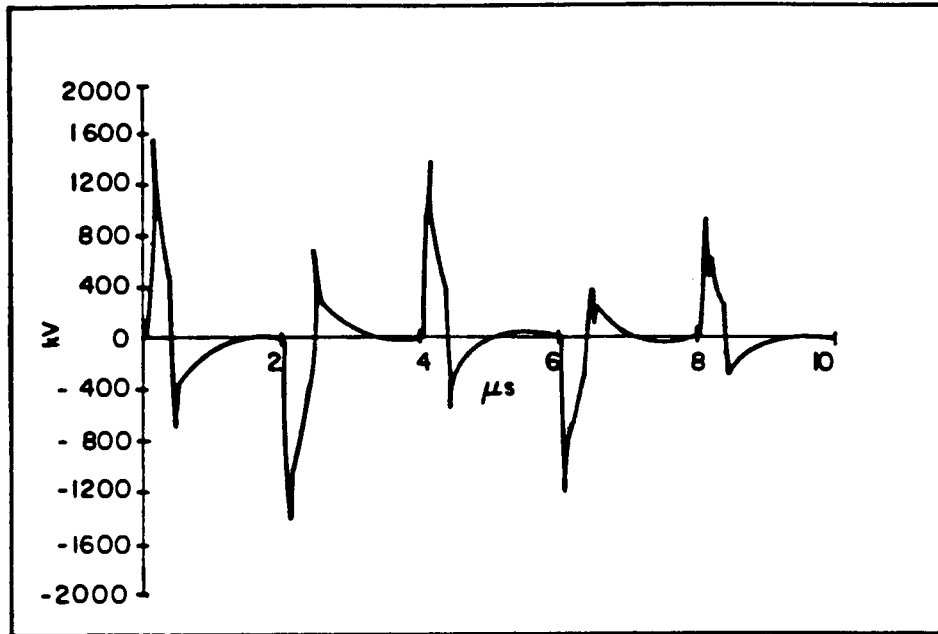
a) Towers spaced at 300m from each other, V_{fo}=500 kV.
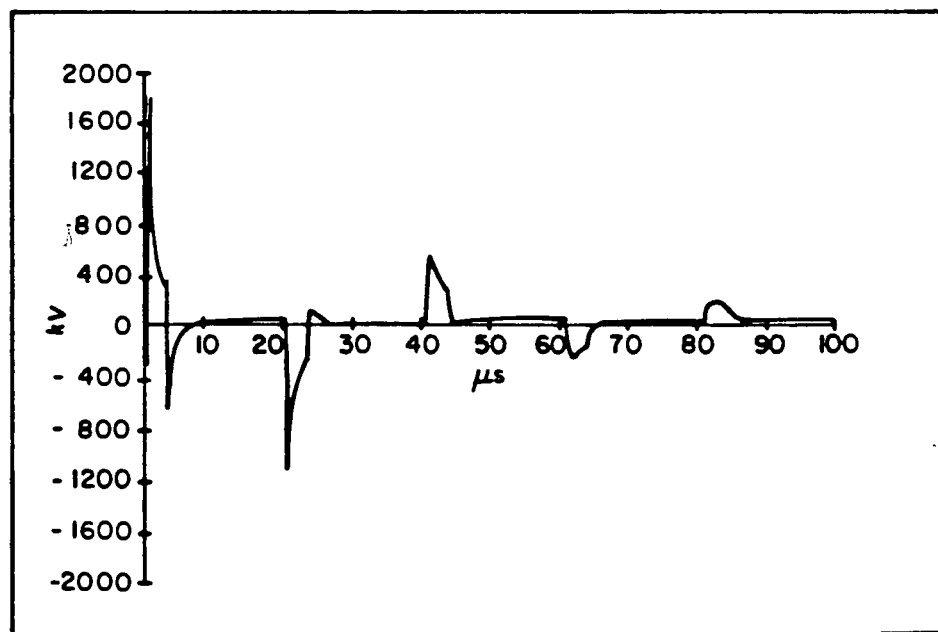
b) No towers represented.

Fig. 33. Plot of HEMP-induced open circuit voltage on a 3 km line 10m above, a .01 mhos/m ground. Z_L=0. ψ=45°, ϕ=0°.

across the arc points. In addition, the tower itself has a characteristic inductance which tends to limit the rise time of the flashover current. These effects deserve further consideration.

BIBLIOGRAPHY

B1. EMP ENGINEERING AND DESIGN PRINCIPLES, Bell Laboratories Publication, Whippany, NJ, 1975.

APPENDIX C

Response of Multiconductor Lines Above Ground

C.1 Introduction

In this appendix numerical solutions for selected multiconductor geometries and HEMP excitations are presented. Numerical results are presented in Section C.2 for frequency domain solutions, in Section C.3 for scattering (antenna) theory solutions, and in C.4 for time domain solutions. A simplified method for determining the effects of multiconductor propagation and shield wires is presented in Section C.5.

C.2 Frequency Domain Solutions

As discussed in Appendix A, the behavior of EMP-induced currents in the loads at the ends of a general multiconductor transmission line shown in Figure C1 can be determined through the current BLT equation given by Equation A9. This equation is based on the existence of multivelocity TEM modes on the multiconductor line. Neglecting the differences in the propagation velocities for the various current modes on the line permits a considerable simplification of the BLT equation as:

$$
\begin{bmatrix} \bar{I}_o \\ \bar{I}_L \end{bmatrix} = \begin{bmatrix} \bar{\bar{U}} - \bar{\bar{\Gamma}}_o & \bar{\bar{0}} \\ \bar{\bar{0}} & \bar{\bar{U}} - \bar{\bar{\Gamma}}_L \end{bmatrix} \begin{bmatrix} -\bar{\bar{\Gamma}}_o & e^{\gamma L}\,\bar{\bar{U}} \\ e^{\gamma L}\,\bar{\bar{U}} & -\bar{\bar{\Gamma}}_L \end{bmatrix} \begin{bmatrix} \bar{I}^- \\ \bar{I}^+ \end{bmatrix} \qquad (C1)
$$

where $\bar{\bar{\Gamma}}_o$ and $\bar{\bar{\Gamma}}_L$ are generalized current reflection coefficient matrices for the z=0 and z=L ends of the line respectively. These are given by:

$$
\bar{\bar{\Gamma}} = \left[\bar{\bar{Z}}_L + \bar{\bar{Z}}_o \right]^{-1} \left[\bar{\bar{Z}}_L - \bar{\bar{Z}}_o \right] \qquad (C2)
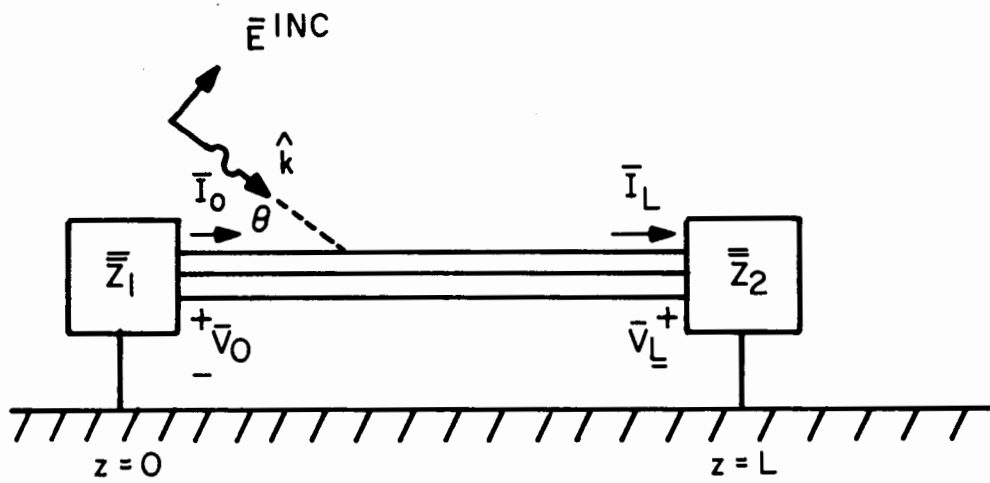$$

Fig. C1. Multiconductor transmission line excited by an incident electromagnetic field.

where $\bar{\bar{Z}}_L$ represents the generalized matrix load impedance at either end of the line and $\bar{\bar{Z}}_0$ is the characteristic impedance matrix of the line. For a general n wire line over a ground plane, all of the above matrices are of order n.

The characteristic impedance matrix of the line is given by:

$$\bar{\bar{Z}}_0 = \frac{1}{\gamma}\ \bar{\bar{Z}}_s \qquad (C3)$$

where $\bar{\bar{Z}}_0$ is the per-unit-length impedance matrix of the line, and γ is the complex propagation constant on the line. For a line having no loss, the per-unit-length impedance becomes simply the per-unit-length inductance matrix and γ is the free space propagation constant, so the line characteristic impedance matrix becomes:

$$\bar{\bar{Z}}_0 = c\ \bar{\bar{L}}_s \qquad (C4)$$

The excitation terms $\bar{\bar{I}}^-$ and $\bar{I}^+$ in Equation C1 are related to the integral of the distributed sourced along the line as:

$$\bar{I}^- = \frac{1}{2}\ \int_0^L e^{\gamma\xi}\ \bar{\bar{Z}}_0^{-1}\ \bar{V}_s'(\xi) + \bar{I}_s'(\xi)\ \ d\xi \qquad (C5)$$

and

$$\bar{I}^+ = -\frac{1}{2}\ \int_0^L e^{\gamma(L-\xi)}\ \bar{\bar{Z}}_0^{-1}\ \bar{V}_s'(\xi) + \bar{I}_s'(\xi)\ \ d\xi \qquad (C6)$$

As discussed in Section 3.2 for the case of EMP excitation of the line, the distributed voltage source vector is equal to the impressed tangential electrical field on each conductor, and is given by Equations

(35) or (38), depending on the nature of polarization of the incident field. For this type of excitation, the distributed current source is zero.

Instead of considering the propagation of current waves on the line as done in Appendix A and obtaining the current BLT equation, it is possible to consider the behavior of voltages at the loads and obtain a voltage BLT equation. In doing this, the behavior of the load voltages at z=0 and z=L may be expressed as:

$$
\begin{bmatrix} \bar{V}_o \\ \bar{V}_L \end{bmatrix} = \begin{bmatrix} \bar{\bar{U}} + \bar{\bar{\rho}}_o & \bar{\bar{0}} \\ \bar{\bar{0}} & \bar{\bar{U}} + \bar{\bar{\rho}}_L \end{bmatrix} \begin{bmatrix} -\bar{\bar{\rho}}_o & e^{\gamma L} \bar{\bar{U}} \\ e^{\gamma L} \bar{\bar{U}} & -\rho_L \end{bmatrix} \begin{bmatrix} \bar{\nu}^- \\ \bar{\nu}^+ \end{bmatrix} \tag{C7}
$$

where the reflection coefficient $\bar{\bar{\rho}}$ is a generalized voltage reflection coefficient matrix given by:

$$
\bar{\bar{\rho}} = \left[\bar{\bar{Z}}_L \bar{\bar{Z}}_o^{-1} + \bar{\bar{U}} \right]^{-1} \left[\bar{\bar{Z}}_L \bar{\bar{Z}}_o^{-1} - \bar{\bar{U}} \right] \tag{C8}
$$

Note that in the single wire case (i.e., all matrices of the order 1), the voltage reflection coefficient is the negative of the current reflection matrix. In the case of a multiconductor line, however, this is not the case, and these two reflection coefficients are related by the more complicated expression:

$$
\bar{\bar{\Gamma}} = \bar{\bar{Z}}_o^{-1} \bar{\bar{\rho}} \bar{\bar{Z}}_o \tag{C9}
$$

The distributed sources in the voltage BLT Equation (C7) take the form:

$$
\bar{\nu}^- = \frac{1}{2} \int_0^L e^{\gamma \xi} \left[\bar{V}_s'(\xi) + \bar{\bar{Z}}_o \bar{I}_s'(\xi) \right] d\xi \tag{C10}
$$

and:

$$\overline{v}^+ = -\frac{1}{2} \int_0^L e^{\gamma(L-\xi)} \left[\overline{V}_s'(\xi) - \overline{\overline{Z}}_0 \, \overline{I}_s'(\xi) \right] d\xi \qquad \text{(C11)}$$

As mentioned earlier, one possible way of representing the behavior of the line is to compute the open-circuit voltage at the z=L end of the line. Thus, the use of Equation (C7) may be used, and a numerical procedure can be developed to perform the indicated matrix manipulations. For the case of every conductor being open-circuited at z=L, the reflection voltage coefficient $\overline{\overline{\rho}}_L$ equals the unit matrix, thereby simplifying Eq. (C7) somewhat. However, if the phase conductors are open but the shield conductors grounded at z=L, the load reflection matrix is not quite so simple. More will be said about this particular loading configuration later. The important point is that this formulation for the multiconductor line permits an arbitrary load configuration at both ends of the line.

For a rigorous solution of Eq. (C7), it is necessary to evaluate the characteristic impedance matrix of the line, $\overline{\overline{Z}}_0$, and the propagation constant, γ, both of which are complex-valued functions of frequency. In studies of a single wire line over a real earth in Section 3.2, it was noted that for most frequencies, the single line impedance was closely approximated by the impedance of the same line over a perfectly conducting earth. Hence, for the multiconductor line, we have approximated the line impedance using Eq. (C4), where the inductance matrix is calculated element by element using the standard expressions for the self and mutual inductances of a line, as summarized in Ref. C1.

For the estimation of the propagation constant of the multiconductor line, an equivalent single wire conductor was placed at the average height of all of the phase conductors over the actual ground, and the complex propagation constant for the line was determined using the calculational techniques developed in Section 3.2. Once this single line γ was determined, it was used in Eq. (C7) for the multiconductor propagation constant.

Geometry of The Line

In order to estimate the effects of an incident EMP on the three phase, shielded transmission line shown in Fig. C2, we will concentrate on a single section of line located between two towers. The assumed tower configuration is that typical of a 345 kV transmission line taken from Ref. C2 as portrayed in Fig. C2 which shows the assumed geometry of the tower and line cross section. The line is taken to be a single circuit, three phase line with the individual phase conductors denoted as #1, #2, and #3 in the figure, and all at an equal height over a conducting earth. Each phase conductor actually consists of two individual conductors, having a 1" diameter and a separation of 18". As discussed in Ref. C3, the two conductors in each phase may be represented by a single conductor having an equivalent radius given by the geometrical mean radius (GMR) of 6.72 cm.

In this line there are two shielded conductors assumed to be located above the phase conductors as shown in the figure. These are denoted as #4 and #5 and are composed of single wires having a diameter of 0.28" (or a radius of 0.37 cm).

The distance between the towers on the line is taken to be 1400' or about 426.7 meters. In analyzing this line, only a single section between two towers will be considered. As shown in Fig. C3, two different load configurations at the z=0 end are considered. The first is a wye configuration for the phase conductors, and the second is a delta configuration. Note that these loadings are highly symmetric and do not generally lead to a mode conversion from the EMP-induced "common" or bulk currents on the line into differential current modes.

In those cases having shield wires, the shields are assumed to be connected at z=0 to the earth through a low impedance. At the opposite end of the line, at z=L, the open-circuit voltage on the line is computed and used as an indication of the behavior in an EMP environment.

20'
6.10 m

25'
(7.62m)

75'
(22.86m)

30'
(9.14m)
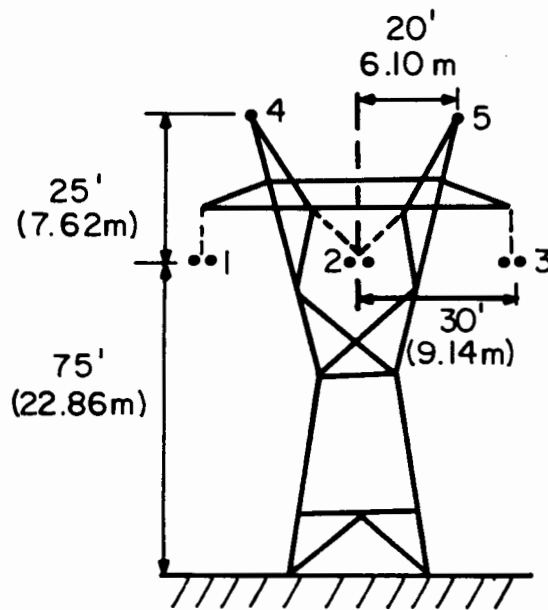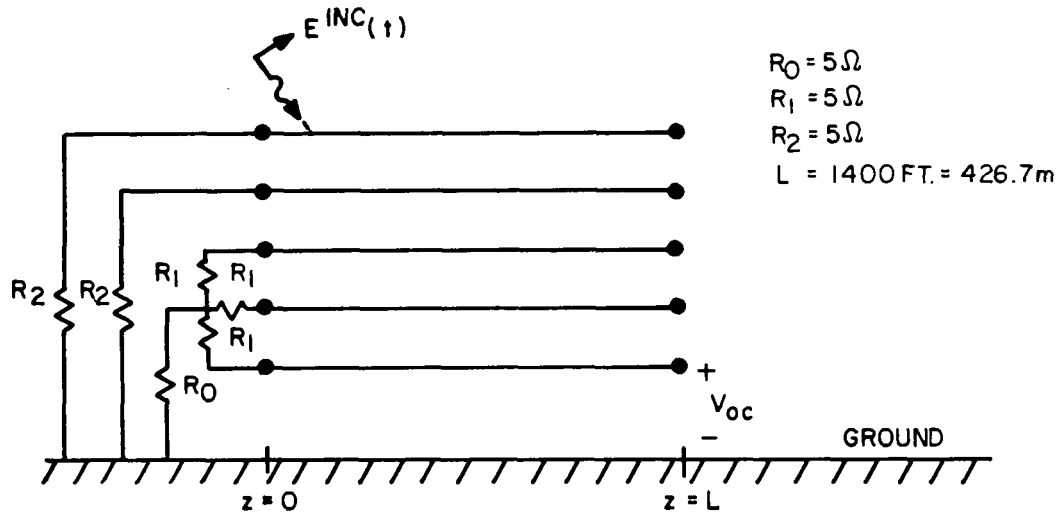
Line Geometry

Phase Conductors #1, #2, #3: 2 1" dia. cables spaced at 18"

GMR = 6.72 cm

Shield Conductors #4, #5   : Single 0.28" dia. cable

(a = .37 cm)

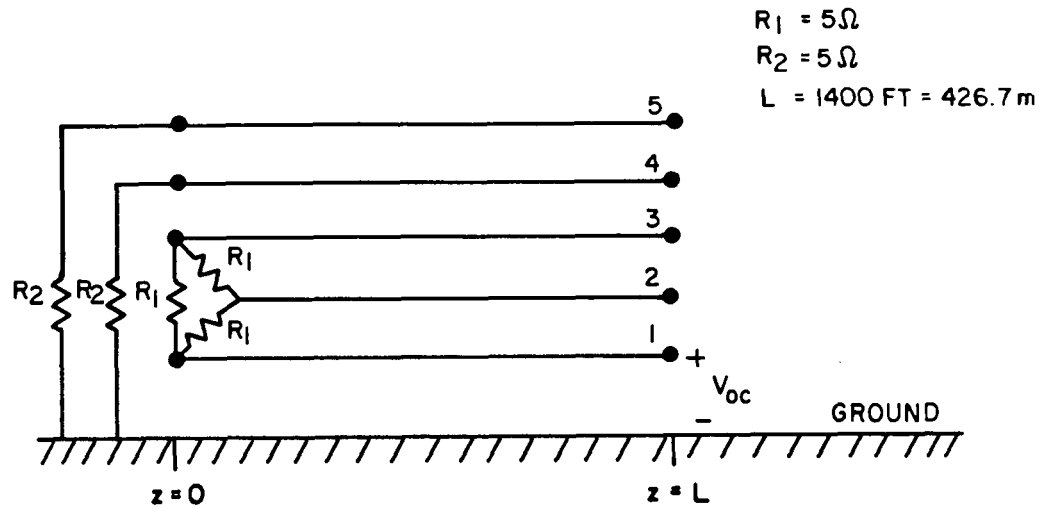Assumed Tower Spacing   : 1400 ft. (426.7 m)

Fig. C2. Cross section of sample 345 kV
3ϕ transmission line.

$R_0 = 5\,\Omega$

$R_1 = 5\,\Omega$

$R_2 = 5\,\Omega$

$L = 1400\,FT. = 426.7m$

a) Wye termination of phase conductors at z=0

Fig. C3. Three phase, single circuit transmission line section with delta and wye terminations and two shield wires.

b) Delta termination of phase conductors at z=0

Fig. C3. (Continued)

Numerical Results

The first case considered is that with a wye connection at the $z=0$ load as shown in Fig. C3a, but with no shield wires present. The load impedance at $z=0$ can best be determined by first writing the load admittance matrix and then inverting it numerically. For the wye connection without shield wires, the load admittance matrix may be expressed as:

$$\bar{Y}_L = \begin{bmatrix} Y_1 & -Y_2 & -Y_2 \\ -Y_2 & Y_1 & -Y_2 \\ -Y_2 & -Y_2 & Y_1 \end{bmatrix} \tag{C12}$$

where the individual elements are expressed in terms of the load resistances as:

$$Y_1 = \left[R_1 + \cfrac{1}{\cfrac{1}{R_0} + \cfrac{2}{R_1}} \right]^{-1} \tag{C13}$$

and

$$Y_2 = \cfrac{\left[1/R_1 \right]^2}{\cfrac{3}{R_1} + \cfrac{1}{R_0}} \tag{C14}$$

For the load admittance matrix at $z=L$, it can be approximated by a matrix having a small value on the diagonal, say, 10^{-6} mhos, and zeros on the off-diagonal elements.

The calculated open-circuit voltage for this load configuration is shown in Fig. C4a for the case of a vertically polarized EMP having the Bell Laboratory waveform (Table 2, Section 2.5), and angles of incidence $\psi=45°$ and $\phi=0°$. For this case, as well as for all further studies in this memo, these incident waveform parameters are fixed, as is the earth dielectric constant of $\epsilon_r=10$, and conductivity $\sigma_g=0.01$ mhos/meter.
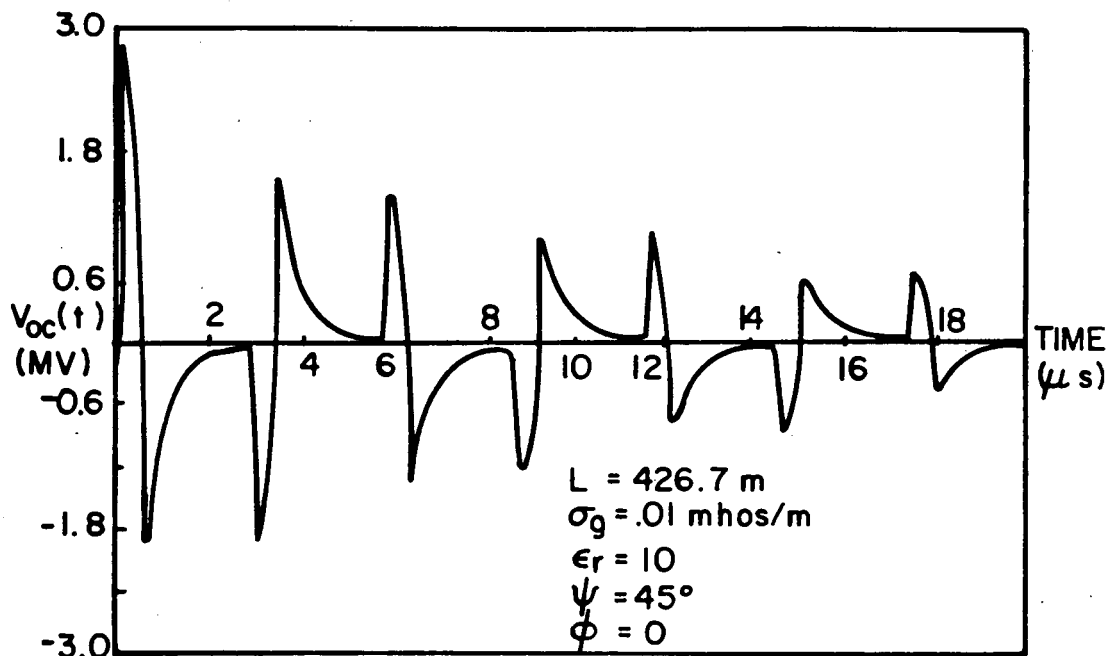
a) Wye connection at z=0
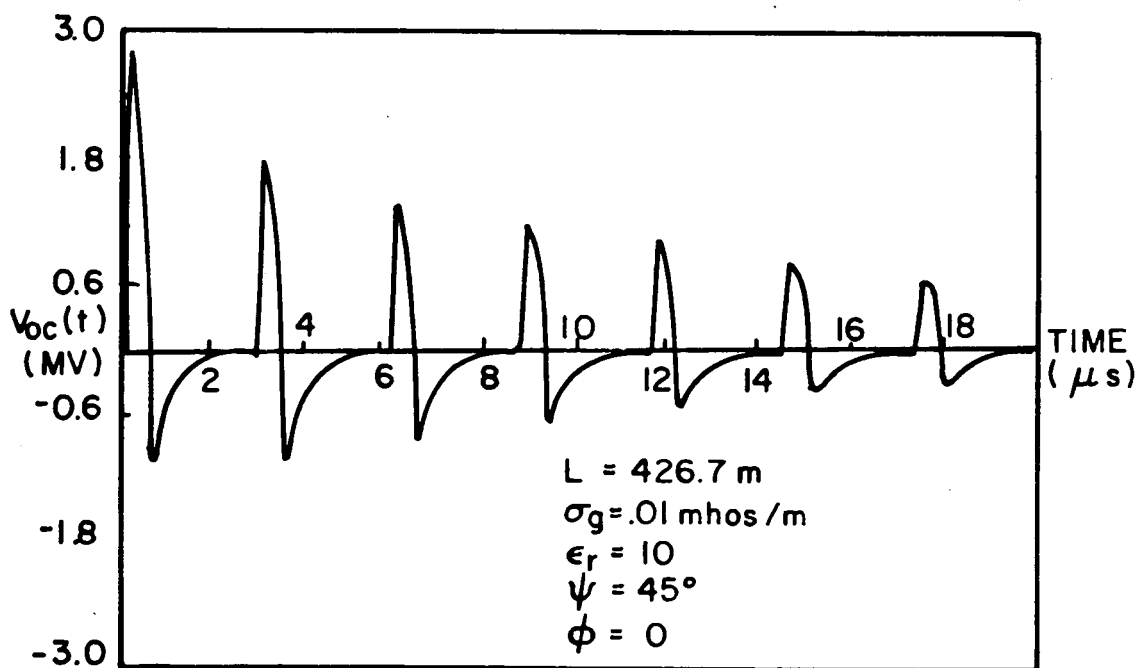
b) Delta connection at z=0

Fig. C4. EMP-induced open circuit voltage on 3φ line
(No shield wires.)

As may be noted in Fig. C4a, there is an initial spike in the open-circuit voltage response that is due to the initial interaction of the EMP with the line in the vicinity of the z=L end of the line, resulting in a peak open-circuit voltage of about 3 MV. Later, as time progresses, there are subsequent reflections on the line which tend to eventually die out due to the ground loss and the small loss in the wye termination. In this figure, there are actually two curves plotted, one for the voltages on wires #1 and #2 which are identical because of symmetry, and the other for the voltage on wire #2. Numerically, there is a difference between these two voltages, but the difference is so small that it is not observable.

Results for the same three conductor, un-shielded line as above, but with a delta load configuration at z=L are shown in Fig. C4b. In this case, the early-time portion of the waveform is exactly the same as for the wye loading until about 1 μs, at which time the observer begins to detect a difference in the response. After that time, there are similar waves bouncing back and forth on the line between the loads, but with different polarities than in the wye case.

In comparing the responses in Fig. C4 with those for an open and shorted single wire line in Appendix B, it is noted that the delta load is similar to that for a single line open-circuited at z=0 and that the wye is similar to a shorted line. In order to provide a more accurate comparison of these multiconductor responses with those of a single wire line, a single conductor having the same length as the multiconductor line, and at the same height over the ground as the phase conductors was analyzed for both load configurations at z=0. Figure C5a shows the resulting open-circuit voltage at z=L for the load shorted at z=0 and Fig. C5b shows the response for the open-circuit load at z=0. Note that there is a very good correlation between these single line responses and those arising from the multiconductor analysis.

This suggests that the trouble and effort of performing a multiconductor analysis for estimating the EMP excitation of a power system might be avoided by using a simple, single line model. It must
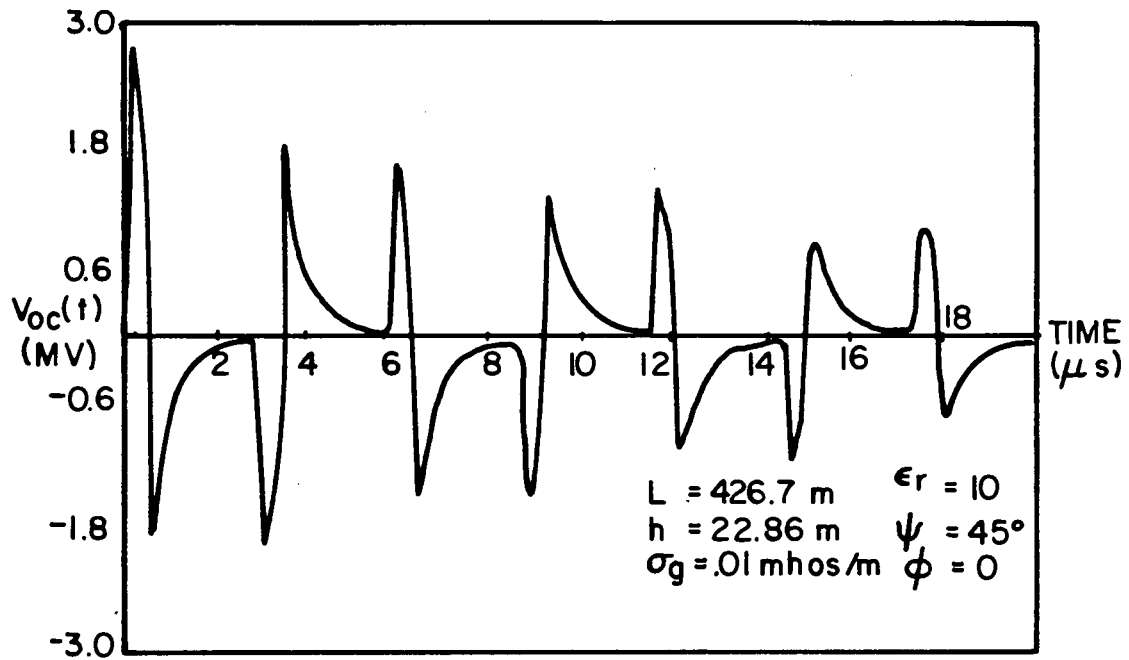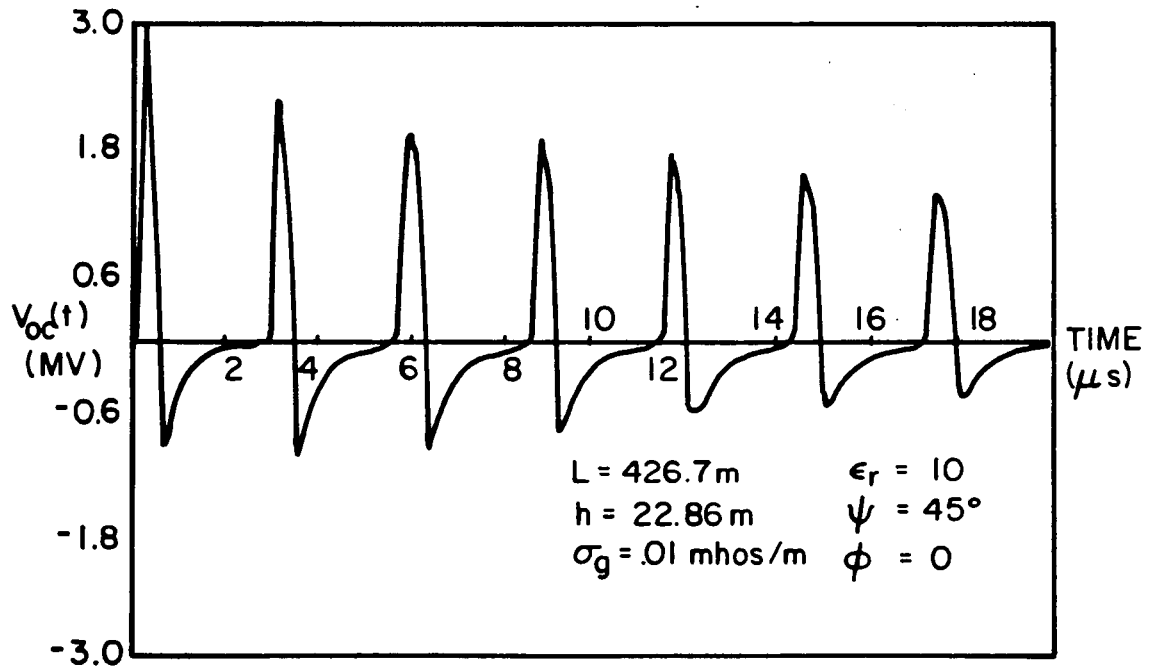
a) Short at z=0

b) Open at z=0

Fig. C5. EMP-induced open circuit voltage for single
conductor terminated in short and open circuit.

be remembered, however, that in this analysis, the individual phase conductors are all at the same height over the earth, and hence all receive the same excitation by the incident field. Moreover, the loading impedances are all symmetric, implying that the bulk or common mode currents are the most strongly excited and naturally correspond to the response of an "equivalent" single wire line. In a more general case with a phase conductor imbalance in the excitation and with arbitrary loads, the differences between the single line and multiconductor responses may be more noticeable. Nevertheless, given the level of uncertainty in the ground parameters, the load details and the non-uniform nature of the actual power line cross section, a single line analysis is probably justified in many cases.

The effect of locating the two shield wires over the phase conductors is illustrated in Fig. C6 for the case of a wye connection at z=0. For this case, the load impedance matrix given in Eq. C12 must be modified by adding two additional rows and columns to account for the termination resistances, R_2, on the shield wires, as shown in Fig. C3. Figure C6a shows the transient open-circuit voltage on the phase conductors (the solid line), and the corresponding open-circuit voltage on the shield conductors (dotted). Note that the early-time response of the phase conductor voltage is virtually identical with that in Fig. C4a for the unshielded line, indicating that the shield wires have no effect at early-time at the open end.

For the data shown in Fig. C6b, the shield wires at z=L are shorted to ground, and the resulting open-circuit phase voltages calculated (the solid line). The load admittance matrix at z=L may be expressed as:

$$\bar{\bar{Y}}_L = \begin{bmatrix} 10^{-6} & 0 & 0 & 0 & 0 \\ 0 & 10^{-6} & 0 & 0 & 0 \\ 0 & 0 & 10^{-6} & 0 & 0 \\ 0 & 0 & 0 & 10^6 & 0 \\ 0 & 0 & 0 & 0 & 10^6 \end{bmatrix} \qquad \text{(C16)}$$
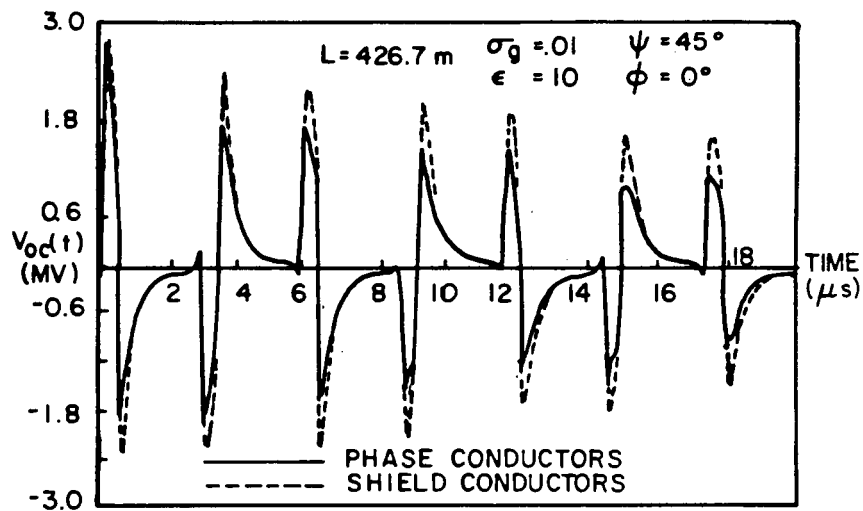
a) Phase conductor and shield conductor voltages for shield wires ungrounded at z=L
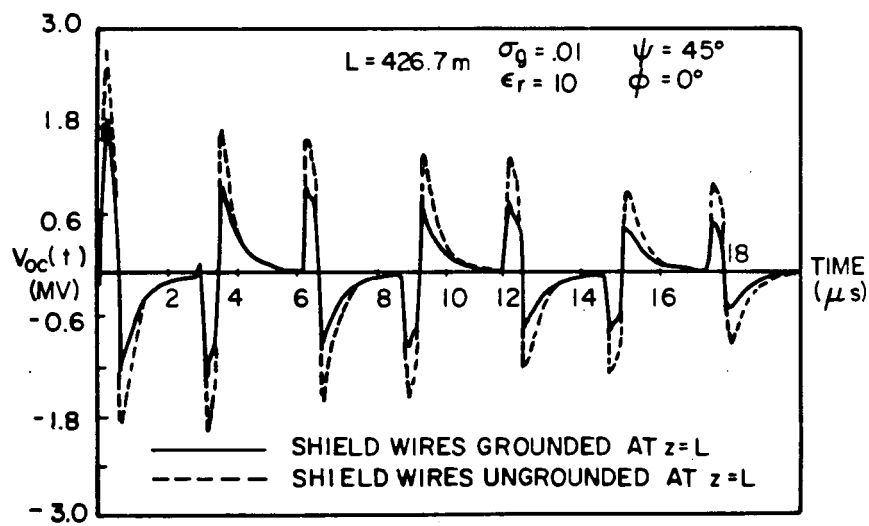
b) Comparison of phase conductor voltages

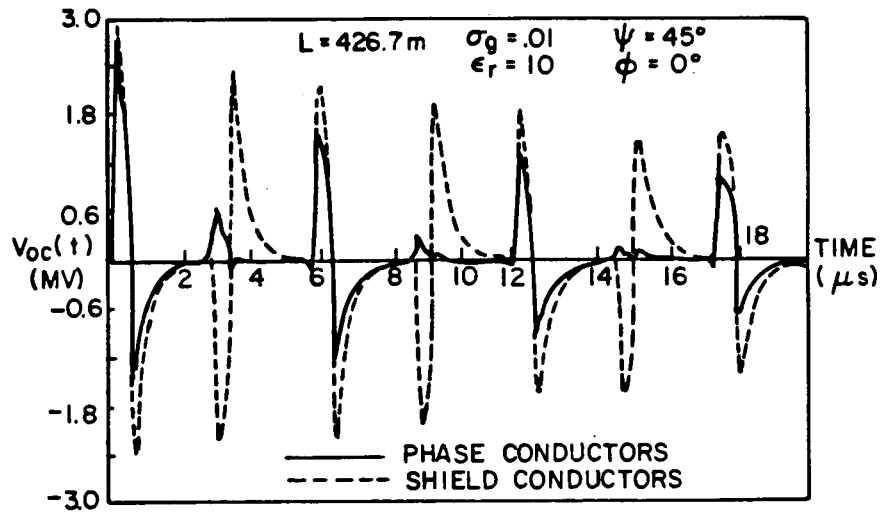Fig. C6. Computed HEMP-induced open-circuit voltages at z=L for a wye load configuration at z=0.

where 10^{-6} ohms has been chosen to represent the resistance of a short-circuit, and 10^{-6} ohms represents an open-circuit.

The results for this loading configuration at z=L may be compared with the same voltage with the shield wires ungrounded at z=L, which are shown by the dotted curve. In this case, it is noted that there is a substantial shielding effect provided by the shield wires. The peak open-circuit voltage on the phase conductors is reduced from slightly less than 3 MV to about 1.8 MV.

The same numerical study on the effects of shield wires for a line with a delta load on the phase conductors at z=0 is shown in Fig. C7. As in the previous case, the shield wires are seen to substantially reduce the response if they are grounded at the observation end of the line.

From the numerical studies performed, it is apparent that the early-time, open-circuit voltage at an observation point on the line is independent of the loading characteristics at the opposite end of the line. The late-time response is dictated by the loading characteristics, with a balanced delta load behaving as an open-circuit to the common mode response, and the grounded, balanced wye appearing as a short-circuit.

It has been noted that for the present case involving a high degree of symmetry in the line loading and excitation, the unshielded multiconductor line response can be estimated very accurately by a single-line transmission line over the earth. In the case of a shielded multiconductor line, however, the loading impedances are no longer symmetric, and such a simplification is no longer possible. In this case it is noted that if the shield wires are connected to ground right at the cross section on the line where the open-circuit phase voltages are observed, the shield wires have the tendency to reduce the early-time peak in the response. However, if the shield wires are also

a) Phase conductor and shield conductor voltages for shield wires ungrounded at z=L
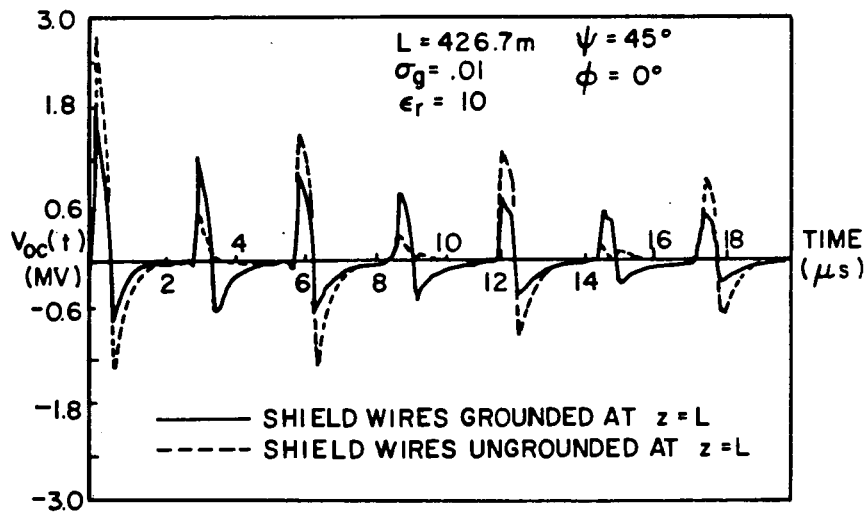
b) Comparison of phase conductor voltages

Fig. C7. Computed HEMP-induced open-circuit voltages at z=L for a delta load configuration at z=0.

open-circuited (even though they may be grounded somewhere else along the line), they are noted to have a negligible effect on the early-time response.

The calculational models described here are greatly simplified, in that the true multiconductor propagation is not taken into account. If a rigorous analysis were to be performed, it would be necessary to compute the various eigenmodes and propagation velocities for a multiconductor line over a lossy earth. This would entail calculating the per-unit-length impedance and admittance matrices as discussed in Ref. C4 and then diagonalizing the resulting complex propagation matrix at every frequency to solve the BLT equation. This task remains for future investigations into the effects of EMP on power systems.

C.3 Scattering Theory Solutions

Solutions for multiconductor transmission lines for early times can be obtained from a linear time-domain scattering theory [C5]. Although the theory is accurate for late times as well as early times, the numerical methods employed to solve the equations generally provide solutions for only the early time period.

The current induced on a two wire transmission line by a vertically polarized electric field with a waveform of $52,500 \left[e^{-4 \times 10^{6}t} - e^{-478 \times 10^{8}t} \right]$ v/m is shown in Fig. C8 [C5].

Early time solutions for the shielded, single circuit, three phase transmission line shown in Fig. C9 are given in Figures C10, C11, and C12 for the same electric field waveform assumed for the two wire transmission line [C5]. A striking difference between these solutions and those obtained with transmission line theory occurs at an incidence angle of 0.1 radians. The solutions obtained from transmission line theory show increasing times to peak, increasing pulse widths, and increasing magnitudes as the incidence angle becomes smaller in contrast to the shorter times to peak, decreasing pulse widths, and constant magnitudes obtained from linear, time-domain scattering theory.
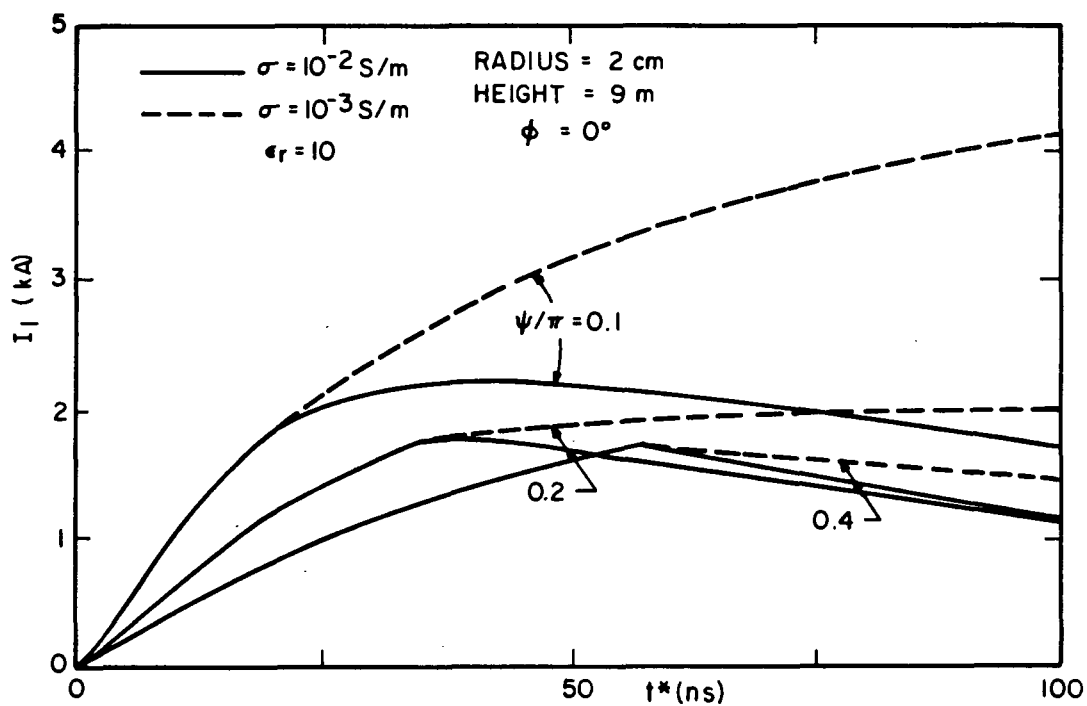
Fig. C8. Total current induced on conductor #1 which is 9 m
away from conductor #2 and at the same height as #2 from ground
for conductivity σ = 10⁻² S/m or σ = 10⁻³ S/m. At "+", a multiple
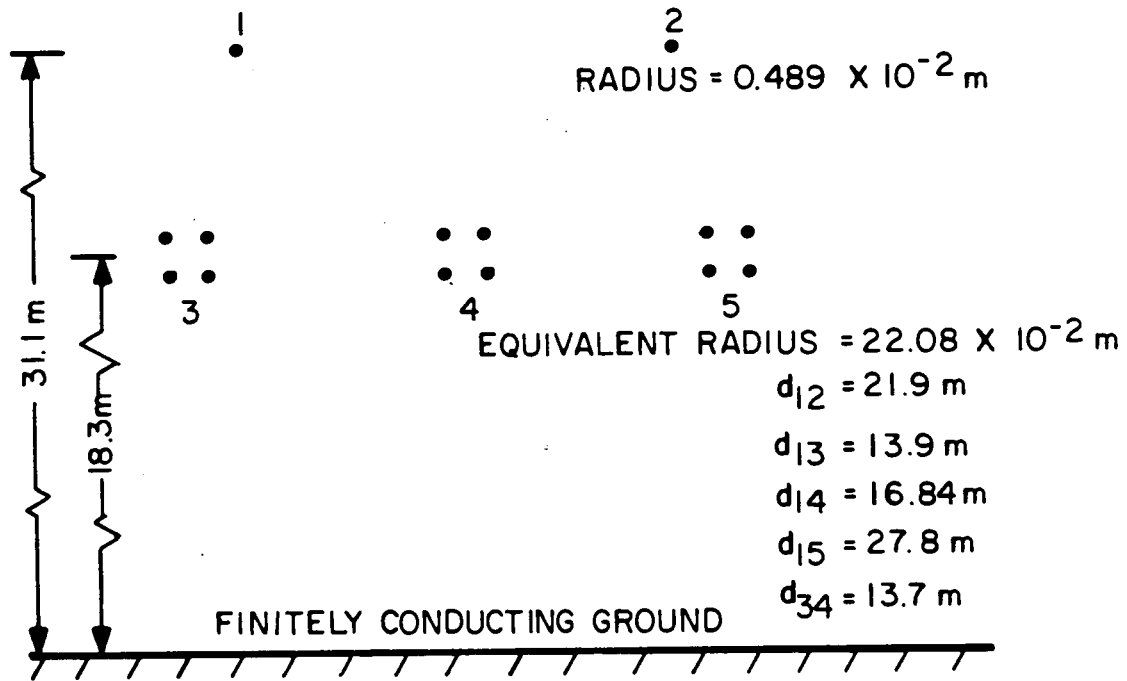scattered field will arrive at wire #1 [C5].

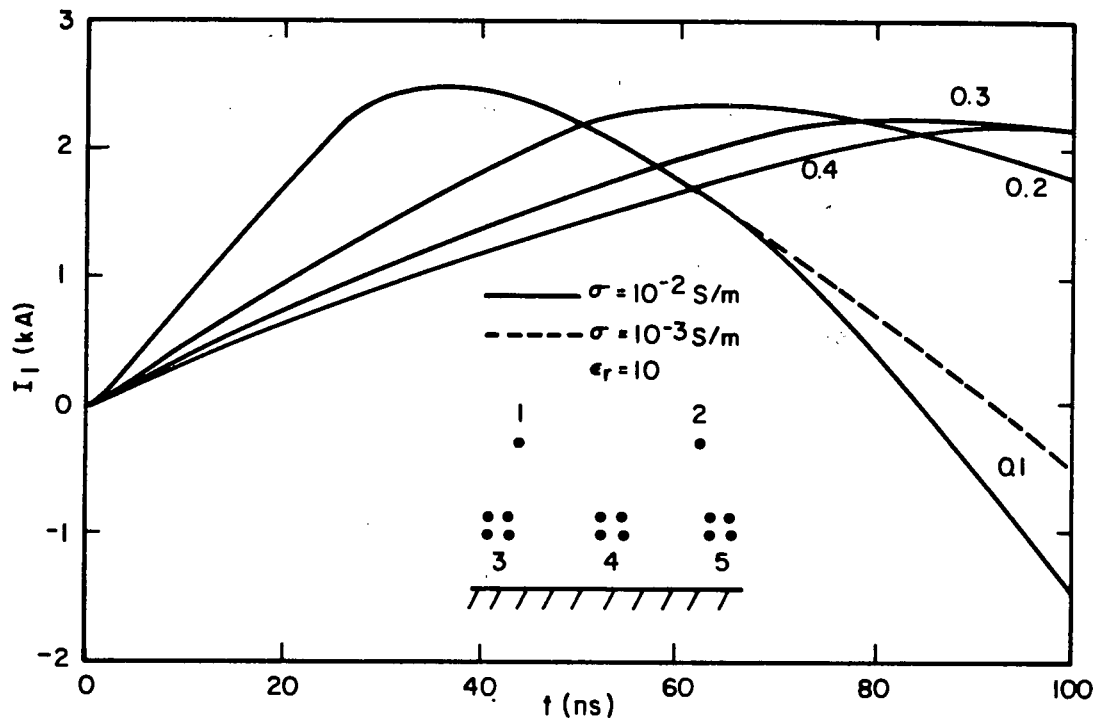Fig. C9. A typical configuration of a 3φ 765 kV single-circuit transmission line.

Fig. C10. Total current induced on shield wire #1 for
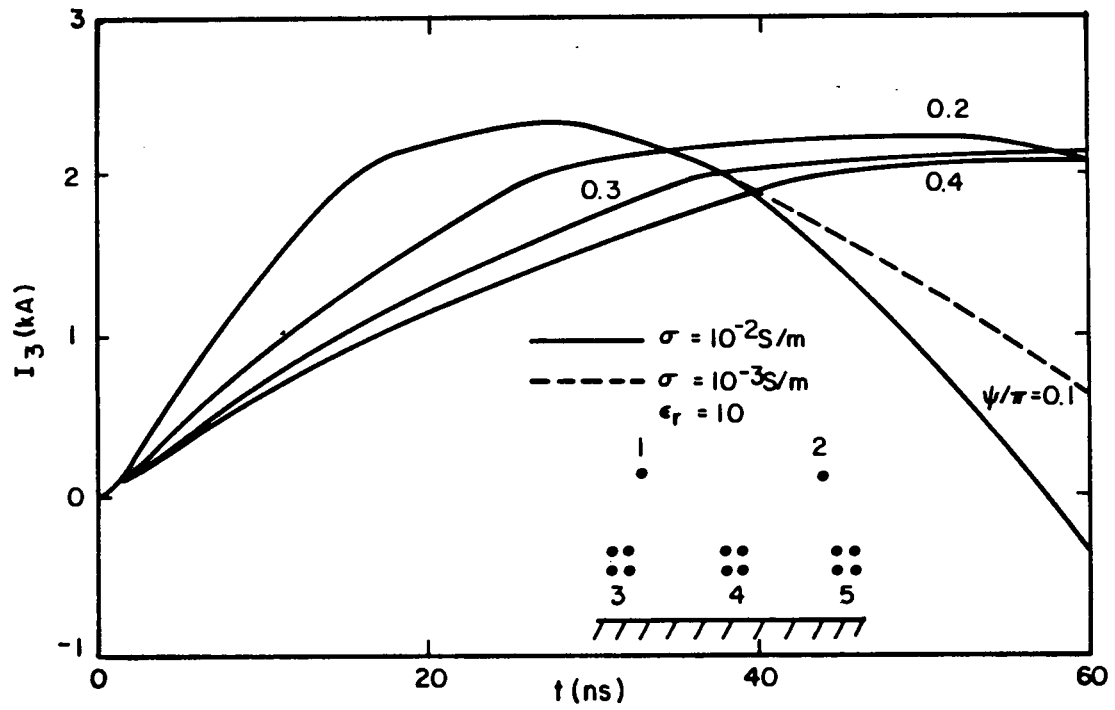ground conductivity $\sigma = 10^{-2}$ S/m or $\sigma = 10^{-3}$ S/m [C5].

Fig. C11. Total current induced on phase wire #3 for ground conductivity $\sigma = 10^{-2}$ S/m or $\sigma = 10^{-3}$ S/m.
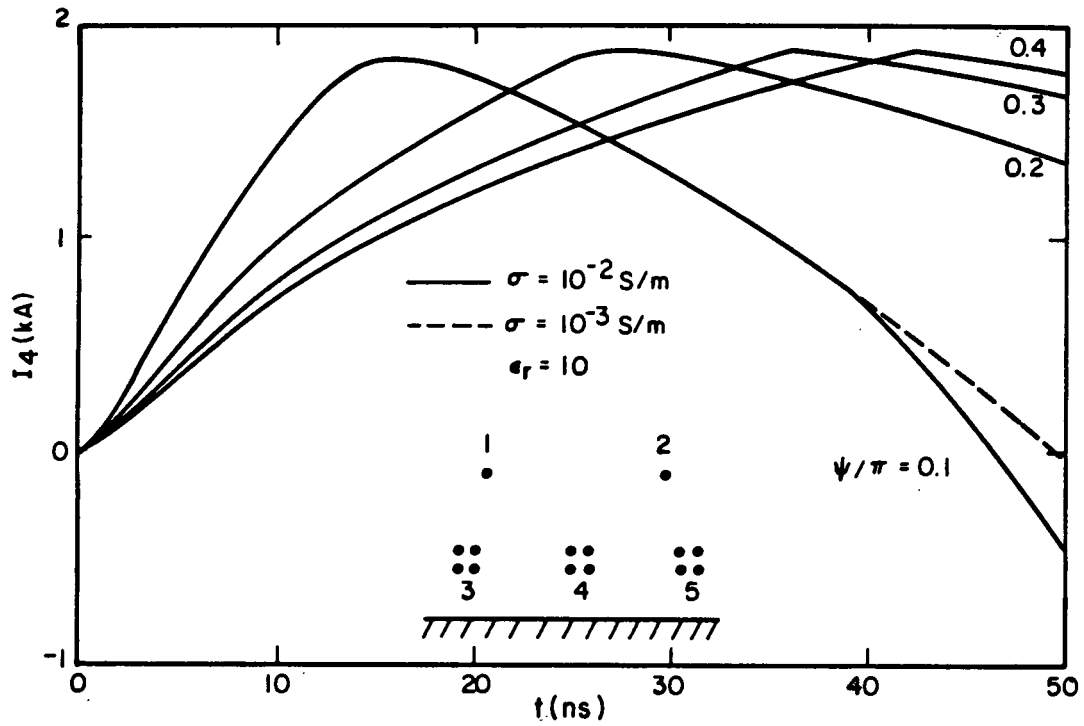
Fig. C12. Total current induced on phase wire #4 for
ground conductivity $\sigma = 10^{-2}$ S/m or $\sigma = 10^{-3}$ S/m.

C.4 Time Domain Multiconductor

Transmission Line Solutions

The EMPT transmission line transients program is widely used to study transients on power system transmission lines. This program can not be used in its present form to determine the voltage induced on transmission line because of the inability to include distributed voltage sources along a conductor. However, this program may be used to estimate the effect of shield wires and multiconductor propagation on the voltage or current response at an observation point as illustrated by the following example.

Effect of Shield Wires on The Response of Phase Conductors of Transmission Lines

The procedure to estimate the response of a multiconductor transmission line can be summarized as follows. First, divide the line into segments; in this case the spans between towers. Second, calculate a first estimate for the HEMP induced responses of the different conductors of each segment, assuming no coupling between the different conductors but modeling the terminations accurately. Third, set up an electromagnetic and electrostatic frequency dependent coupling model for the line. Fourth, using the voltage (or currents) obtained above as the driving sources for the line segments at both ends of the segment, find the corrected response for each span. Fifth, use superposition to find the composite response from the responses of each span.

The analysis of the effects of shield wires and non-corona attenuation are illustrated in the following example.

Responses of The Conductors Assuming No Coupling Between Them

In this example only the response of the horizontal conductor is calculated. Calculation of the complete response considering both the

vertical and horizontal elements might be necessary in an actual assessment.

The geometry of a typical 132 kV line chosen for our example is shown in Fig. C13. The span length is assumed to be 241 meters. A vertically polarized HEMP wave having the "Bell" waveform with a peak magnitude of 50 kV/m and angles of incidence $\Psi=30°$ and $\phi=0°$ is assumed. The phase conductors are terminated by their characteristic impedance at the beginning of the span. The ground wires are shorted to ground at the beginning of the span. Figures C14 and C15 show the induced open circuit voltage at the end of one span for the ground and phase conductors.

Coupling Model Used

The complex line constants were calculated over a frequency range of 1 to 10×10^6 Hz. The two ground wires were retained in these calculations, and, hence, five different propagational modes were obtained for the line. For the purposes of this analysis, only the portion between 0 and .2 μs of the voltage waveform of Figures C14 and C15 is represented. Hence, the circuit parameters for 1 MHz are used. In general, an FFT analysis needs to be done on the coupled responses and a frequency dependent model for the line should be used.

Calculation of The Coupled Conductors

For the three cases run for this analysis, it is assumed that the excitation voltage sources were 2056 and 1612 kV for the ground (shield) and phase wires, respectively. These correspond to half of the open circuit voltages calculated above and shown in Figures C14 and C15. The phase conductors are terminated in their characteristic impedance at the end of the span.
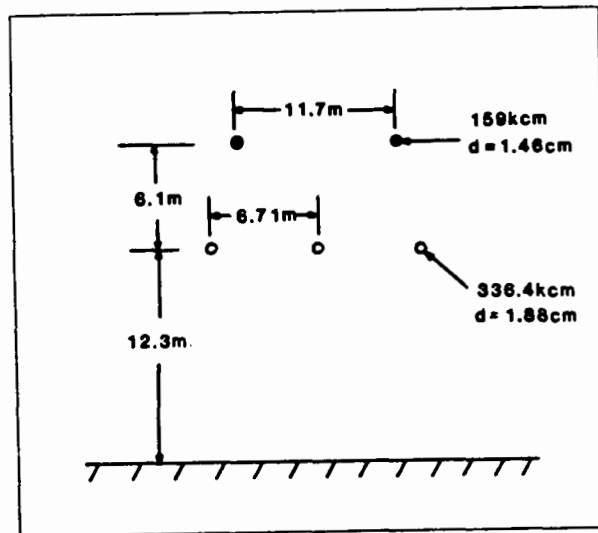
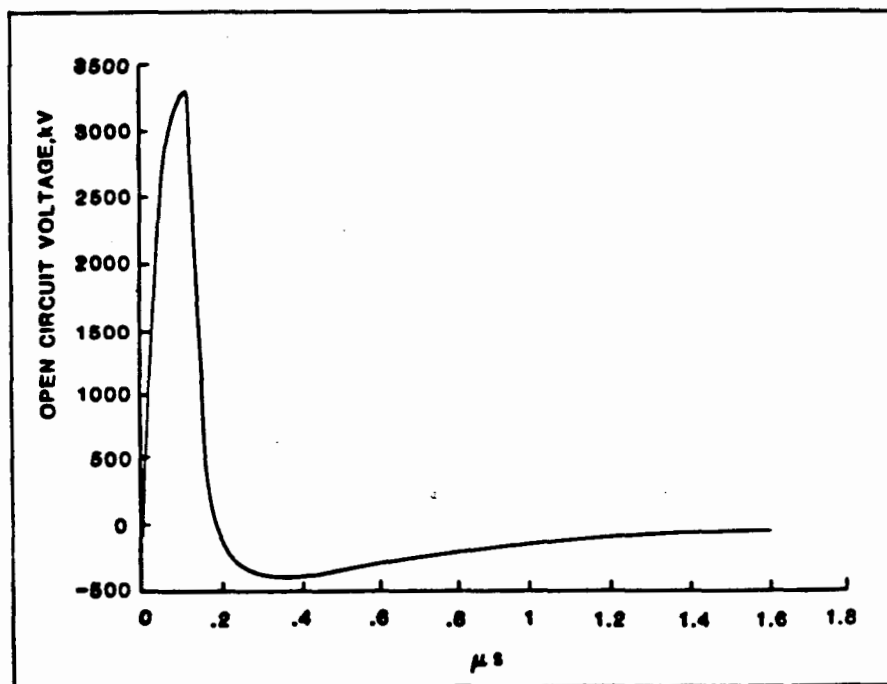Fig. C13. Typical 132-kV line physical layout.

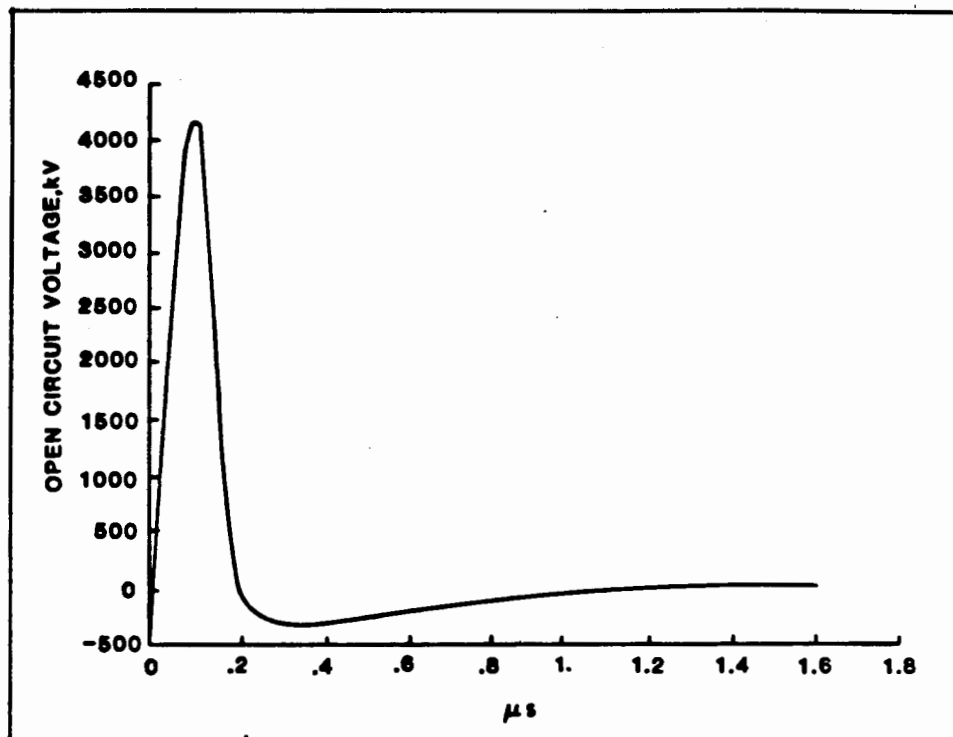Fig. C14. Open circuit voltage at the end of one span (241m) for the phase conductors ψ=30°, φ=0°, conductivity = .01 mhos/m.

Fig. C15. Open circuit voltage at the end of one span for the ground wires ψ=30°, φ=0°, conductivity = .01 mhos/m.

Case 1:

Only one span of the line is represented. Ground wires are not connected to the tower. This case is run to establish the propagation attentuation.

Case 2:

Same as Case 1, but with the ground wires solidly grounded, tower not represented.

Case 3:

Two spans are represented. Towers at the end of the first and second span are represented by an 18.4 m, 200 Ω surge impedance for the tower and 20 Ω footing resistance.

Case Results

Table C1 shows the results for the three different cases described above. From this table it can be deduced:

From Case 1:

- The attenuation constant for the ground wires is approximately 15% per span (241 m).

- The attenuation constant for the phase conductor is approximately 12% per span.

Table C1

Peak Voltage Recorded In kV

	Tower 1			Tower 2		
	Center Phase	Outer Phase	Shield Wire	Center Phase	Outer Phase	Shield Wire
Case 1...	1404	1395	1744			
Case 2...	996	941	0			
Case 3...	1142	1107	683	851	806	185

From Case 2:

● The phase conductor voltages for the case of a solidly grounded ground conductor are reduced by a factor 38-40% when coupling and attenuation are considered.

From Case 3:

● The voltages of the phase conductors at the end of the first span are reduced by a factor 29-31% when coupling and attenuation are considered.

● The voltages of the phase voltage at the second tower are reduced by a factor 47-50% when coupling and attenuation were considered.

Composite Response of The Different Spans

Using superposition, for the 132-kV line under consideration and for the assumed HEMP polarization, the voltage at the station is primarily a function of the first span from the station. The contributions from the other consecutive spans do not alter the peak magnitude and the initial rise time of this voltage as seen in Fig. C16.

C.5 A Simplified Method to Determine The Effect of Ground Wires on The Phase Conductor Responses

In the above cases, a multi-phase transients program is used to obtain the responses. In this section, a simplified method to estimate the effect of the ground wires is presented. This method predicts the response of the phase conductors through the use of "coupling factors" of the circuit.

Coupling Factor of A Two Conductor System

For the two conductor systems of Fig. C17, one can write the following two equations which relate the traveling wave currents (i) and voltages (e) on the two conductors.
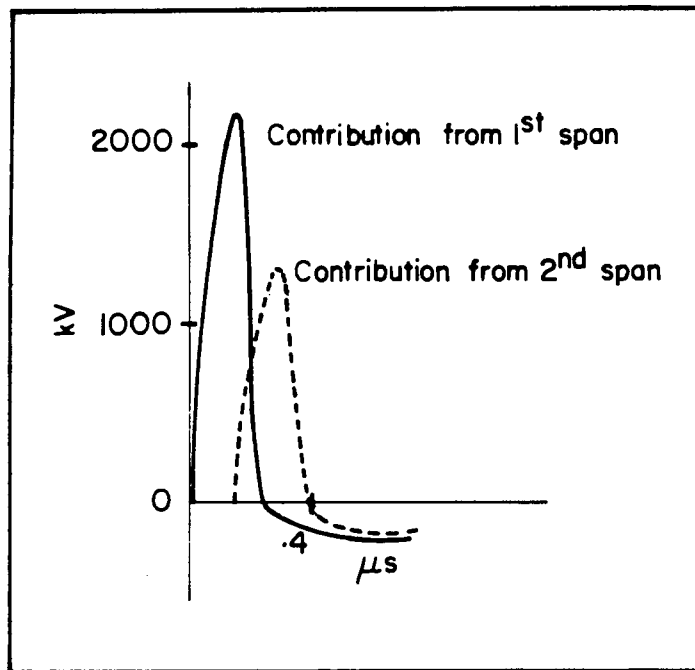
a) Contribution of the first two spans of the line.
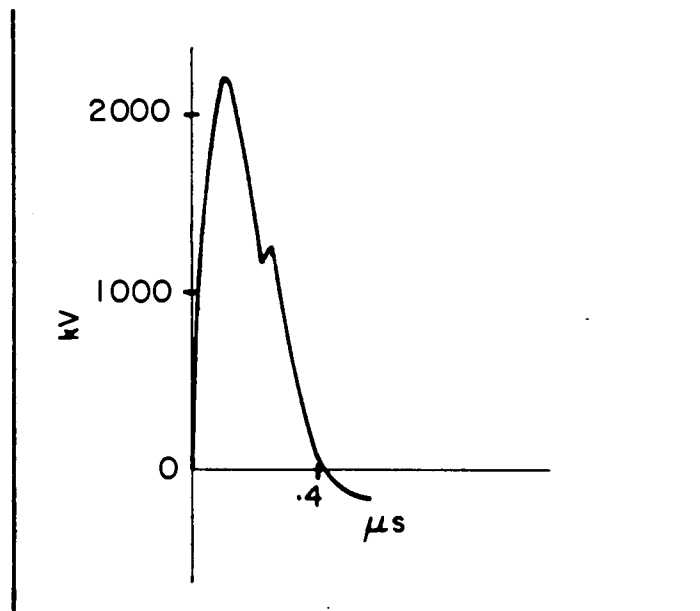
b) Composite waveshape of voltage at the end of the line.

Fig. C16. Twice the traveling wave voltage appearing at the end of the 132-kV line due to the first two spans.
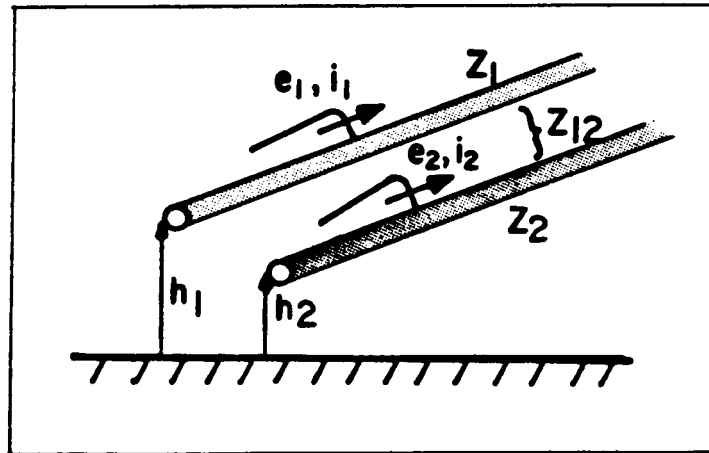
Fig. C17. Two conductor systems with corresponding surge impedances.
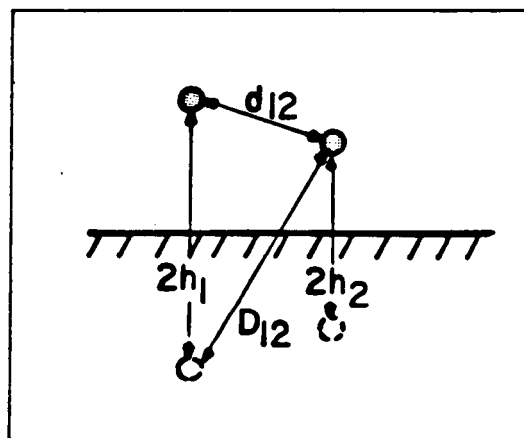

Fig. C18. Physical layout of the two conductor systems of Figure C17.

$$e_1 = i_1 \, Z_1 + i_2 \, Z_{12} \tag{C17}$$

$$e_2 = i_1 \, Z_{12} + i_2 \, Z_2 \tag{C18}$$

whereby:

$$Z_1 = 60 \ln \frac{2h_1}{r_1} \tag{C19}$$

$$Z_2 = 60 \ln \frac{2h_2}{r_2} \tag{C20}$$

$$Z_{12} = 60 \ln \frac{D_{12}}{d_{12}} \simeq 60 \ln \frac{2h_1}{d_{12}} \tag{C21}$$

and r_1 and r_2 are the radii of the two conductors and h_1, h_2, d_{12}, and D_{12} are as defined per Fig. C18.

Coupling Factor of One Ground Wire and One Phase Conductor

If a traveling wave voltage and current are impressed on one conductor only, a voltage will be induced or coupled on to the other conductor.

Let $i_2 = 0$ in Equations (C17) and (C18), then:

$$e_1 = i_1 \, Z_1 \tag{C22}$$

$$e_2 = i_1 \, Z_{12} \tag{C23}$$

$$e_2 = \frac{Z_{12}}{Z_1} \, e_1 = C e_1 \tag{C24}$$

where $\dfrac{Z_{12}}{Z_1}$ is called the coupling factor, C.

Coupling Factor of Two Ground Wires and One Phase Conductor

In many practical cases, the coupling factor between two ground wires and one phase conductor, as in Fig. C19, is needed. This is derived as follows.

Let the voltage on the ground wires be equal to e. Also, no current is injected in the phase conductor so that the current in the phase conductor, $i_c = 0$. Therefore:

$$e = e_1 = i_1 Z_1 + i_2 Z_{12} \qquad (C25)$$

$$e = e_2 = i_1 Z_{12} + i_2 Z_2 \qquad (C26)$$

$$e_c = i_1 Z_{1c} + i_2 Z_{2c} \qquad (C27)$$

Let $Z = Z_1 = Z_2$, then:

$$e_c = \frac{e}{Z + Z_{12}} (Z_{1c} + Z_{2c}) = \frac{e}{(\frac{Z + Z_{12}}{2})} (\frac{Z_{1c} + Z_{2c}}{2}) \qquad (C28)$$

$$e_c = \frac{(Z_{1c} + Z_{2c})/2}{Z_g} e = Ce \qquad (C29)$$

where $Z_g = \dfrac{Z + Z_{12}}{2}$ is the equivalent ground wire surge impedance.

Therefore, the coupling factor, C, is equal to the average mutual surge impedance divided by the equivalent ground wire surge impedance. The above is true for two ground wires and one phase conductor. For n ground wires and one conductor, and within 1% accuracy, one can write:
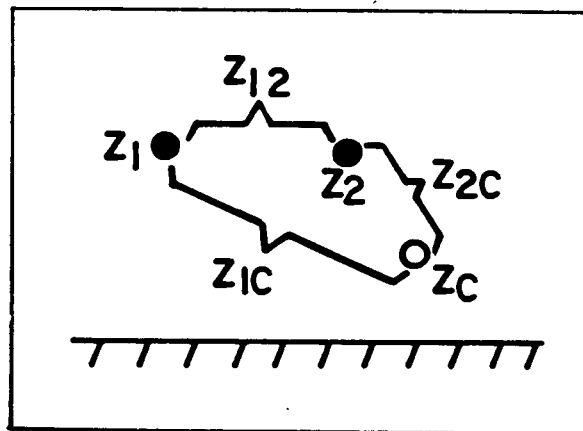
$$C = \frac{Z_m}{Z_g} \qquad (C30)$$

Fig. C19. A three conductor system: two
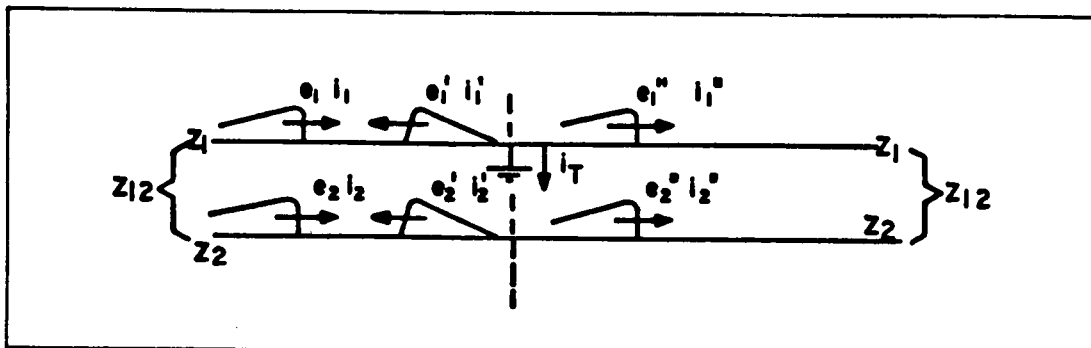ground wires and one phase conductor.

Fig. C20. One phase conductor and one
grounded ground wire.

where:

$$Z_g = \frac{Z + (n-1) Z_{mg}}{n}$$ (C31)

Z_{mg} is the average mutual surge impedance of the ground wires.

Z is the average self surge impedance of the ground wires.

Z_m is the average mutual surge impedance between the n ground wires and the phase conductor.

n is the number of conductors.

Simplified Method for The Calculation of Phase Voltages On Lines with Shield Wires

For the system of the two lossless conductors of Fig. C20, it can be shown that:

$$e_c'' = e_c - Ce_g$$ (C32)

If the conductors are lossy, Equation (C32) becomes:

$$e_c'' = e_c K_2 - K_1 Ce_g$$ (C33)

whereby:

C is the coupling factor between the two conductors.

K_1 is the attenuation for Conductor 1.

K_2 is the attenuation for Conductor 2.

e_g is the induced voltage on Conductor 1.

e_c is the induced voltage on Conductor 2.

Case of The 132-kV Line

In a manner similar to the above, it can be shown that, for the subject 132 kV line, the coupling between the phase conductors and the shield wires is approximately 27%. From Case 1, K_1 and K_2 are $(.88)^n$ and $(.85)^n$, respectively, where n is the number of 241 m spans.

For the case of grounding the shield wires at the first tower, Equation (C33) yields:

$$(1612).88 - (.85)(2056)(.27) = 947 \text{ kV}$$

This agrees quite closely with the results of Case 2.

In the case where the ground wires are not grounded directly, as in Case 3, the phase voltage at the first tower is reduced, but not as much as depicted by Equation (C33). The voltages at the second tower, however, agree nicely with (C33) as shown below:

Phase Voltage at the Second Tower =

$$(1612)(.88)^2 - (.85)^2(2056)(.27) = 846 \text{ kV}$$

The small difference between the values calculated by (C33) and computer simulations are attributed to the coupling between the different phases.

It can be concluded from the above that the simplified method can be used to estimate accurately the phase voltages to include the effects of ground wires.

Conclusions on The Effect of Ground Wires

The following can be concluded from the above discussion.

Neglecting propagational attenuation, one should expect a minimum of (1-C) reduction factor in the phase voltages (C is typically 25-35%). This reduction is obtained after the first span for lines with low tower footing resistance (TFR), and after the second or third span for higher TFR (say 20-30 ohms). If attenuation and unequal excitation of the ground and phase wires are considered, a further reduction is expected.

A systematic methodology to determine the open circuit voltages arriving at the station due to HEMP can be summarized as follows:

- Determine the excitation for one span for the phase and ground wires assuming no coupling between any conductor.
- Determine the propagational attenuation for the power line.

- Using the coupling factor method or a rigorous multi-phase, multi-mode analysis program, determine the effect of ground wires on the phase conductor.

- Start with first span out of the station and sum the contribution of the consecutive spans.

BIBLIOGRAPHY

C1. Lee, K. S. H., ed., EMP INTERACTION: PRINCIPLES, TECHNIQUES, AND REFERENCE DATA-EMP Interaction 2-1, AFWL-TR-80-402, December, 1980.

C2. TRANSMISSION LINE REFERENCE BOOK, 345 kV AND ABOVE, Electric Power Research Institute Publication, 1982.

C3. ELECTRICAL TRANSMISSION AND DISTRIBUTION REFERENCE BOOK, Westing-house Electric Corporation Publication, 1964.

C4. Ianovici, M., and F. M. Tesche, "Use of General Multiconductor Transmission Line Analysis Code for the Study of EMP Effects in HV Networks," Presented at the 1984 Nuclear EMP Meeting (NEM), Baltimore, MD., July, 1984.

C5. Lee, K. S. H., F. C. Young, N. Enqheta, "Interaction of High-Altitude Electromagnetic Pulse (HEMP) with Transmission Lines: An Early-Time Consideration," AFWL EMP Interaction Note 435, December, 1983.

APPENDIX D

Numerical Examples for Responses of
Buried Cables

In this appendix, normalized currents induced on buried conductors for various combinations of HEMP waveforms, burial depths, and soil conductivities are shown.

Figure D1 shows the magnitude of the peak current, I_p, which can circulate on a long underground conductor. In the case of a concentric cable, this will be the current on the metal sheath rather than the inner conductor. The incident electric field is considered to be single exponential of the form $e^{-t/\tau}$ where $\tau=.25\mu$ sec, vertically polarized and has the same orientation as that of the conductor ($\phi=0°$). The results are independent of the elevation incidence angle, ad $D(\psi,\phi)$ is only a function of ϕ for this kind of polarization.

It can be concluded from Fig. D1, that the peak induced current is inversely proportional with respect to the square root of the ground conductivity for small burial depths:

$$I_p \; \alpha \; \frac{1}{\sqrt{\sigma_g}} \qquad\qquad (D1)$$

Also, as is expected, the peak current decreases with increasing depths, however, for highly lossy grounds, and for small depths (e.g., less than 5m), the peak induced current is nearly independent of the depth.

Figure D2, extracted from Reference [D1], shows the variation of the peak current with different decay time constants of the incident electric field. These curves are applicable to all cases where $\tau>>\tau_e$.

Figures D3, D4 and D5 show that complete waveforms for the HEMP induced currents on long buried conductors for different ground conductivities and buried depths.
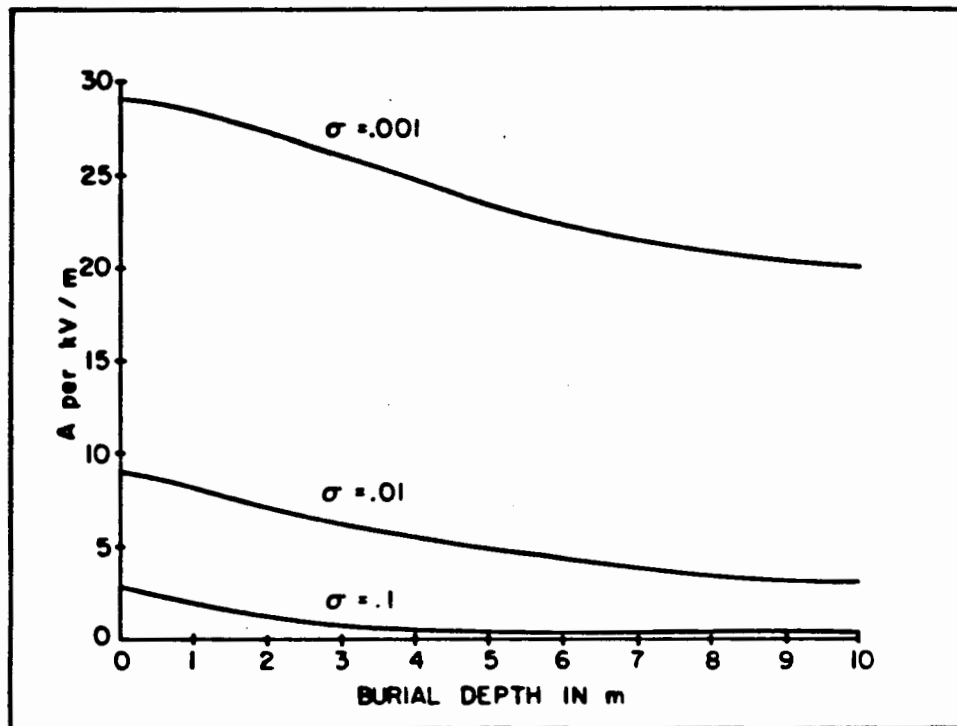
Fig. D1. Normalized HEMP induced current in a long
buried conductor for different ground conductivities
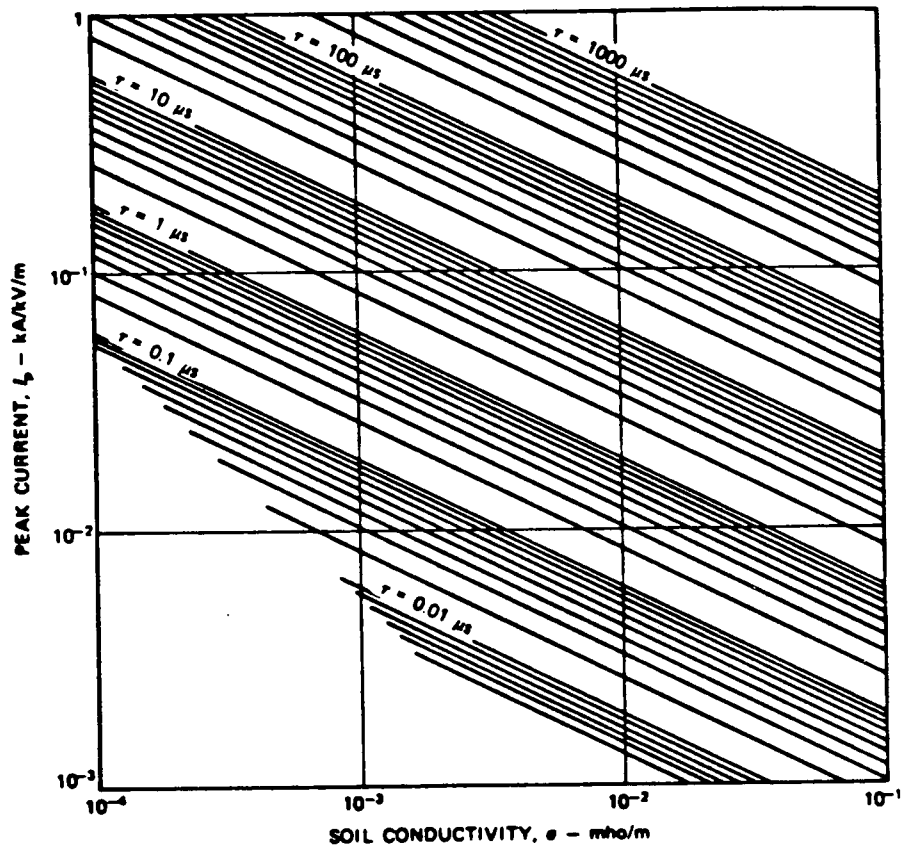(.001, .01 and .1 mhos/m) and buried depths.

Fig. D2. Peak cable current as a function of soil conductivity and incident exponential pulse-decay time constant [D1].
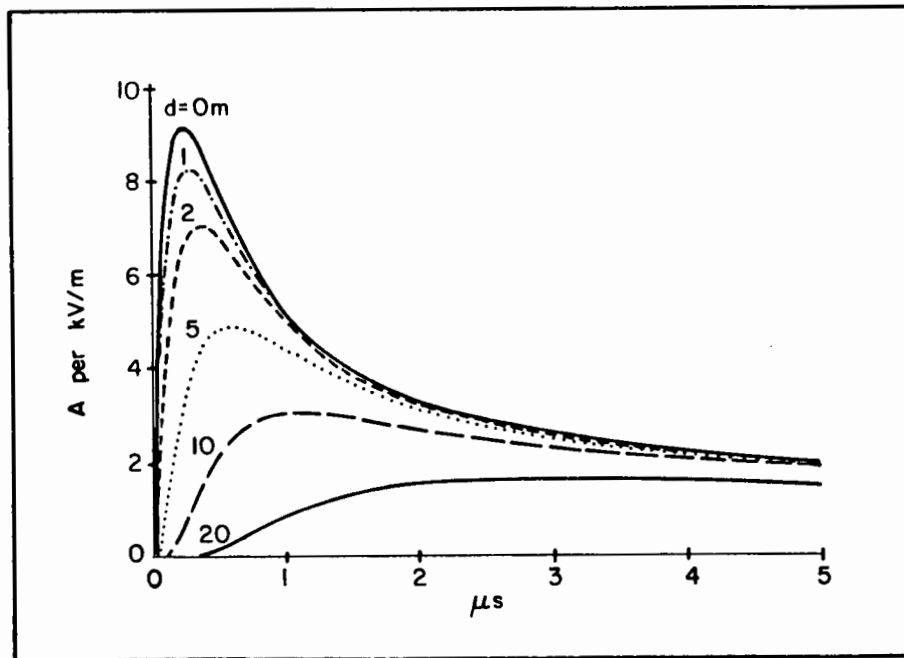
Fig. D3. Normalized HEMP-induced current on a long buried conductor in earth with a conductivity of $\sigma_g = 10^{-2}$ mhos/meter for several burial depths.
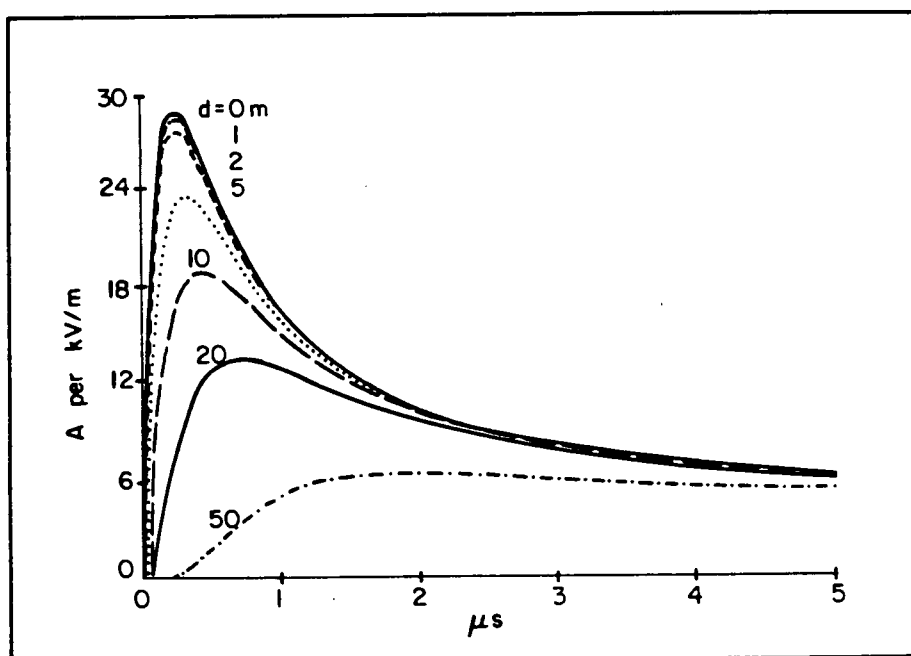
Fig. D4. Normalized HEMP-induced current on a long buried conductor in earth with conductivity $\sigma_g=10^{-3}$ mhos/meter for several burial depths.
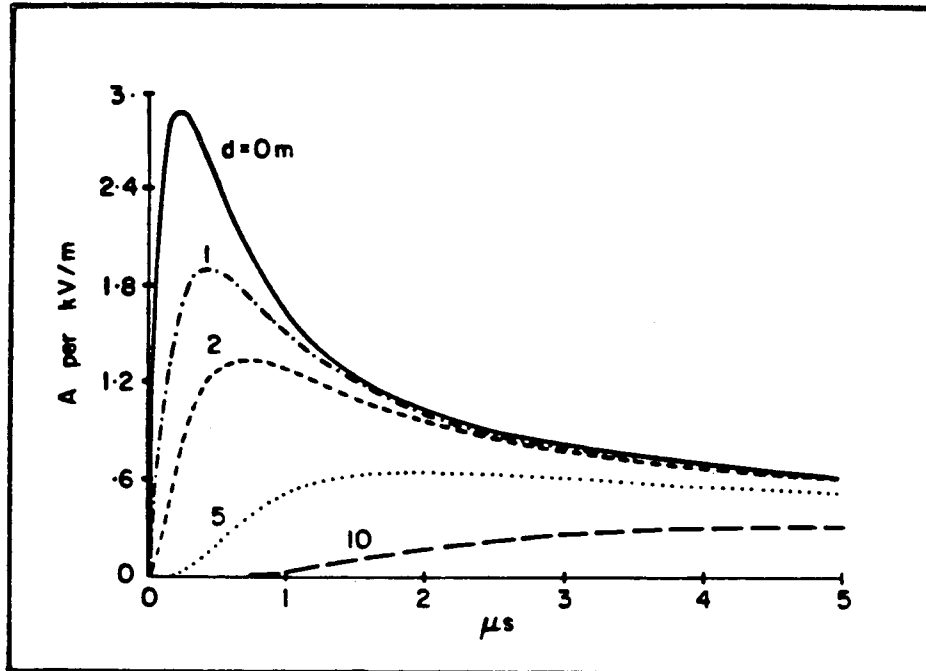
Fig. D5. Normalized HEMP-induced current on buried
conductor in earth with a conductivity of $\sigma_g = 10^{-1}$
mhos/meter for several burial depths.

BIBLIOGRAPHY

D1. Vance, E. F., "Electromagnetic Pulse Handbook for Electric Power
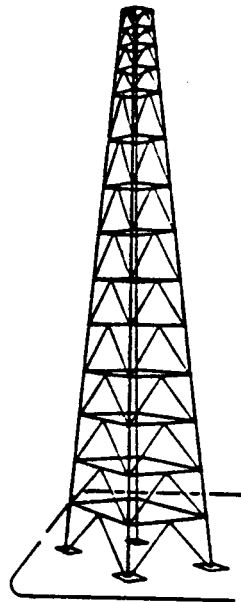   Systems," DNA Report No. 3466F, February 4, 1975.

APPENDIX E

Examples of Antennas Commonly Used
for Various Frequency Bands

Description of Antenna Types

There are many different types of antennas, and some are more susceptible to EMP excitation than are others. An antenna may be viewed as a simple matching transformer which transforms the impedance of the final stage of a transmitter or receiver to the impedance of free space, so as to maximize the efficiency of energy transmission.
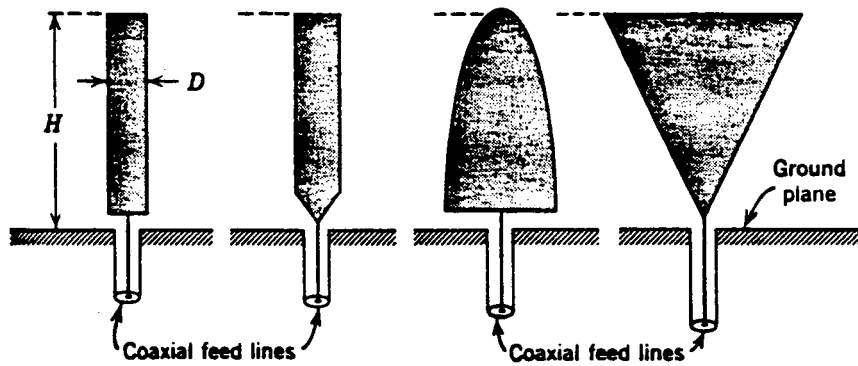
Because electromagnetic radiation is possible over a wide range of frequencies, there are many different designs for antennas. Those antennas designed to operate in the MF and HF frequency ranges are usually most affected by EMP, since their operating frequencies occur in a band where the EMP signal has a strong spectral content. However, in an assessment of a system, all energy gathering antennas should be examined for possible adverse effects.

The monopole class of antenna is a common design, ranging from very low frequency antenna towers used in commercial AM radio stations to UHF blade antennas on aircraft and other vehicles. Figure E1 shows variations of this type of antenna. A spiral monopole antenna as shown in Figure E2 is also commonly found in communications equipment operating in the UHF regime. In this class of radiator, the antenna is driven against the ground plane which might be the earth or the conducting skin of a vehicle.

Another class of antenna is the dipole. Unlike the monopole, the dipole does not require the presence of the earth or a ground plane for its operation. Figure E3 shows two HF dipole antennas which are commonly found in voice communications systems. Folded dipole antennas shown in Figure E4 are commonly found in VHF communications, with a common example being the commercially available FM antennas for the home. Figure E5 shows several other dipole antenna types.

a) Tower antenna

b) General monopole antennas

Fig. E1. Examples of monopole antennas [E1].

d—diameter of wire
D—diameter of helix
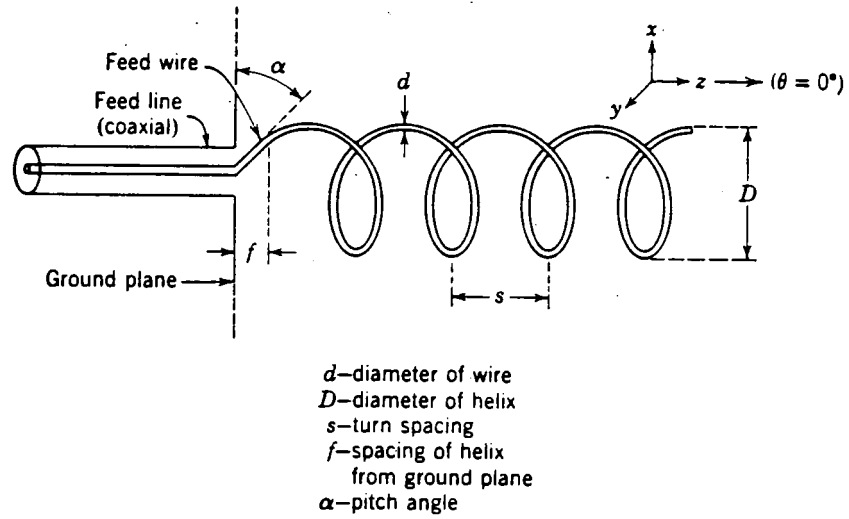s—turn spacing
f—spacing of helix
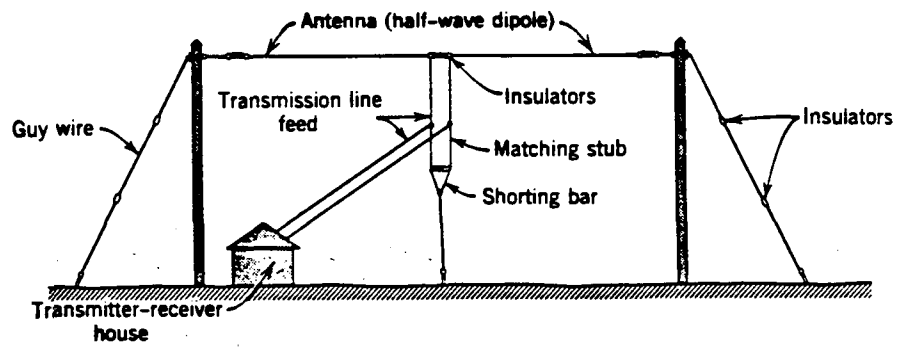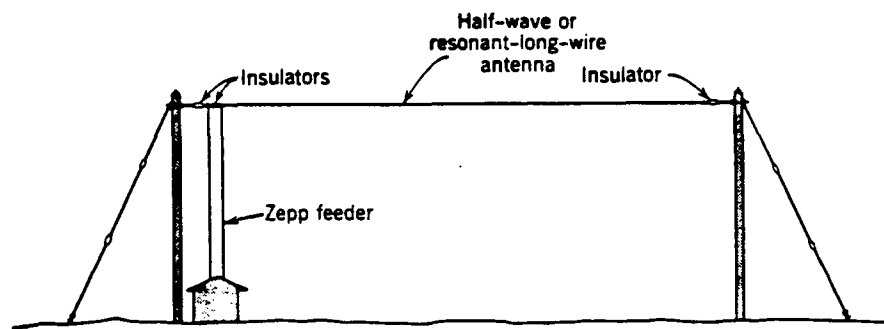   from ground plane
α—pitch angle
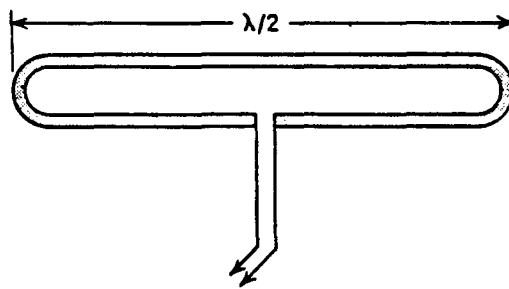
Fig. E2.   Spiral monopole antenna [E1].
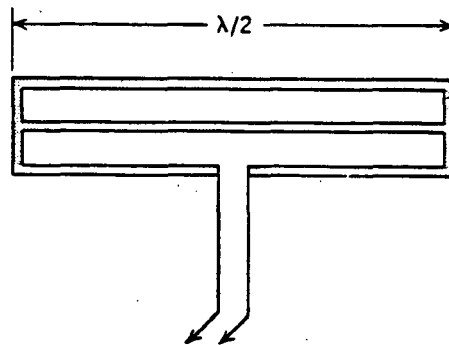
a) Center fed antenna

b) Zepp fed antenna
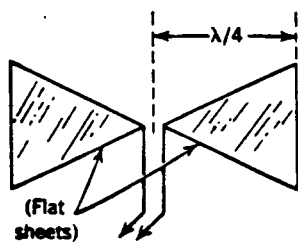
Fig. E3. Examples of HF dipole antennas [E1].
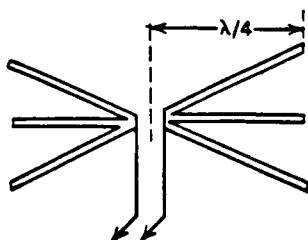
a) Folded dipole antenna
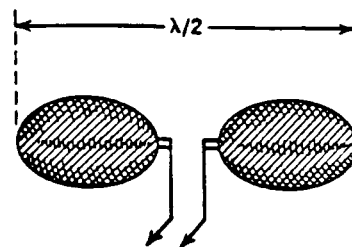

b) Three-wire folded dipole antenna
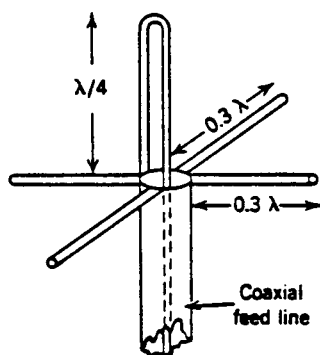
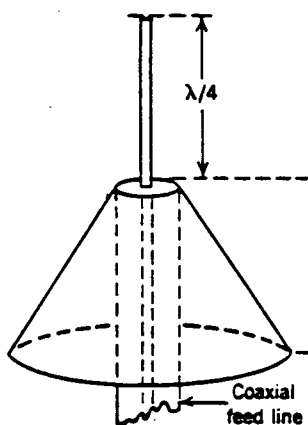Fig. E4. Folded dipole antennas [E2].

(a)
Triangular dipole

(b)
Fan dipole

(c)
Ellipsoidal dipole

(d)
Folded Monopole with
simulated ground

(e)
Conical skirt
antenna
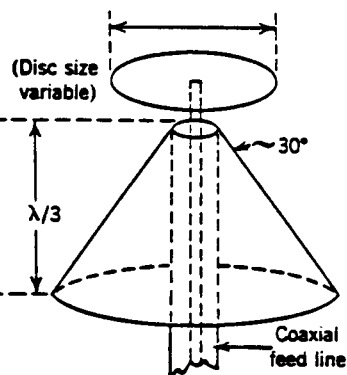
(f)
Discone antenna
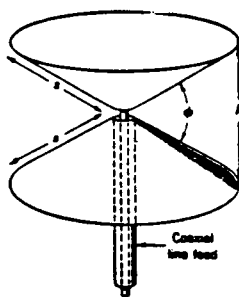
(g)
Biconical antenna

Fig. E5. Examples of dipole type antennas [E1].

At the microwave frequencies, say from 500 Mhz and above, antennas tend to look different from the low frequency devices. Waveguide horns as shown in Figure E6 are commonly used to provide a slow transition from the bounded waveguide propagation to the free space propagation of EM energy. A leaky waveguide as illustrated in Figure E7 also serves as an antenna in this frequency range, and microwave reflector antennas as shown in Figure E8 are also commonly used.

Other types of antennas are also found. Flush-mount antennas are common in vehicles, with the slot antenna of Figure E9 being one example. In addition, the frequency independent antennas shown in Figure E10 are common, especially for communications over several different frequencies, such as found in commercial television.

BIBLIOGRAPHY

E1. Blake, Lamont V., _Antennas_, John Wiley and Sons, New York, 1966.

E2. Schelkunoff, S. A. and S. T. Friis, _Antennas, Theory and Practice_, John Wiley and Sons, New York, 1952.

Fig. E6. Examples of microwave horn antennas [E1].

Fig. E7.   Slotted waveguide antenna [E1].

a) Microwave dish antennas

b) Pill-box antenna

Fig. E8. Examples of microwave reflector antennas [E1].

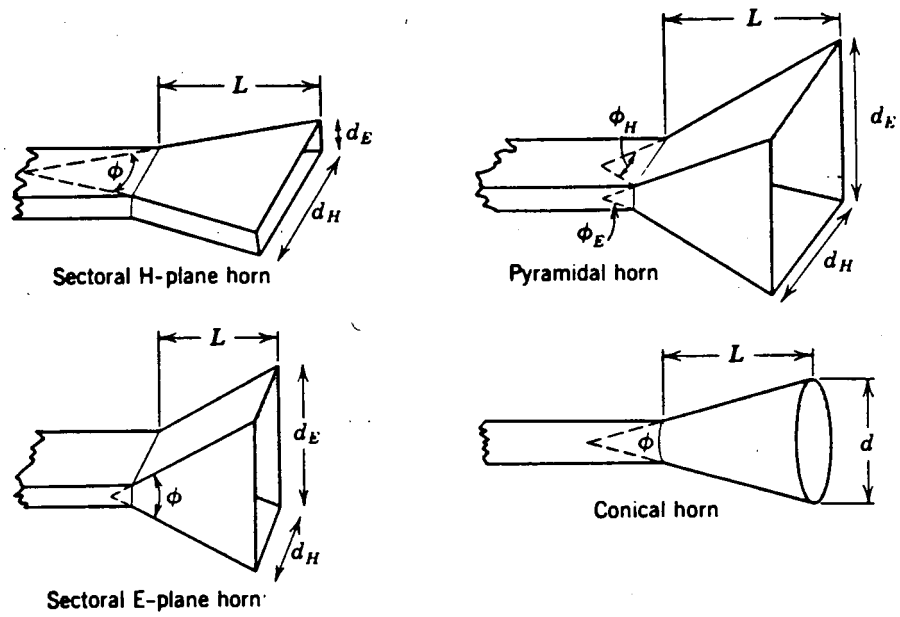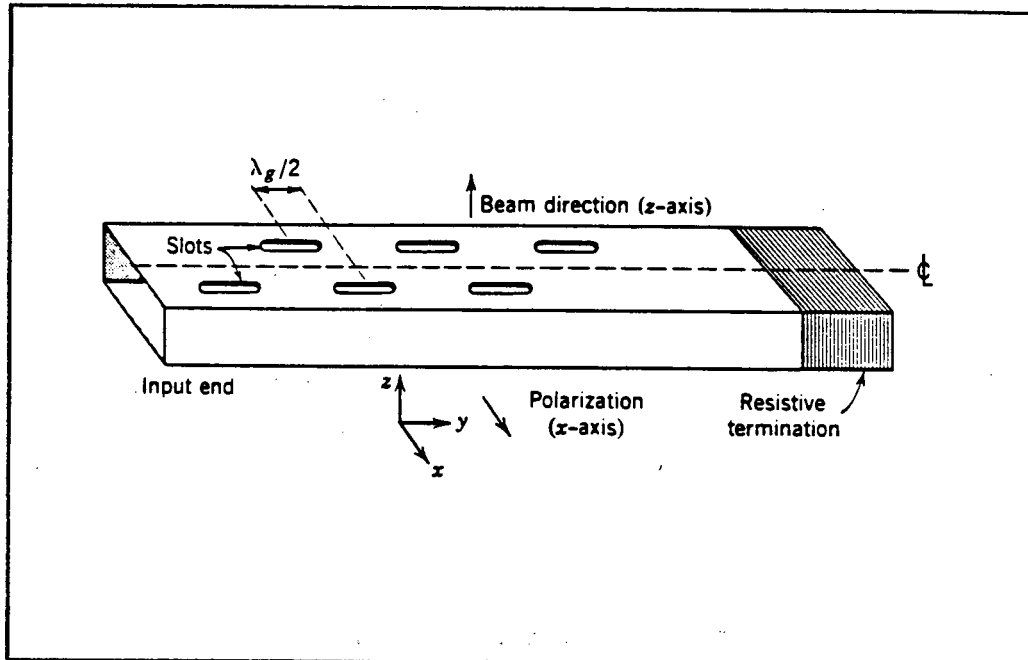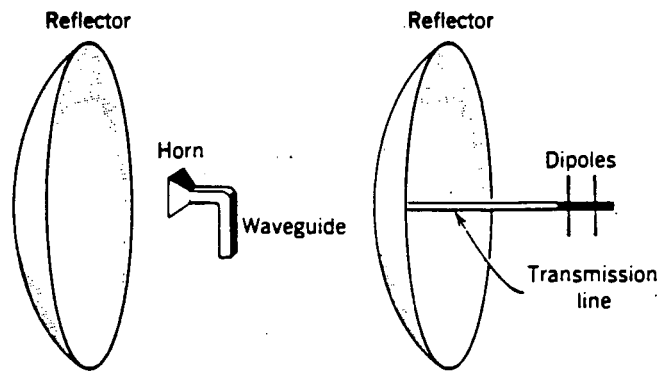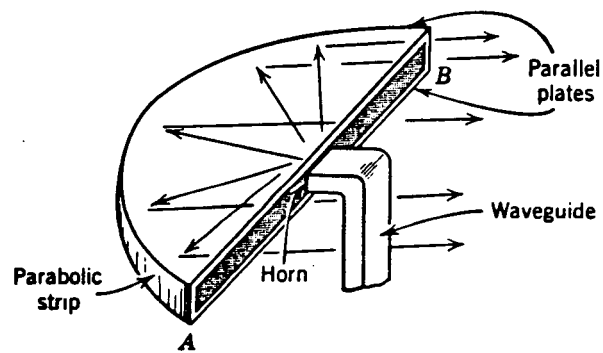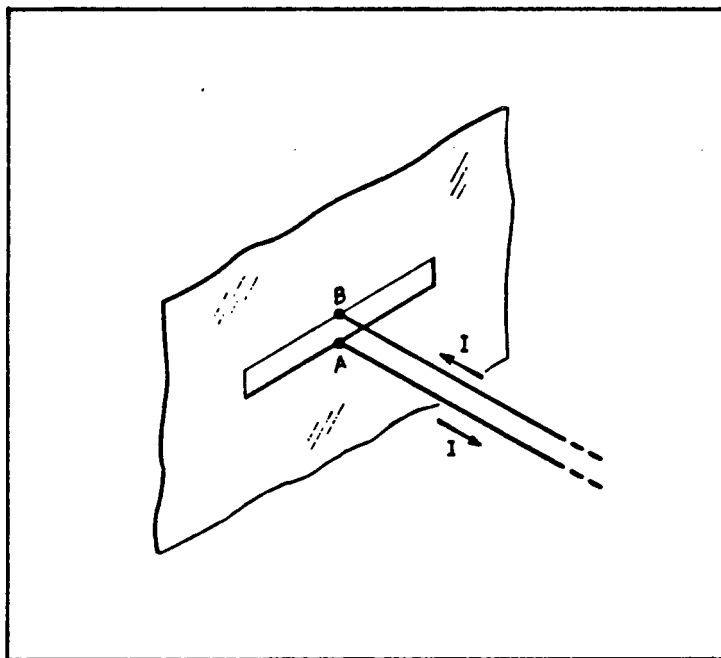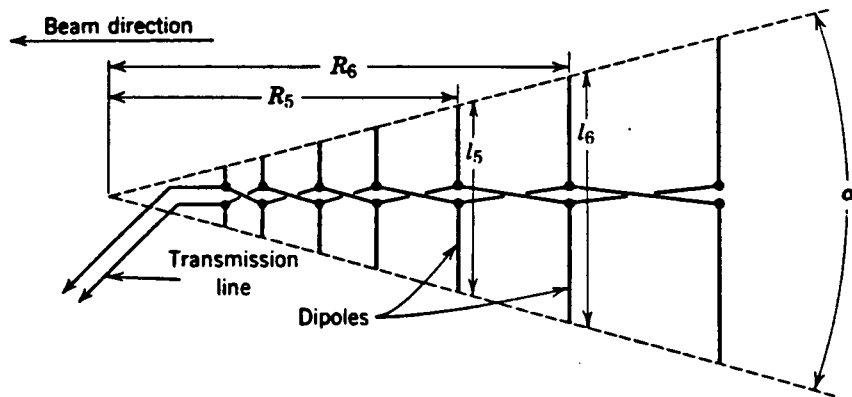Fig. E9. Slot antenna [E2].

a) Log-periodic antenna
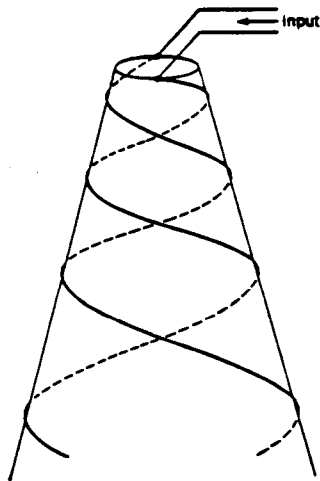
b) Conical Spiral
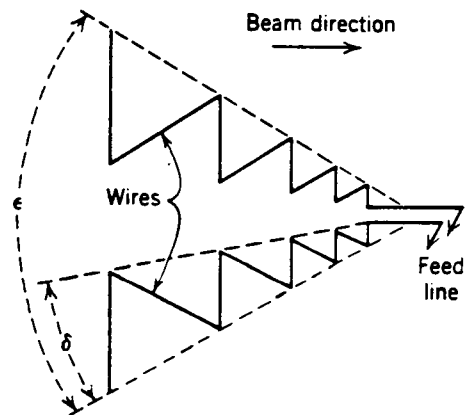
c) Zig-zag antenna

Fig. E10. Examples of frequency independent antennas [E1].

APPENDIX F

Definitions of Electrical Insulation Strengths
for Power Apparatus

Electrical insulation may be classified as (1) external or internal or (2) self-restoring or non-self-restoring, and tests applied to determine insulating strength characteristic are dependent on these classifications. For example, an insulation classified as self-restoring indicates that after flashover the insulation is restored to its original strength condition. This classification is, thus, mainly applied to air-porcelain insulations (external insulation), and tests may be designed which permit flashovers. In contrast, for non-self-restoring insulations, any flashover or puncture results in insulation failure. These insulations are usually internal insulations, e.g., transformers. Tests for these insulations are at such a level that there is a low probability of failure.

Tests may also be classified as investigative or proof tests. The investigative or engineering research tests are those which are used to investigate the insulation strength, its characteristics and abnormalities, whereas the proof tests are those used to demonstrate that a specific apparatus or insulation meets its "rated" insulation strength. Most tests on tower insulations or on bus support insulators are investigative while most tests on transformers and other internal insulation structures are proof tests.

Equipment or air/porcelain insulation strength may be defined by its strength to three types of overvoltages: (1) lightning surges (2) switching surges, and (3) power frequency voltages. The values used to specify insulation strength are:

1. BIL - Basic Lightning Impulse Insulation Level

    The electrical strength of insulation expressed in terms of the crest value of a standard lightning impulse, which has a front of 1.2 μs and a time-to-half-value of 50 μs (usually designated as "1.2/50 μs"). The BIL may be either a statistical BIL or a conventional BIL. The

statistical BIL applies specifically to self-restoring insulation, and is defined as that crest value of the standard lightning impulse for which the insulation exhibits a 10% probability of failure. The conventional BIL specifically applies to non-self-restoring insulations and is the crest value of the standard lightning impulse for which a disruptive discharge does not occur. The probability of failure for the conventional BIL is generally not known.

2. BSL - Basic Switching Impulse Insulation Level

   This is identical to the BIL except a standard switching impulse (250/2500 μs) is used.

3. CFO - Critical Flashover Voltage

   The electrical strength expressed as the crest value of an impulse of any specific wave shape for which the insulation exhibits a 50% probability of flashover. Thus, a CFO may apply to a lightning impulse (CFO_{LI}) or to a switching impulse (CFO_{SI}).

4. Chopped-Wave Insulation Strength

   The electrical insulation strength expressed as the crest value of a standard lightning impulse (1.2/50 μs) which is chopped by an air gap on the tail of the impulse. Chopping times for proof tests are usually 3 μs except for circuit breakers where chopping times are 3 and 2 μs.

5. Front-of-Wave Insulation Strength

   The electrical insulation strength expressed as the maximum value of lightning impulse which has an approximate linear steepness. Normally only used for transformer and then only when specified by the purchaser.

6. Time-Lag Curve

   Curves of crest or maximum voltage of a lightning impulse (usually a 1.2/50 μs impulse) as a function of time-to-flashover. Used primarily, and usually exclusively, for self-restoring insulations and for investigative tests. By varying magnitude of impulse, flashovers for a specific insulation structure will flashover on the tail of the wave for low magnitude, and on the fronts for high magnitudes.

As noted, tests for all of the above strengths employ either a lightning or switching impulse. Chopped-wave and front-of-wave tests, in general, have a greater effect on turn-to-turn internal insulation. The other tests are more applicable to the strength of the major insulation to ground.

Tests using power frequency voltages are also specified for most apparatus. For high voltage equipment these tests are applied to establish performance for system operating voltages and temporary overvoltages. Power frequency tests are also performed on external insulations such as line insulators to determine their performance under contaminated or polluted conditions.

ORNL/Sub/83-43374/1/V2
Dist. Category 97a,b,c

INTERNAL DISTRIBUTION

1-24.	P. R. Barnes	36.	B. W. McConnell
25.	R. B. Braid	37.	J. W. Michel
26.	R. S. Carlsmith	38.	M. O. Pace
27.	F. C. Chen	39-43.	D. J. Slaughter
28.	L. G. Christophorou	44.	R. A. Stevens
29.	R. I. Crutcher	45-46.	J. P. Stovall
30.	S. J. Dale	47.	Central Research Library
31.	W. Fulkerson	48.	Document Reference Section
32.	P. A. Gnadt	50.	Energy Information Library
33.	T. L. Hudson	51-52.	Laboratory Records - RC
34.	F. C. Maienschein	53.	Laboratory Records Department
35.	J. W. MacDonald	54.	ORNL Patent Section

EXTERNAL DISTRIBUTION

55. R. Bellem, Director for Radiation, Defense Nuclear Agency, Washington, DC 20305

56. V. D. Albertson, Department of Electrical Engineering, 123 Church Street, S.W., University of Minnesota, Minneapolis, MN 55455

57. H. W. Askins, Jr., The Citadel, Charleston, SC 29409

58. C. E. Baum, AFWL/NTAAB, Kirkland AFB, NM 87117-6008

59. J. N. Bombardt, R&D Associates, 105 E. Vermijo Street, Suite 450, Colorado Springs, CO 80903

60. G. E. Brackett, Code H25, Navy Surface Weapons Center, 1091 New Hampshire Avenue, Silver Springs, MD 20903-5000

61. E. H. Brehm, Department GK/CN32, Brown, Boveri, and Cie, Aktiengesell Schaft, Postfach 351, D-6800 Mannheim 1, WEST GERMANY

62. F. C. Buchholz, Pacific Gas & Electric Co., 77 Beale Street, Room 2933, San Francisco, CA 94106

63. J. F. Buck, Wisconsin Electric Power Company, 231 W. Michigan, Milwaukee, WI 53201

64. L. M. Burrage, McGraw-Edison, P.O. Box 100, 11131 Adams Road, Franksville, WI 53126

65. H. S. Cabayan, Lawrence Livermore Laboratory, P.O. Box 5504, Livermore, CA 94550

66. F. L. Cain, Georgia Institute of Technology, Engineering Experiment Station, Atlanta, GA 30332

67. J. G. Carbonell, Associate Professor of Computer Science, Carnegie-Mellon University, Pittsburgh, PA 15213

68. R. N. Carlile, Department of Electrical and Computer Engineering, University of Arizona, Tucson, AZ 85721

79. I. J. Carney, Nuclear Survivability Organization, Boeing Aerospace Company, P.O. Box 3999, Seattle, WA 98124

70. V. L. Chartier, Bonneville Power Administration, P.O. Box 491-ER, Vancouver, WA 98666

71. K. K. Chen, Sandia National Laboratory, Drawer 1333, P.O. Box 5800, Kirkland AFB, NM 87185

72. R. F. Chu, Philadelphia Electric Company, 2301 Market Street, MS 10-1, P.O. Box 8699, Philadelphia, PA 19101

73. H. E. Church, Aluminum Company of America, 1501 Alcoa Building, Pittsburgh, PA 15219

74. B. Cikotas, DCES (R-620), Defense Communications Agency, 1860 Wiehle Avenue, Reston, VA 22090-5500

75. C. F. Clark, Bonneville Power Administration, P.O. Box 3621, Portland, OR 97208

76. R. E. Clayton, Power Technologies, P.O. Box 1058, 1482 Erie Boulevard, Schenectady, NY 12301-1058

77. A. Clerici, Sanelmi, Via Pergolesi 25, 20124 Milano, Italy

78. H. W. Colborn, North American Electric Reliability Council, Research Park, Terhume Road, Princeton, NJ 08540-3573

79. P. L. Collins, VP-TPO, Defense Intelligence Agency, Washington, D.C. 20301-6111

80. D. E. Cooper, Southern California Edison Company, P.O. Box 800, 2244 Walnut Grove Avenue, Rosemead, CA 91770

81. R. Cortina, ENEL-Centro Ricerca, Automatica, VIA Volta 1, Cologno Monzese (MI), ITALY

82. G. Dahlen, Royal Institute of Technology, S-100-44, Stockholm, SWEDEN

83. J. Darrah, Headquarters NORAD/G5, Peterson AFB, CO 80914

84. Defense Technical Information Center, Cameron Station, Alexandria, VA 22314

85. J. J. Dougherty, Electric Power Research Institute, P.O. Box 10412, Palo Alto, CA 94303

86. W. M. Druen, 8200 South Memorial Parkway, Suite D, Huntsville, AL 35802

87. J. C. Engimann, Commonwealth Edison, 1319 S. First Avenue, Maywood, IL 60153

88. D. M. Ericson, Jr., Sandia National Laboratory, Division 6414, Kirkland AFB, NM 87185

89. W. E. Ferro, Electric Research and Management, Inc., P.O. Box 165, State College, PA 16804

90. W. G. Finney, Project Manager, Stanley Consultants, Inc., Stanley Building, Muscatine, IA 52761

91. M. Fitzgerald, MITRE Corp., P.O. Box 208, Bedford, MA 01730

92. F. Fisher, General Electric Corporation, Electric Utility Systems Engineering Department, Building 5, Room 306, Schenectady, NY 12345

93. P. B. Fleming, Science and Engineering Associates, Inc., Mariners Square, Suite 127, 1900 North Northlake Way, P.O. Box 31819, Seattle, WA 98103

94. R. Fullwood, Science Applications, Inc., 5 Palo Alto Square, Suite 200, Palo Alto, CA 94304

95. R. Gates, Federal Emergency Management Agency, Research Division, 500 C Street, S.W., Washington, DC 20472

96. M. R. Gent, North American Electric Reliability Council, Research Park, Terhume Road, Princeton, NJ 08540-3573

97. S. M. Gillis, Economic and Public Policy, Department of Economics, Duke University, 4875 Duke Station, Durham, NC 27706

98. W. Graham, R&D Associates, P.O. Box 9695, Marina Del Rey, CA 90291

99. J. J. Grainger, 5004 Hermitage Drive, Raleigh, NC 27612

100. I. S. Grant, Power Technologies, Inc., 1482 Erie Blvd., Schenectady, NY 12305

101. A. R. Gritzke, U.S. Department of Navy, Theater Nuclear Warfare Project Office, Washington, DC 20360

102. J. Gut, Research Intitute for Protective Construction, Auf der Mauer 2, CH-8001 Zurich, SWITZERLAND

103. V. Guten, R-52, National Security Agency, Fort G. Mead, MD 20755

104. M. H. Hesse, JEC 5008, Rensselaer Polytechnic Institute, Troy, NY 12181

105. D. Higgins, JAYCOR, Santa Barbara Facility, P.O. Box 30281, 360 South Hope Avenue, Santa Barbara, CA 93105

106. D. W. Hilson, Tennessee Valley Authority, 1100 Chestnut Street, Tower 2, Chattanooga, TN 37402

107. F. C. Holdes, Pacific Gas & Electric Company, 3235-18th Street, San Francisco, CA 94110

108. W. S. Howington, Noranda Aluminum, Inc., P.O. Box 70, New Madrid, MO 63869

109. R. Hutchins, BDM Corporation, 1801 Randolph, S.W., Albuquerque, NM 87106

110. J. Hunt, Emergency Preparedness Administrator, San Diego Gas and Electric Company, P.O. Box 1831, San Diego, CA 92112

111. V. Inkis, Ontario Hydro, U7E1, 700 University Avenue, Toronto, Canada M5G1X6

112. Wasyl Janischewskyj, Electrical Engineering Dept., University of Toronto, Toronto, Canada M5S1A4

113. H. P. Johnson, Georgia Power Company, 270 Peachtree Street, 11th Floor, Atlanta, GA 30303

114. V. K. Jones, Science and Engineering Associates, Inc., Mariners Square, Suite 127, 1900 North Northlake Way, P.O. Box 31819, Seattle, WA 98103

115. F. R. Kalhammer, Vice-President, Electric Power Research Institute, 3412 Hillview Avenue, P.O. Box 10412, Palo Alto, CA 94303

116. W. Karzas, R&D Associates, P.O. Box 9695, Marina Del Rey, CA 90291

117. R. E. Kasperson, Professor of Government and Geography, Graduate School of Geography, Clark University, Worcester, MA 01610

118. K. W. Klein, Forrestal Building, Room 5E-052, 1000 Independence Avenue, S.W., Washington, DC 20585

119. J. Koepfinger, System Planning Department 21-2, Duquesne Light Company, 1 Oxford Centre, Pittsburgh, PA 15279

120. N. Kolcio, American Electric Power, 1 Riverside Plaza, Columbus, OH 43216

121. J. Labadie, IRT, 6800 Poplar Place, McLean, VA 22131

122. H. T. Lam, South Carolina Public Service Authority, 1 Riverwood Dr., Monks Corner, SC 29461

123. T. R. LaPorte, Professor, Political Science, Institute of Government Studies, University of California, 109 Moses Hall, Berkeley, CA 94720

124. R. C. Latham, Duke Power Company, P.O. Box 33189, Charlotte, NC 28242

125. A. Latter, R&D Associates, P.O. Box 9695, Marina Del Rey, CA 90291

126. J. S. Lawler, Department of Electrical Engineering, University of Tennessee, Knoxville, TN 37916

127. K. S. H. Lee, Dikewood Division of Kaman Science Corp., 2800 28th Street, Suite 3780, Santa Monica, CA 90405

128. J. R. Legro, Westinghouse Electric Corporation, Advanced Systems Technology, 777 Penn Center Boulevard, Pittsburgh, PA 15235

129. M. Lessen, Consulting Engineer, 12 Country Club Drive, Rochester, NY 14618

130. Library, JAYCOR, 205 S Whiting Street, Alexandria, VA 22304

131. J. Lloyd, ED-SD, U.S. Army Engineering, USAEDH, P.O. Box 1600, Huntsville, AL 35087

132. J. Locasso, Rockwell International, 3370 Meraloma Avenue, P.O. Box 4192, Mail Code 031-BB17, Anaheim, CA 92803

133. C. L. Longmire, Mission Research Corporation, P.O. Drawer 719, Santa Barbara, CA 93102

134. W. C. Maklin, IRT Corporation, 6800 Poplar Place, McLean, VA 22101

135. R. M. Maliszewski, American Electric Power Service Corp., 1 Riverside Plaza, P.O. Box 16631, Columbus, OH 43216-6631

136. J. N. Mallory, Southern California Edison Co., P.O. Box 800, Rosemead, CA 91770

137. J. D. Martin, Harris Corporation, PRD Electronics Division, 6801 Jericho Turnpike, Syossett, NY 11791

138. P. S. Maruvada, Hydro-Quebec Institute of Research, 1800 Montee Ste-Julie, Varennes, Quebec, CANADA J0L2P0

139. R. G. McCormack, CERL, Corps of Engineers, P.O. Box 4005, Champaign, IL 61820

140. G. F. Meenaghan, Vice President for Academic Affairs and Dean of the College, The Citadel, Charleston, SC 29409

141. C. Menemenlis, University of Patras, Patras, GREECE

142. I. N. Mindel, IIT Research Institute, 10 West 35th Street, Chicago, IL 60616

143. D. L. Mohre, Cajun Electric Power Corp., P.O. Box 15440, Baton Rouge, LA 70895

144. B. B. Mrowca, Baltimore Gas & Electric Co., P.O. Box 1475, Baltimore, MD 21203

145. K. Muller, IABG, Einsteinstrasse 20, 8012 Ottobrunn, WEST GERMANY

146. E. M. Murtha, Booz Allen and Hamilton, General Services Administration, 18th & F Streets, N.W., Washington, DC 10405

147. H. P. Neff, Department of Electrical Engineering, University of Tennessee, Knoxville, TN 37916

148. B. O. Nettles (Code 203), Naval Electronic Systems Engineering Center, Charleston, 4600 Marriott Drive, North Charleston, SC 29418

149. D. R. Nevius, North American Electric Reliability Council, Research Park, Terhume Road, Princeton, NJ 08540-3573

150. G. B. Niles, Baltimore Gas & Electric Company, Principal Eng. Room 1020, P.O. Box 1475, Baltimore, MD 21203

151. B. Noel, Los Alamos National Laboratory, Mail Station 5000, P.O. Box 1663, Los Alamos, NM 87545

152. B. Nowlin, Arizona Public Service Company, P.O. Box 21666, Phoenix, AR 85036

153. R. Oats, Atomic Weapons Research Establishment, Building D57, Aldermaston, Reading, RG74PR, England

154. G. Orrell, Dep. Associate Director for National Preparedness, Federal Emergency Management Agency, 500 C Street, S.W., Washington, DC 20555

155. L. Paris, University of Pisa, Via Diotisalvi 2, 56100 PISA, ITALY

156. R. Parker, RDA, P.O. Box 9335, Albuquerque, NM 87119

157. R. Parkinson, Science Applications, Inc., 5150 El Camino Real, Suite B-31, Los Altos, CA 94022

158. A. Pigini, CESI-Via Rubahimo 59-Milano, ITALY

159. J. B. Posey, Ohio Brass Co., 380 N. Main Street, Mansfield, OH 44903

160. M. Rabinowitz, Electric Power Research Institute, 3412 Hillview Avenue, P.O. Box 10412, Palo Alto, CA 94303

161. W. A. Radaski, Metatech Corp., 358 South Fairview Avenue, Suite E, Goleta, CA 93117

162. J. J. Ray, Bonneville Power Administration, P.O. Box 3621, Portland, OR 97208

163. T. J. Reed, Westinghouse Electric Corporation, Advanced Systems Technology, 777 Penn Center Boulevard, Pittsburgh. PA 15235

164. R. L. Retallach, American Electric Power, 1 Riverside Plaza, Columbus, OH 43216

165. J. Richardson, National Academy of Science, 2101 Constitution Avenue, Washington, DC 20418

166. F. Rosa, Nuclear Regulatory Commission, Division of Systems Integration, MS P1030, Washington, DC 20555

167. D. H. Sandell, Harza Engineering Co., 150 South Wacker Drive, Chicago, IL 60606

168. J. A. Sawyer, MITRE Corp., MS-H070, P.O. Box 208, Bedford, MA 01703

169. R. A. Schaefer, Metatech Corp., 20 Sunnyside Avenue, Suite D, Mill Valley, CA 94941

170. M. Schechter, A.D.A., P.O. Box 2250(81), Haifa, 31021, ISRAEL

171. D. Serafin, Lawrence Livermore Laboratory, P.O. Box 5504, Livermore, CA 94550

172. H. Singaraju, Air Force Weapons Laboratory, Kirkland AFB, NM 87117

173. A. C. Smith, Jr., Beam Research Program, Lawrence Livermore National Laboratory, P.O. Box 808, Livermore, CA 94550

174. J. C. Smith, McGraw-Edison Company, Power Systems Group, P.O. Box 440, Canonsburg, PA 15317

175. R. Smith, DNA, RAEE, 6801 Telegraph Road, Alexandria, VA 22310

176. W. Sollfrey, RAND Corp., 1700 Main Street, Santa Monica, CA 90406

177. H. Songster, Electric Power Research Institute, Electrical Systems Division, 3412 Hillview Avenue, P.O. Box 10412, Palo Alto, CA 94303

178. G. K. Soper, Defense Nuclear Agency, Washington, DC 20305

179. S. Spohn, DB-6E2, Defense Intelligence Agency, Washington, DC 20301-6111

180. J. R. Stewart, Power Technologies, Inc., P.O. Box 1058, 1482 Erie Boulevard, Schenectady, NY 12301-1058

181. R. L. Sullivan, Department of Electrical Engineering, College of Engineering, University of Florida, Gainesville, FL 32611

182. I. O. Sunderman, Lincoln Electric System, P.O. Box 80869, Lincoln, NE 68501

183. R. W. Sutton, Science Applications, Inc., 1710 Goodridge Drive, P.O. Box 1303, McLean, VA 22102

184. F. M. Tesche, LuTech, Inc., 3742 Mt. Diablo Boulevard, Lafayette, CA 94549

185. L. Thione, CESI-Via Rubattino 54 20734, Milano, ITALY

186. R. J. Thomas, 302 Phillips Hall, Cornell University, Ithaca, NY 14853

187. R. Torres, BDM Corporation, 1801 Randolph, S.W., Albuquerque, NM 87106

188. W. Tyler, NT, Kirkland AFB, NM 87117

189. M. A. Uman, Department of Electrical Engineering, University of Florida, Gainesville, FL 32611

190. E. F. Vance, Route 3, Box 268A, Fort Worth, TX 76140

191. D. R. Volzka, Wisconsin Electric Power Company, 231 West Michigan Street, Milwaukee, WI 53201

192. J. Vora, Nuclear Regulatory Commission, MS 5650 NL, Washington, DC 20555

193. C. D. Whitescarber, Martin Marietta Orlando Aerospace, Sandlake Road Complex (SLRC), Mail Point 399, P.O. Box 5837, Orlando, FL 32855

194. W. P. Wigner, 8 Ober Road, Princeton, NJ 08540

195. M. W. Wik, Forsvarets Materielverk, S-11588 Stockholm, SWEDEN

196. C. B. Williams, IRT Corp., 7650 Convoy Court, P.O. Box 80817, San Diego, CA 92138

197. W. H. Williams, Division Manager, AT&T Information Systems, Building 83, Room 1B23, 100 Southgate Parkway, Morristown, NJ 07960

198. D. D. Wilson, Power Technologies, Inc., P.O. Box 1058, Schenectady, NY 12301

199. U. P. Wissmann, AEG-Telefunken, General Electric Company, 1 River Road, Building 36-444, Schenectady, NY 12345

200. H. W. Zaininger, Zaininger Engineering Company, 3408 Vance Court, San Jose, CA 95132

201. Institute for Energy Analysis, ORAU - Library

202. Assistant Manager for Energy Research & Development, DOE/ORO Oak Ridge, TN 37830

203-856. Given for distribution as shown in DOE/TIC-4500 under Category UC-97a,b,c (Electric Energy Systems, Transmission, Power Distribution, Systems Development and Control)